

Aus dem Institut für Aktive Polymere
Helmholtz-Zentrum Hereon, Teltow

**Modulating ultrathin films of semi-crystalline oligomers
by Langmuir technique**

zur Erlangung des akademischen Grades

"Doktor der Naturwissenschaften"

(Dr. rer. nat)

in der Wissenschaftsdisziplin

"Materialien in den Lebenswissenschaften"

Kumulative Dissertation

eingereicht an der

Mathematisch-Naturwissenschaftlichen Fakultät

der Universität Potsdam

 **Helmholtz
Graduate School**
Macromolecular Bioscience



von

Shivam Saretia

aus Bhopal, Indien

Potsdam, 2021

Hauptbetreuer: Prof. Dr. Andreas Lendlein
Universität Potsdam

Gutachter: Prof. Dr. Andreas Lendlein
Universität Potsdam

Prof. Dr. Svetlana Santer
Universität Potsdam

Prof. Dr. Michel Goldmann
Université de Paris

Ort und Tag der Disputation: Universität Potsdam, Golm; Februar 16, 2022

Published online on the
Publication Server of the University of Potsdam:
<https://doi.org/10.25932/publishup-54210>
<https://nbn-resolving.org/urn:nbn:de:kobv:517-opus4-542108>

Statement of Authenticity

I, Shivam Saretia, formally submit my PhD dissertation entitled “Modulating ultrathin films of semi-crystalline oligomers by Langmuir technique” to the Institute of Chemistry, Faculty of Mathematics and Natural Sciences of the University of Potsdam, Germany, for the acquirement of the academic degree of Doctor of Natural Sciences (Dr. ret. nat.) in the Department of Chemistry.

I hereby declare that the work presented in this dissertation is my own original work based on the research carried out at the Institute of Active Polymers, Helmholtz-Zentrum Hereon in Teltow, Germany, from May 2016 to Sept 2021 under the supervision of Prof. Dr. Andreas Lendlein. To the best of my knowledge and belief, this dissertation does not contain any work previously published or written by another person, except where due reference is made in it. No portion of this work has been previously submitted in the support of any other degree to another university or institute. Any contribution made by other co-workers to this research is explicitly acknowledged in the dissertation.

Shivam Saretia

Acknowledgement

Throughout the duration of this dissertation I have received a great deal of support and assistance. First and foremost, I would like to express my sincere gratitude to my supervisor, Prof. Andreas Lendlein, whose expertise was invaluable in developing the research, pushed me to sharpen my thinking, and elevated my work to a higher level.

I am truly thankful to my Group leader, Dr. Rainhard Machatschek, for his valuable guidance in the later half of this dissertation. Your insights on formulating the research methodology, interpretation of the findings, and drafting the manuscripts were immensely helpful in completing this dissertation, and broadening my skills. Without Dr. Burkhard Schulz, my Group Leader in the first half of my Dissertation, this thesis would have not been possible. His plentiful knowledge, continuous support and patience were instrumental in laying the foundation of this dissertation. His perception continues to inspire me throughout my academic and daily life. I would also like to acknowledge and thank Prof. Nan Ma and Dr. Toralf Roch for their contributions to the early stages of my PhD research.

I acknowledge Prof. Svetlana Santer and Prof. Michel Goldmann for their effort and time in reviewing my thesis. I also thank Prof. Yan Lu for chairing the examination committee for my PhD defense.

My genuine thanks to Dr. Karl Kratz and Dr. Marc Behl for their coordination to conduct characterization experiments in their labs. For their assistance with the experimental techniques, I am very thankful to Olaf Lettau, Daniela Radzik, Susanne Schwanz, Dr. Karola Lützow, Dr. Maria Balk, Victor Izraylit, Dr. Skadi Lau and Dr. Natalia Tarazona. Special thanks to Manuela Keller for her countless assistance in my experiments and for keeping the lab running smoothly. Thank you Wing Tai Tung, Thanga Bhuvanesh and Falko Rottke for your helping hand in my various works as well as for being amusing officemates.

Many thanks to Ms. Sabine Benner and Ms. Karolin Schmäzlin for coordinating the submission of my manuscripts to Journals. I would like to compliment Dr. Michael Schroeter, Patricia Ebel, and Dr. Anne Schöne for their efforts in coordination of mentoring committee. I also acknowledge Mario Zahn, Stephanie Altenkirch, and Sebastian Goeldner and Christin Skala for their general assistance, especially coordinating activities during the pandemic.

Gratitude to my parents and brother for their wise counsel and indispensable support throughout my life. I am also very grateful to my friends and colleagues at Hereon, who provided stimulating discussions as well as immense encouragement.

Finally, I am grateful for the financial support by the Helmholtz Association of German Research Centers through program-oriented funding and Helmholtz Graduate School for Macromolecular Bioscience, and by the University of Potsdam.

Table of Contents

Abstract.....	VI
Zusammenfassung.....	VIII
Abbreviations and symbols.....	XI
List of Figures.....	XIII
1. Introduction.....	1
1.1. Polymeric films as biomaterials	1
1.1.1. Current trends in research and applications	3
1.1.2. Semi-crystalline polymer films	5
1.1.3. Hydrolytic and enzymatically catalyzed degradation	8
1.2. Fabrication methods for ultrathin films	11
1.2.1. Langmuir technique.....	12
1.2.2. Langmuir films of polymers: crystallization, degradation, and chemical reactions.....	15
2. Motivation and Aims	18
3. Hypotheses and Concept.....	20
4. Organization of the thesis	22
5. Publications.....	23
5.1. Effect of water on crystallization and melting of telechelic oligo(ϵ -caprolactone)s in ultrathin films	23
5.2. Degradation kinetics of oligo(ϵ -caprolactone) ultrathin films: influence of crystallinity.....	25
5.3. Highly crystalline PCL ultrathin films as thermally switchable biomaterial coatings	27
5.4. Reversible 2D networks of oligo(ϵ -caprolactone) at the air-water interface...	29
6. Discussion.....	31
6.1. Nanostructured ultrathin films by crystallization under defined conditions ...	31
6.2. Degradation of (ultra)thin films from semi-crystalline oligomers	35
6.3. Reaction of polymer/oligomer end-groups in ultrathin films	37
7. Conclusion and Outlook	40
8. References.....	44
Appendix I	57
Appendix II.....	68
Appendix III.....	81
Appendix IV.....	97
Appendix V: List of Publications and Contributions to Conferences	107
Appendix VI: Curriculum Vitae	109

Abstract

Polymeric films and coatings derived from semi-crystalline oligomers are of relevance for medical and pharmaceutical applications. In this context, the material surface is of particular importance, as it mediates the interaction with the biological system. Two-dimensional (2D) systems and ultrathin films are used to model this interface. However, conventional techniques for their preparation, such as spin coating or dip coating, have disadvantages, since the morphology and chain packing of the generated films can only be controlled to a limited extent and adsorption on the substrate used affects the behavior of the films. Detaching and transferring the films prepared by such techniques requires additional sacrificial or supporting layers, and free-standing or self-supporting domains are usually of very limited lateral extension. The aim of this thesis is to study and modulate crystallization, melting, degradation and chemical reactions in ultrathin films of oligo(ϵ -caprolactone)s (OCL)s with different end-groups under ambient conditions. Here, oligomeric ultrathin films are assembled at the air-water interface using the Langmuir technique. The water surface allows lateral movement and aggregation of the oligomers, which, unlike solid substrates, enables dynamic physical and chemical interaction of the molecules. Parameters like surface pressure (π), temperature and mean molecular area (MMA) allow controlled assembly and manipulation of oligomer molecules when using the Langmuir technique. The π -MMA isotherms, Brewster angle microscopy (BAM), and interfacial infrared spectroscopy assist in detecting morphological and physicochemical changes in the film. Ultrathin films can be easily transferred to the solid silicon surface via Langmuir-Schaefer (LS) method (horizontal substrate dipping). Here, the films transferred on silicon are investigated using atomic force microscopy (AFM) and optical microscopy and are compared to the films on the water surface.

The semi-crystalline morphology (lamellar thicknesses, crystal number densities, and lateral crystal dimensions) is tuned by the chemical structure of the OCL end-groups (hydroxy or methacrylate) and by the crystallization temperature (T_c ; 12 or 21 °C) or MMAs. Compression to lower MMA of $\sim 2 \text{ \AA}^2$, results in the formation of a highly crystalline film, which consists of tightly packed single crystals. Preparation of tightly packed single crystals on a cm^2 scale is not possible by conventional techniques. Upon transfer to a solid surface, these films retain their crystalline morphology whereas amorphous films undergo dewetting.

The melting temperature (T_m) of OCL single crystals at the water and the solid surface is found proportional to the inverse crystal thickness and is generally lower than the T_m of bulk PCL. The impact of OCL end-groups on melting behavior is most noticeable at the air-solid interface, where

the methacrylate end-capped OCL (OCDME) melted at lower temperatures than the hydroxy end-capped OCL (OCDOL). When comparing the underlying substrate, melting/recrystallization of OCL ultrathin films is possible at lower temperatures at the air-water interface than at the air-solid interface, where recrystallization is not visible. Recrystallization at the air-water interface usually occurs at a higher temperature than the initial T_c .

Controlled degradation is crucial for the predictable performance of degradable polymeric biomaterials. Degradation of ultrathin films is carried out under acidic (pH \sim 1) or enzymatic catalysis (lipase from *Pseudomonas cepcia*) on the water surface or on a silicon surface as transferred films. A high crystallinity strongly reduces the hydrolytic but not the enzymatic degradation rate. As an influence of end-groups, the methacrylate end-capped linear oligomer, OCDME ($\sim 85 \pm 2$ % end-group functionalization) hydrolytically degrades faster than the hydroxy end-capped linear oligomer, OCDOL ($\sim 95 \pm 3$ % end-group functionalization) at different temperatures. Differences in the acceleration of hydrolytic degradation of semi-crystalline films were observed upon complete melting, partial melting of the crystals, or by heating to temperatures close to T_m . Therefore, films of densely packed single crystals are suitable as barrier layers with thermally switchable degradation rates.

Chemical modification in ultrathin films is an intricate process applicable to connect functionalized molecules, impart stability or create stimuli-sensitive cross-links. The reaction of end-groups is explored for transferred single crystals on a solid surface or amorphous monolayer at the air-water interface. Bulky methacrylate end-groups are expelled to the crystal surface during chain-folded crystallization. The density of end-groups is inversely proportional to molecular weight and hence very pronounced for oligomers. The methacrylate end-groups at the crystal surface, which are present at high concentration, can be used for further chemical functionalization. This is demonstrated by fluorescence microscopy after reaction with fluorescein dimethacrylate. The thermoswitching behavior (melting and recrystallization) of fluorescein functionalized single crystals shows the temperature-dependent distribution of the chemically linked fluorescein moieties, which are accumulated on the surfaces of crystals, and homogeneously dispersed when the crystals are molten. In amorphous monolayers at the air-water interface, reversible cross-linking of hydroxy-terminated oligo(ϵ -caprolactone) monolayers using dialdehyde (glyoxal) lead to the formation of 2D networks. Pronounced contraction in the area occurred for 2D OCL films in dependence of surface pressure and time indicating the reaction progress. Cross-linking inhibited crystallization and retarded enzymatic degradation of the OCL film. Altering the subphase pH to ~ 2 led to cleavage of the covalent acetal cross-links. Besides as

model systems, these reversibly cross-linked films are applicable for drug delivery systems or cell substrates modulating adhesion at biointerfaces.

Zusammenfassung

Ultradünne Filme/Beschichtungen aus semikristallinen oligomeren Makromolekülen sind für medizinische und pharmazeutische Anwendungen von Bedeutung. Dabei kommt der Materialoberfläche eine besondere Bedeutung zu, da diese die Interaktion mit dem umgebenden biologischen System ermöglicht. Zur Modellierung der Oberfläche werden 2D Systeme und ultradünne Filme verwendet. Herkömmlichen Techniken zu deren Präparation wie Spin-Coating oder Dip-Coating haben jedoch Nachteile, da sich die Morphologie und Kettenpackung der erzeugten Filme nur sehr bedingt kontrollieren lässt und sich die Adsorption auf dem verwendeten Substrat auf das Verhalten der Filme auswirkt. Zum Ablösen oder Übertragen der mit Hilfe dieser Techniken hergestellten Filme sind zusätzliche Opfer- oder Transferschichten erforderlich. Zudem können mit diesen Methoden nur freistehende oder selbsttragende Filme von sehr geringer lateraler Ausdehnung hergestellt werden. Das Ziel dieser Arbeit ist es, Kristallisation, Schmelzen, Abbau und chemische Reaktionen in ultradünnen Filmen von Oligo(ϵ -caprolacton)en (OCL)s mit unterschiedlichen Endgruppen unter Umgebungsbedingungen zu untersuchen und zu kontrollieren. Dazu wurden ultradünne Filme an der Luft-Wasser-Grenzfläche mit der Langmuir-Technik erzeugt. Die Wasseroberfläche erlaubt eine ungestörte Bewegung und Aggregation der Oligomere, was, im Gegensatz zu festen Substraten, dynamische physikalische und chemische Interaktion der Moleküle miteinander ermöglicht. Die Langmuir-Technik erlaubt mit Hilfe von Parametern wie Temperatur, Oberflächendruck (π) und Fläche pro Wiederholheit eine kontrollierte Manipulation der Oligomere. Kompressionsisothermen, Brewster-Winkelmikroskopie und Grenzflächen-Infrarotspektroskopie halfen beim Nachweis morphologischer und physikalisch-chemischer Veränderungen im Film. Die ultradünnen Filme wurden über das Langmuir-Schäfer-Verfahren (Kontakt mit Substrat in paralleler Orientierung zur Grenzfläche) auf Siliziumsubstrate übertragen. Danach wurden die übertragenen Filme mittels AFM und optischer Mikroskopie untersucht und mit Filmen an der Wasseroberfläche verglichen.

Die teilkristalline Morphologie (Lamellendicke, Kristallzahldichte und laterale Dimension der Kristalle) von Polymerfilmen kann durch die chemische Struktur der OCL-Endgruppen (Hydroxy oder Methacrylat) und durch die Kristallisationstemperatur (T_c ; 12 oder 21 °C) oder die Fläche pro Wiederholeinheit beeinflusst werden. Die Kompression auf eine sehr kleine Fläche pro Wiederholeinheit von $\sim 2 \text{ \AA}^2$ führt zur Bildung eines hochkristallinen Films, der aus dicht gepackten

Einkristallen besteht. Eine Synthese von derartigen Filmen im cm^2 Maßstab ist mit herkömmlichen Techniken nicht möglich. Nach Übertragung auf eine feste Oberfläche behielten die teilkristallinen Filme ihre Morphologie, während amorphe Filme das für Polymere charakteristische Entnetzungsverhalten aufwiesen.

Die Schmelztemperaturen (T_m) von OCL-Einkristallen an der Wasser- und Festkörperoberfläche waren proportional zur inversen Kristalldicke und im Allgemeinen niedriger als die T_m von PCL im Festkörper. Der Einfluss der OCL-Endgruppen auf das Schmelzverhalten war an der Luft-Feststoff-Grenzfläche am deutlichsten, wo OCL mit Methacrylat-Endgruppen bei niedrigeren Temperaturen schmolz als OCL mit Hydroxyl-Endgruppen. Das Schmelzen/Rekristallisieren ultradünner OCL-Filme an der Luft-Wasser-Grenzfläche erfolgte bei niedrigeren Temperaturen als an der Luft-Feststoff-Grenzfläche, wo keine Rekristallisation beobachtet wurde. Die Rekristallisation geschmolzener Filme an der Luft-Wasser-Grenzfläche erfolgte normalerweise bei einer höheren Temperatur als der anfänglichen T_c .

Der kontrollierte Abbau ist entscheidend für die Performance von abbaubaren Polymeren als Biomaterialien. Der Abbau ultradünner Filme erfolgte hydrolytisch entweder unter saurer ($\text{pH} \sim 1$) oder enzymatischer Katalyse (Lipase aus *Pseudomonas cepcia*) auf der Wasseroberfläche oder als übertragene Filme auf Siliziumoberflächen. Eine hohe Kristallinität reduzierte die hydrolytische Abbaurate stark, aber die enzymatische dagegen wenig. Das lineare Oligomer mit Methacrylat Endgruppen ($\sim 85 \pm 2$ % Endgruppenfunktionalisierung) wurde bei unterschiedlichen Temperaturen schneller hydrolytisch abgebaut als das lineare Oligomer mit Hydroxyl Endgruppen ($\sim 95 \pm 3$ % Endgruppenfunktionalisierung). Unterschiede in der Beschleunigung des hydrolytischen Abbaus von teilkristallinen Filmen wurden beim vollständigen Schmelzen, teilweisen Schmelzen der Kristalle, oder durch erwärmen in die Nähe von T_m beobachtet. Daher eignen sich Filme aus dicht gepackten Einkristallen als Barrierschichten mit thermisch schaltbarer Degradationsrate.

Chemische Reaktionen in ultradünnen Filmen können angewandt werden, um funktionalisierte Moleküle zu verbinden und ihnen Stabilität zu verleihen oder Stimuli-sensitive Vernetzungen zu erzeugen. Hier wurden die Reaktionen der Endgruppen transferierter Einkristalle auf festen Oberflächen und amorphen Monoschichten an der Luft-Wasser-Grenzfläche untersucht. Da die Kettenenden defekte in den Einkristallen darstellen würden, werden sie bei der Kristallisation an der Kristalloberfläche angeordnet. Die Dichte der Endgruppen ist umgekehrt proportional zum Molekulargewicht und daher bei Oligomeren besonders hoch. Hier wurden mit Methacrylatendgruppen versehene OCL Moleküle verwendet. Diese Gruppen können chemisch

weiter umgesetzt und für eine Funktionalisierung der Kristalle verwendet werden. Dies wurde fluoreszenz-mikroskopisch nach der Reaktion mit Fluoresceindimethacrylat nachgewiesen. Das thermische Schalten (Schmelzen und Umkristallisieren) von Fluorescein-funktionalisierten Einkristallen erzeugt eine temperaturabhängige Verteilung der chemisch verknüpften Fluorescein-Einheiten, die sich auf den Oberflächen der Kristalle ansammeln und beim Schmelzen der Kristalle homogen dispergiert werden. In amorphen Monoschichten an der Luft-Wasser-Grenzfläche führt die reversible Vernetzung von Hydroxy-terminierten Oligo(ϵ -caprolacton) Monoschichten unter Verwendung eines Dialdehyds (Glyoxal) zur Bildung von zweidimensionalen (2D) Netzwerken. Bei 2D-OCL-Filmen trat eine ausgeprägte Kontraktion der Fläche in Abhängigkeit von Oberflächendruck und Zeit auf, was den Fortschritt der Reaktion anzeigte. Die Vernetzung hemmte die Kristallisation und verzögerte den enzymatischen Abbau des OCL-Films. Eine Änderung des pH-Wertes der Subphase auf ~ 2 führte zur Spaltung der kovalenten Acetalvernetzungen. Außer als Modellsysteme wäre der Einsatz dieser reversibel vernetzten Filme für den Einsatz als Drug-Delivery-Systeme oder als Oberflächen zur Steuerung der Adhäsion von Zellen möglich.

Abbreviations and symbols

1D	One-dimensional
2D	Two-dimensional
3D	Three-dimensional
A(t)	Film area after a degradation time interval t
A ₀	Initial film area
AFM	Atomic force microscopy
BAM	Brewster angle microscopy
G	Gibbs free energy
<i>I</i>	Normalized differential intensity
IR	Infrared
LB	Langmuir-Blodgett
LMD	Langmuir monolayer degradation
LS	Langmuir-Schaefer
MMA	Mean molecular area
<i>M_n</i>	Number-average molar mass
<i>n_{air}</i>	Refractive index of air
<i>n_{water}</i>	Refractive index of water
OCDME	Oligo(ϵ -caprolactone) dimethacrylate
OCDOL	Oligo(ϵ -caprolactone) diol
OCL	Oligo(ϵ -caprolactone)
PCL	Poly(ϵ -caprolactone)
PE	Polyethylene
PEG	Poly(ethylene glycol)
PEO	Poly(ethylene oxide)
PFC	Perfluorinated compound

PGA	Polyglycolide
PHB	Poly(β -hydroxybutyrate)
PI	Polyimide
PLA	Poly lactide
PLGA	Poly(lactide-co-glycolide)
PM-IRRAS	Polarization modulation-infrared reflection-adsorption spectroscopy
POM	Polarized optical microscopy
PP	Polypropylene
PTFE	Polytetrafluoroethylene
PU	Polyurethane
T_c	Crystallization temperature
T_g	Glass transition temperature
T_m	Melting temperature
$T_{m\text{ end}}$	Endpoint temperature of melting
$T_{m\text{ onset}}$	Onset temperature of melting
T_m°	Equilibrium melting point of an infinitely large crystal
T_{rec}	Recrystallization temperature
UV	Ultraviolet
$\Delta A_{\text{rel}}(t)$	Normalized area reduction
$\Delta A_t(t)$	Absolute area change
ΔH_m	Enthalpy of fusion
ΔS_m	Entropy of fusion
θ_B	Brewster's angle
π	Surface pressure

List of Figures

Figure 1: Applications of polymer thin films and coatings in life science	3
Figure 2: Three-layer model of confined polymer crystallization at a solid surface	7
Figure 3: Acid (a) and base (b) catalyzed hydrolysis of the ester bond.....	9
Figure 4: Effect of crystallinity on the degradation of a bulk polymeric system in an aqueous environment	10
Figure 5: Selected methods for preparing ultrathin films	11
Figure 6: (a) Schematic representation of the Langmuir technique for monolayer preparation of an ideal amphiphile. (b) Deposition scheme of Langmuir ultrathin film on a solid substrate by Langmuir-Blodgett method and Langmuir-Schaefer method.....	13
Figure 7: Principle of Brewster angle microscopy for visualizing films at the air-water interface.....	14
Figure 8: Principle of Polarization Modulation Infrared Reflection Adsorption Spectroscopy at the air-water interface	15
Figure 9: Ultrathin films (amorphous or semi-crystalline) as model representations for complex bulk interfaces	19
Figure 10: Schematic illustration of Langmuir ultrathin films: Preparation, transfer, and investigation at different interfaces for thermoswitching, degradation, and reaction of end-groups	20

1. Introduction

Ultrathin films in biomaterial research are designed as platforms fulfilling engineering and biological aspects, where molecules are assembled in the x-y or a 2D plane. The perspectives on defining materials that are confined in a 2D plane differ between disciplines. Biologists frequently refer to thin sheets, or a layered scaffold consisting of a network of fibers (1D; one-dimensional material) in a confined space as a 2D material.¹ Physicists on the other hand do not consider the assembly of a 1D material in laterally confined geometries as a 2D material. They define materials based on their topology, mechanical behavior, and dimensions, whereas chemists strictly define the features for 2D material to be a sheet-like monomolecular film with laterally connected repeat units having end-groups along all edges.² The molecules forming 2D materials are generally based on atoms, groups of atoms, or organic molecules, such as monomers from the graphene family, chalcogenides, and oxides, generally with an application motivated towards mechanoelectronics.^{3,4}

Ultrathin films with non-toxicity, predictable bio response, and regulated (bio)degradation are highly relevant for medical applications. The synthesis methods used should be ecologically friendly and capable of producing large-scale, homogenous films that can be coated on a variety of surfaces. Because of structural effects and unknown processes, toxicities from typical graphene-based 2D materials are not uncommon. Its possible negative impacts on species in marine and terrestrial environments are also a source of future concern.^{5,6}

1.1. Polymeric films as biomaterials

Polymers can be used to create ultrathin films with distinct characteristics. Polymeric films do not require special handling or storage conditions and are more stable than the sensitive films made from proteins, peptides, or nucleic acids, which also require time-consuming and costly isolation and purification step.^{7,8} Regarding the polymeric film thickness, a thin film ≥ 200 nm, an ultrathin film ≤ 100 nm, and a 2D ultrathin film has thickness \leq its random coil size.⁹

The molecular weight is an important characteristic governing the degradation and bioelimination of polymers used in a nanostructured device.¹⁰ For example, the degradation time of a high molecular weight poly(lactide-*co*-glycolide) (PLGA) in an implanted drug release device can exceed 6 months.^{11,12} From the perspective of compliance, it is not desirable to retain an empty drug matrix in the body for a long time period. Depending on the release time period, low-molecular-weight polymers (~ 10 kDa) might be a more suitable choice for such applications as these demonstrate a faster renal clearance and allow various linker

chemistries for conjugation of drugs with high concentration.¹³ Therefore, compared to high-molecular-weight polymers, oligomers are often in focus for the delivery of drugs, especially for therapeutic applications.^{14, 15} Oligomers are also important in the study of structure-activity relationships because their molecular structure is more easily controllable than that of their polymeric counterparts.^{14, 15} Oligomers, therefore, are emerging molecules for the creation of various complex systems such as electroactive devices¹⁶, three-dimensional (3D) printed actuators¹⁷, smart coatings¹⁸, and solar cells¹⁹.

According to the International Union of Pure and Applied Chemistry (IUPAC), an oligomer has an intermediary molecular mass, and its properties vary significantly with the removal of one or a few of the repeating units.²⁰ In materials science, for example, PCL telechelics with number-average molar mass (M_n) approximately up to 5000 g·mol⁻¹ have been considered as oligomers.²¹ Semi-crystalline oligomers are interesting candidates for creating ultrathin films because they offer tunable degradation, end-group functionalization capability, and well-described synthesis routes. Their mechanical and degradation behavior in bulk are often adjusted by varying molar mass, crystallinity, or copolymerization with other polymers. Amongst polyesters, PLGA due to its favorable properties for in vivo sustained release of therapeutics has been widely researched and also applied to prepare drug delivery systems (e.g. injectable microparticles²²).^{23, 24} However, acidic degradation products of PLGA pose a problem, since they can deactivate peptide or protein-based drugs²⁵ and can cause an unfavorable systemic response²⁶. Another relevant degradable polyester is polylactide (PLA), which is widely applied for food packaging and single-use items, however, PLA exhibits poor heat stability and water barrier properties (moisture absorption makes PLA brittle).²⁷ Polyglycolide (PGA) has a similar chemical structure to PLA, however, it is more expensive to synthesize when compared to other (bio)degradable polymers.²⁸ The temperature of PGA degradation (~250 °C) is also near to its T_m (220-230 °C), making it susceptible to thermal degradation.²⁹ Poly(ϵ -caprolactone) (PCL) is a polyester well documented in bulk, with T_m and T_c in the physiological temperature ranges. Because of the hydrolyzable ester linkages in PCL, it is entirely degradable, with low acidity of the reaction products. PCL is soluble in a range of solvents and its end-groups can be post-functionalized with relevant reactive groups such as hydroxy, methacrylate, and boronic acids. PCL crystallization and degradation are also documented to some extent for thin and ultrathin films. As a result, a vast number of studies use PCL to develop nanostructured medical devices, drug delivery systems, and substrate coatings.^{21, 30}

1.1.1. Current trends in research and applications

Polymeric coatings are applied in everyday life, for example, to control friction, sun reflection, or to improve dirt release characteristics. As protectants, polymeric coatings can significantly extend the life of coated items against deterioration caused by external elements such as sunshine, moisture, dust, microorganisms, and so on. Such protective coatings lower the overall carbon footprint because the frequency of replacement of the covered object is reduced.⁸

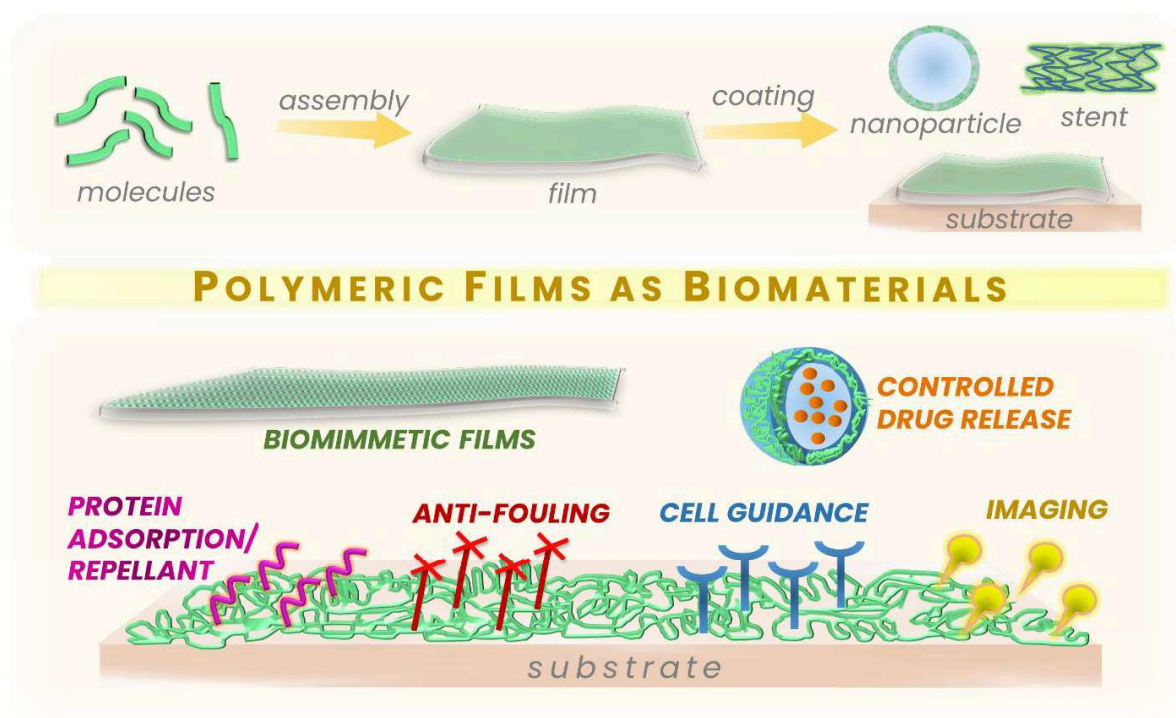


Figure 1: Applications of polymer thin films and coatings in life science

In the health care field, polymer films are applicable as biocompatible coatings for implants (protein-repellant coatings, anti-thrombogenic coatings, membrane-mimetic films, antibacterial coatings), tissue engineering (controlling protein adsorption and cell adhesion onto scaffolds), drug delivery, and gene therapy (e.g. pH-dependent drug, protein and nucleic acid delivery via nanoparticles)³¹⁻³³ (Figure 1).

Stimuli-responsivity is an essential feature in polymeric ultrathin films for a variety of applications such as self-healing³⁴, on-demand reflectivity,³⁵ anti-microbial activity,^{36, 37} or changing surface dynamics³⁸. The stimuli-responsivity in ultrathin films is imparted via crystals, embedded nanoparticles, reversible bonds, etc., and is triggered by external stimuli of light, temperature, pH, ion exchange, voltage, magnetic field, mechanic stress, plasma, ultrasonication, solvent, gas, or guest.³⁹ A medical device designed using a light-sensitive polymer offers remote operability, however employing light as a trigger in medicine is

hampered by poor or no light penetration in deep body tissues. Temperature and pH are important stimuli that occur naturally in the physiological system and do not require the device to be transparent or conductive in order to function.⁴⁰ It is also well known that sites of inflammation and most tumors differ from their surrounding tissues by having an acidic pH. As a means of targeting such sites, pH-sensitive polymeric coatings have a wide interest in targeted drug delivery vehicles. Temperature-sensitive polymeric films, for example, are used for easy cell detachment from cell culture surfaces.⁴¹ Thermally switchable films are also applied for packaging food and sustaining the environment for preservation. In some other examples, crystallinity plays an important role for thermally switchable films for temperature regulation (crystalline PE nanofibers)⁴² or mechanical stiffness control (salt seed crystals)⁴³.

Polymeric films are also utilized as model biointerfaces to acquire molecular insights into bulk systems. Polymeric thin films, for example, are used to study the interfacial phenomenon of crystallization, degradation, and interactions with biomolecules.⁴⁴ In particular, several studies on polymer crystallization dynamics utilizing ultrathin polymeric films on solid surfaces have been published. Utilizing single crystals, the influence of polymer properties such as chain ends on protein interaction is also demonstrated.⁴⁵ Altering surface chemistry of polymer single crystals using the immense end-groups presented on the surface is an emerging field in pharmaceutical science. For example, amino-functionalized PLA single crystals (grown from dilute solutions) are explored as vaccine delivery vehicles to virus-associated tumors.⁴⁶ Surface chemistry of single crystals from polylysine, and copolymers of poly(ethylene glycol) (PEG) and PLA are also explored for loading of drugs.^{45, 47}

Surface chemistry is also effective in creating bioactive surfaces for regulating cellular responses.⁴⁸ For instance, peptides^{49, 50}, growth factors, and glysoaminiglycans^{51, 52} are cross-linked on PCL surface for specific cell adhesion and proliferation. Such reactions explore and demand chemistries in an aqueous environment and under ambient conditions to maintain the viability of biomolecules. Also, modification of surfaces of medical devices or implants in a non-destructive environment is critical to preserve functionality and intended bioresponsivity.

For predicting the bioresponse of medically applicable coatings or nanostructured devices, the influence of unavoidable variables such as aqueous environment and temperature is highly important. For instance, PCL scaffolds incorporated with hydrogels have the ability to treat bone defects or bioengineer the cartilaginous tissue surrounding bone joints.^{53, 54} Yet, the strains or frictional heat produced by joint movements, or device handling during implantation, can alter their physicochemical properties and therefore can affect their tissue regeneration

capability.^{55, 56} Therefore, for health care needs and translation of semi-crystalline materials to real-life applications, the complex interplay between aqueous environment, crystalline states, degradation and chemical reactions in confine systems is highly relevant.

1.1.2. Semi-crystalline polymer films

The function of crystallinity in a material is to provide temperature-sensitive physical cross-links. The effect of crystallinity on the mechanical response is significant in the temperature range between T_g and T_m while below, T_g the effect is negligible. The T_g of some clinically applied polymers is well below room temperature, e.g. $-78\text{ }^\circ\text{C}$ for poly(ethylene oxide) (PEO), $-60\text{ }^\circ\text{C}$ for PCL and $5\text{ }^\circ\text{C}$ for (poly[β -hydroxybutyrate]) (PHB),⁵⁷ enabling their processing at room temperature (between T_g and T_m) by a process such as by cold-drawing to produce films of high strength⁵⁸.

For methods such as melt extrusion and crystallization studies via melt,⁵⁹ polymer needs to be melted above T_m . However, PHB has a very narrow processing window, due to very low resistance to thermal degradation. T_m of bulk PHB is around $170\text{-}180\text{ }^\circ\text{C}$ and its processing temperature should be at least $180\text{-}190\text{ }^\circ\text{C}$, where it is susceptible to rapid thermal degradation.⁵⁹ To improve the processability of this polymer, the addition of additives, plasticizers, or blending with other polymers is required.⁶⁰ Whereas T_m of bulk PCL is around $64\text{ }^\circ\text{C}$, and its thermal degradation products are only observable at a temperature above $340\text{ }^\circ\text{C}$.⁶¹ This large processing window for manipulation under ambient temperatures is one of the reasons why PCL is applied as a model polymer for investigating crystallization in (ultra)thin films.⁶²

In the polymer crystallization process, the first step is the formation of nuclei that can occur when chain segments become aligned. This can happen spontaneously in an undercooled melt (homogeneous nucleation) or be promoted by extraneous particles (heterogeneous nucleation). With an increase in the size of the nuclei, free energy first increases to a certain maximum value and then drops and becomes negative to form a stable nucleus. After nucleation, the growth of crystals occurs by the addition of folded polymer chains at the crystal growth front.⁶³ The melting of a polymer crystal occurs when its Gibbs free energy G is equal to the free energy of the melt. Therefore:

$$G_{\text{cryst}}(T_m) = G_{\text{melt}}(T_m)$$
$$\Delta G_m = G_{\text{melt}}(T_m) - G_{\text{cryst}}(T_m) = \Delta H_m - T_m \Delta S_m = 0$$

$$T_m^\circ = \frac{\Delta H_m}{\Delta S_m}$$

where T_m° is the equilibrium melting point of an infinitely large crystal. ΔH_m and ΔS_m are the enthalpy and entropy of fusion of the crystalline segments respectively.^{64, 65}

Crystallization of polymers can be induced by evaporating a dilute solution, cooling a melt, lateral strain, annealing, or stretching/drawing processes. Depending on the crystallization process and its conditions, different crystalline morphologies are obtained. Single crystals (uniform thickness with well-defined, regular chain packing) can be produced from dilute solutions and ultrathin films, while spherulites (lamellar structures arranged in circular symmetry) are commonly observed from the cooling of the melt.⁴⁵

A long going debate evolved around the chain conformation in single crystals. For this, the chain assembly process is described by two competing models - the regular folded array (adjacent re-entry of chains) and the more generally accepted switchboard model (folding of chains with random reentry). For crystallization from the cooling of a melt, density measurement and scattering studies suggest that there is no significant reordering of chain conformation, which is explained by the solidification model (variation of switchboard model). This model explains that lamellar structure involves the straightening of sections of the polymer coil followed by the alignment of these sequences in regular arrays. Hence, a lamellar structure is formed by a minimal amount of chain movement and this is evidenced by rapid crystal growth on the cooling of the melt.⁶³

In confined crystallization, apart from polymer features and processing parameters, the film thickness and substrate are highly influential parameters. The number of active nuclei and the rate of crystal growth decrease with the film thickness. For instance, confined crystallization of PCL on solid surface prohibits isotropic spherulitic growth, leading to the formation of unique crystalline morphologies such as branched edge-on lamellae (~200 nm), flat-on axialites, (~30 nm), and dendrites (15 nm and below).⁶⁶ Thickness also affects the chain orientation in crystals. For example in confined crystallization of polyethylene (PE) and polypropylene (PP), thicker films preferentially produce edge-on lamellae (chain alignment is parallel to the layer plane) whereas flat-on lamellae (chain orientation perpendicular to the layers) are mostly observed in thinner films.⁶²

The methods and preparation conditions produce a variety of anomalies and challenges in polymer film crystallization.⁶⁷ Many studies employ spin coating, where, following the deposition of the polymer solution on the substrate, the assembly is subjected to a high rotation

rate, which wastes the majority of the solution due to centrifugal forces.⁶⁸ In another method, semi-crystalline films with different pore sizes can be made using gas blowing. This technique is complicated by the requirement of molds that are subsequently required to control the insertion of gas bubbles within the sandwiched film.^{69 70} For example, CO₂ is passed through a sandwiched polyurethane (PU) film between two additional polyimide (PI) films. Here, the gas bubble sizes are used for influencing the film crystallization and overall film morphology.⁷¹ Solvent evaporation is another method of polymer thin film crystallization where crystallization can be influenced by factors such as choice of substrate characteristics, choice of solvents, and its rate of evaporation. The major disadvantages of this method include environmental concerns of the release of solvents and incomplete solvent removal.⁷² However, residual organic solvents may be needed to enhance polymer chain mobility in confined environments. For example, residual solvents can act as a plasticizer, increasing PCL chain mobility for large-sized crystals formation.⁷³ Yet, residual organic solvents pose a risk for biological applications and are thus removed via vacuum or heating that can lead to dewetting of the polymeric coating.⁷⁴ In another method of preparing semi-crystalline coating via melt, thermal history, or the amount of time the films are kept above the T_m , has a significant impact on crystallization. For example, heating times of 30 mins or more above the T_m of PCL, result in slower crystallization when compared to a heating time of 1 minute.⁷³ Also, in order to initiate isothermal crystallization in thin films of polymers such as from PEO and PCL, heterogeneous nucleation by residues, dust particles, or manually scratching the substrate is often required.⁹

Interactions between the substrate and polymer chains have a dramatic influence on crystallization. At the polymer-substrate interface, chain mobility is highly reduced as explained by a three-layer model (Figure 2). Polymer chains near the substrate have a higher T_g than the remainder of the film due to limited chain mobility, and therefore their diffusion to the crystal growth front is hindered.

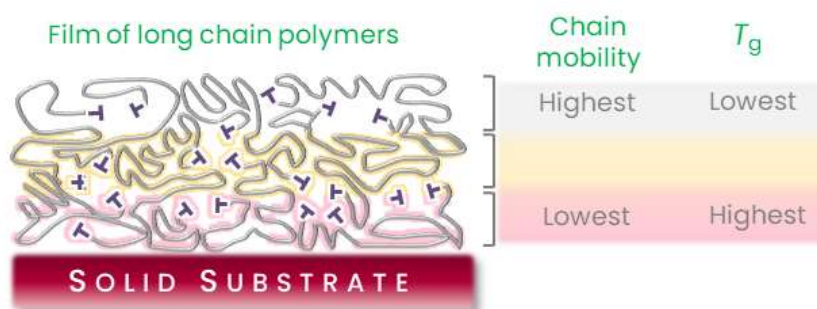


Figure 2: Three-layer model of confined polymer crystallization at a solid surface

Polymer crystallization also differs at two contrasting substrates namely sticky walls (slow crystallization with flat-on orientation) and slippery walls (fast crystallization with edge-on orientation) with strong attractive and repulsive force at the substrate-polymer interface, respectively.^{9, 75} When using amorphous polymeric substrates for crystallization of PCL and PEO, additives/stabilizers within substrate lead to the discrepancies between the experiment and theoretical models for crystallization.⁷⁶ Submicrometer morphology and roughness also dramatically affect the polymer crystallization. For example, isothermal crystallization of isotactic PP melt in contact with an aluminum plate is considerably faster than that with a stainless-steel plate due to differences in the submicrometer morphology.⁷⁷ For PCL films, even a minute scratch on the solid surface can change the chain packing of a growing flat-on lamella to a thicker edge-on lamella.⁶⁷ Depending on the substrate wettability, molecular orientation gets varied too as seen for polyamide ~50 nm films, which on the hydrophilic Si(OH) substrate dominantly form edge-on lamellae while flat-on lamellae are favored for films on the more hydrophobic Mica surface.⁷⁸ In terms of melting, interactive forces on a polymer-solid interface may lead to a decrease or increase in the overall free energy on melting.^{79, 80} Altogether, the effect of the solid substrate on polymer crystallization and the melting transition is complex and highly dependent on surface dynamics.

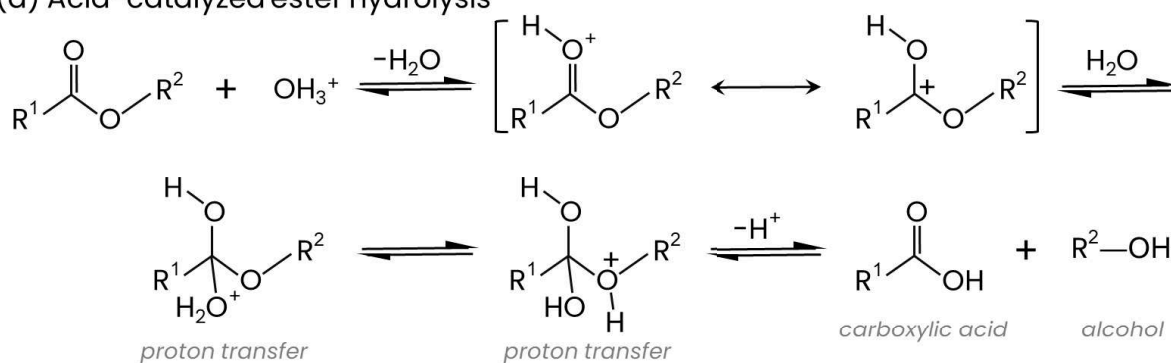
1.1.3. Hydrolytic and enzymatically catalyzed degradation

Controlled degradation of ultrathin films is a relevant function for medical application. When considering ultrathin films, diffusion of reactants and reaction products is much faster than the chain scission reaction itself. Degradation experiments can be completed within a few minutes to hours, in contrast to experiments with bulk materials that can take months to years.⁴⁴ Therefore, thin or ultrathin films are employed for predicting mechanisms of bulk degradation and for the interaction studies with catalytic species in a highly controlled environment.

Material degradation can occur physically, e.g. by light, high temperature, and mechanical stress, or by chemical reactions. For medical applications, chemical degradations via hydrolysis, potentially under enzymatic catalysis, is of high interest.⁸¹ Generally, the hydrolytic degradation of polyesters occurs by random scission of the ester backbone, with the hydrophilicity of the chains as an important governing factor. In Figure 3, the acid and base-catalyzed hydrolysis of ester bonds are presented. Under acid catalysis, the carbonyl oxygen of the ester group is protonated by a hydronium ion. Subsequently, a water molecule attacks the carbonyl carbon to give a tetrahedral intermediate, which is either cleaved to a carboxylic acid and an alcohol, or the original ester is regenerated. Under alkaline conditions, a hydroxide anion

attacks the carbonyl carbon and a tetrahedral intermediate is produced, which either reverts to the ester, or produces carboxylate and alcohol. The last reaction step is irreversible, making the alkaline hydrolysis generally more efficient. In the hydrolytic degradation process, water molecules act as both reactant and reaction medium. Catalytic ions or enzymes produce water-soluble degradation fragments by polymer chains scission (random or chain end cleavage). The local degradation rate depends on local water concentration and chain mobility, both of which are restricted in crystals.⁴⁴

(a) Acid-catalyzed ester hydrolysis



(b) Base-catalyzed ester hydrolysis

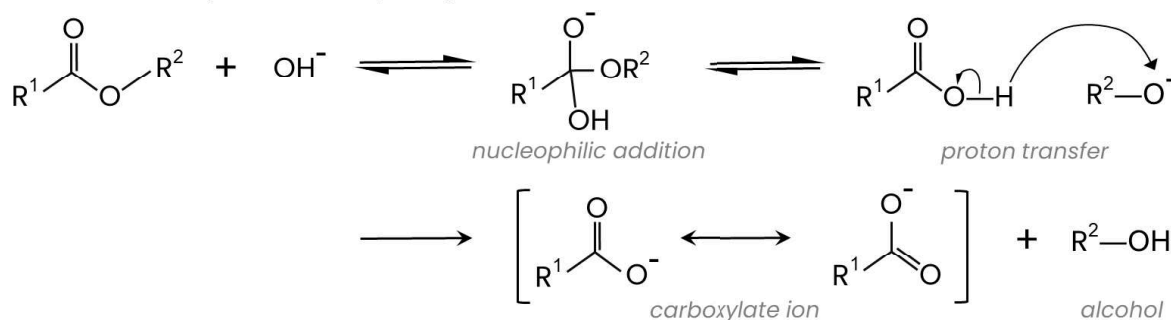


Figure 3: Acid (a) and base (b) catalyzed hydrolysis of the ester bond

Bulk degradation occurs when water uptake is faster than the chain scission rate. The mass loss rate occurs from the entire volume, and over time, the object may develop cracks, limiting mechanical performance or causing the object to break into several pieces.⁸¹ In an ideal surface erosion process, the material is lost solely from the polymer matrix surface at a rate proportional to the surface area. In general, materials wherein water cannot easily permeate the bulk, or that have a very chain scission rate, exhibit surface erosion.⁸² Figure 4 depicts the effect of crystallinity on the degradation of a bulk polymer in an aqueous environment. Depending on the polymer characteristics, in a system with high material crystallinity, the bulk material can degrade primarily by surface erosion due to slower water diffusion than the molecular degradation rate (Figure 4). Whereas in a material with low crystallinity, due to faster water

uptake than the chain scission rate, a bulk degradation process can occur depending on polymer features (Figure 4). For example, due to the difference in crystallinity, poly(*rac*-lactide) (d,l-PLA; amorphous; primarily bulk degradation) degrades much faster than the stereoregular poly(*L*-lactide) (l-PLA; semi-crystalline; primarily surface erosion).^{83, 84} However, the general effect of crystallinity on degradation kinetics is not well understood.⁸⁵ A slower degradation of crystallites during degradation of a semi-crystalline bulk material might be caused by lower water access in crystals or also due to a slower rate of bond scission. Often an increase in crystallinity is observed during degradation.⁸⁶ Here, it is uncertain if the released fragments are crystallizing or if the amorphous phase is degrading faster than the crystalline segments.⁴⁴

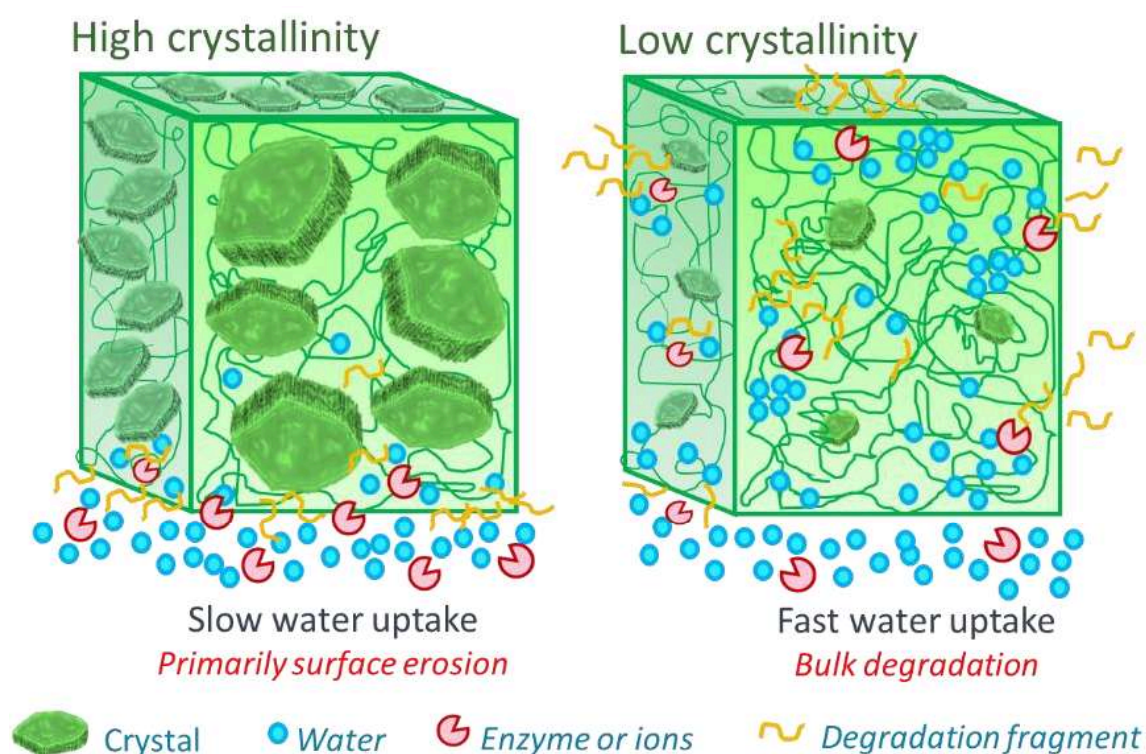


Figure 4: Effect of crystallinity on the degradation of a bulk polymeric system in an aqueous environment

Due to the large size of enzymes and often high catalytic rate, enzymatic degradation can primarily occur at the surface of a bulk material. Often lipases are employed for degradation studies, which have an active catalytic triad consisting of serine, histidine, and aspartate/glutamic acid. Different factors influence enzymatic degradation, most importantly, the combination of enzyme and polymer, and the activity of the enzyme in the degradation conditions.^{44, 81} For instance, the lipase from *Pseudomonas cepacia* is stable and active over a wide pH range (3-11.5 for 24 h at 30 °C) with the highest activity performance at physiological pH ~7.4. At very low or high pH values, the activity of the enzyme is reduced.⁸⁷

1.2. Fabrication methods for ultrathin films

In top-down approaches, 2D ultrathin films are exfoliated from highly organized layers, e.g. exfoliation of graphene from highly oriented pyrolytic graphite. Different approaches such as (scratching/removal via adhesive tapes,), chemical (intercalators separating individual layers), or electrochemical (voltage) have been developed.⁸⁸ Since these approaches rely on the existence of sheet-like structures within the 3D materials, it is not applicable for oligomers or polymers, unless they also have a sheet-like structure. A schematic representation of techniques for ultrathin film preparation is shown in Figure 5.

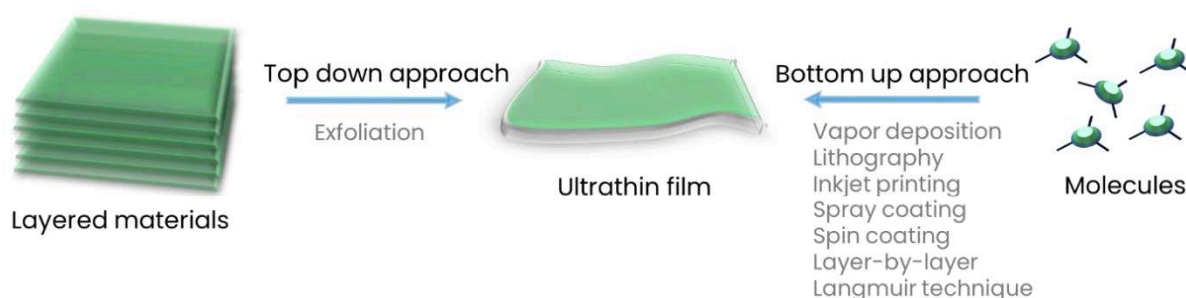


Figure 5: Selected methods for preparing ultrathin films

In the bottom-up approach, the molecules are assembled or reacted in a 2D plane to form an ultrathin film. A widely applied technique for preparing ultrathin films of small molecules is chemical/physical vapor deposition. The downside of this method is limited control over the morphology, susceptibility of polymer degradation, and the difficulty to study the films in situ.⁸⁹ Several other solvent techniques use ambient conditions suitable for polymers and biomolecules. These are limited in the types of molecules that can be investigated, for example, polyelectrolytes in the Layer-by-Layer method, lipid-like molecules in the self-assembly method, and amphiphiles in the Langmuir technique.^{90, 91} The Langmuir technique outperforms any method when it comes to controlling the lateral packing density and studying the behavior of oligomers/polymers confined in a 2D plane using the coupled in situ characterization methods. Since polymers/oligomers on the water surface can move freely, their chain packing and orientation are adjustable to induce dynamic processes such as crystallization and 2D reactions. Degradation of an ultrathin film can be carried in a close simulation of the physiological environment. In principle, a practically infinitely long 2D layer can be formed and lifted from the air-water interface to solid surfaces for further characterization. Though the Langmuir technique requires some operator skills and expensive instrumentation, it surpasses

other ultrathin film preparation methods in terms of controlling film thickness, homogenous deposition, and real-time characterization of versatile macromolecules.^{44, 92}

1.2.1. Langmuir technique

The Langmuir technique enables the formation of a monolayer of amphiphilic molecules over a liquid surface.^{93, 94} A typical instrumental setup of this method consists of the Langmuir trough made from hydrophobic polytetrafluoroethylene (PTFE) holding the aqueous liquid (subphase), over which the solution of amphiphile is spread using a microsyringe. Subsequent evaporation of solvent and compression of amphiphiles leads to the formation of a monolayer (Figure 6a). By software-controlled operation of the movable barriers, compression and expansion of the film can be achieved. The barriers are made up of polyoxymethylene, a hydrophilic material, or PTFE, and are heavy enough to prevent any leakage of the monolayer beneath the barrier. The trough is thermostated by circulating water in channels placed underneath the PTFE trough.^{93, 95}

The surface tension of a liquid changes in the presence of a monolayer of amphiphilic molecules. Surface tension arises due to the energetic costs of creating an interface. The molecules within the bulk of a liquid exert and experience forces in all directions. Whereas, molecules on the surface of a liquid experience an imbalance of forces. This creates excess energy in comparison to the bulk, denoted as surface free energy leading to the occurrence of surface tension with the unit of $\text{N}\cdot\text{m}^{-1}$. The variable measured by the Langmuir technique is surface pressure π and is given by the relationship, $\pi = \gamma_0 - \gamma$, where γ_0 is the surface tension in absence of a monolayer and γ is the surface tension with the film present.⁹⁶ In a Langmuir trough, π is usually measured by the Wilhelmy plate method. In this method, the force pulling on a partially immersed and suspended plate in the liquid subphase is measured. This force is then converted into surface tension with the help of a simple two-point calibration.⁹³ The thin Wilhelmy plate is usually made from platinum, but plates made of glass, quartz, mica, and paper are also used. While the platinum plate can be reused by cleaning with a blow torch or Piranha solution, paper plates are discarded after each use and require a long stabilization time (~ 1 h).⁹⁵

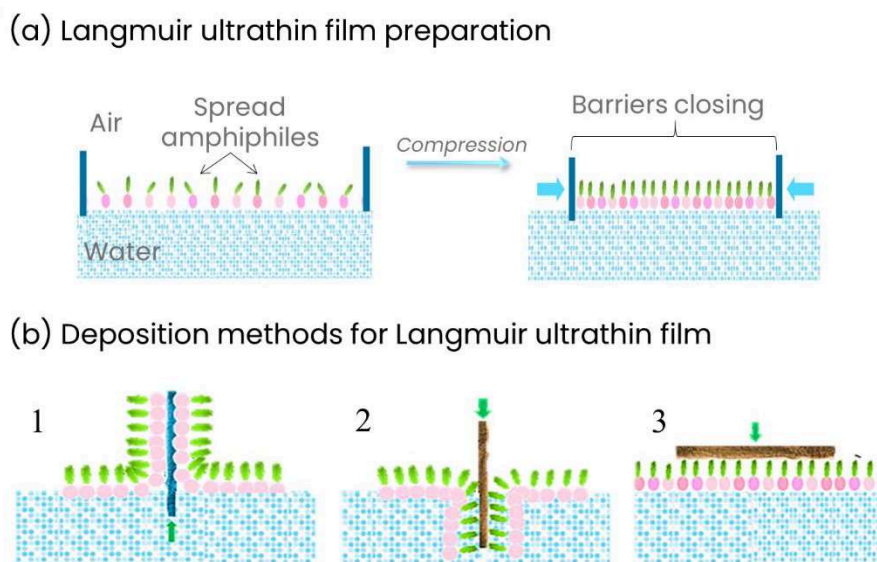


Figure 6: (a) Schematic representation of the Langmuir technique for monolayer preparation of an ideal amphiphile (pink: polar part; green; non-polar part). (b) Deposition scheme of Langmuir ultrathin film on a solid substrate by (b: 1-2) Langmuir-Blodgett method and (b: 3) Langmuir-Schaefer method (hydrophilic substrate = blue; hydrophobic substrate = brown)

The MMA of the film is continuously determined by an in-built software system by monitoring the distance between the barriers and correlating it with the number of spread molecules on the liquid surface. The number of spread molecules is deduced using the formula, $N = N_A (C \cdot V / M)$, where N_A is Avogadro Constant [$6.02214076 \cdot 10^{23} \text{ mol}^{-1}$], C is concentration [$\text{mol} \cdot \text{L}^{-1}$], V is volume [L] and M is molecular mass [$\text{g} \cdot \text{mol}^{-1}$].⁴⁷ The number of spread molecules, N when divided by the area between the barriers, yields the MMA. For insoluble molecules, the MMA can be determined with remarkable precision given that the only relevant errors in its determination are concentration and volume measurement uncertainties, both of which can be kept below 1%.

Transfer of a monolayer as a coating is carried out through horizontal or vertical dipping/pulling of the solid substrate (Figure 6b). Langmuir films, after deposition to the solid substrate, are henceforth called Langmuir-Blodgett (LB) films or Langmuir-Schaefer (LS) films (named after the scientists who invented the corresponding methods of film deposition). In the LB method, the solid substrate is dipped up and down through the film while simultaneously keeping the π constant by a computer-controlled feedback system (Figure 6b: 1-2). In the LS method, the solid substrate is horizontally lowered to get in contact with the film, followed by the transfer of film via adsorption (Figure 6b: 3).⁹⁵ With subsequent cycles, multilayers can be deposited using each method. With each transfer, the number of transferred molecules are theoretically identifiable.^{93, 97}

To visualize the film morphology, Brewster angle microscopy (BAM) is an established technique for the air-water interface.⁷⁵ The principle of this optical technique is depicted in Figure 7. At a particular angle of incidence (Brewster's Angle⁹⁸), $\theta_B = \tan^{-1} \frac{n_{\text{water}}}{n_{\text{air}}}$, light with a polarization parallel to the plane of incidence is perfectly transmitted through the water and no reflection is produced at the detector. The wavelength dependence of the refractive index of water determines the wavelength dependence of the Brewster angle. The best contrast is obtained using lasers as a single-wavelength light source, with the Brewster angle for $\lambda = 658 \text{ nm}$ being 53.1° .

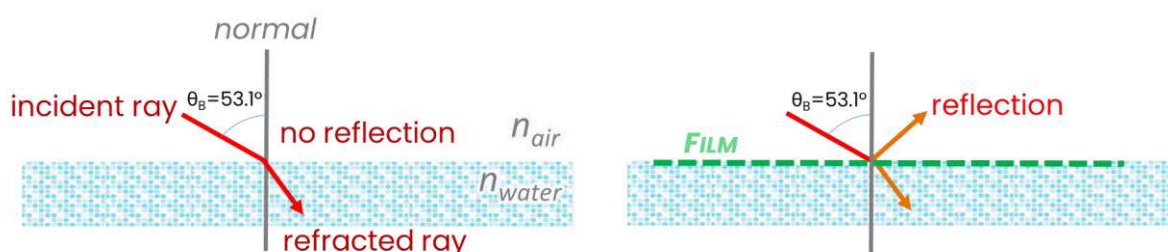


Figure 7: Principle of Brewster angle microscopy for visualizing films at the air-water interface. After the spreading of molecules and formation of the Langmuir film, the refractive index at the air-water interface changes. Subsequently, the polarization of the reflected ray gets differed, and a certain fraction of the light is reflected. The output is in the form of a video/image with a black and white contrast between the water phase and the matter (aggregates or crystals in films) at the air-water interface.⁷⁵

Polarization modulation-infrared reflection-adsorption spectroscopy (PM-IRRAS) is used for determining vibrational bands of film at the air-liquid surface (Figure 8). An infrared (IR) laser is reflected off the air-water interface at a grazing angle. The incoming beam's polarization is modulated at a high frequency between s- and p-polarization, and a normalized differential intensity is calculated using $I_{\text{PM}} = \frac{I_p - I_s}{I_p + I_s} = \frac{\Delta}{\Sigma}$, where I_s is 0 for a conducting surface, and the absorption band is formed exclusively by the component of the dipole moment that is parallel to the plane of incidence. Water, which is a dielectric, is excluded from this simple selection criteria. Instead, the optimum signal-to-noise ratio was computed for an organic monolayer at the air-water interface at an angle of incidence of $\approx 72^\circ$.^{99, 100}

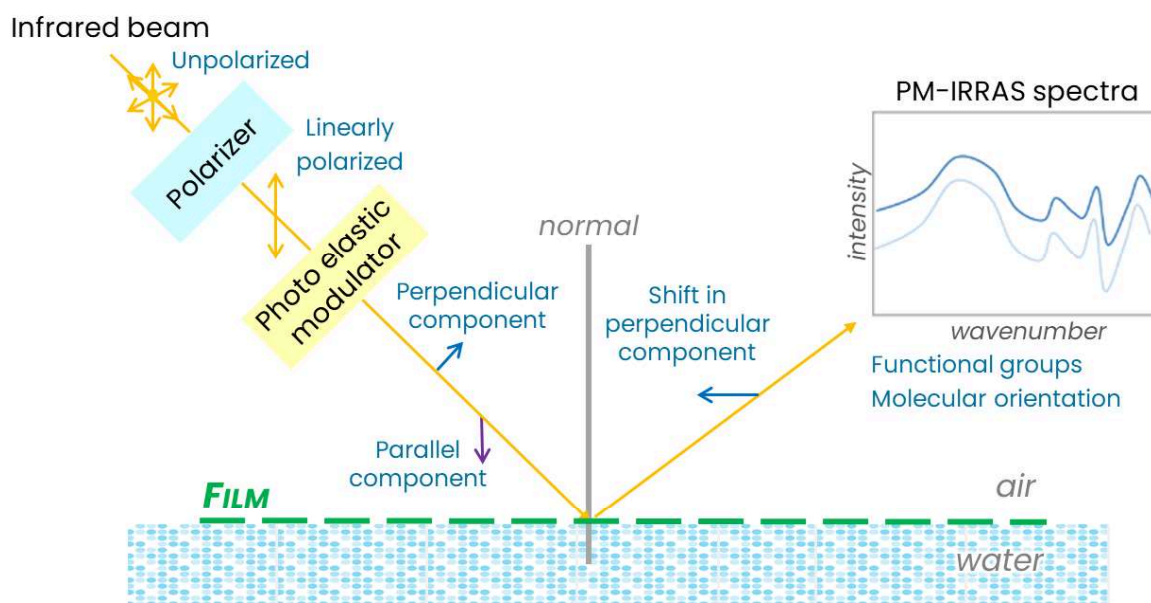


Figure 8: Principle of polarization modulation-infrared reflection-adsorption spectroscopy at the air-water interface

Dipole moments parallel to the air-water interface produce a negative Δ , whereas dipole moments perpendicular to the air-water contact produce a positive Δ . If the signal intensities for both orientations were identical, complete cancellation would be observed for dipoles oriented at 45° to the air-water contact. Hence, for randomly oriented dipoles like water or CO_2 , I_{PM} would be zero. However, because the parallel component's signal intensity was larger than the perpendicular component's signal intensity, the 'vanishing' angle is moved to a higher angle of 39° with regard to the surface normal. As a result, the water absorption band in PM-IRRAS observations at the air-water interface was decreased but not eliminated. Furthermore, the photoelastic modulator's transmittance, like water's reflectance, is strongly wavelength-dependent. In comparison to these effects, the intensity modulation generated by the organic layer's vibrational absorption bands was negligible. To eliminate these contributions, the layer's signal was compared to the bare subphase: $S = \frac{I_{\text{sample}}}{I_{\text{bare}}} - 1$. The optical response of the subphase varies due to water evaporation and variations in humidity, and the normalizing of spectra recorded long after the measurement of the bare subphase is compromised. A water level adjustment device is therefore installed to mitigate this effect.¹⁰⁰

1.2.2. Langmuir films of polymers: crystallization, degradation, and chemical reactions

Confined crystallization in Langmuir ultrathin films at the air-water interface have different regimes. Chains at the polymer-water interface have higher degrees of flexibility than the ones

at the polymer-solid interface. At low π , the regime is comparable to that of a dilute solution, while with increasing compression, the regime shifts to that of a concentrated solution that crystallizes due to the lateral strain by the barriers. The quasi-2D confinement produces more regular crystals than the crystallization from melts. Importantly, in Langmuir film crystallization, the layers have a negligible shear modulus, meaning the effects of chain entanglements on crystallization can be excluded, allowing to study crystallization without transport restriction. This may explain why the crystal habits from star shape PCL-tetrol molecules are found comparable to the ones from linear OCL diols in the Langmuir films.¹⁰¹ In that context, crystallization from Langmuir films resembles crystallization from dilute solution.⁴⁴ However, an impact of molar mass on crystallization in Langmuir films is observable, where, a maximum growth rate at an intermediate M_n of 8000 g·mol⁻¹ is observed for linear hydroxy end-capped PCLs.¹⁰²

The Langmuir technique also allows studying the degradation of ultrathin films at the air-liquid interface under controlled parameters. For instance, the effect of enzyme activity, oligomer molecular architecture, and crystallinity on degradation is investigated to a certain extent in Langmuir ultrathin films. In this regard, work has proved to give unique molecular-level insights into the influence of diverse enzymes and catalytic species on the degradation of polymeric biomaterials. Langmuir film degradation curves (film area change versus time at constant π) allow the estimation of the mass loss and also the chain scission mechanism. The absolute area change $\Delta A_t(t)$ in the film occurs due to the formation of water-soluble scission fragments and is given by $\Delta A_t(t) = A_0 - A(t)$, where A_0 is the initial film area and $A(t)$ is the film area after a degradation time interval t . The relevant variable is the normalized area reduction, which is stated as $\Delta A_{rel}(t) = \frac{A_0 - A(t)}{A_0} = 1 - \frac{A(t)}{A_0}$. Overall, the information extracted from a degradation curve depends on the selection of the model and its complexity.^{44, 103}

Polymerization of Langmuir films is a complex process and is generally aimed to stabilize 2D morphologies. Overall, generally applied monomers for carrying out polymerization reactions by the Langmuir technique were small amphiphiles. For instance, by 2D cross-linking of photo reactive methacrylate groups, phase separating behavior in lipids and stabilization of the binary system is realized.¹⁰⁴ π and MMA play an important role in the 2D polymerization, as demonstrated for aniline based surfactants (small amphiphiles) reaction in presence of a strong oxidizing agent in the subphase.¹⁰⁵ Ionic charge and adsorption phenomenon also offers the opportunity for 2D polymerization of ultrathin films. For instance, the monomer styrene sulfonate dissolved in the subphase is adsorbed to a positively charged monolayer, where a

spontaneous 2D anionic polymerization occurs.^{106, 107} Ionic interactions are also used for harmonizing phase kinetics and morphology of ultrathin films at the air-liquid interface, where the carboxylic head group of polydiacetylene is interacted with different divalent metal cations.¹⁰⁸ Such studies elaborate the strategies for measuring polymerization kinetics utilizing the changes in film behavior (area, π , or morphology), relative surface viscosity, or spectroscopic techniques.

For polymers/oligomers, presumably due to difficulty in the assembly of flexible chain ends, only a few studies describe their 2D cross-linking by the Langmuir technique.^{104, 105, 108-119} For example, a stable semi-interpenetrating 2D oligomeric network is achieved by embedding cross-linked methacryloxypropyl-terminated polydimethylsiloxane in cellulose acetate butyrate matrix.¹⁰⁹ In another study, self-condensable silanes are utilized for 2D cross-linking where real-time rheological measurements are used to estimate the surface viscosity dynamics. By virtue of silane-based pendant groups, cross-linked polybutadiene networks at the air-water interface, containing PEO pores of controlled size are also accomplished.^{111, 112} Overall, the reaction method, monomers' chemical groups' placement, quantity, electronegativity, and behavior in an aerial or aquatic environment are critical controlling variables for the polymerization of oligomers/polymers in Langmuir films.

2. Motivation and Aims

Predicting physical and chemical phenomena in the presence of water is crucial for clinically applied (bio)degradable synthetic materials such as ϵ -caprolactone-based polymers. OCL telechelics are often used as starting materials for active or stimuli-sensitive polymers because it is possible to use OCL crystals as thermal switches around physiological temperatures. Controlled OCL crystallization and degradation offers to improve the stability and a predictable bio response for different biomaterials, for example, hydrogel networks for 3D printing¹²⁰, scaffolds for tissue engineering¹²¹, or nanoparticles for drug delivery systems¹²². Such thermally active devices must meet strict safety, reliability, and temperature control criteria. However, aqueous environment and temperature fluctuations are often unavoidable during the processing, handling, or ultimate function of the system. Especially for nanostructured devices, even minutes of environmental changes can cause dynamic physiochemical changes that can alter its bioresponse. The lifetime of OCL at physiological temperatures and pH is in the range of years, so predicting the behavior of these materials with time needs to systematically address a range of phenomena.

Ultrathin films can be designed to model the inner and outer surfaces of structured polymer devices in order to investigate and control the influencing parameters (Figure 9). The modulation of chain assembly of oligomers/polymers plays a dominant role in structuring ultrathin films/coatings, yet is largely affected by the underlying solid surface. As a prerequisite for preparing uniform semi-crystalline coatings, most conventional techniques, such as spin coating, solvent evaporation, and melt cooling, require that the substrate be ideally smooth, have unvarying wettability, and be compatible with an organic solvent for pretreatment or crystallization. These interfacial properties are hardly evident in implants or medical devices, which can have cracks, crevices, and dynamic wettability as a result of the different material compositions of various device parts. Any additional thermal treatments required for the formation of a polymeric coating on implants may also impair their ability to function. The organic solvents used for processing are then either incompatible with the implant surface or do not entirely evaporate. Chemical reactions in confinement are further challenged by the need for an aqueous environment with ambient conditions.

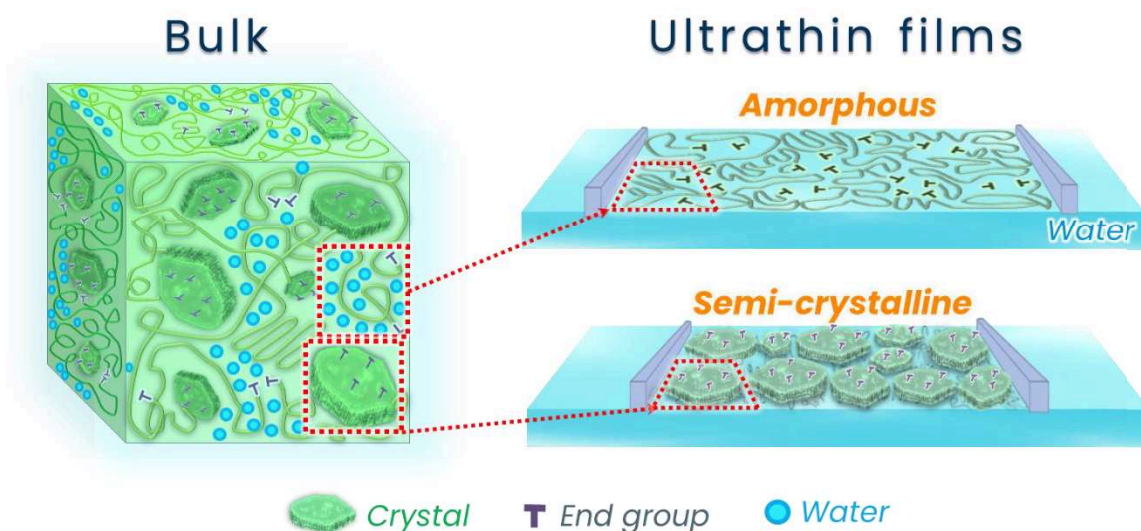


Figure 9: Ultrathin oligomeric films (amorphous or semi-crystalline) as model representations for complex bulk interfaces

The Langmuir technique employs an air-water interface for systematically designing ultrathin films, circumventing any unwanted defects that are usually present at the air-solid interface. The process parameter of lateral pressure from barriers compression allows the possibility to control chain assembly and interactions with the reactive groups. This becomes relevant for PCL-based materials, where cell adhesion or targeted drug delivery needs to be improved by a chemical modification of the film.¹²¹ The liquid subphase acts as a medium for degrading enzymes/ions or reagents. The coupled optical microscopy and spectroscopy techniques allow to simultaneously measure different processes ongoing within the film. This feature enables to the creation of improved nanostructured systems such as bioactive coatings that rely on chemical reactions, degradation, or stimuli response to function⁴⁸. Under controlled parameters, the nanostructured Langmuir film from the air-water interface can be transferred systematically as a coating on various surfaces.

Overall, the aim of this research is to elucidate molecular mechanisms of how the aqueous environment influences the interplay of crystallization, melting transitions, degradation, and the reaction of end-groups in ultrathin films. For this purpose, the underlying substrate is varied as the water or a solid surface, to incur the effect on chain mobility during melting transitions and degradation. The melting of functionalized OCL single crystals is pursued to change the expression of functional moieties on the surface of a material to create thermoswitchable coatings for advanced applications. Chemical reactions are aimed at ambient room temperature or physiologically applicable conditions in an aqueous environment to create structured materials or to trigger a defined response.

3. Hypotheses and Concept

This work is based on the hypothesis that the physical and chemical processes determining the dynamic behavior of OCL in aqueous environments (crystallization, degradation, and reaction of end-groups) can be systematically investigated in Langmuir ultrathin films. This allows to predict and design the behavior of OCL based materials at biointerfaces, as well as in high-water-content systems such as implants, hydrogels, and scaffolds. By varying chemical attributes like end-groups or arm number and system parameters like packing density, temperature, or pH, the semi-crystalline morphology and its influence on degradation and chemical reactions can be studied. Additionally, it is hypothesized that the air-water interface gives a more realistic representation than ultrathin films adsorbed to solid substrates, where dynamic phenomena are obstructed by the reduced molecular mobility. This effect can be identified by comparing the behavior of oligomer films on the air-water interface and after transfer to solid substrates.

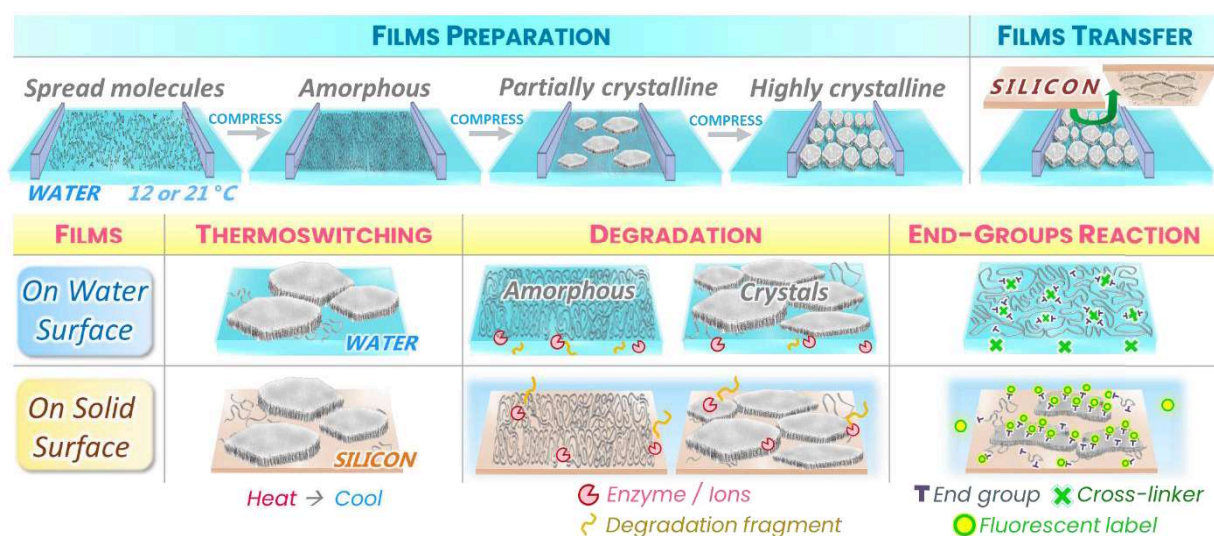


Figure 10: Schematic illustration of Langmuir ultrathin films: Preparation, transfer, and investigation at different interfaces for thermoswitching, degradation, and reaction of end-groups

The OCL telechelics selected for this study are within the molecular weight range of 5000 to 8000 $\text{g}\cdot\text{mol}^{-1}$, where these macromolecules are known to form large microscopically observable crystals.¹⁰² This allows for straightforward characterization of crystallization, melting behavior, and surface functionalization progress. The end-group effect on the chain packing for crystallization or cross-linking is also accentuated due to the low molecular weights of oligomers. The concept of this study aims to demonstrate the effect of the aqueous environment on the interplay between crystallization, degradation, and the reaction of end-groups of OCL at different interfaces.

1. π induced crystallization of oligomers at the air-water interface is a dynamic material process dependent on the nuclei, molar mass but importantly on the chain mobility. The semi-crystalline morphology in the ultrathin film is varied by the crystallization of films by the function of MMA and temperature. Chain mobility during melting transitions is affected by the variation of substrates (water or silicon). By comparison between air-water, air-solid and bulk behavior, the effect of water and confinement on OCL thermal transitions become apparent.
2. Ultrathin film of different semi-crystalline morphologies at the air-water interface represent interfaces from bulk materials of different crystallinity interacting with the degradation medium. Hence, interaction with enzymes/ions and degradation kinetics can be explored for the fundamental understanding of bulk polymer network degradation as a function of crystallinity in ultrathin films. Distinguishing the degradation kinetics in crystalline regions and amorphous regions can be achieved by preparing and degrading amorphous and semi-crystalline films at the air-water interface. Further, ultrathin films of different semi-crystalline morphologies are explored as thermoswitchable coatings by transfer and degradation at solid surfaces. The influence of thermoswitching (melting and recrystallization of semi-crystalline films) on degradation is investigated for ultrathin films at both water and silicon surface.
3. The reaction of end-groups at the air-water or air-solid interface is investigated by different reaction chemistries. At the air-water interface, acetal cross-links are formed by reacting hydroxy end-groups of amorphous OCL films with glyoxal as dialdehyde. Chemical cross-links resulting in the development of a 2D OCL network formation should alter film crystallization or degradation, which could prove the joining of flexible reactive end-groups of oligomers in the monolayer on the water surface. Acetal links are also dynamic pH reversible bonds, a phenomenon that is useful to prove cross-linking at the air-water interface. The accumulation of end-groups on crystal surfaces offers to form a densely functionalized surface on the former, which disperses upon melting. This effect is demonstrated using the methacrylate end-groups present on transferred single crystals on the silicon surface, which enables photochemical reaction with fluorescein dimethacrylate. Fluorescence intensity changes during crystal melting are used to gain insights into chain ends distributions during the melting/recrystallization process.

4. Organization of the thesis

This cumulative dissertation focuses to understand the impact of an aqueous environment on the interplay of crystallization, melting transitions, degradation, and end-group reaction in ultrathin films. Where, Langmuir technique is applied to systematically adjust the molecular assembly for influencing the physical and chemical processes. The content of the incorporated chapters is outlined below:

Chapter 1 titled ‘Introduction’ provides a summary of the research background as well as key advancements in the field of research related to the thesis.

Chapter 2 titled ‘Motivation and aims’ outlines the motivation for initiating the project, and is followed by the aims of this thesis.

Chapter 3 titled ‘Hypotheses and concept’ describes the formulated hypotheses and the concept employed to achieve the aims of this thesis. The concept describes ultrathin films preparation, transfer, and investigation at different interfaces for thermoswitching, degradation, and the reaction of end-groups.

Chapter 4 titled ‘Organization of the thesis’ presents the organizational framework of this thesis.

Chapter 5 titled ‘Publications’ provides a summary and contribution of the four publications (5.1-5.4) - Appendix I-IV in fulfilling the concept. The concept of OCL ultrathin film crystallization, transfer on the silicon substrate, and melting transitions is realized and described in Chapter 5.1 (Appendix I). The effect of crystallinity, end-groups, and temperature on the hydrolytic degradation and enzymatically catalyzed degradation of films is systematically investigated in Chapter 5.2 (Appendix II) and Chapter 5.3 (Appendix III), respectively. The reaction of end-groups on crystals surface is demonstrated in Chapter 5.3 (Appendix III), whereas the reaction of OCL end-groups in amorphous films to form reversible 2D networks is achieved in Chapter 5.4 (Appendix IV).

Chapter 6 titled ‘Discussion’ is an overall discussion of the findings of this work.

Chapter 7 titled ‘Summary and Outlook’ summarizes the findings and prospective implications of this research.

5. Publications

5.1. Effect of water on crystallization and melting of telechelic oligo(ϵ -caprolactone)s in ultrathin films

Linear OCL telechelics differing in functional end groups were crystallized in ultrathin films at the air-water interface. Crystallization parameters varied using the Langmuir technique were the MMA for isochoric crystallization and the water temperature. The melting and recrystallization were investigated on the water surface and in transferred films on silicon. The key findings were:

- OCL functional end-groups and T_c affect π -MMA isotherms, crystal habits, and melting/recrystallization temperatures
- In accordance with the Gibbs-Thomson equation, the OCL crystal melting temperatures are proportional to inverse crystal thickness, which is also proportional to the film MMA prior to crystallization. Therefore, the crystal thickness correlates with the film thickness prior to crystallization
- Crystallization and melting in ultrathin films at the air-water interface follows similar laws as in bulk, albeit with generally lower transition temperatures
- OCL ultrathin films at the water surface melt at lower temperatures than the transferred films on the solid substrates in absence of water

5.1.1. Contribution to the Publication

Literature study:

- Different thin film crystallization methods of PCL: their advantages and limitations
- Factors influencing PCL crystallization and melting/recrystallization
- OCL end-groups, molecular weight, crystallization temperature, and substrate properties

Study design with discussion and advice from co-authors:

- Selection of ultrathin film crystallization method and molecular parameters suitable for OCL single crystal growth
- Identification of parameter range (MMA, temperature) to construct Gibbs-Thomson plots

- Establishing a methodology combining AFM of transferred films and optical microscopy together with a suitable temperature profile for reproducible (re)crystallization experiments

Experimental work:

- Crystallization of OCL diol (OCDOL) or OCL dimethacrylate (OCDME) under different conditions using the Langmuir technique
- LS transfers of films crystallized at different conditions onto silicon substrates
- Heating and subsequent cooling of OCL films present at the air-water (BAM and temperature-controlled Langmuir trough) or air-solid interface (POM with temperature-controlled stage) to identify the T_m and T_{rec}

Contribution to analysis and interpretation of experimental data:

- Real-time optical microscopy to determine T_m and T_{rec} of OCL films present at the air-water or air-solid interface
- Calculation of crystals thickness based on height images from AFM using the image processing software WsXM
- Processing and graphical representation of data to identify the hypothesized linear dependencies between thermal transitions, crystal thickness, and MMA

Manuscript:

- Providing initial draft of the manuscript according to comments from co-authors
- Revision and finalization of the manuscript according to comments from co-authors

5.1.2. Publication I (Appendix I)

Shivam Saretia, Rainhard Machatschek, Thanga Bhuvanesh and Andreas Lendlein, **Effect of Water on Crystallization and Melting of Telechelic Oligo(ϵ -caprolactone)s in Ultrathin Films**, *Advanced Materials Interfaces*, 8, 2001940, 2021, DOI: 10.1002/admi.202001940

5.2. Degradation kinetics of oligo(ϵ -caprolactone) ultrathin films: influence of crystallinity

Semi-crystalline and amorphous ultrathin films of linear OCLs differing in end-groups were prepared at the air-water interface at room temperature using the Langmuir technique. Both films at the air-water interface and films transferred to silicon surfaces were hydrolytically degraded at pH 1.2. The effect of melting crystals to accelerate the degradation rate was investigated. The key findings were:

- Hydrolytic degradation rates of ultrathin films of OCL are as follows: amorphous > partially crystalline > highly crystalline
- OCL crystallites have ca 2-3x lower hydrolytic degradation rates than the amorphous part. This finding can be used to predict the influence of crystallinity on degradation in bulk
- The hydrolytic degradation is accelerated in all semi-crystalline films by the melting of crystals
- Transferred highly crystalline films only partially degrade after 72 h, while the transferred amorphous films degrade within 48 h
- Compared to enzymatically accelerated degradation of highly crystalline films by *Pseudomonas cepacia* lipase, which completes within few minutes, hydrolytic degradation of highly crystalline films at pH 1.2 takes several hours at 37 °C

5.2.1. Contribution to the Publication

Literature study:

- Aspects of PCL hydrolytic degradation and the influencing factors
- Effect of crystallinity on bulk PCL hydrolytic degradation in vitro and in vivo

Study design with discussion and advice from co-authors:

- Selection of OCL telechelics and identification of crystallization conditions at the air-water interface for film preparation
- Conditions for LS transfer of films to silicon and subsequent degradation conditions
- Design of experimental procedure allowing for a highly crystalline film with zero crystal growth rate

Experimental work:

- Determining the onset of acid-catalysis for OCL degradation as initial experimental design
- Preparation of highly crystalline films
- Films degradation investigated at the water surface by the Langmuir monolayer degradation (LMD) technique and on silicon using POM

Contribution to analysis and interpretation of experimental data:

- Processing and graphical representation of experimental data to construct degradation curves
- Evaluation of hydrolytic degradation curves of OCL films in dependence to crystallinity and temperature
- Evaluation of morphological changes during hydrolytic degradation of LS transferred OCL films using POM

Manuscript:

- Providing initial draft of the manuscript according to the outline discussed with co-authors
- Revision and finalization of the manuscript according to comments from co-authors

5.2.2. Publication II (Appendix II)

Shivam Saretia, Rainhard Machatschek, and Andreas Lendlein, **Degradation kinetics of oligo(ϵ -caprolactone) ultrathin films: influence of crystallinity**, MRS Advances, 2021, DOI: 10.1557/s43580-021-00067-4

5.3. Highly crystalline PCL ultrathin films as thermally switchable biomaterial coatings

Highly crystalline ultrathin films of linear OCL differing in end-groups were prepared and their melting transitions were studied at the air-water interface using the Langmuir technique. The highly crystalline films were degraded under enzymatic catalysis at physiologically applicable temperatures both at the air-water interface and after transfer to solid surfaces. The high density of methacrylate end-groups at the crystal surfaces were post-functionalized using fluorescein dimethacrylate as a chemically linked label and the change in fluorescence intensity during thermoswitching of the film was investigated. The key findings were:

- Extreme compression of OCL molecules at the air-water interface yields highly crystalline films
- Morphology and melting temperatures of highly crystalline films can be varied by OCL functional end-groups and water temperature
- Highly crystalline films are transferrable to silicon surfaces, with minor crystal fractures, by the LS method
- Highly crystalline OCDOL films degrade slower by ~3x under enzymatic catalysis than the amorphous films on both water and solid surface
- Highly crystalline films of ODCME functionalized with fluorescein dimethacrylate showed a pronounced change in fluorescence intensity during thermoswitching of the film, hence assembly of functional molecules at the surfaces of highly crystalline films can be switched with temperature

5.3.1. Contribution to the Publication

Literature study:

- Biomaterial coatings using thermal transitions for switching of functions or properties
- Large scale synthesis methods for polymer single crystals: advantages and limitations
- Enzymatically catalyzed degradation of PCL and the influence of crystallinity

Study design with discussion and advice from co-authors:

- Selection of OCLs, the enzyme for degradation and substrate for film transfer
- Approach for highly crystalline films preparation, characterization, and transfer
- Enzymatic degradation conditions of films at different interfaces

- Functionalization of end-groups at OCL crystals surface by chemically linked fluorescein compound

Experimental work:

- Extreme compression of OCL molecules with hydroxy or methacrylate end-groups to MMA $\sim 2 \text{ \AA}^2$ on the water surface at 12 or 21 °C
- Film characterization for morphology and melting transitions by BAM and for LS transferred films by POM
- Enzymatic degradation of different films using *Pseudomonas cepacia* lipase enzyme
- Photoreaction of fluorescein dimethacrylate with methacrylate end-groups at the OCDME crystal surfaces
- Fluorescence microscopy during thermoswitching of fluorescein functionalized, highly crystalline OCDME films

Contribution to analysis and interpretation of experimental data:

- Determination of OCL crystals morphology and packing at MMA $\sim 2 \text{ \AA}^2$ on the water at 12 or 21 °C using BAM
- Processing of experimental degradation data and graphical representation as degradation curves of OCL films in dependence on crystallinity, end-groups, and temperature
- Evaluation and processing of AFM height images LS transferred OCL films which were subjected to different durations of enzymatically catalyzed degradation

Manuscript:

- Providing initial draft of the manuscript according to the outline discussed with co-authors
- Revision and finalization of the manuscript according to comments from co-authors

5.3.2. Publication III (Appendix III)

Shivam Saretia, Rainhard Machatschek, and Andreas Lendlein, **Highly crystalline PCL ultrathin films as thermally switchable biomaterial coatings**, MRS Advances, 6, 283–290, 2021, DOI: 10.1557/s43580-021-00020-5

5.4. Reversible 2D networks of oligo(ϵ -caprolactone) at the air-water interface

Using glyoxal as a water-soluble dialdehyde, OCL telechelics with hydroxy end-groups were cross-linked at different π 's at the air-water interface at room temperature. At different reaction times, the acetalization reaction progression in OCL films was identified by the interfacial IR. To investigate indirect proofs of cross-linking, different cross-linked networks were compared with non-cross-linked films for their change in film area, crystallization, and enzymatic degradation. The key findings were:

- The interfacial acetalization reaction process was revealed by OCL films contraction at the air-water interface, which was higher when OCL 2D networks were formed at elevated π values (higher hydroxy end-groups concentration in the film) or with longer reaction time
- Due to film contraction by acetalization reaction, compression isotherms of OCL 2D networks shifts to lower MMA values at the air-water interface. Where, the MMA corresponding to the highest value static elasticity modulus decreases from $\sim 35 \text{ \AA}^2$ for the non-cross-linked film to $\sim 15 \text{ \AA}^2$ for the OCL 2D network formed after 18 h reaction time at 7 mN m^{-1}
- Branching centers formed via acetalization in the OCL 2D network retard crystallization and enzymatic degradation of OCL chains
- By changing water pH to 2.5, acetal cross-links in OCL 2D networks are reversible at the air-water interface

5.4.1. Contribution to the Publication

Literature study:

- Reversibly cross-linked polymer networks
- Cross-linked ultrathin films of oligomers at the air-water interface
- Cross-linking effect on crystallization and degradation

Study design with discussion and advice from co-authors:

- OCLs selection and optimal cross-linking conditions at the air-water interface
- Characterization approaches to understand cross-links formation
- Conditions for reversal of cross-linking reaction

Experimental work:

- OCL diol and four arm OCL tetrol cross-linking by glyoxal at different π 's
- Characterization by BAM for morphology, isotherms for films contraction, and PM-IRRAS for chemical characterization
- Effect of cross-linking on OCL film crystallization and enzymatic degradation by *Pseudomonas cepacia* lipase
- Reversion of acetal cross-links by decreasing the pH

Contribution to analysis and interpretation of experimental data:

- Determination of morphological changes in OCL film during cross-linking reaction using BAM
- Data processing and graphical representation as degradation/stability curves
- Evaluating compressibility modulus from π -MMA isotherms of OCL films cross-linked at different constant π s or reaction time

Manuscript:

- Providing initial draft of the manuscript according to the outline discussed with co-authors
- Revision and finalization of the manuscript according to comments from co-authors

5.4.2. Publication IV (Appendix IV)

Shivam Saretia, Rainhard Machatschek, Burkhard Schulz and Andreas Lendlein, **Reversible 2D networks of oligo(ϵ -caprolactone) at the air-water interface**, Biomedical Materials, 14(3), 034103, 2019, DOI: 10.1088/1748-605X/ab0cef

6. Discussion

Semi-crystalline polymers/oligomers through their controlled crystallization, degradation, and chemical functionalization can endow ultrathin films with unique properties and broaden their application in health and materials research. Here, approaches to prepare polymer ultrathin films and enable crystallization under defined conditions are discussed along with the findings in this thesis (Chapter 5.1). Thereafter, hydrolytic (Chapter 5.2) and enzymatically (Chapter 5.3) catalyzed degradation of semi-crystalline oligomers is described, along with the aspects of oligomer degradation that were controlled using the Langmuir in this work. To further highlight the control of molecular assembly by the Langmuir technique, the results of the reaction of OCL end-groups in ultrathin films are discussed and compared to similar studies (Chapter 5.4).

6.1. Nanostructured ultrathin films by crystallization under defined conditions

Adjusting crystalline morphology in ultrathin films is of interest for preparing coatings with pre-defined behavior and for the fundamental understanding of bulk interfaces. Crystallinity also plays an important role for thermal switching of a wide range of coatings acting as thermal regulators⁴², stiffness control⁴³, and shape change¹²³. Yet, controlling semi-crystalline morphology in coatings is challenged by the solid surface dynamics and use of organic solvents. The presence of an aqueous environment is also frequently inevitable during processing or system operation, which has been overlooked in the literature.

The work presented in this thesis overcomes crystallization challenges at solid surfaces by using the water surface for crystallizing the oligomers by the Langmuir technique. The findings in Chapter 5.1-5.3 explicitly demonstrate the effect of water on crystallization, and on melting transitions of the films crystallized independent of the solid substrate. Polymeric films prepared on the water surface are also environmentally, health, and safety friendly because they use a small amount of oligomers/solvents (a few micrograms). The organic solvent is only used to dissolve the polymer, which is then evaporated before crystallization. Fundamental insights of polymer crystallization were gained using Brewster angle microscopy, which identified the oligomer single crystals formation and melting transitions on the water surface. The thickness, amount, and morphology of single crystals in ultrathin films were easily varied by changing process parameters (π , temperature...) while taking into account oligomer structural features (end-groups, molecular weight...). A major challenge for large-scale synthesis of polymer single crystals is addressed in Chapter 5.3, where the high density of single crystals in the film was achieved by compression of the film. By means of changing MMA and temperature, a

dense and compact highly crystalline polymeric film, thermally switchable at physiologically applicable conditions is prepared. For their applicability as degradable coatings, hydrolytic and enzymatically catalyzed degradation of highly crystalline films is investigated at different temperatures in Chapter 5.2-5.3. Unlike other conventional techniques, there is no material waste because all polymers crystallized on the water surface are practically transferrable to the solid surface. Films were transferred to the solid surface via the water surface using the scalable Langmuir-Schaefer method that retains the semi-crystalline morphology of films with high structural fidelity.

Aside from the preparation technique, several other factors, such as film thickness, T_c , chain mobility, and polymer-substrate interactions influence crystallization in a confined space. Film thickness in particular exhibits a dramatic effect on polymer crystallization. For example, as layer thickness decreases, so does the overall crystallization rate in PEO ($T_g = -78\text{ }^\circ\text{C}$) in films with thicknesses ranging from 100 nm to 40 nm.¹²⁴ This is also true for Langmuir films of OCL, where films with a greater initial thickness (lower MMA) produced larger and thicker single crystals, indicative of a faster crystallization process (Chapter 5.1; Appendix I: Figure 4). This finding is also interesting in the context of chain entanglements, which do not seem to have a decisive effect on crystallization from thin films. Otherwise, monolayers, where chains cannot overlap or entangle, would show faster crystallization than slightly thicker films. In line with the substrate effect on chain mobility is the finding that PHB ($T_g = 5\text{ }^\circ\text{C}$) appears to be entirely amorphous after 6 months in films of thicknesses up to 27 nm on a glass surface, despite the fact that it can crystallize to a high degree with large spherulites in bulk.¹²⁵ This is due to an extreme increase of the T_g at the polymer-solid interface. Where, a $30\text{ }^\circ\text{C}$ increase in T_g for PEO, brings it to around $-40\text{ }^\circ\text{C}$, which is still well below room temperature.¹²⁶ However, a similar change in T_g for PHB immobilizes the polymer chain on the solid glass surface at room temperature.^{125, 127} In Langmuir films, the chain restriction observed at the polymer-solid interface does not occur. Therefore, while PHB ultrathin films crystallization on solid surfaces is inhibited for months, Tarazona et al demonstrated that crystallization of PHB in Langmuir films on the water surface can occur within minutes.¹²⁸ Hobbs et al also showed that in PHB 1-20 μm thick films, the presence of water is thought to be acting as a weak plasticizer. Where, water influenced the T_g and led to the change in activation energy for transport of chain segments to the growth front.¹²⁹ Kikkawa et al supported these findings using friction force measurements and AFM observations on the surface of 300 nm PLA films. Where, the molecular motion on the surface of the films enhanced due to the presence of water molecules.¹³⁰

The immobilization of chains on solid surfaces is also very well demonstrated by the fact that recrystallization of molten films on solid substrates was impeded, whereas it was observed at a high temperature at the air-water interface (Chapter 5.1; Appendix I: Figure 3). Parameters that were investigated previously and discussed in Chapter 1.2.2 are the effect of molecular weight¹⁰² and architecture (linear or star shape)¹⁰¹ on the crystallization process of medically relevant polymers. In this thesis, the parameters of temperature, MMA, and chain end functionalization were further investigated. It was unequivocally demonstrated that the effect of the MMA is to determine the initial film thickness, with the aforementioned consequences. In that context, an additional effect of crystallization π seems unlikely. The effect of T_c in monolayers and thin films is similar to bulk systems: As T_c decreases, nucleation density increases, and lamella thickness decreases, resulting in a lower T_m . There was no discernible effect on the crystallization rate, as the films produced at lower T_c contained more but smaller crystals (Chapter 5.1; Appendix I: Figure 2). This was to be expected, since chain mobility in OCL layers is very high, as indicated by interfacial shear moduli below $10^{-4} \text{ N}\cdot\text{m}^{-1}$. Therefore, lowering the water temperature does not seem to decrease the oligomer crystallization rate.

The chain orientation of crystals in ultrathin films on a solid surface can respond dynamically when cooling below the T_c . Yu et al investigated isothermal crystallization of PCL ultrathin films (~8-10 nm) on mica surface, where temperatures below 30 °C result in a mixture of two different morphologies, flat-on lamellae, and edge-on lamellae. During the melting process, the edge-on lamellae melt first, followed by the flat-on lamellae. The edges of the lamellae became smoother as the temperature increased, and the flat-on lamellae thickened. They found that the polymer recrystallization phenomenon was difficult to discern because it occurred during the heating process, but this resulted in multiple melting peaks.¹³¹

In contrast to Yu et al, Chapter 5.1 (Appendix I: Figure 2) demonstrates that exclusively single crystals with flat-on orientation are produced during isothermal crystallization of OCL with different end-groups at 12 or 21 °C at the air-water interface. Here, OCL ultrathin films are crystallized at different MMAs that led to the formation of even thinner semi-crystalline films with thicknesses less than 7 nm. As observed in bulk and similar to findings of Yu et al, the lamellar thickness in ultrathin films increased with increasing T_c . The fact that semi-crystalline oligomers on the air-water interface can be melted at temperatures much lower than in the bulk or at the air-solid interface is a major highlight (Chapter 5.1; Appendix I: Figure 6). This enables the development of thermoresponsive films that can respond to small temperature changes in nature caused by sunlight or electrical appliances. In contrast to the results of Yu et al, the

recrystallization process is observable via optical microscopy in the OCL films at the air-water interface. The recrystallized structures at the air-water interface were formed during the cooling of the melted film. The T_{rec} was found higher than the initial T_c , where the recrystallized structures were morphologically different in shape and size than the initial OCL crystals.

Confined space in ultrathin films and added restriction on chain mobility on the solid substrate leads to dynamic changes in the semi-crystalline morphology. For example, Mareau et al found that the truncated lozenge-shape of PCL crystals observed in thicker films (~ 200 nm) becomes distorted in thinner films (15 nm or below) depending on the T_c .⁶⁶ In contrast to these findings, T_c does affect the lateral size and thickness of the crystals but does not seem to deform the morphological outer hexagonal shape of the crystals from hydroxy-end capped OCL (Chapter 5.1; Appendix I: Figure 3). Even in films as thin as ~ 5 nm, deformation of crystal edges does not occur due to unrestricted chain transport to the crystal growth front, suggesting the lack of any strong adhesion effect at the polymer-water interface. Rather, the bulky end-groups have a major influence on crystal habits via lateral chain packing kinetics, which result in wavy edges for OCL dimethacrylate crystals (Chapter 5.1; Appendix I: Figure 2).

Although the amount of end-groups is generally small in comparison to the amount of polymer backbone, the effect on the chain assembly can be dramatic.¹³² Kawazu et al, for example, demonstrated the effect of end-groups on the crystallization rate of PCL confined in a nanocylinder. To their surprise, the crystallization rate of PCL with certain bulky end-groups (e.g. cholesterol) was substantially higher than that of PCL with small acetyl groups. This was explained by the complex chain mobility due to combined effects by the end-groups, and nano-cylinder diameter (~ 13 nm) which was close to PCL lamellar thickness.¹³³ In Chapter 5.1 (Appendix I: Figure 2-3), π -area isotherms, melting transitions, and optical microscopy are compared to investigate the effect of end-groups on crystallization. Spread oligomers on the water were in a dilute regime at low π s prior to crystallization. This allowed flexible chain ends to occupy preferential positions within the layer without being influenced by the underlying substrate. After a certain π , the end-groups have a dramatic influence on the π -MMA isotherm and semi-crystalline morphology, where as expected, bulkier end-groups slowed down the crystallization rate.

The T_m s of semi-crystalline films on solid surfaces do not have clear interdependencies on film thicknesses due to the polymer-substrate interactions. For instance, Wang et al found in poly[ethylene-co-vinyl acetate] (random copolymer with 90.5 wt % ethylene; $T_m = 95$ °C), and linear low-density PE ($T_m = 117$ °C) films (460 to 10 nm; spun-cast from polymer/toluene

solutions on a silicon substrate), a dramatic decrease of T_m for films thinner than 100 nm was observed. This T_m depression cannot be anticipated from the conventional Gibbs-Thomson relationship, and the effect was attributed to the modification in the effective heat of fusion by the polymer-silicon surface interactions.¹³⁴ In that context, Flieger et al found that a thicker PCL film (127 nm; $T_m = 63$ °C) can melt at a lower temperature than a thinner film (13 nm; $T_m = 84$ °C) on solid graphite surfaces.¹³⁵ Here, one can speculate that the underlying substrate has a different effect, as graphite is assumed to have weak interaction with adsorbing molecules. In contrast to the findings above, (Chapter 5.1; Appendix I: Figure 5) shows that the T_m s of semi-crystalline OCL films are proportional to the inverse crystal thickness as predicted by the Gibbs-Thomson equation. The crystal thickness, in turn, increases with a higher T_c , and is inversely proportional to the crystallization MMA . The dependency of T_m on thickness is also retained for transferred semi-crystalline films on the solid surface, making the Langmuir technique a viable and predictable option to prepare semi-crystalline coatings. Altogether, the data shown in Chapter 5.1 highlights the effect of the underlying substrate (water or silicon) on the kinetics and thermodynamics of OCL crystallization from ultrathin films.

6.2. Degradation of (ultra)thin films from semi-crystalline oligomers

The films/coatings with controlled degradation enable the simple and safe integration of the implants, as well as the drug delivery with predetermined release profiles.⁸² The overall degradation pathway depends on the in vivo conditions. For example, degradation of PCL films occurs via surface erosion in saliva and gastric juice, but via bulk erosion in bile and PBS. It is plausible that surface erosion in saliva occurred due to enzymatic catalysis by amylase, whereas in gastric juice, pepsinogen could catalyze the degradation. Also, the accelerated hydrolysis at the low pH (~ 1) of gastric juice shifts the degradation behavior towards surface erosion.⁷⁸ For prediction of degradation pathway, it becomes highly relevant to study the influences of different variables. In that context, (ultra)thin films are important platforms for studying and understanding degradation mechanisms in a relatively faster and more efficient manner. Yet, the way a polymeric thin film degrades is also influenced by the method of film preparation. For instance, Hermanová et al showed that films made by the solution casting method enzymatically degraded faster than the films prepared by compression molding due to the easier accessibility of ester bonds in the amorphous phase of spherulites.¹³⁶ In our work, mass transport processes, such as the diffusion of water into or the diffusion of fragments out of a material, do not occur in Langmuir ultrathin films. As a result, it becomes easier to comprehend polymer degradation mechanisms (e.g., degradation kinetics, identification of degradation

products, influencing factors) at the molecular level. The aspects of mass transport processes must be assessed separately in different experiments and simulations.^{44, 137}

Chemical modification of polymers can have interesting effects on degradation, but it necessitates synthesis, purification, and characterization. For example, the addition of perfluorinated segments to the PCL chain increases the polymer's hydrophobicity and decreases the rate of enzymatic degradation in the early period. Here, the lipase-catalyzed degradation occurred only in the PCL chains, thereby enriching the perfluorinated chain segments on the material surface.¹³⁸ However, the industrial production and application of perfluorinated compounds (PFC)s present a range of health issues. PFCs can bioaccumulate in the human body, and their high serum concentrations have been linked to elevated uric acid, blood cholesterol levels, an increased risk of heart, lung, and thyroid diseases, and even bladder cancer incidences.^{139 140} In another study, the thermal stability of ultrathin polyurea films on the silicon surface is increased by the cross-linking reaction.⁹⁵ In this thesis, additional options for altering the degradation of ultrathin films are demonstrated by varying chain termination (end-groups), adjusting film crystallinity (Chapter 5.2; Appendix II: Figure 2), and cross-links density (Chapter 5.4; Appendix IV: Figure 6).

In a previous study about the influence of end-groups on degradation, Jiang et al compared the influence of hydrophilic (amino) and hydrophobic (methoxy) groups on the degradation of single crystals of amphiphilic block copolymers. These studies concluded that the enzyme interaction was affected by the end-groups' wettability leading to differences in the surface of degraded crystals.¹⁴¹ In another study, Su et al showed that in PHB single crystal, the degradation proceeds at crystal edges due to the presence of loose chain packing.^{45, 142} In our work (Chapter 5.2; Appendix II: Figure 3), the chain packing of single crystals from hydroxy end-capped OCL differed from the ones from methacrylate end-capped OCL. However, the single crystals from OCL dimethacrylate showed channels after degradation, suggesting that the loose chain packing regions are also present within the crystals possibly as an influence from the bulky end-group. Overall, these findings show that changing the composition and functional terminal groups of polymers can be an effective method to control the surface characteristics of polymeric devices.

Chapter 5.2 (Appendix II: Figure 2) also compares amorphous film degradation with semi-crystalline films which shows that the increase in crystallinity in the film slowed down the hydrolytic degradation of films compared to the amorphous film by several hours. A similar effect of crystallinity on reducing material degradation was also found in bulk. Hence, the

effectiveness of ultrathin films in portraying bulk interfaces to elucidate molecular mechanisms remains viable. Degradation is also performed on LS transferred films on silicon, which aids in determining the influence of the solid substrate on degradation (Chapter 5.2; Appendix II: Figure 3). Due to the adhesion effect of polymer chains on the solid substrate, transferred LS films on silicon hydrolytically degraded slower compared to the films on the water surface. Heating or thermal switching of crystals to melted (amorphous) state accelerates the hydrolytic degradation of the ultrathin films. However, after cooling back to the initial temperature, the hydrolytic degradation proceeds as before. This is an important finding when applying crystals for strengthening materials or as thermoresponsive functional moieties in devices or coatings for drug release.⁸² However, we found that enzyme lipase from *Pseudomonas cepacia* is catalyzing the degradation of single crystals with great efficiency. Therefore, when designing materials for tunable enzymatic degradation, other approaches than tuning crystallinity should be considered. In Chapter 5.4 we demonstrated that the enzymatic (Appendix IV: Figure 6), or hydrolytic (Appendix IV: Figure 7) degradation in a cross-linked 2D network can be tailored as a function of acetalization reaction time. Overall, these findings are important for the need for continued improvement of drug delivery for more sensitive molecules like proteins, antibodies, or nucleic acids which can be readily deactivated or unfolded by the hydrophobic or ionic interactions with the delivery vehicle.¹⁴³ In this context, the findings reported in this thesis are expected to provide some guidance for better tailoring the bulk and nanostructured systems for controlling the degradation.

6.3. Reaction of polymer/oligomer end-groups in ultrathin films

End-group chemistry is a versatile and strong tool for tuning polymer characteristics for a specific purpose.¹³² Yet, carrying out reactions on the end-groups in ultrathin films or coatings is an intricate process, especially since flexible chain ends are in lower concentration available compared to the polymer backbone. In this context, polymer single crystals provide opportunities for post-functionalization by the immense end-groups present on its surface. Hence, surface-functionalized crystals are also emerging in the medical field for vaccine delivery⁴⁶, drug delivery^{45, 47}, filtration membranes¹⁴⁴, and as nanomotors^{45, 145, 146}. In this thesis (Chapter 5.3; Appendix III: Figure 6), an efficient approach for performing surface chemistry of methacrylate end-capped PCL single crystals in an aqueous environment at room temperature is demonstrated. Here, a fluorescent dye with the photoreactive group was chemically linked using ultraviolet (UV) light and the melting transitions of the fluorescent dye functionalized single crystals was monitored by fluorescent microscopy. These fascinating results from Chapter 5.3 (Appendix III: Figure 6) helps in following change in phase morphology during

thermally controlled switching of the semi-crystalline coating under an aqueous environment. Hence, apart from providing insight on topological features of polymer single crystals, molecular-level description of the semi-crystalline state is provided through fluorescent labeling. Very recently, Kato et al. also used fluorescence to follow polymer crystallization. In their work, a large fluorophore (tetraarylsuccinonitrile) was inserted within the polymer backbone to understand how polymer architecture affects the growth of spherulites.¹⁴⁷ In another study, molecular structure and single crystals adhesion process were investigated by Zhao et al using fluorescent-labeled anthracene units present at the single crystal edges.¹⁴⁸ Overall, these studies and the findings from this thesis (Chapter 5.3; Appendix III: Figure 6) complement the use of surface chemistry in understanding the molecular processes occurring in a polymer crystal.

At the air-water interface, 2D reactions of flexible chain ends in ultrathin films are important for improving stability for film transfer or imparting functionalization. The degree of movement of chain ends of polymers/oligomers is higher compared to end-groups in small amphiphiles or crystal surfaces. Therefore, strict requirements of chain assembly for covalent reactions are not easily met under the 2D plane. In consequence, only a few studies describe the 2D cross-linking reactions of oligomers or polymers at the air-liquid interface for the last two decades. Selecting appropriate reaction chemistry, process parameters and characterization strategy is crucial before carrying out the reactions.^{104-108, 110-112, 149-176} Polymerization of Langmuir films from small amphiphiles at the air-liquid interface has been investigated comprehensively already before and is generally based on photo^{109-113, 118, 149, 151, 154-158, 160, 161, 169, 171, 174, 176, 177} or electron beam^{162, 178} irradiation, coordination chemistry¹¹⁴⁻¹¹⁷, redox reactions^{106, 152, 153, 159, 165, 166, 172} or polycondensation reactions^{167, 168}. Carrying out polymerization reactions of polymers or oligomers by UV irradiation necessitates the use of certain initiators and, in most cases, an oxygen-free environment. Prolonged photo-irradiation also causes ultrathin film degradation, demanding the development of other reaction chemistries in the 2D plane. In Chapter 5.4, pH reversible acetalization chemistry for 2D cross-linking the oligomers with different molecular architecture (linear or star shape) under ambient conditions is introduced as a novel approach to prepare 2D networks. The reaction does not require special considerations to the aerial environment for cross-linking the oligomeric monolayer. The formation of cross-links in the oligomeric monolayer is shown by the change in film area, crystallization, degradation behavior as well as interfacial spectroscopic measurements (Chapter 5.4; Appendix IV: Figure 1-6).

The findings presented in Chapter 5.4 on OCL 2D networks are also acknowledged in recently reported works on ultrathin films polymerization. For example, 1,2-polybutadiene 2D networks were formed on the water surface by UV irradiation, where cross-linking was investigated with the help of BAM observations and Sum-Frequency Generation spectroscopy.¹⁷⁶ Another study from Haroun et al employs acetalization reaction in the monolayer, the reaction chemistry that is introduced for Langmuir monolayers via the methods established in this thesis. 2D networks of a poly(ethylene glycol)-block-poly(propylene glycol)-block-poly(ethylene glycol) copolymer (10 wt % PEG) was prepared at the air-water interface using a trifunctional aldehyde (benzene-1,3,5-tricarboxaldehyde) in the subphase.¹⁷⁵ Similar to the findings of OCL 2D networks shown in Chapter 5.4 (Appendix IV: Figure 1), the presence of cross-linker in the subphase also contracted their oligomeric monolayer and shifted its compressibility modulus during the acetalization reaction. Therefore, the findings of this thesis are also becoming helpful in the material research field for the guidance of reactions in ultrathin films in a confined plane.

7. Conclusion and Outlook

Semi-crystalline aliphatic oligoesters are degradable materials, which are of relevance as building blocks of biomaterials for medical devices, drug delivery systems, and tissue engineering. Especially, crystals of OCL can melt and recrystallize at physiologically applicable temperatures and therefore find their applicability in designing active nanostructured and microscopic devices. The presented work in this thesis provides a model to prepare and elucidate ultrathin films from semi-crystalline oligomers under ambient conditions using the Langmuir technique. The molecular-level insights of oligomer crystallization, melting transitions, and the reaction of end-groups were provided using the ultrathin films. Oligomer assembly at the air-water interface was adjustable and overcomes the limitations of strong adhesion forces observed on the solid substrate.

Semi-crystalline morphology and thermal transitions in the ultrathin films were tuned by the chemical structure of the OCL end-group (hydroxy or methacrylate), and by T_c (12 or 21 °C) and film MMA as the physical parameters. Ultrathin films of OCL were transferred from the air-water interface onto a solid surface by the Langmuir-Schaefer method. Whereby, single crystals were transferable with minor fractures to the solid surfaces, but amorphous films produced holes due to the process of dewetting.

Melting/recrystallization of different OCL ultrathin films was carried out at the air-water interface and compared to bulk and the air-solid interface. Melting and recrystallization at the air-water interface occurred at much lower temperatures than in bulk or at the air-solid interface. These findings highlight the consideration of underlying substrate when investigating thin or ultrathin films of polymer. Compared to OCL diol films where oligomers are terminated by hydroxy groups, the melting of films having methacrylate end-capped OCL occurred at lower temperatures. This was explained by the thinner OCL dimethacrylate crystals formed under identical conditions compared to the OCL diol crystals. Overall, the melting transitions of OCL diol and OCL dimethacrylate single crystals at the air-water or air-solid interface were proportional to the inverse crystal thickness, in agreement with the Gibbs-Thomson equation. Compared to the air-water interface, semi-crystalline films melting on the silicon surface occurred in a restricted manner where the recrystallization process was also not identifiable by optical microscopy.

Highly crystalline OCL films consisting of tightly packed, identical single crystals were prepared by compression to low MMA of $\sim 2 \text{ \AA}^2$ and explored as functionalized thermoswitchable coatings. This demand of large-scale synthesis of high crystallite density and

adjustable morphology of coatings is not achievable by conventional methodologies such as spin coating and solvent casting. The highly crystalline OCL coatings on silicon were fluorescent-labeled and investigated for change in phase morphology during thermally controlled switching in the aqueous environment. The thermoswitching behavior (melting and recrystallization) of fluorescein functionalized, highly crystalline OCL films showed a temperature-dependent distribution of the chemically linked fluorescein moieties, which were accumulated on the surfaces of single crystals, but redistributed after crystals melting. This redistribution of functionalized bioactive molecules by a small change of thermal stimuli is relevant for subcutaneous implants or tissue culture substrates. Depending on the attached biological cue such as cell adhesion peptides or anti-bacterial molecules, temperature-dependent on-demand cell guidance or anti-pathogenic effect can be achieved on the coated surface.

Another conceivable application of highly crystalline films is friction-reducing coatings, for example on sutures. Here, the temperature at the suture-tissue interface does not increase as long as the heat generated by frictional forces is absorbed by the melting enthalpy of the crystals. Apart from biological applications, highly crystalline films formed via (bio)degradable polymers offer sustainable ways for developing temperature-dependent coatings for thermal reflection.

Polymer single crystals presented in this thesis are also interesting candidates for drug carriers or nanomotors. For the motion of polymer single crystals, surface chemistry alteration via functional end-groups or adsorbed nanoparticles is explored in many studies.^{45, 145, 146} In this context, anisotropy in structural designs is crucial for the directional movement of micro or nano-sized motors.¹⁷⁹ In this thesis, the anisotropy of shape and edges of polymer single crystals (e.g. wavy edges of methacrylate end-capped single crystals) is particularly of interest for the directional motion. Methacrylate functional groups immensely present on single crystals can also aid in the assembly of the platinum or silver nanoparticles that in the presence of hydrogen peroxide solution can produce oxygen bubbles for self-propulsion.

For predicting biological performance, it is important to characterize different factors affecting the degradation behavior, which however is difficult in bulk systems. The ultrathin films were demonstrated as model systems to elucidate the effect of crystallinity, temperature, end-groups, and substrate on OCL degradation. In general, the highly crystalline ultrathin films displayed linear mass-loss at different temperatures, where the OCL dimethacrylate films degraded faster

than the OCL diol films at different temperatures. The strong retardation of degradation of OCL crystals was also observed after films transfer to the solid substrates.

Comparing different semi-crystalline films, a high crystallinity strongly reduced the hydrolytic but not the enzymatic degradation rate. As an influence of end-groups, the methacrylate end-capped oligomer hydrolytically degraded faster than the hydroxy end-capped oligomer at different temperatures. Hence, chain termination was found as an additional option to control the degradation of OCL in ultrathin films.

At physiological temperature, transferred highly crystalline films on silicon degraded slowly and almost linearly. Such behavior is highly demanded for applications like erosion-controlled drug release coatings. After 72 h, the propagation of degradation in transferred single crystals proceeded through the cracks and channels. This effect is attributed to the differences in chain packing and larger free volume in the single crystals from bulky, methacrylate end-group oligomer. Since the transferred single crystals degrade slowly in the non-melted state, they can potentially act as a thermally switchable, diffusion barrier for gases or macromolecules to the underlying surface. The barrier performance would be determined by the frequency of defects and crystalline morphology. The underlying surface can also be a fast degrading polymer whose degradation will be influenced by the crystalline state of the coated film.

Degradation was also measured in real-time during the thermal treatments of semi-crystalline ultrathin films. An acceleration of the hydrolytic degradation of semi-crystalline films was achieved by the crystals melting. By cooling the melted film, the degradation rate again slowed down. Hence, the melting of OCL crystals accelerated degradation for a short while, but after cooling the film, the degradation was nearly the same as before. This is of importance for building devices such as thermally triggered microvalves that employ OCL crystals as thermal switches in an aqueous environment.¹⁸⁰

In the described degradation studies, influences from film crystallinity, thickness, molecular concentration, and π were identified. This is useful in the construction of kinetic models for the degradation of semi-crystalline polymers. In particular, π i.e. lateral surface pressure (5 and 7 mN·m⁻¹) as a parameter appears to impact the dissolution of water-soluble degradation fragments. This is important for implants placed under the skin or other tissues where lateral stress may lead to faster degradation of the implant material. As a consequence, this could lead to unintended behavior of a device such as speedier discharge of a medicament into the bloodstream.

Degradation of OCL in ultrathin films was also found to be influenced by the cross-linking of chain ends that lead to the formation of branching centers in the film. Firstly, as a proof of concept for the two-dimensional cross-linking, OCL 2D networks at the air-water interface were formed using glyoxal, which imparts pH-sensitive reversible acetal cross-links. The course of acetalization reaction was supported by interfacial infrared spectroscopy and changes in the π -MMA isotherms showing film contraction. For OCL 2D networks at the air-water interface, cross-links formation dramatically influenced the crystallization and degradation kinetics. Where, in a cross-linked 2D network formed after 24 h of reaction, the crystallization was inhibited and the degradation slowed for a certain initial period of time.

Glyoxal applied as a cross-linker is less toxic than paraformaldehyde and therefore is an emerging molecule to fixate cells for immunostaining¹⁸¹, however, for in vivo applications, would have to be replaced by a less toxic dialdehyde. The reversibility of acetal cross-links formed using glyoxal in the 2D network was demonstrated by reducing the pH (Chapter 5.4; Appendix IV; Figure 8). The strategy described in this thesis for preparing reversible 2D networks is showcasing mechanisms that are relevant for other pH-reversible systems such as maleimide-functionalized oligomers for tissue regeneration¹⁸² or phenylboronic acid decorated macromolecules to influence cell adhesion¹⁸³. Also in the field of molecular imprinting, reversible cross-linking to create molecular templates in a 2D plane is of fundamental interest, e.g. for sensing applications.¹⁸⁴⁻¹⁸⁷ Such reversibly cross-linked systems can be investigated in ultrathin films that are closely matching the targeted environment. The preparation and characterization and strategies described in our work are likely relevant and applicable for these systems.

As coatings, 2D layers on patterned substrates are used to generate intricate effects such as regulation of the cellular organization.¹⁸⁸ The highly crystalline ultrathin films or 2D networks presented in this thesis, can possibly provide thermomechanical signals for cells. Proteins or cells might stick to coated films depending on their viscoelastic properties, which vary strongly with chain ordering. Approaches for large-scale film synthesis by apparatus modification have been described and were at least temporarily, commercially available.^{92, 189} Hence, the versatility of the Langmuir technique in controlling polymer crystallization and chemistry for the preparation of functional ultrathin films remains immense.

8. References

1. Payamyar, P.; King, B. T.; Öttinger, H. C.; Schlüter, A. D. Two-dimensional polymers: concepts and perspectives. *Chemical Communications* **2016**, 52(1), 18-34 DOI: 10.1039/C5CC07381B.
2. Akinwande, D.; Brennan, C. J.; Bunch, J. S.; Egberts, P.; Felts, J. R.; Gao, H.; Huang, R.; Kim, J.-S.; Li, T.; Li, Y.; Liechti, K. M.; Lu, N.; Park, H. S.; Reed, E. J.; Wang, P.; Yakobson, B. I.; Zhang, T.; Zhang, Y.-W.; Zhou, Y.; Zhu, Y. A review on mechanics and mechanical properties of 2D materials—Graphene and beyond. *Extreme Mechanics Letters* **2017**, 13, 42-77 DOI: 10.1016/j.eml.2017.01.008.
3. Glavin, N. R.; Rao, R.; Varshney, V.; Bianco, E.; Apte, A.; Roy, A.; Ringe, E.; Ajayan, P. M. Emerging applications of elemental 2d materials. *Advanced Materials* **2020**, 32(7), 1904302 DOI: 10.1002/adma.201904302.
4. Schaibley, J. R.; Yu, H.; Clark, G.; Rivera, P.; Ross, J. S.; Seyler, K. L.; Yao, W.; Xu, X. Valleytronics in 2D materials. *Nature Reviews Materials* **2016**, 1(11), 16055 DOI: 10.1038/natrevmats.2016.55.
5. Montagner, A.; Bosi, S.; Tenori, E.; Bidussi, M.; Alshatwi, A. A.; Tretiach, M.; Prato, M.; Syrgiannis, Z. Ecotoxicological effects of graphene-based materials. *2D Materials* **2017**, 4(1), 012001 DOI: 10.1088/2053-1583/4/1/012001.
6. Yuri, V.; Jennifer, M.; Adriele, P.-M. Graphene toxicity as a double-edged sword of risks and exploitable opportunities: a critical analysis of the most recent trends and developments. *2D Materials* **2017**, 4(2), 022001 DOI: 10.1088/2053-1583/aa5476.
7. Smith, J. R.; Lamprou, D. A. Polymer coatings for biomedical applications: a review. *Transactions of the Institute of Materials Finishing* **2014**, 92(1), 9-19 DOI: 10.1179/0020296713Z.000000000157.
8. Kurakula, M.; Naveen, N. R.; Yadav, K. S., Chapter 19 - Formulations for polymer coatings. In *Polymer Coatings: Technology and Applications*, Inamuddin, Boddula, R., Ahamed, M. I., Asiri, A. M., Eds. Scrivener **2020**; pp 415-443 DOI: 10.1002/9781119655145.ch19.
9. Liu, Y.-X.; Chen, E.-Q. Polymer crystallization of ultrathin films on solid substrates. *Coordination Chemistry Reviews* **2010**, 254(9), 1011-1037 DOI: 10.1016/j.ccr.2010.02.017.
10. Machatschek, R.; Lendlein, A. Fundamental insights in PLGA degradation from thin film studies. *Journal of Controlled Release* **2020**, 319, 276-284 DOI: 10.1016/j.jconrel.2019.12.044.
11. Ulbrich, K.; Holá, K.; Šubr, V.; Bakandritsos, A.; Tuček, J.; Zbořil, R. Targeted drug delivery with polymers and magnetic nanoparticles: covalent and noncovalent approaches, release control, and clinical studies. *Chemical Reviews* **2016**, 116(9), 5338-5431 DOI: 10.1021/acs.chemrev.5b00589.
12. Nuo, W.; Xue Shen, W.; Hannia, L.-U.; Donahue, E.; Siddiqui, A. Synthesis, characterization, biodegradation, and drug delivery application of biodegradable lactic/glycolic acid oligomers: I. Synthesis and characterization. *Journal of Biomaterials Science, Polymer Edition* **1997**, 8(12), 905-917 DOI: 10.1163/156856297X00083.
13. Camacho, K. M.; Menegatti, S.; Mitragotri, S. Low-molecular-weight polymer-drug conjugates for synergistic anticancer activity of camptothecin and doxorubicin combinations. *Nanomedicine (Lond)* **2016**, 11(9), 1139-1151 DOI: 10.2217/nmm.16.33.
14. Babudri, F.; Farinola, G. M.; Naso, F. Synthesis of conjugated oligomers and polymers: the organometallic way. *Journal of Materials Chemistry* **2004**, 14(1), 11-34 DOI: 10.1039/B309515K.
15. van Genabeek, B.; Lamers, B. A. G.; Hawker, C. J.; Meijer, E. W.; Gutekunst, W. R.; Schmidt, B. V. K. J. Properties and applications of precision oligomer materials; where

- organic and polymer chemistry join forces. *Journal of Polymer Science* **2021**, 59(5), 373-403 DOI: 10.1002/pol.20200862.
16. Scherlis, D. A.; Marzari, N. π -stacking in thiophene oligomers as the driving force for electroactive materials and devices. *Journal of the American Chemical Society* **2005**, 127(9), 3207-3212 DOI: 10.1021/ja043557d.
 17. Chortos, A.; Hajiesmaili, E.; Morales, J.; Clarke, D. R.; Lewis, J. A. 3D printing of interdigitated dielectric elastomer actuators. *Advanced Functional Materials* **2020**, 30(1), 1907375 DOI: 10.1002/adfm.201907375.
 18. Liu, M.; Liu, P.; Lu, G.; Xu, Z.; Yao, X. Multiphase-assembly of siloxane oligomers with improved mechanical strength and water-enhanced healing. *Angewandte Chemie International Edition* **2018**, 57(35), 11242-11246 DOI: 10.1002/anie.201805206.
 19. Zhang, F.; Wu, D.; Xu, Y.; Feng, X. Thiophene-based conjugated oligomers for organic solar cells. *Journal of Materials Chemistry* **2011**, 21(44), 17590-17600 DOI: 10.1039/C1JM12801A.
 20. Jenkins, A. D.; Kratochvíl, P.; Stepto, R. F. T.; Suter, U. W. Glossary of basic terms in polymer science (IUPAC Recommendations 1996). *Pure and Applied Chemistry* **1996**, 68(12), 2287-2311 DOI: 10.1351/pac199668122287.
 21. Sisson, A. L.; Ekinici, D.; Lendlein, A. The contemporary role of ϵ -caprolactone chemistry to create advanced polymer architectures. *Polymer* **2013**, 54(17), 4333-4350 DOI: 10.1016/j.polymer.2013.04.045.
 22. Blasi, P. Poly(lactic acid)/poly(lactic-co-glycolic acid)-based microparticles: an overview. *Journal of Pharmaceutical Investigation* **2019**, 49(4), 337-346 DOI: 10.1007/s40005-019-00453-z.
 23. Operti, M. C.; Bernhardt, A.; Grimm, S.; Engel, A.; Figdor, C. G.; Tagit, O. PLGA-based nanomedicines manufacturing: technologies overview and challenges in industrial scale-up. *International Journal of Pharmaceutics* **2021**, 605, 120807 DOI: 10.1016/j.ijpharm.2021.120807.
 24. Lee, P. W.; Pokorski, J. K. Poly(lactic-co-glycolic acid) devices: production and applications for sustained protein delivery. *Wiley interdisciplinary reviews. Nanomedicine and nanobiotechnology* **2018**, 10(5), e1516-e1516 DOI: 10.1002/wnan.1516.
 25. Grayson, A. C. R.; Cima, M. J.; Langer, R. Size and temperature effects on poly(lactic-co-glycolic acid) degradation and microreservoir device performance. *Biomaterials* **2005**, 26(14), 2137-2145 DOI: 10.1016/j.biomaterials.2004.06.033.
 26. Fodor-Kardos, A.; Kiss, Á. F.; Monostory, K.; Feczko, T. Sustained in vitro interferon-beta release and in vivo toxicity of PLGA and PEG-PLGA nanoparticles. *RSC Advances* **2020**, 10(27), 15893-15900 DOI: 10.1039/C9RA09928J.
 27. Díaz-Galindo, E. P.; Nestic, A.; Cabrera-Barjas, G.; Dublan-García, O.; Ventura-Aguilar, R. I.; Vázquez-Armenta, F. J.; Aguilar-Montes de Oca, S.; Mardones, C.; Ayala-Zavala, J. F. Physico-chemical and antiadhesive properties of poly(lactic acid)/grapevine cane extract films against food pathogenic microorganisms. *Polymers* **2020**, 12(12), 2967 DOI: 10.3390/polym12122967.
 28. Jem, K. J.; Tan, B. The development and challenges of poly (lactic acid) and poly (glycolic acid). *Advanced Industrial and Engineering Polymer Research* **2020**, 3(2), 60-70 DOI: 10.1016/j.aiepr.2020.01.002.
 29. Gautier, E.; Fuertes, P.; Cassagnau, P.; Pascault, J.-P.; Fleury, E. Synthesis and rheology of biodegradable poly(glycolic acid) prepared by melt ring-opening polymerization of glycolide. *Journal of Polymer Science Part A: Polymer Chemistry* **2009**, 47(5), 1440-1449 DOI: 10.1002/pola.23253.

30. Malikmammadov, E.; Tanir, T. E.; Kiziltay, A.; Hasirci, V.; Hasirci, N. PCL and PCL-based materials in biomedical applications. *Journal of Biomaterials Science, Polymer Edition* **2018**, 29(7-9), 863-893 DOI: 10.1080/09205063.2017.1394711.
31. Farooq, T.; Hameed, A.; Akash, M. S. H.; Rehman, K., Chapter 14 - Polymer coatings for biomedical applications. In *Polymer Coatings: Technology and Applications*, Inamuddin, Boddula, R., Ahamed, M. I., Asiri, A. M., Eds. Scrivener: **2020**; pp 333-346 DOI: 10.1002/9781119655145.ch14.
32. Venda, V.; Wu, L.; Krishnan, S., Polymer thin films for biomedical applications. In *Nanostructured Thin Films and Surfaces*, Kumar, C., Ed. Wiley-VCH: **2011**; Vol. 5, pp 1-51 DOI: 10.1002/9783527610419.ntls0179.
33. Zhou, G.; Niepel, M. S.; Saretia, S.; Groth, T. Reducing the inflammatory responses of biomaterials by surface modification with glycosaminoglycan multilayers. *Journal of Biomedical Materials Research A* **2016**, 104(2), 493-502 DOI: 10.1002/jbm.a.35587.
34. Kim, H.; Yarin, A. L.; Lee, M. W. Self-healing corrosion protection film for marine environment. *Composites Part B: Engineering* **2020**, 182, 107598 DOI: 10.1016/j.compositesb.2019.107598.
35. Zhao, H.; Sun, Q.; Zhou, J.; Deng, X.; Cui, J. Switchable cavitation in silicone coatings for energy-saving cooling and heating. *Advanced Materials* **2020**, 32(29), 2000870 DOI: 10.1002/adma.202000870.
36. Hoque, J.; Ghosh, S.; Paramanandham, K.; Haldar, J. Charge-switchable polymeric coating kills bacteria and prevents biofilm formation in vivo. *ACS Appl Mater Interfaces* **2019**, 11(42), 39150-39162 DOI: 10.1021/acsami.9b11453.
37. Xu, G.; Neoh, K. G.; Kang, E.-T.; Teo, S. L.-M. Switchable antimicrobial and antifouling coatings from tannic acid-scaffolded binary polymer brushes. *ACS Sustainable Chemistry & Engineering* **2020**, 8(6), 2586-2595 DOI: 10.1021/acssuschemeng.9b07836.
38. Rajab, F. H.; Korshed, P.; Liu, Z.; Wang, T.; Li, L. How did the structural ZnO nanowire as antibacterial coatings control the switchable wettability. *Applied Surface Science* **2019**, 469, 593-606 DOI: 10.1016/j.apsusc.2018.10.249.
39. Taleb, S.; Darmanin, T.; Guittard, F., Chapter 8 - Switchable and reversible superhydrophobic surfaces: part one. In *Interdisciplinary Expansions in Engineering and Design With the Power of Biomimicry*, Kokturk, G., Altun, T., Eds. InTech: **2018**; DOI: 10.5772/intechopen.73022.
40. Jessop, P. G.; Cunningham, M. F., Chapter 1 - Introduction to CO₂-switchable materials. In *CO₂-switchable Materials: Solvents, Surfactants, Solutes and Solids*, Jessop, P. G., Cunningham, M. F., Eds. The Royal Society of Chemistry: **2021**; pp 1-6 DOI: 10.1039/9781788012850-00001.
41. Becherer, T.; Heinen, S.; Wei, Q.; Haag, R.; Weinhart, M. In-depth analysis of switchable glycerol based polymeric coatings for cell sheet engineering. *Acta Biomaterialia* **2015**, 25, 43-55 DOI: 10.1016/j.actbio.2015.06.036.
42. Shrestha, R.; Luan, Y.; Shin, S.-M.; Zhang, T.; Luo, X.; Lundh, J.; Gong, W.; Bockstaller, M.; Choi, S.; Luo, T.; Chen, R.; Hippalgaonkar, K.; Shen, S. High-contrast and reversible polymer thermal regulator by structural phase transition. *Science advances* **2019**, 5, eaax3777 DOI: 10.1126/sciadv.aax3777.
43. Yang, F.; Cholewinski, A.; Yu, L.; Rivers, G.; Zhao, B. A hybrid material that reversibly switches between two stable solid states. *Nature Materials* **2019**, 18(8), 874-882 DOI: 10.1038/s41563-019-0434-0.
44. Machatschek, R.; Schulz, B.; Lendlein, A. Langmuir monolayers as tools to study biodegradable polymer implant materials. *Macromolecular Rapid Communications* **2019**, 40(1), 1800611 DOI: 10.1002/marc.201800611.

45. Agbolaghi, S.; Abbaspoor, S.; Abbasi, F. A comprehensive review on polymer single crystals—from fundamental concepts to applications. *Progress in Polymer Science* **2018**, *81*, 22-79 DOI: 10.1016/j.progpolymsci.2017.11.006.
46. Di Bonito, P.; Petrone, L.; Casini, G.; Francolini, I.; Ammendolia, M. G.; Accardi, L.; Piozzi, A.; D'Ilario, L.; Martinelli, A. Amino-functionalized poly(L-lactide) lamellar single crystals as a valuable substrate for delivery of HPV16-E7 tumor antigen in vaccine development. *International journal of nanomedicine* **2015**, *10*, 3447-58 DOI: 10.2147/ijn.s76023.
47. D'Ilario, L.; Francolini, I.; Martinelli, A.; Piozzi, A. Dipyrindamole-loaded poly(l-lactide) single crystals as drug delivery systems. *Macromolecular Rapid Communications* **2007**, *28*(18-19), 1900-1904 DOI: 10.1002/marc.200700224.
48. Oliver, J.-a. N.; Su, Y.; Lu, X.; Kuo, P.-H.; Du, J.; Zhu, D. Bioactive glass coatings on metallic implants for biomedical applications. *Bioactive Materials* **2019**, *4*, 261-270 DOI: 10.1016/j.bioactmat.2019.09.002.
49. Correia, T. R.; Ferreira, P.; Vaz, R.; Alves, P.; Figueiredo, M. M.; Correia, I. J.; Coimbra, P. Development of UV cross-linked gelatin coated electrospun poly(caprolactone) fibrous scaffolds for tissue engineering. *International Journal of Biological Macromolecules* **2016**, *93*, 1539-1548 DOI: 10.1016/j.ijbiomac.2016.05.045.
50. Kim, Y.-H.; Jyoti, M. A.; Song, H.-Y. Immobilization of cross linked Col-I–OPN bone matrix protein on aminolysed PCL surfaces enhances initial biocompatibility of human adipogenic mesenchymal stem cells (hADMSC). *Applied Surface Science* **2014**, *303*, 97-106 DOI: 10.1016/j.apsusc.2014.02.084.
51. Singh, S.; Wu, B. M.; Dunn, J. C. Y. The enhancement of VEGF-mediated angiogenesis by polycaprolactone scaffolds with surface cross-linked heparin. *Biomaterials* **2011**, *32*(8), 2059-2069 DOI: 10.1016/j.biomaterials.2010.11.038.
52. Wang, D.; Wang, X.; Zhang, Z.; Wang, L.; Li, X.; Xu, Y.; Ren, C.; Li, Q.; Turng, L.-S. Programmed release of multimodal, cross-linked vascular endothelial growth factor and heparin layers on electrospun polycaprolactone vascular grafts. *ACS Applied Materials & Interfaces* **2019**, *11*(35), 32533-32542 DOI: 10.1021/acsami.9b10621.
53. Bahcecioglu, G.; Hasirci, N.; Bilgen, B.; Hasirci, V. A 3D printed PCL/hydrogel construct with zone-specific biochemical composition mimicking that of the meniscus. *Biofabrication* **2019**, *11*(2), 025002 DOI: 10.1088/1758-5090/aaf707.
54. Zhong, X.; Ji, C.; Chan, K. L. A.; Kazarian, S.; Ruys, A.; Dehghani, F. Chitosan/poly(ϵ -caprolactone) composite hydrogel for tissue engineering applications. *Journal of materials science. Materials in medicine* **2011**, *22*, 279-88 DOI: 10.1007/s10856-010-4194-2.
55. Uddin, M. S.; Majewski, P. Frictional heating in hip implants – a review. *Procedia Engineering* **2013**, *56*, 725-730 DOI: 10.1016/j.proeng.2013.03.185.
56. Boutry, C. M.; Kaizawa, Y.; Schroeder, B. C.; Chortos, A.; Legrand, A.; Wang, Z.; Chang, J.; Fox, P.; Bao, Z. A stretchable and biodegradable strain and pressure sensor for orthopaedic application. *Nature Electronics* **2018**, *1*(5), 314-321 DOI: 10.1038/s41928-018-0071-7.
57. Manavitehrani, I.; Fathi, A.; Badr, H.; Daly, S.; Negahi Shirazi, A.; Dehghani, F. Biomedical applications of biodegradable polyesters. *Polymers* **2016**, *8*(1), 20 DOI: 10.3390/polym8010020.
58. Ino, K.; Sato, S.; Ushimaru, K.; Saika, A.; Fukuoka, T.; Ohshiman, K.; Morita, T. Mechanical properties of cold-drawn films of ultrahigh-molecular-weight poly(3-hydroxybutyrate-co-3-hydroxyvalerate) produced by *Haloferax mediterranei*. *Polymer Journal* **2020**, *52*(11), 1299-1306 DOI: 10.1038/s41428-020-0379-9.

59. Pachekoski, W.; Dalmolin, C. The influence of the industrial processing on the degradation of poly(hidroxybutyrate)- PHB. *Materials Research* **2013**, *16*, 237-332 DOI: 10.1590/S1516-14392012005000180.
60. Turco, R.; Santagata, G.; Corrado, I.; Pezzella, C.; Di Serio, M. In vivo and post-synthesis strategies to enhance the properties of PHB-based materials: a review. *Front Bioeng Biotechnol* **2020**, *8*, 619266 DOI: 10.3389/fbioe.2020.619266.
61. Vogel, C.; Siesler, H. W. Thermal degradation of poly(ϵ -caprolactone), poly(L-lactic acid) and their blends with poly(3-hydroxy-butyrates) studied by TGA/FT-IR spectroscopy. *Macromolecular Symposia* **2008**, *265*(1), 183-194 DOI: 10.1002/masy.200850520.
62. Samanta, P.; Liu, C.-L.; Nandan, B.; Chen, H.-L., Chapter 13 - Crystallization of polymers in confined space. In *Crystallization in Multiphase Polymer Systems*, Thomas, S., Arif P, M., Gowd, E. B., Kalarikkal, N., Eds. Elsevier: **2018**; pp 367-431 DOI: 10.1016/B978-0-12-809453-2.00013-X.
63. Zhang, M. C.; Guo, B.-H.; Xu, J. A review on polymer crystallization theories. *Crystals* **2017**, *7*(1), 4 DOI: 10.3390/cryst7010004.
64. Hoffman, J. D. Melting process and equilibrium melting temperature of poly(chlorotrifluoroethylene). *Journal of Research of the National Bureau of Standards. Section A, Physics and Chemistry* **1962**, *66A*, 13-28 DOI: 10.6028/JRES.066A.003.
65. Wunderlich, B.; Czornyj, G. A study of equilibrium melting of polyethylene. *Macromolecules* **1977**, *10*(5), 906-913 DOI: 10.1021/ma60059a006.
66. Mareau, V. H.; Prud'homme, R. E. In-situ hot stage atomic force microscopy study of poly(ϵ -caprolactone) crystal growth in ultrathin films. *Macromolecules* **2005**, *38*(2), 398-408 DOI: 10.1021/ma0482359.
67. Yu, C.; Xie, Q.; Bao, Y.; Shan, G.; Pan, P. Crystalline and spherulitic morphology of polymers crystallized in confined systems. *Crystals* **2017**, *7*(5), 147 DOI: 10.3390/cryst7050147.
68. Sahu, N.; Parija, B.; Panigrahi, S. Fundamental understanding and modeling of spin coating process: A review. *Indian Journal of Physics* **2009**, *83*(4), 493-502 DOI: 10.1007/s12648-009-0009-z.
69. Abbas, M.; Zeng, L.; Guo, F.; Rauf, M.; Yuan, X.-C.; Cai, B. A Critical Review on Crystal Growth Techniques for Scalable Deposition of Photovoltaic Perovskite Thin Films. *Materials* **2020**, *13*(21), 4851 DOI: 10.3390/ma13214851.
70. Tong, J.; Dombia, A.; Alieva, A.; Turner, M. L.; Casiraghi, C. Gas blow coating: a deposition technique to control the crystal morphology in thin films of organic semiconductors. *ACS Omega* **2019**, *4*(7), 11657-11662 DOI: 10.1021/acsomega.9b00835.
71. Ge, C.; Zhai, W. Cellular thermoplastic polyurethane thin film: preparation, elasticity, and thermal insulation performance. *Industrial & Engineering Chemistry Research* **2018**, *57*(13), 4688-4696 DOI: 10.1021/acs.iecr.7b05037.
72. Udayakumar, M.; Kollár, M.; Kristály, F.; Leskó, M.; Szabó, T.; Marossy, K.; Tasnádi, I.; Németh, Z. Temperature and time dependence of the solvent-induced crystallization of poly(L-lactide). *Polymers* **2020**, *12*(5), 1065 DOI: 10.3390/polym12051065.
73. Mareau, V. H.; Prud'homme, R. Crystallization of ultrathin poly(ϵ -caprolactone) films in the presence of residual solvent, an in situ atomic force microscopy study. *Polymer* **2005**, *46*, 7255-7265 DOI: 10.1016/j.polymer.2005.06.036.
74. Zhang, H.; Xu, L.; Xu, Y.; Huang, G.; Zhao, X.; Lai, Y.; Shi, T. Enhanced self-organized dewetting of ultrathin polymer blend film for large-area fabrication of SERS substrate. *Scientific Reports* **2016**, *6*(1), 38337 DOI: 10.1038/srep38337.
75. Somasundaran, P. Encyclopedia of surface and colloid science. *CRC Press* **2006** *5*, DOI: 10.1081/E-ESCS-120000001.

76. Ponting, M.; Lin, Y.; Keum, J. K.; Hiltner, A.; Baer, E. Effect of substrate on the isothermal crystallization kinetics of confined poly(ϵ -caprolactone) nanolayers. *Macromolecules* **2010**, 43(20), 8619-8627 DOI: 10.1021/ma101625h.
77. Lin, Y.; Fan, Y. Substrate effect on the crystallization of isotactic polypropylene. *Journal of Applied Polymer Science* **2012**, 125(1), 233-245 DOI: 10.1002/app.35484.
78. Zhong, L.-W.; Ren, X.-K.; Yang, S.; Chen, E.-Q.; Sun, C.-X.; Stroeks, A.; Yang, T.-Y. Lamellar orientation of polyamide 6 thin film crystallization on solid substrates. *Polymer* **2014**, 55(16), 4332-4340 DOI: 10.1016/j.polymer.2014.06.031.
79. Wang, Y.; Rafailovich, M.; Sokolov, J.; Gersappe, D.; Araki, T.; Zou, Y.; Kilcoyne, A. D.; Ade, H.; Marom, G.; Lustiger, A. Substrate effect on the melting temperature of thin polyethylene films. *Physical review letters* **2006**, 96(2), 028303 DOI: 10.1103/PhysRevLett.96.028303.
80. Bernazzani, P.; Sanchez, R. F. Effect of substrate interactions on the melting behavior of thin polyethylene films. *The European physical journal. E, Soft matter* **2008**, 26(4), 427-34 DOI: 10.1140/epje/i2007-10344-7.
81. Woodard, L. N.; Grunlan, M. A. Hydrolytic degradation and erosion of polyester biomaterials. *ACS Macro Letters* **2018**, 7(8), 976-982 DOI: 10.1021/acsmacrolett.8b00424.
82. Visan, A. I.; Popescu-Pelin, G.; Socol, G. Degradation behavior of polymers used as coating materials for drug delivery-a basic review. *Polymers* **2021**, 13(8), 1272 DOI: 10.3390/polym13081272.
83. Rey-Vinolàs, S.; Engel, E.; Mateos-Timoneda, M. A., Chapter 7 - Polymers for bone repair. In *Bone Repair Biomaterials (Second Edition)*, Pawelec, K. M., Planell, J. A., Eds. Woodhead Publishing: **2019**; pp 179-197 DOI: 10.1016/B978-0-08-102451-5.00007-X.
84. Zhang, X.; Espiritu, M.; Bilyk, A.; Kurniawan, L. Morphological behaviour of poly(lactic acid) during hydrolytic degradation. *Polymer Degradation and Stability* **2008**, 93(10), 1964-1970 DOI: 10.1016/j.polymdegradstab.2008.06.007.
85. Burkersroda, F. v.; Schedl, L.; Göpferich, A. Why degradable polymers undergo surface erosion or bulk erosion. *Biomaterials* **2002**, 23(21), 4221-4231 DOI: 10.1016/S0142-9612(02)00170-9.
86. Machatschek, R.; Schulz, B.; Lendlein, A. Quantitative model and thin film studies relating molecular architecture and degradation of multifunctional materials. *Cell Reports Physical Science* **2020**, 1(1), 100009 DOI: 10.1016/j.xcrp.2019.100009.
87. Bornscheuer, U.; Reif, O.-W.; Lausch, R.; Freitag, R.; Scheper, T.; Kolisis, F. N.; Menge, U. Lipase of *Pseudomonas cepacia* for biotechnological purposes: purification, crystallization and characterization. *Biochimica et Biophysica Acta (BBA) - General Subjects* **1994**, 1201(1), 55-60 DOI: 10.1016/0304-4165(94)90151-1.
88. Mannix, A. J.; Kiraly, B.; Hersam, M. C.; Guisinger, N. P. Synthesis and chemistry of elemental 2D materials. *Nature Reviews Chemistry* **2017**, 1(2), 0014 DOI: 10.1038/s41570-016-0014.
89. Yu, J.; Li, J.; Zhang, W.; Chang, H. Synthesis of high quality two-dimensional materials via chemical vapor deposition. *Chemical Science* **2015**, 6(12), 6705-6716 DOI: 10.1039/C5SC01941A.
90. Sakamoto, J.; van Heijst, J.; Lukin, O.; Schlüter, A. D. Two-dimensional polymers: just a dream of synthetic chemists? *Angewandte Chemie International Edition* **2009**, 48(6), 1030-1069 DOI: 10.1002/anie.200801863.
91. Dong, R.; Zhang, T.; Feng, X. Interface-assisted synthesis of 2D materials: trend and challenges. *Chemical Reviews* **2018**, 118(13), 6189-6235 DOI: 10.1021/acs.chemrev.8b00056.

92. Ariga, K.; Yamauchi, Y.; Mori, T.; Hill, J. P. 25th anniversary article: What can be done with the Langmuir-Blodgett method? Recent developments and its critical role in materials science. *Advanced Materials* **2013**, 25(45), 6477-6512 DOI: 10.1002/adma.201302283.
93. Petty, M. C. Langmuir-Blodgett Films: An Introduction. *Cambridge University Press* **1996** 39-63 DOI: 10.1002/adma.19970091019.
94. C., D. M.; Mert, V.; Mauricio, T. Composites of proteins and 2D nanomaterials. *Advanced Functional Materials* **2018**, 28, 1704990 DOI: 10.1002/adfm.201704990.
95. Zhou, H.; Toney, M. F.; Bent, S. F. Cross-linked ultrathin polyurea films via molecular layer deposition. *Macromolecules* **2013**, 46(14), 5638-5643 DOI: 10.1021/ma400998m.
96. Burdon, R. S. Surface tension and the spreading of liquids. *Nature* **2014** 147, 659 DOI: 10.1038/147659c0.
97. Sanchez-Gonzalez, J.; Ruiz-Garcia, J.; Galvez-Ruiz, M. J. Langmuir-Blodgett films of biopolymers: a method to obtain protein multilayers. *Journal of Colloid and Interface Science* **2003**, 267(2), 286-93 DOI: 10.1016/s0021-9797(03)00754-9
98. Brewster, D. On the laws which regulate the polarisation of light by reflexion from transparent bodies. *Philosophical transactions of the Royal Society of London* **1815** 105, DOI: 10.1098/rstl.1815.0010.
99. Blaudez, D.; Turllet, J.-M.; Dufourcq, J.; Bard, D.; Buffeteau, T.; Desbat, B. Investigations at the air/water interface using polarization modulation IR spectroscopy. *Journal of the Chemical Society, Faraday Transactions* **1996**, 92(4), 525-530 DOI: 10.1039/FT9969200525.
100. Machatschek, R.; Saretia, S.; Lendlein, A. Assessing the influence of temperature-memory creation on the degradation of copolyesterurethanes in ultrathin films. *Advanced Materials Interfaces* **2021**, 8(6), 2001926 DOI: 10.1002/admi.202001926.
101. Schöne, A.-C.; Kratz, K.; Schulz, B.; Lendlein, A. Polymer architecture versus chemical structure as adjusting tools for the enzymatic degradation of oligo(ϵ -caprolactone) based films at the air-water interface. *Polymer Degradation and Stability* **2016**, 131, 114-121 DOI: 10.1016/j.polymdegradstab.2016.07.010.
102. Li, B.; Esker, A. R. Molar mass dependent growth of poly(ϵ -caprolactone) crystals in langmuir films. *Langmuir* **2007**, 23(5), 2546-2554 DOI: 10.1021/la062563f.
103. Schöne, A.-C.; Roch, T.; Schulz, B.; Lendlein, A. Evaluating polymeric biomaterial-environment interfaces by Langmuir monolayer techniques. *Journal of The Royal Society Interface* **2017**, 14(130), 20161028 DOI: 10.1098/rsif.2016.1028.
104. Scheibe, P.; Schoenhentz, J.; Platen, T.; Hoffmann-Röder, A.; Zentel, R. Langmuir-Blodgett films of fluorinated glycolipids and polymerizable lipids and their phase separating behavior. *Langmuir* **2010**, 26(23), 18246-18255 DOI: 10.1021/la1029917.
105. Kloppner, L. J.; Batten, J. H.; Duran, R. S. Surface behavior and polymerization of 2- and 3-(1-octadecynyl)aniline at the air-aqueous interface. *Macromolecules* **2000**, 33(21), 8006-8011 DOI: 10.1021/ma9916584.
106. Fichet, O.; Plesse, C.; Teyssié, D. Spontaneous styrene sulfonate polymerization in Langmuir films: evidence for an anionic mechanism. *Colloids and Surfaces A: Physicochemical and Engineering Aspects* **2004**, 244(1), 121-130 DOI: 10.1016/j.colsurfa.2004.05.017.
107. Fichet, O.; Teyssié, D. A new type of spontaneous vinyl monomer polymerization in langmuir films. *Macromolecules* **2002**, 35(14), 5352-5354 DOI: 10.1021/ma020190t.
108. Upcher, A.; Lifshitz, Y.; Zeiri, L.; Golan, Y.; Berman, A. Effect of metal cations on polydiacetylene Langmuir films. *Langmuir* **2012**, 28(9), 4248-4258 DOI: 10.1021/la204735t.

109. El Haitami, A.; Backus, E. H. G.; Cantin, S. Synthesis at the air–water interface of a two-dimensional semi-interpenetrating network based on poly(dimethylsiloxane) and cellulose acetate butyrate. *Langmuir* **2014**, 30(40), 11919-11927 DOI: 10.1021/la502514e.
110. Matmour, R.; J Joncheray, T.; Gnanou, Y.; S Duran, R. Two-Dimensional Polymeric Nanomaterials through Cross-linking of Polybutadiene- b -Poly(ethylene oxide) Monolayers at the Air/Water Interface. *Langmuir* **2007**, 23, 649-58 DOI: 10.1021/la062256+.
111. Matmour, R.; J Joncheray, T.; Gnanou, Y.; S Duran, R. Cross-linking of polybutadiene at the air/water interface: Toward an easy access to two-dimensional polymeric materials. *Journal of Colloid and Interface Science* **2007**, 311, 315-21 DOI: 10.1016/j.jcis.2007.02.065.
112. Carino, S. R.; Duran, R. S.; Baney, R. H.; Gower, L. A.; He, L.; Sheth, P. K. Chemical cross-linking, surface compressional modulus, and viscosity of n-octadecyltrimethoxy silane monolayers. *Journal of the American Chemical Society* **2001**, 123(9), 2103-2104 DOI: 10.1021/ja0055514.
113. Payamyar, P.; Kaja, K.; Ruiz-Vargas, C.; Stemmer, A.; Murray, D. J.; Johnson, C. J.; King, B. T.; Schiffmann, F.; VandeVondele, J.; Renn, A.; Götzinger, S.; Ceroni, P.; Schütz, A.; Lee, L.-T.; Zheng, Z.; Sakamoto, J.; Schlüter, A. D. Synthesis of a covalent monolayer sheet by photochemical anthracene dimerization at the air/water interface and its mechanical characterization by AFM indentation. *Advanced Materials* **2014**, 26(13), 2052-2058 DOI: 10.1002/adma.201304705.
114. Dai, W.; Lee, L.-T.; Schütz, A.; Zelenay, B.; Zheng, Z.; Borgschulte, A.; Döbeli, M.; Abuillan, W.; Konovalov, O. V.; Tanaka, M.; Schlüter, A. D. Three-legged 2,2'-bipyridine monomer at the air/water interface: monolayer structure and reactions with Ni(ii) ions from the subphase. *Langmuir* **2017**, 33(7), 1646-1654 DOI: 10.1021/acs.langmuir.6b04282.
115. Kayal, H.; Ahmida, M. M.; Dufour, S.; Taing, H.; Eichhorn, S. H. Cross-linking of discotic tetraazaporphyrin dyes in 2 and 3 dimensions by "click" chemistry. *Journal of Materials Chemistry C* **2013**, 1(42), 7064-7072 DOI: 10.1039/C3TC31588F.
116. Bauer, T.; Zheng, Z.; Renn, A.; Enning, R.; Stemmer, A.; Sakamoto, J.; Schlüter, A. D. Synthesis of free-standing, monolayered organometallic sheets at the air/water interface. *Angewandte Chemie International Edition* **2011**, 50(34), 7879-7884 DOI: 10.1002/anie.201100669.
117. Dong, R.; Pfeffermann, M.; Liang, H.; Zheng, Z.; Zhu, X.; Zhang, J.; Feng, X. Large-area, free-standing, two-dimensional supramolecular polymer single-layer sheets for highly efficient electrocatalytic hydrogen evolution. *Angewandte Chemie International Edition* **2015**, 54(41), 12058-12063 DOI: 10.1002/anie.201506048.
118. Murray, D. J.; Patterson, D. D.; Payamyar, P.; Bhola, R.; Song, W.; Lackinger, M.; Schlüter, A. D.; King, B. T. Large area synthesis of a nanoporous two-dimensional polymer at the air/water interface. *Journal of the American Chemical Society* **2015**, 137(10), 3450-3453 DOI: 10.1021/ja512018j.
119. Zheng, Z.; Ruiz-Vargas, C. S.; Bauer, T.; Rossi, A.; Payamyar, P.; Schutz, A.; Stemmer, A.; Sakamoto, J.; Schluter, A. D. Square-micrometer-sized, free-standing organometallic sheets and their square-centimeter-sized multilayers on solid substrates. *Macromol Rapid Commun* **2013**, 34(21), 1670-80 DOI: 10.1002/marc.201300624.
120. Cui, Y.; Jin, R.; Zhou, Y.; Yu, M.; Ling, Y.; Wang, L.-Q. Crystallization enhanced thermal-sensitive hydrogels of PCL-PEG-PCL triblock copolymer for 3D printing. *Biomedical Materials* **2021**, 16(3), 035006 DOI: 10.1088/1748-605x/abc38e.

121. Malikmammadov, E.; Tanir, T. E.; Kiziltay, A.; Hasirci, V.; Hasirci, N. PCL and PCL-based materials in biomedical applications. *Journal of biomaterials science. Polymer edition* **2018**, 29(7-9), 863-893 DOI: 10.1080/09205063.2017.1394711.
122. Holländer, J.; Genina, N.; Jukarainen, H.; Khajeheian, M.; Rosling, A.; Mäkilä, E.; Sandler, N. Three-dimensional printed PCL-based implantable prototypes of medical devices for controlled drug delivery. *Journal of pharmaceutical sciences* **2016**, 105(9), 2665-2676 DOI: 10.1016/j.xphs.2015.12.012.
123. Xu, W.; Kwok, K. S.; Gracias, D. H. Ultrathin shape change smart materials. *Accounts of Chemical Research* **2018**, 51(2), 436-444 DOI: 10.1021/acs.accounts.7b00468.
124. Dalnoki-Veress, K.; Forrest, J.; Massa, M.; Pratt, A.; Williams, A. Crystal growth rate in ultrathin films of poly(ethylene oxide). *Journal of Polymer Science Part B: Polymer Physics* **2001**, 39, 2615-2621 DOI: 10.1002/polb.10018.
125. Capitán, M. J.; Rueda, D. R.; Ezquerro, T. A. Inhibition of the crystallization in nanofilms of poly(3-hydroxybutyrate). *Macromolecules* **2004**, 37(15), 5653-5659 DOI: 10.1021/ma049576p.
126. Schönherr, H.; Frank, C. W. Ultrathin films of poly(ethylene oxides) on oxidized silicon. 2. in situ study of crystallization and melting by hot stage AFM. *Macromolecules* **2003**, 36(4), 1199-1208 DOI: 10.1021/ma020686a.
127. Napolitano, S.; Wübberhorst, M. Slowing down of the crystallization kinetics in ultrathin polymer films: a size or an interface effect? *Macromolecules* **2006**, 39, 5967-5970 DOI: 10.1021/ma061304u.
128. Tarazona, N. A.; Machatschek, R.; Lendlein, A. Influence of depolymerases and lipases on the degradation of polyhydroxyalkanoates determined in langmuir degradation studies. *Advanced Materials Interfaces* **2020**, 7(17), 2000872 DOI: 10.1002/admi.202000872.
129. Hobbs, J. K.; Barham, P. J. The effect of water on the crystallization of thin films of poly(hydroxybutyrate). *Polymer* **1997**, 38(15), 3879-3883 DOI: 10.1016/S0032-3861(96)00945-7.
130. Kikkawa, Y.; Fujita, M.; Abe, H.; Doi, Y. Effect of water on the surface molecular mobility of poly(lactide) thin films: an atomic force microscopy study. *Biomacromolecules* **2004**, 5(4), 1187-93 DOI: 10.1021/bm0345007.
131. Yu, X.; Wang, N.; Lv, S. Crystal and multiple melting behaviors of PCL lamellae in ultrathin films. *Journal of Crystal Growth* **2016**, 438, 11-18 DOI: 10.1016/j.jcrysgro.2015.12.021.
132. Kim, J.; Jung, H. Y.; Park, M. J. End-group chemistry and junction chemistry in polymer science: past, present, and future. *Macromolecules* **2020**, 53(3), 746-763 DOI: 10.1021/acs.macromol.9b02293.
133. Kawazu, K.; Nakagawa, S.; Ishizone, T.; Nojima, S.; Arai, D.; Yamaguchi, K.; Nakahama, S. Effects of bulky end-groups on the crystallization kinetics of poly(ϵ -caprolactone) homopolymers confined in a cylindrical nanodomain. *Macromolecules* **2017**, 50(18), 7202-7210 DOI: 10.1021/acs.macromol.7b01536.
134. Wang, Y.; Ge, S.; Rafailovich, M.; Sokolov, J.; Zou, Y.; Ade, H.; Lüning, J.; Lustiger, A.; Maron, G. Crystallization in the thin and ultrathin films of poly(ethylene-vinyl acetate) and linear low-density polyethylene. *Macromolecules* **2004**, 37(9), 3319-3327 DOI: 10.1021/ma030456b.
135. Flieger, A.-K.; Schulz, M.; Thurn-Albrecht, T. Interface-induced crystallization of polycaprolactone on graphite via first-order prewetting of the crystalline phase. *Macromolecules* **2018**, 51(1), 189-194 DOI: 10.1021/acs.macromol.7b02113.
136. Hermanová, S.; Omelková, J.; Voběrková, S.; Bálková, R.; Richtera, L.; Mravcová, L.; Jančář, J. The effect of processing of polycaprolactone films on degradation process

- initiated by aspergillus oryzae lipase. *International Journal of Polymer Analysis and Characterization* **2012**, 17(6), 465-475 DOI: 10.1080/1023666X.2012.696402.
137. Machatschek, R.; Saretia, S.; Lendlein, A. The interplay between network morphology and degradation kinetics of polymers: Theoretical and experimental analysis by means of a 2D model system. *MRS Advances* **2019**, 5(12-13), 679-691 DOI: 10.1557/adv.2019.457.
 138. Liu, Q.; Wang, H.; Chen, L.; Li, W.; Zong, Y.; Sun, Y.; Li, Z. Enzymatic degradation of fluorinated poly(ϵ -caprolactone) (PCL) block copolymer films with improved hydrophobicity. *Polymer Degradation and Stability* **2019**, 165, DOI: 10.1016/j.polymdegradstab.2019.04.018.
 139. Stahl, T.; Mattern, D.; Brunn, H. Toxicology of perfluorinated compounds. *Environmental Sciences Europe* **2011**, 23(1), 38 DOI: 10.1186/2190-4715-23-38.
 140. Johnson, B. M.; Shu, Y.-Z.; Zhuo, X.; Meanwell, N. A. Metabolic and Pharmaceutical Aspects of Fluorinated Compounds. *Journal of Medicinal Chemistry* **2020**, 63(12), 6315-6386 DOI: 10.1021/acs.jmedchem.9b01877.
 141. Jiang, N.; Jiang, S.; Hou, Y.; Yan, S.; Zhang, G.; Gan, Z. Influence of chemical structure on enzymatic degradation of single crystals of PCL-b-PEO amphiphilic block copolymer. *Polymer* **2010**, 51(11), 2426-2434 DOI: 10.1016/j.polymer.2010.03.058.
 142. Su, F.; Iwata, T.; Tanaka, F.; Doi, Y. Crystal structure and enzymatic degradation of poly(4-hydroxybutyrate). *Macromolecules* **2003**, 36(17), 6401-6409 DOI: 10.1021/ma034546s.
 143. Hoare, T. R.; Kohane, D. S. Hydrogels in drug delivery: Progress and challenges. *Polymer* **2008**, 49(8), 1993-2007 DOI: 10.1016/j.polymer.2008.01.027.
 144. Wang, J.-J.; Yang, H.-C.; Wu, M.-B.; Zhang, X.; Xu, Z.-K. Nanofiltration membranes with cellulose nanocrystals as an interlayer for unprecedented performance. *Journal of Materials Chemistry A* **2017**, 5(31), 16289-16295 DOI: 10.1039/C7TA00501F.
 145. Wang, J.; Gao, W. Nano/microscale motors: biomedical opportunities and challenges. *ACS Nano* **2012**, 6(7), 5745-5751 DOI: 10.1021/nn3028997.
 146. Liu, M.; Liu, L.; Gao, W.; Su, M.; Ge, Y.; Shi, L.; Zhang, H.; Dong, B.; Li, C. Y. A micromotor based on polymer single crystals and nanoparticles: toward functional versatility. *Nanoscale* **2014**, 6(15), 8601-8605 DOI: 10.1039/C4NR02593H.
 147. Kato, S.; Furukawa, S.; Aoki, D.; Goseki, R.; Oikawa, K.; Tsuchiya, K.; Shimada, N.; Maruyama, A.; Numata, K.; Otsuka, H. Crystallization-induced mechanofluorescence for visualization of polymer crystallization. *Nature Communications* **2021**, 12(1), 126 DOI: 10.1038/s41467-020-20366-y.
 148. Zhao, Y.; Bernitzky, R. H. M.; Kory, M. J.; Hofer, G.; Hofkens, J.; Schlüter, A. D. Decorating the edges of a 2D polymer with a fluorescence label. *Journal of the American Chemical Society* **2016**, 138(28), 8976-8981 DOI: 10.1021/jacs.6b05456.
 149. Dubault, A.; VeyssiÉ, M.; Liebert, L.; Strzelecki, L. Cross-linked polymerization of monolayers of 1-n-octadecyloxy-2-3-diacryloyloxy propane. *Nature Physical Science* **1973**, 245(145), 94-95 DOI: 10.1038/phyci245094a0.
 150. Beredjick, N.; Burlant, W. J. Polymerization of monolayers of vinyl and divinyl monomers. *Journal of Polymer Science Part A-1: Polymer Chemistry* **1970**, 8(10), 2807-2818 DOI: 10.1002/pol.1970.150081007.
 151. Day, D.; Hub, H. H.; Ringsdorf, H. Polymerization of mono- and bi-functional diacetylene derivatives in monolayers at the gas-water interface. *Israel Journal of Chemistry* **1979**, 18(3-4), 325-329 DOI: 10.1002/ijch.197900050.
 152. Kunitake, M.; Nishi, T.; Yamamoto, H.; Nasu, K.; Manabe, O.; Nakashima, N. Preparation and characterization of two-dimensional cross-linked monolayers and langmuir-blodgett films of oligo(dimethylsiloxane) copolymer. *Langmuir* **1994**, 10(9), 3207-3212 DOI: 10.1021/la00021a051.

153. Arslanov, V. V.; Sheinina, L. S.; Kalinina, M. A. Immobilization of functionalized molecules and nanoparticles in organic 2D networks as a method for the preparation of stable supramolecular devices. *Protection of Metals* **2008**, 44(1), 1-21 DOI: 10.1134/S0033173208010013.
154. Rabe, J. P.; Rabolt, J. F.; Brown, C. A.; Swalen, J. D. Polymerization of two unsaturated fatty acid esters in Langmuir-Blodgett films as studied by IR spectroscopy. *Thin Solid Films* **1985**, 133(1), 153-159 DOI: 10.1016/0040-6090(85)90435-3.
155. Day, D. R.; Ringsdorf, H. The monolayer polymerization of 10,12-nonacosadiynoic acid studied by a spectroscopic technique. Polyreactions in ordered systems, 19. *Die Makromolekulare Chemie* **1979**, 180(4), 1059-1063 DOI: 10.1002/macp.1979.021800424.
156. Day, D.; Ringsdorf, H. Polymerization of diacetylene carbonic acid monolayers at the gas-water interface. *Journal of Polymer Science: Polymer Letters Edition* **1978**, 16(5), 205-210 DOI: 10.1002/pol.1978.130160501.
157. Naegele, D.; Ringsdorf, H. Polyreactions in ordered systems: Polymerization of octadecyl methacrylate in monolayers at the gas-water interface. *Journal of Polymer Science: Polymer Chemistry Edition* **1977**, 15(12), 2821-2834 DOI: 10.1002/pol.1977.170151202.
158. Dérue, V.; Alexandre, S.; Valleton, J. M. Polymerization of an elaidic acid langmuir film prepared on a terbium-containing subphase. *Journal of Colloid and Interface Science* **1999**, 213(2), 546-551 DOI: 10.1006/jcis.1999.6166.
159. Zhang, X.; Lv, Y.; Yang, H.-C.; Du, Y.; Xu, Z.-K. Polyphenol coating as an interlayer for thin-film composite membranes with enhanced nanofiltration performance. *ACS Applied Materials & Interfaces* **2016**, 8(47), 32512-32519 DOI: 10.1021/acsami.6b10693.
160. Berkovic, G.; Rasing, T.; Shen, Y. R. Study of monolayer polymerization using nonlinear optics. *The Journal of Chemical Physics* **1986**, 85(12), 7374-7376 DOI: 10.1063/1.451325.
161. Letts, S. A.; Fort, T.; Lando, J. B. Polymerization of oriented monolayers of vinyl stearate. *Journal of Colloid and Interface Science* **1976**, 56(1), 64-75 DOI: 10.1016/0021-9797(76)90147-8.
162. Hatada, M.; Nishii, M.; Hirota, K. Radiation-induced polymerization of monomolecular film of octadecyl acrylate at gas-water interface. *Journal of Colloid and Interface Science* **1973**, 45(3), 502-506 DOI: 10.1016/0021-9797(73)90165-3.
163. Scheibe, G.; Schuller, H. Über die polymerisation monomolekularer filme von vinylisobutyläther. *Zeitschrift für Elektrochemie, Berichte der Bunsengesellschaft für physikalische Chemie* **1955**, 59(9), 861-862 DOI: 10.1002/bbpc.19550590907.
164. Gee, G.; Rideal, E. K. Reaction in monolayers of drying oils I - The oxidation of the maleic anhydride compound of β -Elaeostearin. *Proceedings of the Royal Society of London. Series A - Mathematical and Physical Sciences* **1935**, 153(878), 116-128 DOI: 10.1098/rspa.1935.0224.
165. Dubault, A.; Casagrande, C.; Veyssie, M. Two-dimensional polymerization processes in mono- and diacrylic esters. *The Journal of Physical Chemistry* **1975**, 79(21), 2254-2259 DOI: 10.1021/j100588a011.
166. Dérue, V.; Alexandre, S.; Valleton, J. M. Polymerization of aminoethyl elaidamide in langmuir and Langmuir-Blodgett films studied by SFM. *Langmuir* **1999**, 15(11), 3852-3858 DOI: 10.1021/la9809325.
167. Lindén, M.; Slotte, J. P.; Rosenholm, J. B. Two-dimensional gelation: octadecyltrimethoxysilane at the air/water interface. *Langmuir* **1996**, 12(18), 4449-4454 DOI: 10.1021/la960256b.

168. Takahashi, A.; Yamamoto, H. Polycondensation in monomolecular layers of poly(p-vinylphenol), formaldehyde, and hexamethylenetetramine. *Polymer Journal* **1980**, 12(2), 79-85 DOI: 10.1295/polymj.12.79.
169. Lindén, M.; Györvary, E.; Peltonen, J.; Rosenholm, J. B. UV-induced reactivity of linoleic acid monolayers. The influence of subphase conditions. *Colloids and Surfaces A: Physicochemical and Engineering Aspects* **1995**, 102, 105-115 DOI: 10.1016/0927-7757(95)03278-L.
170. Viitala, T.; Peltonen, J. UV-induced reaction kinetics of dilinoleoylphosphatidylethanolamine monolayers. *Biophysical Journal* **1999**, 76(5), 2803-2813 DOI: 10.1016/S0006-3495(99)77434-5.
171. Matmour, R.; Joncheray, T. J.; Gnanou, Y.; Duran, R. S. Cross-linking of polybutadiene at the air/water interface: Toward an easy access to two-dimensional polymeric materials *Journal of Colloid and Interface Science* **2007**, 311(1), 315-321 DOI: 10.1016/j.jcis.2007.02.065.
172. Kloeppner, L. J.; Duran, R. S. Langmuir film polymerization of 1,22-bis(2-aminophenyl)docosane: a two-dimensional cross-linked polyalkylaniline. *Journal of the American Chemical Society* **1999**, 121(35), 8108-8109 DOI: 10.1021/ja990142x.
173. de Samaniego, M. S. S.; Miller, A. F. 2-dimensional network formation from a graft copolymer at the air-water interface. *Macromolecular Symposia* **2007**, 256(1), 167-174 DOI: 10.1002/masy.200751019.
174. Rolandi, R.; Paradiso, R.; Fendler, J. H. Polymerized monolayers from a styrene functionalized surfactant. *Colloids and Surfaces* **1989**, 35(2), 343-351 DOI: 10.1016/0166-6622(89)80307-5.
175. Haroun, F.; El Haitami, A.; Ober, P.; Backus, E. H. G.; Cantin, S. Poly(ethylene glycol)-block-poly(propylene glycol)-block-poly(ethylene glycol) Copolymer 2D Single Network at the Air–Water Interface. *Langmuir* **2020**, 36(31), 9142-9152 DOI: 10.1021/acs.langmuir.0c01398.
176. Vaillard, A.-S.; El Haitami, A.; Dreier, L. B.; Backus, E. H. G.; Cantin, S. Confinement and cross-linking of 1,2-polybutadiene in two dimensions at the air–water interface. *Langmuir* **2020**, 36(4), 862-871 DOI: 10.1021/acs.langmuir.9b03297.
177. Bubeck, C. Reactions in monolayers and Langmuir-Blodgett films. *Thin Solid Films* **1988**, 160(1), 1-14 DOI: 10.1016/0040-6090(88)90041-7.
178. Hatada, M.; Nishii, M. Polymerization induced by electron-beam irradiation of octadecyl methacrylate in the form of a multilayer or monolayer. *Journal of Polymer Science: Polymer Chemistry Edition* **1977**, 15(4), 927-935 DOI: 10.1002/pol.1977.170150414.
179. Pena-Francesch, A.; Giltinan, J.; Sitti, M. Multifunctional and biodegradable self-propelled protein motors. *Nature Communications* **2019**, 10(1), 3188 DOI: 10.1038/s41467-019-11141-9.
180. Lendlein, A.; Gould, O. E. C. Reprogrammable recovery and actuation behaviour of shape-memory polymers. *Nature Reviews Materials* **2019**, 4(2), 116-133 DOI: 10.1038/s41578-018-0078-8.
181. Richter, K. N.; Revelo, N. H.; Seitz, K. J.; Helm, M. S.; Sarkar, D.; Saleeb, R. S.; D'Este, E.; Eberle, J.; Wagner, E.; Vogl, C.; Lazaro, D. F.; Richter, F.; Coy-Vergara, J.; Coceano, G.; Boyden, E. S.; Duncan, R. R.; Hell, S. W.; Lauterbach, M. A.; Lehnart, S. E.; Moser, T.; Outeiro, T. F.; Rehling, P.; Schwappach, B.; Testa, I.; Zapiec, B.; Rizzoli, S. O. Glyoxal as an alternative fixative to formaldehyde in immunostaining and super-resolution microscopy. *The EMBO journal* **2018**, 37(1), 139-159 DOI: 10.15252/embj.201695709.

182. Folikumah, M. Y.; Behl, M.; Lendlein, A. Thiol-thioester exchange reactions in precursors enable pH-triggered hydrogel formation. *Biomacromolecules* **2021**, 22(5), 1875-1884 DOI: 10.1021/acs.biomac.0c01690.
183. António, J. P. M.; Russo, R.; Carvalho, C. P.; Cal, P. M. S. D.; Gois, P. M. P. Boronic acids as building blocks for the construction of therapeutically useful bioconjugates. *Chemical Society Reviews* **2019**, 48(13), 3513-3536 DOI: 10.1039/C9CS00184K.
184. Liu, S.; Pan, J.; Zhu, H.; Pan, G.; Qiu, F.; Meng, M.; Yao, J.; Yuan, D. Graphene oxide based molecularly imprinted polymers with double recognition abilities: the combination of covalent boronic acid and traditional non-covalent monomers. *Chemical Engineering Journal* **2016**, 290, DOI: 10.1016/j.cej.2016.01.061.
185. Madikizela, L. M.; Tavengwa, N. T.; Tutu, H.; Chimuka, L. Green aspects in molecular imprinting technology: from design to environmental applications. *Trends in Environmental Analytical Chemistry* **2018**, 17, 14-22 DOI: 10.1016/j.teac.2018.01.001.
186. Lee, K.-S.; Kim, D. S.; Kim, B. S. Biodegradable molecularly imprinted polymers based on poly(ϵ -caprolactone). *Biotechnology and Bioprocess Engineering* **2007**, 12(2), 152-156 DOI: 10.1007/BF03028642.
187. Gagliardi, M.; Bertero, A.; Bifone, A. Molecularly imprinted biodegradable nanoparticles. *Scientific Reports* **2017**, 7, 40046 DOI: 10.1038/srep40046.
188. Moreira, J.; Vale, A. C.; Alves, N. M. Spin-coated freestanding films for biomedical applications. *Journal of Materials Chemistry B* **2021**, 9(18), 3778-3799 DOI: 10.1039/D1TB00233C.
189. Xu, L.; Tetreault, A. R.; Khaligh, H. H.; Goldthorpe, I. A.; Wettig, S. D.; Pope, M. A. Continuous Langmuir–Blodgett deposition and transfer by controlled edge-to-edge assembly of floating 2D materials. *Langmuir* **2019**, 35(1), 51-59 DOI: 10.1021/acs.langmuir.8b03173.

Appendix I: Effect of Water on Crystallization and Melting of Telechelic Oligo(ϵ -caprolactone)s in Ultrathin Films

Shivam Saretia, Rainhard Machatschek, Thanga Bhuvanesh, and Andreas Lendlein*

The thermal behavior of ultrathin, semi-crystalline films of oligo(ϵ -caprolactone)s (OCLs) with hydroxy or methacrylate end groups, is studied by the Langmuir technique in dependence on mean molecular areas and crystallization temperatures. The films on solid substrate as obtained by Langmuir–Schaefer transfer exhibit different lamellar thicknesses, crystal number densities, and lateral sizes. The melting temperature of OCL single crystals at the water and solid surface is proportional to the inverse crystal thickness and generally lower than in bulk PCL. An influence of OCL end groups on the melting behavior is observed mainly at the air–solid interface, where methacrylate end capped OCL melts at lower temperatures than hydroxy end capped OCL. Comparing the underlying substrate, melting/recrystallization of OCL ultrathin films is achievable at lower temperatures at the air–water interface than at the air–solid interface, where recrystallization is not identifiable. Recrystallization at the air–water interface generally occurs at higher temperature than the initial crystallization temperature. The surface pressure, as an additional thermodynamic variable, seems to further affect the crystallization behavior, with crystal thickness and lateral growth rate increasing with surface pressure. The results presented here are important when designing temperature-sensitive or active nanostructured materials or interfaces based on OCL.

1. Introduction

Poly(ϵ -caprolactone) (PCL) is an important material in biomaterial applications, especially as a thermal switch with a transition close to physiological conditions.^[1] PCL oligomers (OCLs) are therefore important building blocks for multifunctional

materials owing to biodegradability, while known synthesis pathways into various end group functionalized telechelics enable flexible strategies for creating thermoreversible crystalline regions.^[2] The interface to the predominantly aqueous environment is of paramount importance for the performance of OCL based materials in biological systems, since nearly all interactions are mediated upon direct contact. The behavior of polymer chains at the interface is very different from the behavior of chains in the bulk, which are buried and strongly entangled, while the chains at the interface are far less restricted. Due to the interaction with water molecules, the energetic situation of polymer chains at the interface will also differ from their counterparts in bulk.^[3] Limiting of chain flexibility by entanglements and crystallites as well as low free volume means that water uptake into bulk PCL is restricted. Yet, water might still interact favorably with the chains and act as a partial solvent. Then, their phase

transitions like crystallization,^[4] as well as other temperature dependent phenomena such as the glass transition,^[5–7] are strongly affected. This is especially applicable for swellable networks and nanostructured materials, where water uptake is near instantaneous and can therefore affect the whole material, not just its surface.^[8] Adequately predicting the switching behavior of OCL-based multifunctional materials in medical applications clearly necessitates taking into account the influence of water, especially at the polymer–water interface.

Thin film experiments are the common approaches to study the behavior of polymer chains at interfaces. These experiments are usually carried out on substrates and in the absence of water and are probably not well suited to replicate the crystallization of chains at the surface of a medical device. On solid surfaces, the polymer chain mobility is extremely constrained, and the solid surface defects cause crystallization by heterogeneous nucleation or prefreezing (formation of thin crystalline layer above melting temperature, T_m).^[9–11] The melting temperature of crystalline films on solid surface can be thickness dependent, for example, from PCL 23K film on a graphite surface, a 127 nm film melts at 63 °C while a thinner 13 nm film melts at 84 °C.^[9] A recrystallization can typically not be observed due to its occurrence during the heating process or dewetting and irreversible adsorption of melted partially crystalline polymer film on solid surfaces.^[12,13]

S. Saretia, Dr. R. Machatschek, T. Bhuvanesh, Prof. A. Lendlein
Institute of Active Polymers
Helmholtz-Zentrum Geesthacht and Berlin-Brandenburg
Center for Regenerative Therapies
Kantstraße 55, 14513 Teltow, Germany
E-mail: andreas.lendlein@hzg.de

S. Saretia, T. Bhuvanesh, Prof. A. Lendlein
Institute of Chemistry
University of Potsdam
Karl-Liebknecht-Straße 24–25, 14476 Potsdam, Germany

 The ORCID identification number(s) for the author(s) of this article can be found under <https://doi.org/10.1002/admi.202001940>.

© 2021 Helmholtz-Zentrum Geesthacht. *Advanced Materials Interfaces* published by Wiley-VCH GmbH. This is an open access article under the terms of the Creative Commons Attribution License, which permits use, distribution and reproduction in any medium, provided the original work is properly cited.

DOI: 10.1002/admi.202001940

Here, we hypothesize that we can understand the influence of water on the thermodynamic transitions of PCL by studying the crystallization and melting of OCL from Langmuir films in dependence of subphase temperature and surface pressure (π). While one would not expect water to be a good substrate for investigating relatively hydrophobic polymers such as PCL or polylactide, experiments with polymers in Langmuir films have taught us that these molecules form 2D polymer solutions at the air–water interface, with the chains of some medically relevant (co)polyesters adopting extended conformations as in good solvents.^[4,14] The ability of these (co)polyesters to form stable investigable films at the air–water interface is due to the hydration of their polar chemical groups, which anchor to the water surface and overall impart an amphiphilic nature to the spread hydrophobic polymer.

Langmuir monolayers are ideally suited for this task, because they avoid the influence of an underlying solid substrate and allow the chains to get swollen by water. During crystallization at the air–liquid interface, the layers have a negligible shear modulus or viscosity, meaning that the effects of chain entanglements on crystallization can be excluded, allowing the study of crystallization without restriction on chain transport, resulting in a crystallization process close to thermodynamic equilibrium.

While polymer crystallization in Langmuir monolayers has been thoroughly investigated,^[4,15,16,17,18] there is an open question, which has so far not been addressed. In bulk and in solution, crystallization is regulated by the degree of undercooling under a characteristic crystallization temperature T_c^* . In Langmuir monolayers of polyesters such as poly(3-*R*-hydroxybutyrate) or PCL,^[4,18,19] crystallization depends on the surface pressure as a second thermodynamic state variable, and crystallization is only observed above a critical surface pressure π^* . The influence of undercooling on the crystallization from melt or solution in terms of crystallization and nucleation rates as well as lamella thickness is extremely well described. It remains to be seen whether the surface pressure has a similar effect as temperature, so that with increasing “overpressure”, crystals become thinner while nucleation and growth rates increase.

To answer this question, crystals grown under different conditions are transferred to solid substrates and their thickness is measured via atomic force microscopy (AFM), which further allows the construction of Gibbs–Thomson plots for OCL crystals in contact with water. We expect the equilibrium melting temperature $T_{m,\infty}$, and also the characteristic crystallization temperature T_c^* , to be substantially lower than in bulk or for crystals at the air–solid interface. The end groups of telechelics, which are used to build architecture materials but have not been converted in a chemical reaction, have different polarity and sterical requirements and will probably also affect the crystallization behavior. We expect the transitions in water shifting to lower temperature when end groups are more hydrophilic.

For this study, two different telechelic OCLs having either hydroxy or methacrylate end groups are applied. Hydroxy and methacrylate end capped polymers are valuable for construction of architected materials, where diols are joined via diisocyanate linkers and methacrylates form networks, both under ambient conditions.^[1,4] OCLs with dimethacrylate or diol end groups are therefore commonly used to introduce thermal switching capability into (multi)functional materials. Yet, these end groups also differ in size and hydrophilicity, and therefore

serve as a representation of either small and hydrophilic, or large and hydrophobic chain terminations, which could occur depending on material architecture. In bulk, it was reported that the influence of end group functionalization on T_m of ethylene glycol initiated OCL diols (OCDMEs) and OCL dimethacrylates (OCMEs) was very small when number average molecular weights (M_n) were above 4000 g mol⁻¹.^[20,21] Therefore, the applied OCL samples for this study are within a M_n range of 4000 to 8000 g mol⁻¹ with a polydispersity index of 1.2, where OCL molecules are also known to form laterally large crystals, which are observable by Brewster Angle Microscopy (BAM) at the air–water interface.^[17] The OCDOL and OCDME used for this study were initiated by either 1,4-butanediol or diethylene glycol. While even for short OCDOLs with M_n of about 1200 g mol⁻¹, the effect of the central initiating unit on the crystallization in bulk is negligible,^[22] at the air–water interface, an influence cannot be ruled out due to the “anchoring effect” of ethylene glycol.^[23]

Crystallization is carried out at air–water interface at constant film area induced by cooling and compressing using the Langmuir trough barriers, resulting in isothermal crystallization with a rate that decreases with time at constant crystallization temperature T_c . In that way, it is possible to observe isolated crystals whereas under constant pressure, films become almost entirely crystalline. Two water subphase temperatures of 12 °C and 21 °C are used as isothermal crystallization temperatures. The melting and recrystallization of OCL films at the air–water interface is studied by altering water subphase temperature at a constant rate. The thermal behavior of partially crystalline OCL films is monitored by in situ Brewster angle microscopy and surface pressure changes. Partially crystallized and recrystallized OCL films from the air–water interface are transferred to silicon substrates via the Langmuir–Schaefer (LS) method (Figure 1) for crystal thickness and morphological investigation by atomic force microscopy. On these samples, using polarizing optical microscopy equipped with a heating stage, the melting temperature at the air–solid interface is studied by heating with a constant rate of 2 °C ± 0.4 °C min⁻¹. The results are analyzed with regard to the Gibbs Thomson equations for crystallization and melting, to facilitate a prediction of the melting temperatures of PCL crystals in aqueous environments. To determine the influence of water, crystallization and melting of OCL at the air–water interface will be compared to results from bulk and from the air–solid interface.

2. Results and Discussion

2.1. OCDOL and OCDME Crystallization at Air–Water Interface at Different MMA and T_c

In the initial step of OCL film crystallization at the air–water interface, compression of spread molecules yields a typical mean molecular area (MMA) versus surface pressure isotherm (Figure 2a,b). The MMA is the mean surface area occupied per ϵ -caprolactone repeat unit, calculated from the number of spread repeat units and the total area of the film. In the OCL surface pressure versus area isotherms, a sudden decrease in surface pressure at MMA <30 Å² is accompanied with the

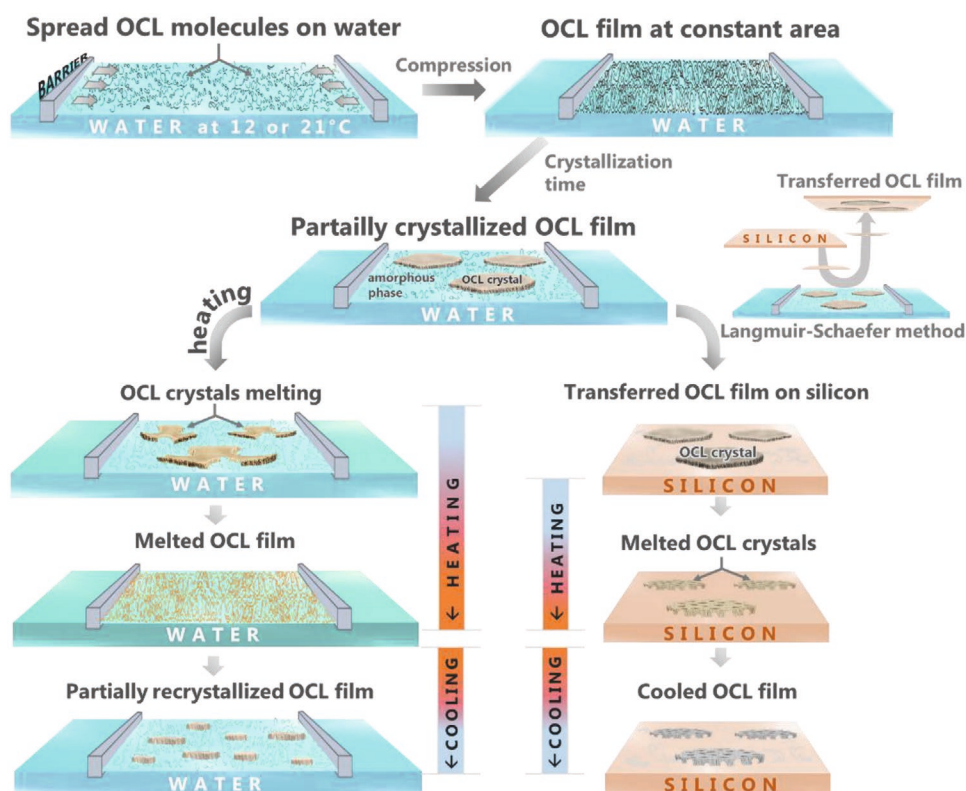


Figure 1. Schematic representation of experimental protocol employed for studying thermodynamics of crystallization and melting of OCL in ultrathin films.

formation of observable crystals in the Brewster Angle microscope. This critical surface pressure π^* in the OCDOL film isotherm (Figure 2a) occurs at $\approx 24 \text{ \AA}^2$ MMA on water at 12 °C or 21 °C, while the OCDME film (Figure 2b) shows the critical surface pressure at a lower MMA of $\approx 18 \text{ \AA}^2$ on water at 12 °C. The OCDME film isotherm (Figure 2b) on water at 21 °C does not show a pronounced critical surface pressure compared to the surface pressure versus area isotherms of OCDME at 12 °C or OCDOL at 21 °C or 12 °C.

2.1.1. Influence of End Groups on Maximum MMA for Crystallization

The BAM images in Figure 2 illustrate the crystal morphologies observed in the OCL films withheld for ≈ 2 h on water at 12 °C or 21 °C, at constant MMA of 22, 18, 15, 12 or 8.5 \AA^2 . At the given MMAs, all OCL films show formation of crystals except the OCDME film held at an MMA of 22 \AA^2 . Here, the OCDOL film is compressed to just above its critical surface pressure, while the OCDME film is slightly below the critical condition. The absence of crystallization in the OCDME film after several hours at 22 \AA^2 shows that the shifted critical surface pressure is not of kinetic origin. Rather, the methacrylate end-groups increase the nucleation barrier for OCL chains at the air–water interface. We emphasize that the difference is not an effect of the M_n , since OCDOLs with a M_n of 3500 g mol^{-1} have a very similar crystallization behavior in Langmuir films when

compared to OCDOLs with a M_n of 8000 g mol^{-1} .^[17] At the air–water interface, there might also be an influence of the central diol unit used as polymerization initiator. The OCDME has a diglyme unit, which is more hydrophilic than the butadiol used for OCDOL, which could contribute to the higher nucleation barrier by anchoring the chains to the interface and preventing the desorption of segments required for crystallization. Yet, this significantly higher nucleation barrier of OCDME correlates well with the bulk properties, where bulk OCDME has a lower T_c of 18 °C, while bulk OCDOL has a T_c of 29 °C, which agrees to a previous study using ethylene glycol initiated oligomers.^[21]

2.1.2. Influence of End Groups on Crystal Habits

The morphology of OCDME crystals is characterized by a parallelogram shape with wavy edges (Figure 2d–7–12), whereas the hydroxy end capped OCL crystals have smoother edges and are less elongated (Figure 2c–1–6). The lateral shape of PCL crystals is determined by the prevalence of (110) and (100) growth sectors. Striations which run outward from the single crystal center, in (110) sectors are continuous and run parallel to the boundaries between the sectors (110) and (100). Striations in (100) sectors are not elongated but granular and non-continuous, and are less pronounced.^[24] These sectors differ in viscoelastic properties^[24] and can be identified as dark and bright areas in the BAM image of the roughly hexagonal OCDOL crystals (Figure 2c). The thermal stability of (100) sectors was found

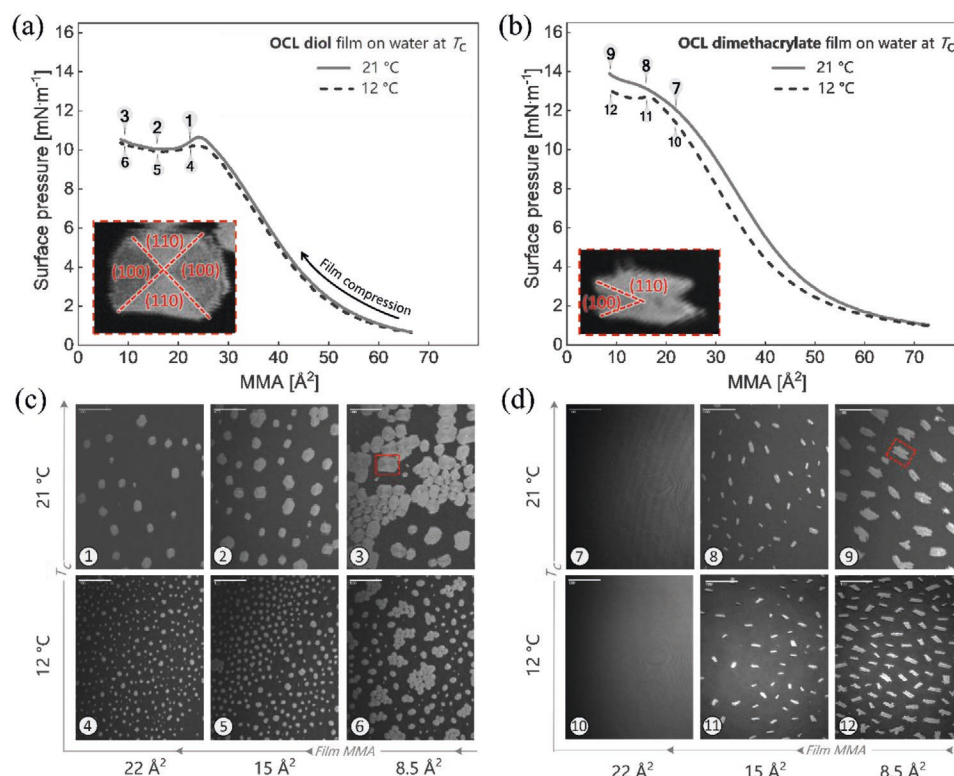


Figure 2. Film compression isotherms of a) OCDOL and b) OCDME at the air–water interface at two different temperatures (12 °C or 21 °C) of the water subphase. The insets show the crystals formed upon high compression at crystallization MMA 8.5 Å². The different growth sectors are marked based on contrast. BAM images (scale bar = 100 μm) for c) OCDOL and d) OCDME were acquired after ≈130 min crystallization time at specific isothermal (constant subphase temperature, 12 °C or 21 °C) and isochoric (constant MMA, 22, 18, 15, 12, or 8.5 Å²) conditions. The boxes mark the positions of the crystals shown in (a) and (b).

to be lower than the one of (110) sectors by other authors.^[24] This suggests that optically darker sectors in the BAM images, which melt at lower temperature are (100) growth sectors (see inset in Figure 2a; and Figure S4, Supporting Information). The elongated shape of the OCDME crystals suggests a prevalence of (110) sectors, in agreement with the generally slightly higher T_m of these crystals at the air–water interface. The greater lateral size of the OCDOL crystals indicates that the prevalence of (110) sectors in OCDME crystals is due to a reduction of the growth rate of (100) sectors in response to the methacrylate end groups. This observation is supported by the inset in Figure 2b where one of the (100) growth sectors is missing from the OCDME crystal.

2.1.3. Influence of Crystallization Temperature on Number Density and Size

OCL films on water at 12 °C (Figures 2c–4–6 and 2d–10–12) show higher number of crystals per unit area, but of smaller crystal size, compared to OCL films on water at 21 °C (Figures 2c–1–3 and 2d–7–9). This dependence of lateral size and number density on crystallization temperature is also seen in the OCDME film at MMA 8.5 Å², but not apparent at MMA 15 Å² (Figure 2d). In OCDOL films at a water temperature of 21 °C, the number of crystals per unit area increases with lowering of crystallization MMA, whereas such a trend is hard to identify for the

other cases. However, under all conditions, the crystals appear laterally bigger at lower MMA, indicating that the growth rate or duration increases with crystallization surface pressure or decreasing MMA.

2.2. Crystallization, Melting, and Recrystallization of OCDOL and OCDME Films

Figure 3 shows the typical plot of surface pressure and temperature as the function of time during a crystallization–melting–recrystallization experiment at the air–water interface. At the constant temperature of the water subphase (12 °C or 21 °C), spread OCL molecules are compressed (increase of surface pressure; typical OCL Langmuir isotherm) to a specific MMA (8.5 Å²) and withheld for 2 h (stabilization of surface pressure). This results in a partially crystalline OCL film at the air–water interface, prepared under isochoric (constant trough area) and isothermal (constant water temperature T_i) conditions (Figure 3c–1,d–4). Here, the surface pressure serves as a convenient indicator for crystal growth. When chain segments are detached from the air–water interface and attached to a crystal, the surface pressure decreases, and hence, a constant surface pressure indicates zero crystal growth. For melting of the partially crystalline OCL film, the water is heated at a constant rate (Figure 3a,b), and the melting temperature range of the partially crystalline OCL film lying on the water surface is identified using

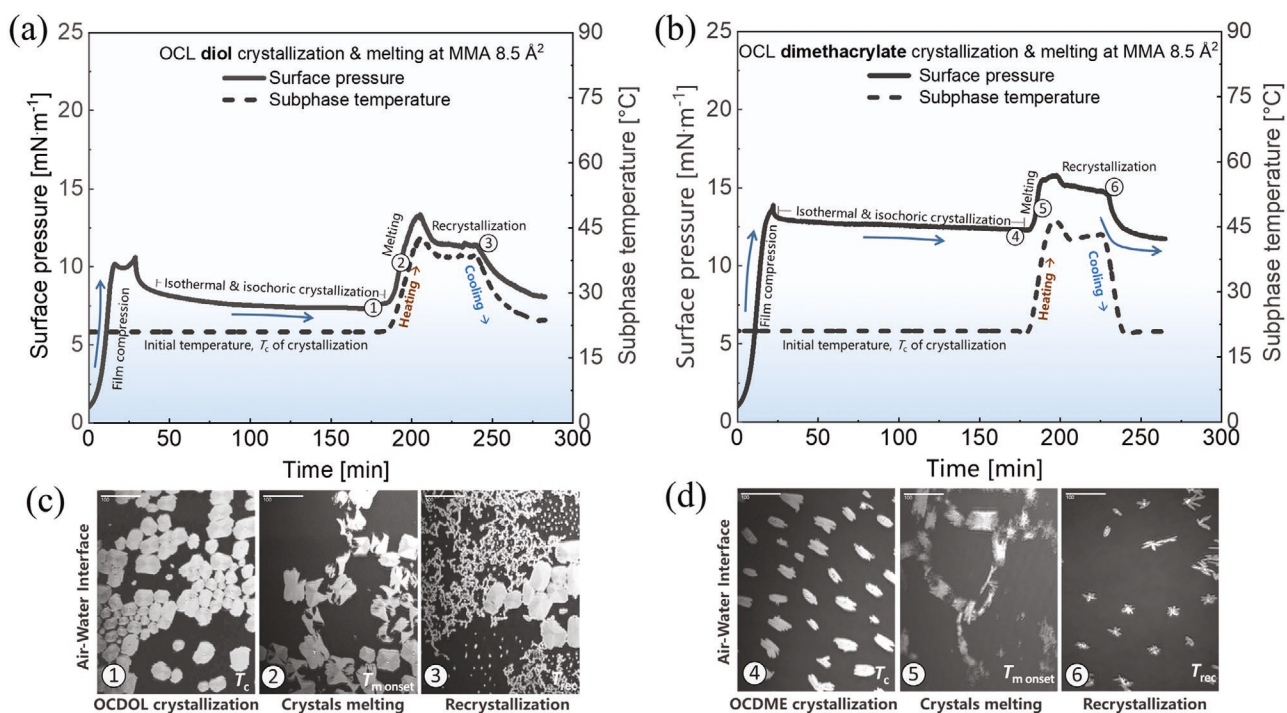


Figure 3. Plot of surface pressure and temperature during a) OCDOL and b) OCDME crystallization, melting, and recrystallization experiment. BAM images (scale bar = 100 μm) c) OCDOL and d) OCDME films acquired at different temperatures and time points. The heating to T_m leads to an increase in surface pressure. Upon cooling to T_{rec} , the layer recrystallizes at nearly constant surface pressure. The surface pressure returns to its initial value upon cooling to the initial temperature (T_c).

the Brewster angle microscopy (see Figure S4a,b, Supporting Information). On the water surface, at $T_{m,onset}$, melting begins in the partially crystalline film where the crystals observable as bright regions in the BAM images start to disappear (Figure 3c-2 and 3d-5). For the OCDOL crystals, the growth sectors appearing darker melt first (see Figure 3c-2). At $T_{m,end}$, melting ends where the BAM image shows absence of any crystalline bright regions (see Figure S4, Supporting Information). The molten OCL film at the air–water interface is recrystallized by cooling the water subphase (Figure 3c-3,d-6). During the cooling of the water subphase, at recrystallization temperature (T_{rec}) the recrystallized entities start to appear as bright regions in the BAM (see Figure S4, Supporting Information), and the film is withheld for 30 mins to allow for recrystallization (Figure 3a,b). The water is cooled further to the initial isothermal crystallization temperature T_c . Here, the surface pressure remains approximately constant over time, indicating that there is no driving force for further crystallization in partially recrystallized OCL. To identify thickness; topography and T_m at the air–solid interface, Langmuir–Schaefer transfers to silicon solid substrates are carried out in separate experiments, both of as-crystallized OCL films, as well as of partially recrystallized OCL films (Figures 4–6).

2.3. Relation of Crystal Thickness with Crystallization MMA and T_c

In Figure 4, the graph and the AFM images of transferred OCL films illustrate the effect of crystallization conditions (MMA or T_c) on the lamellar thickness and morphology. Clearly, the

inverse crystal's thickness is directly proportional to the crystallization MMA, that is.

$$\frac{1}{\text{Crystal thickness}} \propto \text{Crystallization MMA} \propto \text{Film area} \quad (1)$$

In general, for an incompressible film:

$$\frac{1}{\text{Film thickness}} = \frac{\text{Film area}}{\text{Film volume}} \quad (2)$$

This finding suggests that for these ultrathin films, the crystal thickness is directly proportional to the film thickness prior to crystallization. Interestingly, the slope is identical for all conditions and end groups. This even includes recrystallization upon cooling, except for OCDOL crystals formed at 12 °C, where the crystal thickness depends much stronger on the film area. While there is an onset surface pressure for crystallization (critical surface pressure π^*), for OCDOL at both crystallization temperatures and OCDME at 12 °C, the surface pressure π does not increase beyond π^* . Yet, there is a pronounced impact of the MMA, indicating that the film thickness rather than surface pressure, controls the crystallization behavior. The idea of a zero growth layer thickness is in line with the constant surface pressure observed after a certain crystallization period (Figure 3a,b). Here, the layer has reached its minimum layer thickness required for crystallization. If such a zero growth layer thickness did not exist, crystallization would continue until the whole film is crystalline.

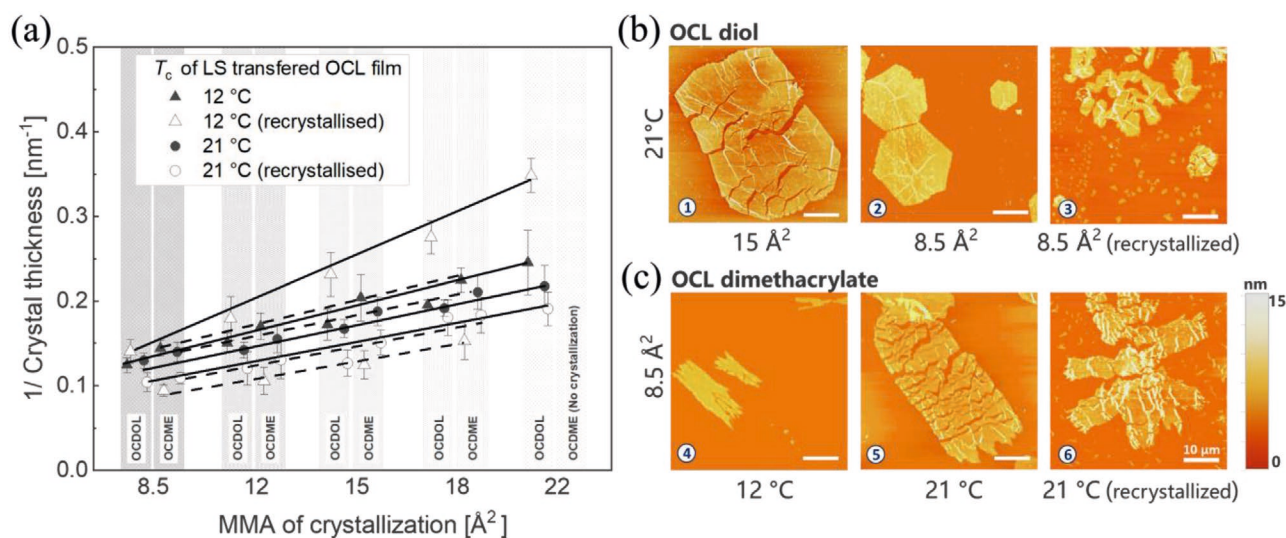


Figure 4. Inverse crystal thickness as a function of mean molecular area (MMA) of OCL crystallization at the air–water interface. a) Trends for both as OCDOL (solid lines) and OCDME (dashed lines) films are represented. Selected topographical AFM images of Langmuir–Schaefer transferred b) OCDOL and c) OCDME at different conditions of crystallization and recrystallization.

The crystallization temperatures (12 °C or 21 °C) of OCL film at the air–water interface largely affect the morphology and number of crystals while the effect of T_c (12 °C or 21 °C) on the crystals thicknesses difference is small (± 0.5 to 1 nm). There is a clear trend

in the lateral crystal dimensions, which increase with decreasing MMA. As observed in bulk polymer crystallization, lowering of the isothermal crystallization temperature at the air–water interface to 12 °C results in a larger nucleation density and slightly reduced

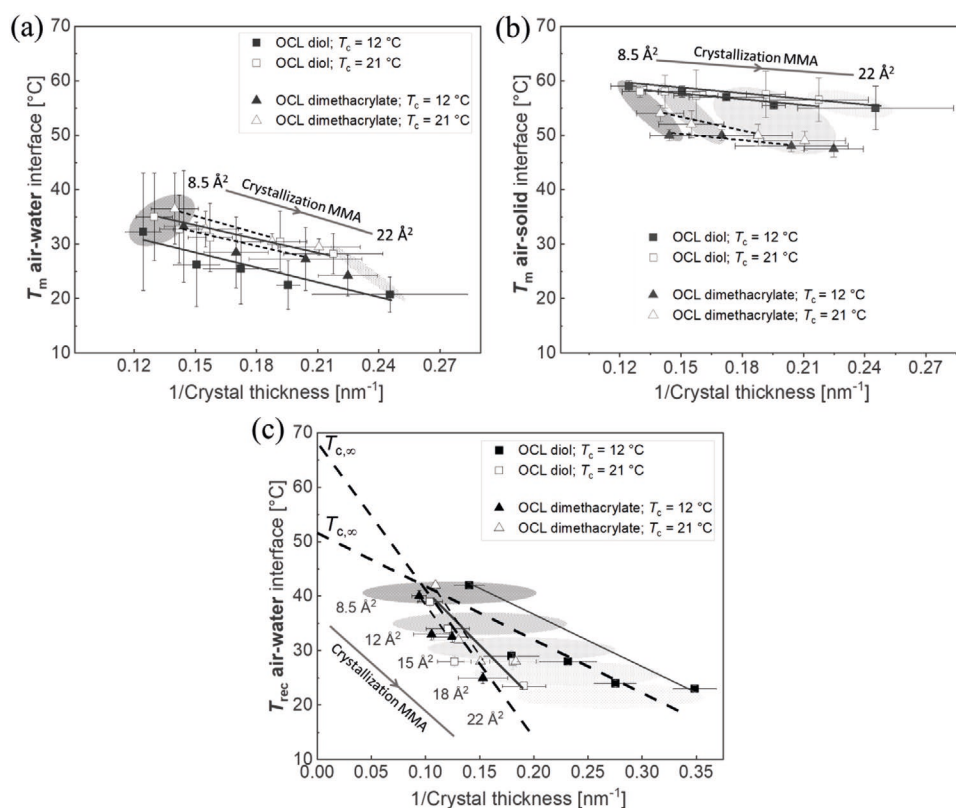


Figure 5. Gibbs–Thomson plot of inverse OCL crystal thickness on function of melting temperature endpoint at the a) air–water interface and b) air–solid interface. Dependence of temperature of OCDOL (straight line) and OCDME (dashed line) to the inverse crystal thickness is represented. c) Gibbs–Thomson plot of recrystallization temperature as a function of inverse OCL crystal thickness at the air–water interface.

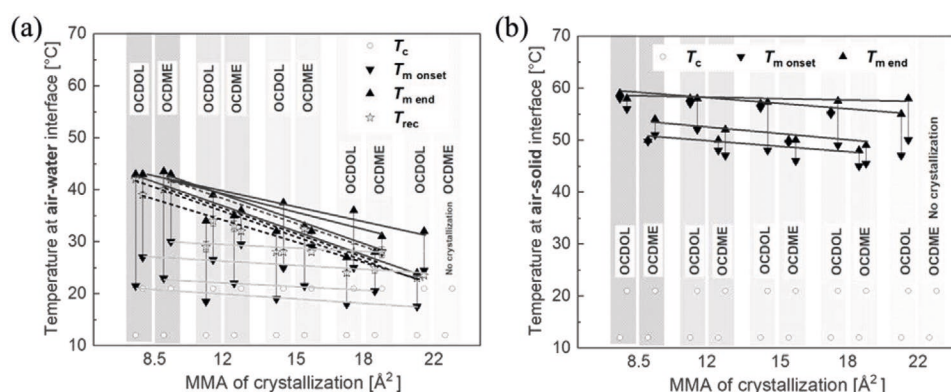


Figure 6. OCL crystallization MMA on function of melting and recrystallization temperatures at the a) air–water interface and the b) air–solid interface. Dependence of $T_{m,end}$ (straight line; dark), $T_{m,onset}$ (straight line; light gray) and T_{rec} (dashed line; dark) to crystallization MMA is represented.

thickness (Figure 4a). The lateral size of the crystals is smaller (Figure 2c,d) at lower crystallization temperature of 12 °C. This is probably due to a higher crystal number density. The higher nucleation density is also indicated by OCDME compression isotherms where a dip is observed at 12 °C, but not at 21 °C (Figure 2b).

The morphology of films of OCDOL (Figure 3c-3) and OCDME (Figure 3d-6) recrystallized at the air–water interface differ from the crystallized film (Figures 3c-1 and 3d-6) but the overall aspect ratio of the crystals is preserved upon recrystallization. These in situ observations by BAM are substantiated by AFM investigation of crystallized and recrystallized OCL films transferred to silicon surfaces (Figure 4b). AFM images of the partially recrystallized OCL films from the water surface show that the morphology and thickness of the recrystallized structures (Figure 4b-3) is different from the crystals prior to melting (Figure 4b-2). Except for the OCDOL film crystallized at 12 °C, in all the OCL films, the recrystallized structures are thicker than the melted OCL crystals, since recrystallization occurs at higher temperatures than crystallization upon compression. The partially recrystallized OCDOL film (Figures 3c-3 and 4b-3) shows presence of connected lamellae, small and large crystals, while the partially recrystallized OCDME film has crystals with protruding lateral lamellae (Figures 3d-6 and 4c-6). It is generally expected that the recrystallized structures are different from as-crystallized structures. By definition, there is no chain-overlap in a monolayer, and hence, there are no entanglements. The lowest MMA of 8.5 Å² corresponds to a thickness of less than three layers, and there are properly not many entanglements created when compressing the monolayer to that state. When single crystals grow from this almost non-entangled film, the chains will cross over during attachment or back-folding. That means that the layer created by melting the single crystals contains more entanglements than the layer before crystallization, and hence, recrystallization proceeds under more constricted conditions than the first crystallization, which explains the disrupted crystal shapes.

2.4. Relation of T_m and T_{rec} with Crystal Thickness, Crystallization MMA, and T_c

The dependence of the melting temperature of lamellar structures on their thickness is described using the Gibbs–Thomson relation,

$$T_m = T_{m,\infty} \left[1 - \frac{2\sigma_e}{l h_f (T_{m,\infty})} \right] \quad (3)$$

where $T_{m,\infty}$ is the melting temperature of infinitely thick crystals, l is thickness of the lamellae, σ_e is surface free energy, and h_f is the enthalpy of fusion. The M_n of the oligomers, OCDOL and OCDME used here is in a range where the bulk melting temperature still increases with M_n , albeit very weakly.^[21] While $M_n(\text{OCDME})$ is lower than the $M_n(\text{OCDOL})$, the Gibbs–Thomson equation is valid for each molecular weight fraction independently. Also, the crystal thickness in our experiments was not affected by the chain length, since the average contour length of the molecules here was around 40 nm (OCDME) or 70 nm (OCDOL). A Gibbs–Thomson plot of T_m versus inverse crystal thickness (Figure 5), shows that the $T_{m,end}$ of partially crystalline OCL films on the water or solid surface is indeed proportional to the inverse crystal thickness, that is,

$$\begin{aligned} &\text{Crystal } T_{m,end} \text{ at air – water} \\ &\text{or air – solid interface} \propto \frac{1}{\text{Crystal thickness}} \end{aligned} \quad (4)$$

The slope of the Gibbs–Thomson plot is much higher for the OCL films on the water surface (Figure 5a) compared to the OCL films on the solid surface (Figure 5b). Also, the stabilities are inverted on the solid substrate, with OCDME crystals showing a substantially lower T_m than the OCDOL crystals. The melting temperature is on average roughly 10 °C lower. The M_n in part accounts for this, with the equilibrium melting point of OCLs with a M_n of 4000 g mol⁻¹ being about 6 °C lower than the equilibrium melting point of the OCL with a M_n of 8000 g mol⁻¹.^[25]

A second Gibbs–Thomson plot is constructed for the recrystallized structures (Figure 5c), where again all materials and conditions exhibit the same behavior except for the OCDOL film crystallized at 12 °C, where the crystal thickness decreases much stronger with T_{rec} . In the OCDOL films crystallized at 12 °C, with lowering of crystallization MMA, the crystal thickness increases but the increase in lateral size is less compared with other crystallization conditions (Figure 2c,d). This perhaps

leads to the anomaly of obtained slopes of Gibbs–Thomson plot for OCDOL films crystallized at 12 °C (Figure 5).

2.5. Dependence of T_m and T_{rec} of OCL Films on the Interface Type

Figure 6 describes the dependence of melting/recrystallization temperature on the functional end groups (hydroxy or methacrylate) and crystallization conditions (MMA or T_c) of OCL films at different surfaces (water or solid silicon substrate). At the air–water interface, the temperature where the most stable crystals in OCDOL and OCDME films melt ($T_{m,end}$), decreases linearly with the MMA. This is expected since $T_m \sim -\frac{1}{\text{Crystal thickness}} \sim -\text{MMA}$ (Equations (1) and (3)). There is a good agreement between materials and conditions on the dependence of $T_{m,end}$ on the mean molecular area before crystallization, except for OCDOL at 21 °C, which shows a lower dependence of T_m on MMA. The recrystallization temperature decreases linearly with the MMA of the film, and therefore with the thickness of the molten layer prior to recrystallization. This implies that the layer thickness influences the thermodynamics of crystallization, with thinner layers requiring greater undercooling to crystallize. Then, the thinner crystals formed in more undercooled Langmuir films are also less stable.

The temperature where the crystals with the lowest stability melt depends only weakly on the MMA of crystallization, which agrees with the idea that the crystal thickness decreases with the thickness of the amorphous layer. When the crystals grow, the thickness of the amorphous layer decreases, resulting in thinner crystals. Crystallization stops at a “zero growth” layer thickness, resulting in a minimum crystal thickness and hence $T_{m,onset}$. The “zero growth” layer thickness decreases with temperature, resulting in a $T_{m,onset}$ that depends on T_c , but not MMA. The slight dependence of $T_{m,onset}$ on the MMA shown in Figure 6a might also be an artifact of the finite heating rates, meaning that the laterally larger crystals formed at lower MMA disappear at slightly higher temperature. At the air–water interface, $T_{m,onset}$ of ODME films is higher than the $T_{m,onset}$ of OCDOL films, potentially because of the different stabilities of (110) and (100) sectors. Yet, on solid surfaces, the $T_{m,onset}$ is lower for the films than for the bulk, which agrees more with the bulk situation where the higher M_n leads to a higher melting temperature.

Altogether, OCL ultrathin films prepared under different crystallization conditions, melt at higher temperature ranges on solid surface (45 °C to 60 °C) compared to films on water surface (20 °C to 45 °C). Also, the dependence of the melting temperature on the crystal thickness is much lower at the air–solid interface. By extrapolating the T_m versus the inverse crystal thickness to infinite crystal thickness, we obtain the equilibrium melting temperatures $T_{m,\infty}$ for both conditions. At the air–water interface, $T_{m,\infty}$ is between 42 °C to 48 °C while at the air–solid interface, $T_{m,\infty}$ is between 53 °C (OCDME) and 65 °C (OCDOL). These values are smaller than the $T_{m,\infty}$ of PCL in bulk, which are 75 °C for a M_n of 8000 g mol⁻¹ and 69 °C for 4000 g mol⁻¹.^[25] Thus, both water and bulky end-groups lead to a lowering of the equilibrium melting point. The melting point in ultra thin films on silicon is lower than the melting point in bulk as well, despite the adsorption to the solid substrate. From

the plot of the recrystallization temperature versus inverse crystal thickness (Figure 5c), we determine the crystallization temperature of infinitely thick PCL crystals at the air–water interface $T_{c,\infty}$. This temperature is at ≈ 55 °C for the OCDOL and at ≈ 70 °C for the OCDME. The finding that $T_{c,\infty}$ is smaller than $T_{m,\infty}$ is in agreement with crystallization in bulk.^[26] Altogether, crystallization and melting in ultra thin films at the air–water interface follows similar laws as in bulk, albeit with generally lower transition temperatures. The slope of T_m versus inverse crystal thickness at the air–water interface (Figure 5a) is much greater than at the air–solid interface (Figure 5b). Since $T_{m,\infty}$ is also smaller, this suggests that the ratio of surface energy to crystallization enthalpy is much greater at the air–water than at the air–solid interface. This is because the amorphous OCL forms a 2D solution at the air–water interface, but the crystalline phase is not stabilized, leading to a decrease of the enthalpy of crystallization.

Considering the interfaces, OCL films melting is achievable at lower temperature range on the water surface than at the solid surface by a temperature, which is roughly 20 °C lower (Figure 6). During the melting of OCL ultrathin film on a substrate, the crystals may preferentially start to melt at the points of contact between the crystal and the substrate. On the water surface, OCL chains may have large point of contacts due to the fluidic and penetrable nature of small water molecules. Besides, during heating of the substrate for melting the OCL film, the degree of molecular motion within the aqueous liquid subphase is higher compared to the bulk solid substrate. On the solid surface with the OCL film, points of contact between the OCL chains and the rigid flat solid surface may be fewer but of strong adhesion forces, which modify the melting process of the crystals. Therefore, on the solid surface, the OCL crystals melting (Figure 6b) proceeds in a constrained environment, with a lower supply of crystalline chain folds into the neighboring amorphous phase. The crystalline polymer chains on the water surface can melt and recrystallize (Figure 6a) easily due to a larger mobility in comparison with the polymer chains on the solid surface. During heating of the LS transferred OCL films at the air–solid surface, droplets of melt are formed inside the periphery of the crystals (not illustrated here; see Figure S5, Supporting Information). During cooling of the melted OCL film on the solid surface, the T_{rec} is not identifiable since the partially recrystallized OCL film does not visually differ from the melted OCL film at the air–solid interface.

Regarding the role of end groups, the most obvious one is the change in crystal habits because of the different prevalence of (100) and (110) growth sectors. The greater sterical requirements of the methacrylate groups may also account for the wavy edges observed in some of the OCL methacrylate crystals. The uniform edges of OCDOL crystals suggest that hydrophilic but lower molar mass hydroxy groups essentially pose minimal steric hindrance in OCL chain folding for crystallization. The higher nucleation barrier for the methacrylate end-capped molecules is apparent from the crystal number density and the higher critical surface pressure π^* . The higher $T_{c,\infty}$ shows that a greater degree of supercooling is indeed required to nucleate these crystals. Compared to the OCDOL central unit, the OCDME central unit is more polar but also of a higher molar mass. According to literature, the central diol unit plays

Table 1. Bulk characteristics of OCL samples.

Sample	M_n (GPC) [g mol ⁻¹]	M_n (¹ H NMR) [g mol ⁻¹]	End group functionalization (¹ H NMR) [%]	PDI (GPC)	T_c (DSC) [°C]	T_m (DSC) [°C]
	8300	7900	95 ± 3	1.2	29 ± 4.5	56 ± 4
	5900	4300	85 ± 2	1.2	18 ± 4.5	39 ± 4.5

Endgroups functionalization determined by ¹H NMR analysis is within the limits of experimental error of signal integration. The shift of M_n to higher values in GPC than ¹H NMR can be related to fractionation of the reaction products by precipitation. The temperature range of T_c and T_m is estimated by extrapolation of slopes of exotherms and endotherms from DSC measurement.

a negligible role in the crystallization of OCLs in bulk,^[22] but at the air–water interface, the more hydrophilic central unit in the OCDME might increase the nucleation barrier for crystallization by anchoring the chains to the water phase,^[23] along with the bulkier methacrylate end groups.

An interesting observation is the inversion of the crystals' stability at the air–water interface and the air–solid interface. A potential explanation is the ability of functional end groups to act as diluents for the polymer melt, which results in a lowering of the melting temperature.^[27] Here, it seems intuitive that hydroxy groups are stronger diluents in an aqueous environment, whereas methacrylate groups are hydrophobic and more effective in air.

3. Conclusion

Partially crystalline ultrathin films of OCL diol and OCL dimethacrylate were prepared at the air–water interface at different film mean molecular areas (22, 18, 15, 12 or 8.5 Å²) and aqueous subphase temperatures (21 °C or 12 °C). Melting/recrystallization was studied for partially crystalline OCL ultrathin films directly at the air–water interface, and also at the air–solid interface after Langmuir–Schaefer transfer to a silicon substrate. Thickness and topographic evaluation was performed for as-crystallized and recrystallized OCL films on silicon substrates. Methacrylate groups affected the chain packing and led to a higher prevalence of (110) growth sectors in OCL single crystals grown at the air–water interface.

In comparison to OCL spherulites in bulk, for investigating thermal properties in ultrathin films, crystallization temperature, end group functionalization, central core group, M_n but also the single crystal's thickness is taken into account. The melting/recrystallization temperatures of OCL diol and OCL dimethacrylate single crystals at the air–water interface or air–solid interface were proportional to the inverse crystal thickness, in agreement to the Gibbs–Thomson equation. The M_n corrected equilibrium melting temperature at the air–solid interface occurs at temperatures, which are about 10 °C lower than those in bulk, while the equilibrium melting temperature at the air–water interface is about 25 °C lower than in bulk. While a critical surface pressure π^* for crystallization was observed, both the lateral crystal size and thickness increased with initial film thickness, which is defined by the MMA for isochoric crystallization, while the initial crystallization surface pressure was almost identical.

The methacrylate groups lead to a considerable lowering of the melting point only in the absence of water. These are important considerations when, for example, using OCL crystals as thermal switches for medical applications. A recrystallization process is noticed with measurable parameters only at the air–water interface, where the recrystallized structures are thicker than the melted crystals, as they form at higher temperatures. This study highlights not only the precisely controllable parameters at the air–water interface for preparing single crystals with defined thermal transitions, but also the importance to take the presence of water into account when using PCL crystals as thermal switches in aqueous environments. In future, we will exploit the high density of functional end groups at OCL crystal surfaces to construct stimuli responsive nanostructured materials with adjustable switching temperatures.

4. Experimental Section

Materials: Oligo(ϵ -caprolactone) diol (OCDOL, trade name CAPA 2803, Solvay Caprolactones, Warrington, U.K.) and oligo(ϵ -caprolactone) dimethacrylate (OCDME, Sigma–Aldrich) were used without any further purification. OCDOL basic characterization was described in detail previously.^[28] **Table 1** summarizes the bulk material characteristics of the OCDOL and OCDME used in this study.

The M_n was determined by gel permeation chromatography (GPC). The set up consisted of a mixed D column (600 mm × 7.5 mm, Polymer Laboratories Ltd.), a T60A dual detector, and a refractive index detector (Shodex RI-101, Showa Denko, Japan). Chloroform (HPLC grade, Roth) was used as the eluent at a flow rate of 1.0 mL min⁻¹, and polystyrene as the standard for universal calibration. Structure elucidation and M_n analysis were performed by ¹H NMR (proton nuclear magnetic resonance) using a Bruker Avance 300 spectrometer (300 MHz), in CDCl₃ (99.8%, VWR) at 25 °C ± 0.5 °C. The degree of methacrylation, D_m was determined from ¹H NMR spectra by the formula, $D_m = (I_{<k>} / I_{<y>}) \times 100\%$, where $I_{<k>}$ and $I_{<y>}$ are the proton intensities of methylene groups in the methacrylate double bonds (=CH₂) and the methylene signals (–CH₂–) of the central diol unit (see Figure S1, Supporting Information). The M_n determined previously via quantification of hydroxy group concentration (OH-value) by potentiometric titration was 8000 g mol⁻¹.^[28] For OCDME, infrared analysis (Nicolet spectrometer; Figure S2, Supporting Information) shows methacrylate peaks at ≈1620 cm⁻¹ (C=C bonds), 810 cm⁻¹ (=CH) and 1408 cm⁻¹ (=CH₂). Thermal properties of OCL bulk samples were evaluated on differential scanning calorimetry (DSC) 204F1 (Perkin Elmer; see Figure S3, Supporting Information). With the nitrogen purge, the sample in first heating cycle was heated from 4 °C to 150 °C, followed by first cooling cycle to –100 °C and a final second heating cycle till 150 °C. The rate of heating or cooling was 10 K min⁻¹. Thermal properties were determined from the first cooling and second heating cycle run.

Crystallization Study at Air–Water interface: Langmuir Technique: Surface pressure, MMA, and temperature curves were recorded in a

Langmuir trough (KSV NIMA, Finland) placed on an active vibration isolation system (Halcyonics variobasic 40, Accurion, Germany) within a laser safety cabinet. A water bath, circulating exteriorly below the trough's teflon base, controlled the temperature of the filled liquid subphase in the Langmuir trough. BAM images were recorded in real time on Langmuir trough with ellipsometer nanofilm_ep3 (Accurion, Göttingen, Germany) equipped with a high performance CCD camera, a 10× magnification lens with a maximum lateral resolution of 2 μm, and a 658 nm class IIIB laser source. π was measured by the Wilhelmy technique with a calibrated sensor placed at the center between the barriers. The trough was cleaned thoroughly with ethanol (HPLC grade; Bernd Kraft, Duisburg, Germany) followed by chloroform (HPLC grade, Roth, Germany). The deionized water filled in Langmuir trough was obtained by a Milli-Q Gradient A-10 water purification system (Millipore, 18.2 MU cm, toc < 4 ppb). The deionized water was filled and removed at least three times. By monitoring the surface pressure, the purity of the Langmuir trough and the aqueous subphase was controlled. In the final aqueous subphase, while closing the barriers, the total change of the surface pressure was below 0.2 mN m⁻¹. For all OCL samples, the chloroform stock solutions had concentrations in the range of 0.2 to 0.4 mg mL⁻¹. The solution was applied drop-wise onto the air–water interface using a microsyringe (Hamilton Co., Reno, NV, USA). The chloroform was allowed to evaporate for 30 min before the start of OCL film compression. The rate of compression and expansion of monolayer was 10 mm min⁻¹. The Langmuir trough software (KSV NIMA) used the input variables of spread amount of OCL solution at air–water interface, trough surface area, and M_n of repeat unit (ϵ -caprolactone; 114 g mol⁻¹) to calculate the OCL film MMA. The output curves show relationships between MMA, surface pressure, temperature, compression speed and time. Under isothermal conditions, the OCL films were compressed and held at different MMAs (crystallization MMA) and OCL crystallization was observed in real time by BAM. Under constant compression rate, the surface pressure point after which OCL crystals first started to appear in the BAM was defined here as the critical surface pressure π^* . For crystals melting, aqueous subphase was heated at the rate of 2 °C ± 0.5 °C min⁻¹ until a clear BAM image without any crystalline structures is observed. For recrystallization, the aqueous subphase was cooled, and withheld for 30 min at the temperature T_{rec} where the recrystallized structures could be observed in BAM images.

Crystallization Study at Air–Solid Interface: Langmuir–Schaefer Films: Partially crystalline, and recrystallized OCL films at different MMAs were transferred onto silicon substrates (Plano GmbH, Germany) by Langmuir–Schaefer (LS) method. Briefly, acetone cleaned silicon substrate was horizontally brought in contact with the partially crystalline or recrystallized OCL film on the water surface. The melting point of LS transferred partially crystalline OCL films were evaluated using an optical microscope equipped with crossed polarizers and a temperature-controlled stage. Thickness and morphology of LS transferred films of partially crystalline and recrystallized OCL films were determined using AFM.

Atomic Force Microscopy: The topography of the OCL films in air was performed using a Nanowizard AFM (JPK Instruments, Germany) operating in the intermittent contact mode at 21 °C ± 0.5 °C. Tips used were made of silicon (285 KHz resonance frequency; 42 N m⁻¹ force constant; Nano World). To determine the crystal thickness from AFM images, WSxM 5.0 software was used^[29].

Polarized Optical Microscopy with Temperature-Controlled Stage: Polarized optical microscopy was performed at Zeiss Axio Imager A1m microscope (Carl Zeiss, Jena, Germany) equipped with crossed polarizers and a Linkam LTS 350 heating stage (Linkam Scientific Instruments Ltd., Tadworth, United Kingdom). 40× magnification objective (Zeiss A-plan) was used in reflection mode with the temperature rate change of 2 °C ± 0.4 °C min⁻¹ in air.

Statistics Experimental Errors and Error Considerations with Respect to Instrumentation: All OCL films melting and recrystallization experiments at air–water interface or air–solid interface were performed more than two times. At the air–water interface, the systematic error range of the surface pressure sensor was ±0.3 mN m⁻¹ and temperature sensor was ±0.2 °C. The experimental error in spreading polymer

solution and environmental impurities led to irregularity in OCL film MMA measurement by ±1 Å². The instrumentation error of rate of heating or cooling at the air–water or air–solid interface was less than ± 0.5 °C min⁻¹. For thermal analysis of bulk material, the DSC had an instrumentation error of ± 0.5 °C. The statistical error of the crystal thickness was calculated by mean deviation of the values obtained from at least three AFM images (see Figure S6, Supporting Information). The statistical error of the melting temperature is given as a temperature range between the points where the first signs of melting and complete melting were observed.

Supporting Information

Supporting Information is available from the Wiley Online Library or from the author.

Acknowledgements

The authors acknowledge the support in material characterization by Dr. Maria Balk for GPC, Ms. Susanne Schwanz for DSC, Dr. Karola Lützwow for NMR, Dr. Anne-Christin Schöne for potentiometric titration, and Mr. Olaf Lettau for infrared spectroscopy. This study was financially supported by the Helmholtz Association through programme-oriented funding and the Helmholtz Graduate School of Macromolecular Bioscience (MacroBio), grant no. VH-GS-503.

Open access funding enabled and organized by Projekt DEAL.

Conflict of interest

The authors declare no conflict of interest.

Data Availability Statement

Research data are not shared.

Keywords

crystallization, melting, oligo(ϵ -caprolactone)s

Received: November 4, 2020

Revised: January 8, 2021

Published online: February 8, 2021

- [1] A. Lendlein, O. E. C. Gould, *Nat. Rev. Mater.* **2019**, *4*, 116.
- [2] A. L. Sisson, D. Ekinici, A. Lendlein, *Polymer* **2013**, *54*, 4333.
- [3] R. Machatschek, B. Schulz, A. Lendlein, *Macromol. Rapid Commun.* **2018**, *40*, 1800611.
- [4] S. Saretia, R. Machatschek, B. Schulz, A. Lendlein, *Biomed. Mater.* **2019**, *14*, 034103.
- [5] D. S. Fryer, R. D. Peters, E. J. Kim, J. E. Tomaszewski, J. J. de Pablo, P. F. Nealey, C. C. White, W.-I. Wu, *Macromolecules* **2001**, *34*, 5627.
- [6] L. Cristofolini, P. Cicuta, M. P. Fontana, *J. Phys.: Condens. Matter* **2003**, *15*, S1031.
- [7] H. Kim, H. Lee, H. Jung, Y. Choi, M. Meron, B. Lin, J. Bang, Y.-Y. Won, *Soft Matter* **2015**, *11*, 5666.
- [8] M. Gagliardi, *Macromol. Theory Simul.* **2019**, *28*, 1800063.
- [9] A.-K. Flieger, M. Schulz, T. Thurn-Albrecht, *Macromolecules* **2018**, *51*, 189.

- [10] W. Kossack, A. Seidlitz, T. Thurn-Albrecht, F. Kremer, *Macromolecules* **2016**, 49, 3442.
- [11] M. Tariq, O. Dolynchuk, T. Thurn-Albrecht, *Macromolecules* **2019**, 52, 9140.
- [12] X. Yu, N. Wang, S. Lv, *J. Cryst. Growth* **2016**, 438, 11.
- [13] V. H. Mareau, R. E. Prud'homme, *Macromolecules* **2005**, 38, 398.
- [14] A.-C. Schöne, S. Falkenhagen, O. Travkova, B. Schulz, K. Kratz, A. Lendlein, *Polym. Adv. Technol.* **2015**, 26, 1402.
- [15] N. Hasan, C. Fuchs, C. Schwieger, K. Busse, O. Dolynchuk, J. Kressler, *Polymer* **2020**, 196, 122468.
- [16] B. Li, H. Marand, A. R. Esker, *J. Polym. Sci., Part B: Polym. Phys.* **2007**, 45, 3200.
- [17] B. Li, A. R. Esker, *Langmuir* **2007**, 23, 2546.
- [18] A.-C. Schöne, K. Kratz, B. Schulz, J. Reiche, S. Santer, A. Lendlein, *Polym. Adv. Technol.* **2015**, 26, 1411.
- [19] N. Tarazona, R. Machatschek, A. Lendlein, *Biomacromolecules* **2019**, 21, 761.
- [20] A. Lendlein, A. M. Schmidt, R. Langer, *Proc. Natl. Acad. Sci. USA* **2001**, 98, 842.
- [21] A. Lendlein, A. M. Schmidt, M. Schroeter, R. Langer, *J. Polym. Sci., Part A: Polym. Chem.* **2005**, 43, 1369.
- [22] J. E. Báez, Á. Marcos-Fernández, A. Martínez-Richa, P. Galindo-Iranzo, *Polym.-Plast. Technol. Eng.* **2017**, 56, 889.
- [23] a) J. P. Kampf, C. W. Frank, E. E. Malmström, C. J. Hawker, *Langmuir* **1999**, 15, 227; b) K. K. Adatia, A. Holm, A. Southan, C. W. Frank, G. E. M. Tovar, *Polym. Chem.* **2020**, 11, 5659.
- [24] E. Núñez, G. J. Vancso, U. W. Gedde, *J. Macromol. Sci., Part B: Phys.* **2008**, 47, 589.
- [25] E. Núñez, C. Ferrando, E. Malmström, H. Claesson, P. E. Werner, U. W. Gedde, *Polymer* **2004**, 45, 5251.
- [26] T. Y. Cho, W. Stille, G. Strobl, *Colloid Polym. Sci.* **2007**, 285, 931.
- [27] B. Heck, G. Strobl, M. Grasruck, *Eur. Phys. J. E* **2003**, 11, 117.
- [28] A.-C. Schöne, K. Kratz, B. Schulz, A. Lendlein, *Polym. Degrad. Stab.* **2016**, 131, 114.
- [29] I. Horcas, R. Fernández, J. M. Gómez-Rodríguez, J. Colchero, J. Gómez-Herrero, A. M. Baro, *Rev. Sci. Instrum.* **2007**, 78, 013705.

**ADVANCED
MATERIALS**
INTERFACES

Supporting Information

for *Adv. Mater. Interfaces*, DOI: 10.1002/admi.202001940

Effect of Water on Crystallization and Melting of Telechelic
Oligo(ϵ -caprolactone)s in Ultrathin Films

*Shivam Saretia, Rainhard Machatschek, Thanga Bhuvanesh,
and Andreas Lendlein**

Supporting Information

Effect of water on crystallization and melting of telechelic oligo(ϵ -caprolactone)s in ultrathin films

Shivam Saretia^{1,2}, Rainhard Machatschek¹, Thanga Bhuvanesh^{1,2}, Andreas Lendlein^{1,2}*

¹ Institute of Active Polymers, Helmholtz-Zentrum Geesthacht and Berlin-Brandenburg Center for Regenerative Therapies, Kantstraße 55, 14513 Teltow, Germany

² Institute of Chemistry, University of Potsdam, Karl-Liebknecht-Straße 24-25, 14476 Potsdam, Germany

E-mail: andreas.lendlein@hzg.de

¹H NMR analysis of OCL diol and OCL dimethacrylate

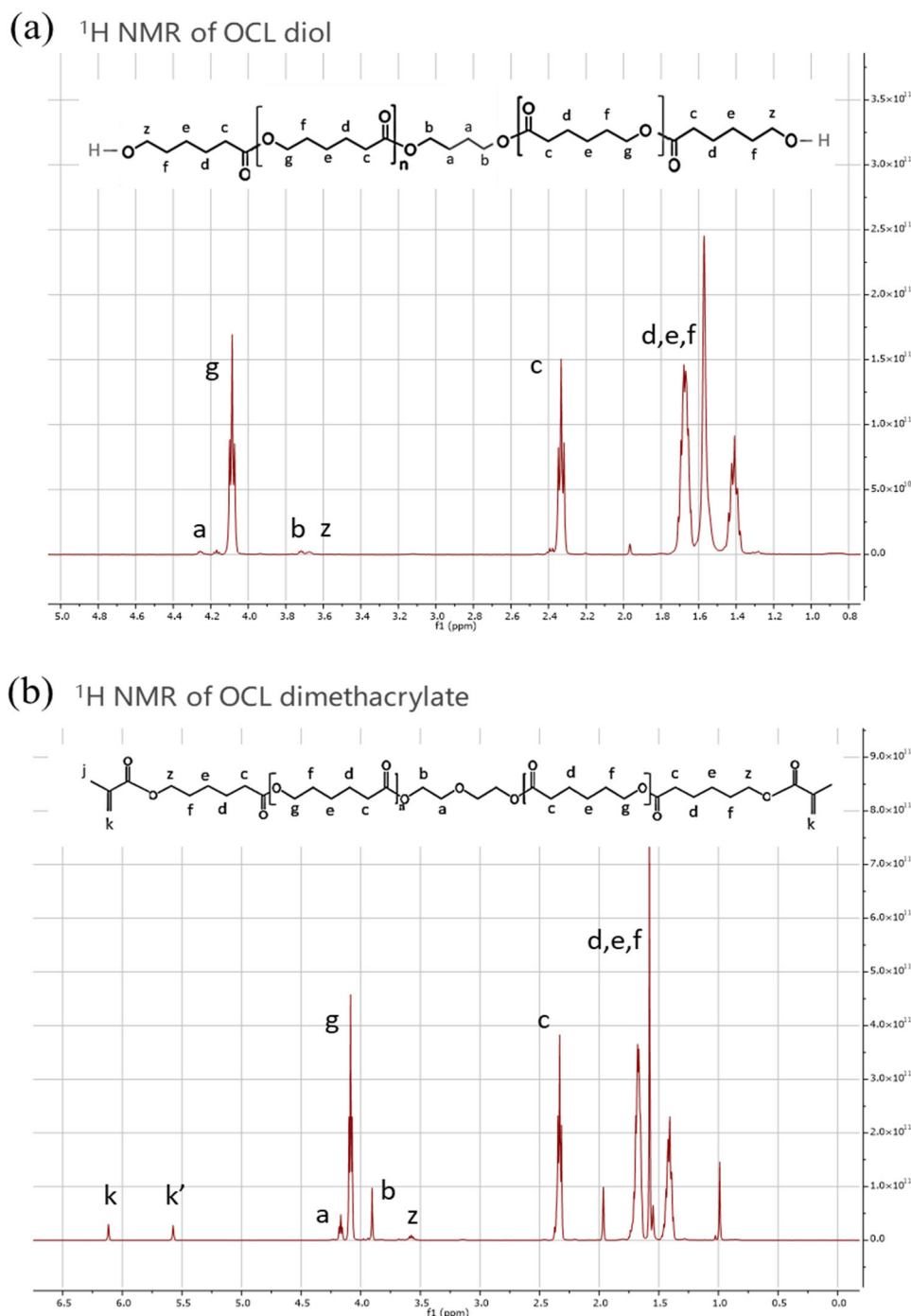


Figure S1: ¹H NMR spectra of oligo(ϵ -caprolactone) (OCL) diol (OCDOL) (a) and OCL dimethacrylate (OCDME) (b) in deuterated chloroform at room temperature.

By ¹H NMR, the number average molecular weight, M_n was determined by calculating the number of repeating monomer units, $n = ((\text{sum of CH}_2 \text{ proton integrals})/\# \text{ of CH}_2 \text{ protons})/(\text{integral per proton value})$. Value of n for OCL diol is 69 and for OCL dimethacrylate is 34. For calculating the M_n , following formula used is, $M_n = (\text{MW end groups}) + (\text{MW core})$

group) + (MW repeating caprolactone unit)(n). M_n of OCL diol = $(31+31) + (104) + (114)(69) = 7900$ to 8200 g mol^{-1} . M_n of OCL dimethacrylate = $(69 + 69) + (104) + (114)(34) = 4200$ to 4300 g mol^{-1} . Degree of end group functionalization, from OCL diol $^1\text{H NMR}$ spectra (a) was calculated by the formula, $D_{\text{OCDOL}} = (I_{<z>} / I_{<a \text{ or } b>}) \times 100 \%$, coming out to be $\geq 95 \%$. Degree of end group functionalization from OCL dimethacrylate $^1\text{H NMR}$ spectra (b) was calculated as $D_{\text{OCDME}} = (I_{<k>} / I_{}) \times 100 \%$, yielding $\sim 85 \%$. Methyl peak at 1 ppm in OCL dimethacrylate $^1\text{H NMR}$ spectra (b) is possible by the methyl groups from trimethylamine used in synthesis pathway by the manufacturer.

Infrared analysis of OCL dimethacrylate

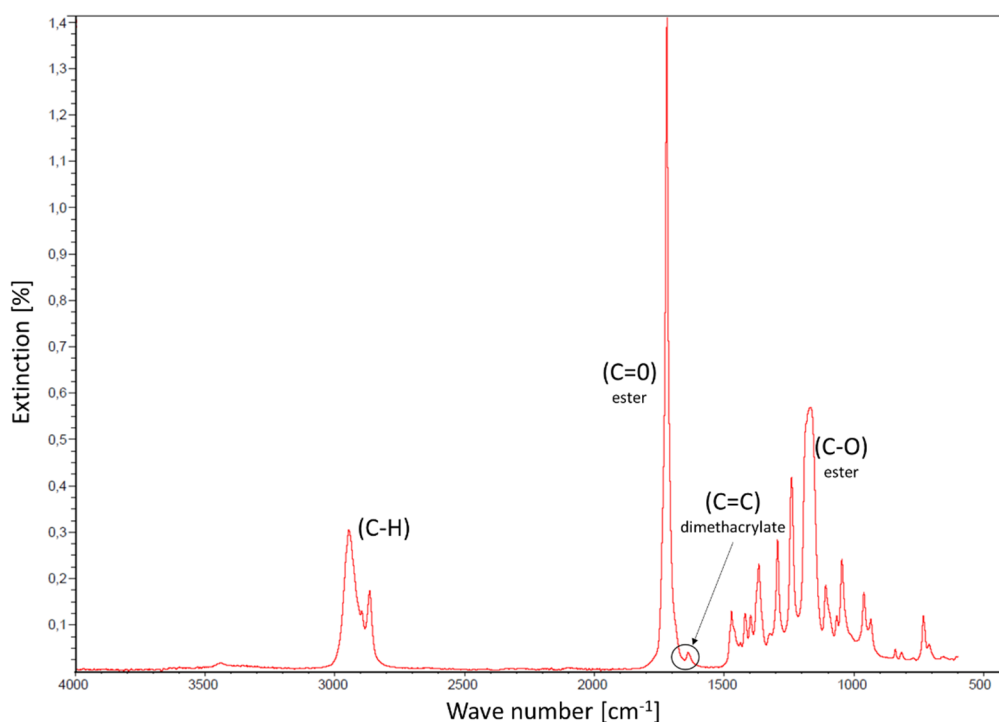
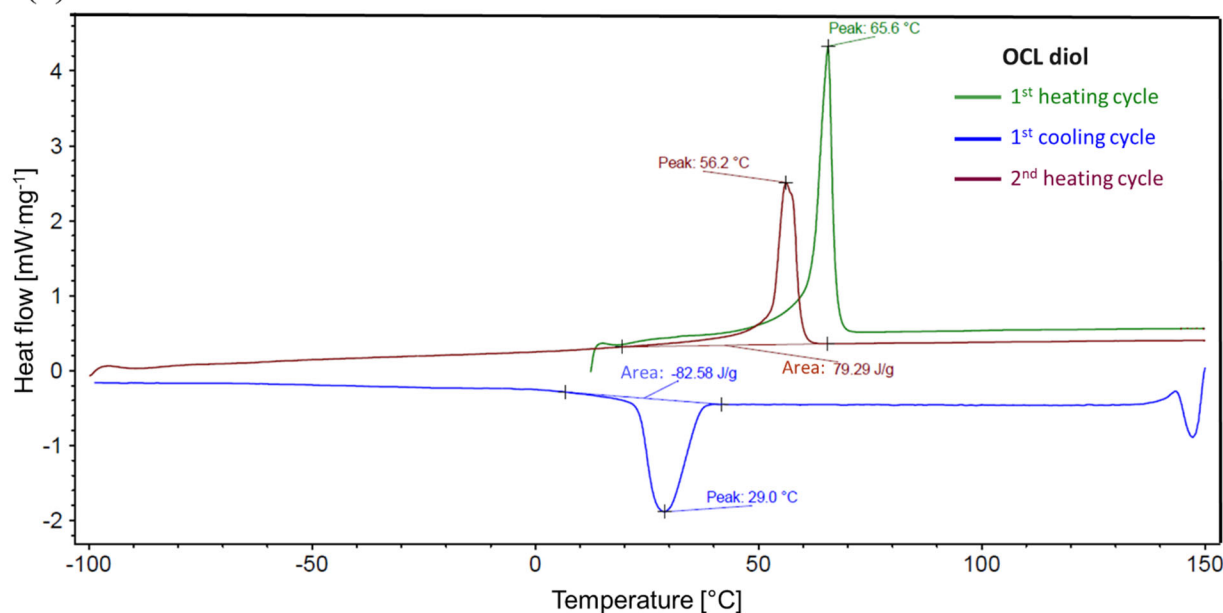


Figure S2: Infrared (IR) spectra of OCL dimethacrylate of solid sample under vacuum at room temperature.

Infrared analysis (Nicolet spectrometer) was carried out for solid sample of OCL dimethacrylate. IR spectra revealed typical stretches for OCL dimethacrylate. At $\sim 1620 \text{ cm}^{-1}$, a small peak due to C=C bonds from dimethacrylate is visible. The stretches at 810 cm^{-1} (=CH) and 1408 cm^{-1} (=CH₂) are also contributed from methacrylates.

DSC analysis of OCL diol and OCL dimethacrylate

(a) DSC curve of OCL diol



(b) DSC curve of OCL dimethacrylate

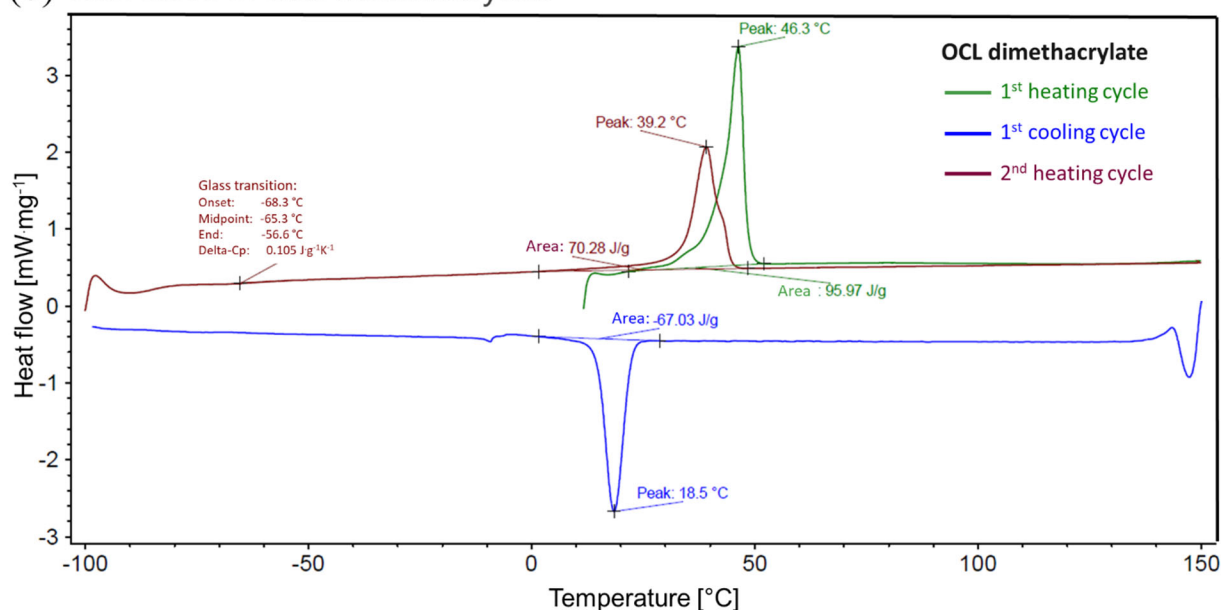
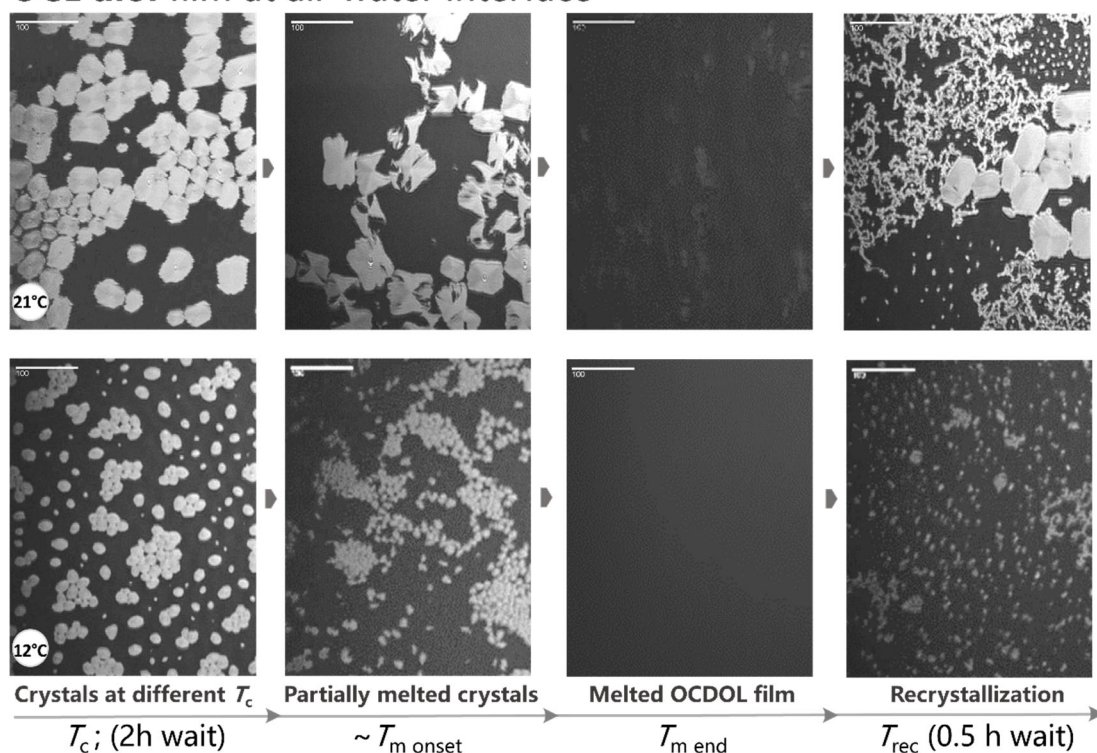


Figure S3: DSC (Differential Scanning Calorimetry) curves of (a) OCL diol and (b) OCL dimethacrylate

Thermal properties of OCL bulk samples were evaluated on DSC 204F1 (Perkin Elmer). With the nitrogen purge, the sample in first heating cycle (green) was heated from 4 °C to 150 °C, followed by first cooling cycle (blue) to -100 °C and a final second heating cycle (red) till 150 °C. The rate of heating or cooling was 10 K min⁻¹. Thermal properties are determined from the first cooling and second heating cycle run.

Melting and recrystallization of OCL diol and OCL dimethacrylate films at air-water interface

(a) OCL diol film at air-water interface



(b) OCL dimethacrylate film at air-water interface

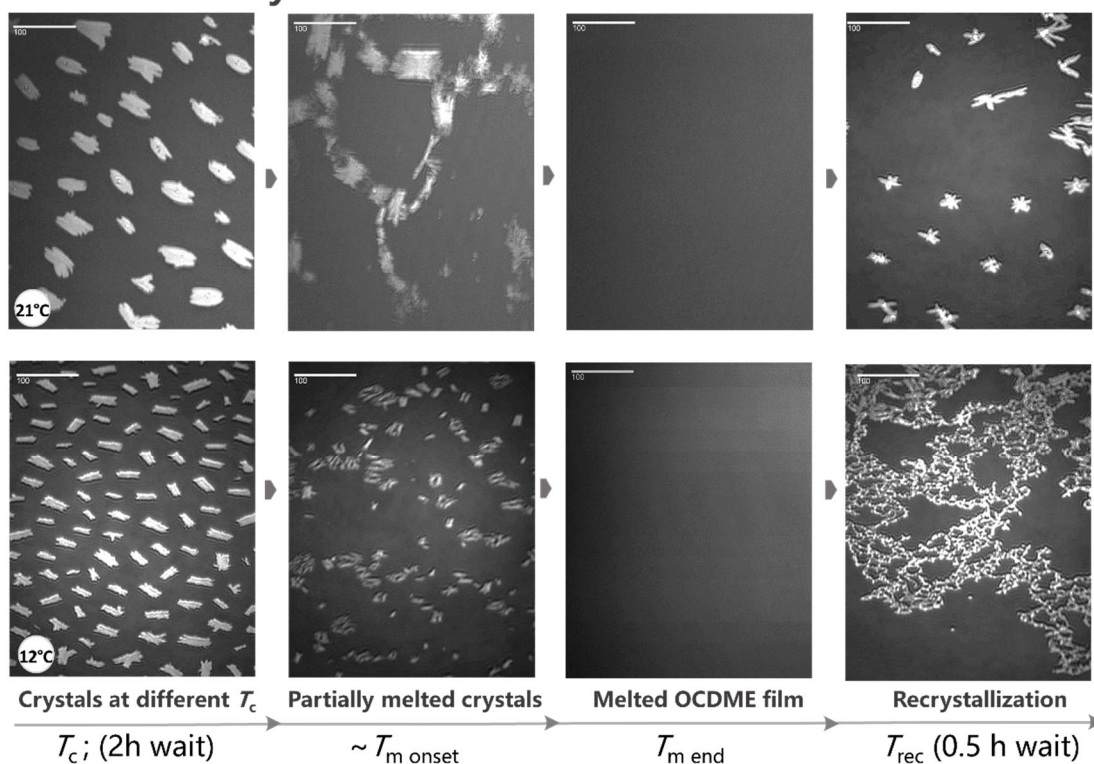


Figure S4: Brewster angle microscopy images at **air-water interface** acquired during identification of melting/recrystallisation temperatures of OCL diol (a) and OCL dimethacrylate (b) films crystallized at mean molecular area (MMA) 8.5 \AA^2 (scale bar = 100 \mu m)

Melting and recrystallization of OCL diol film at air-solid interface

OCL diol film at air-solid interface

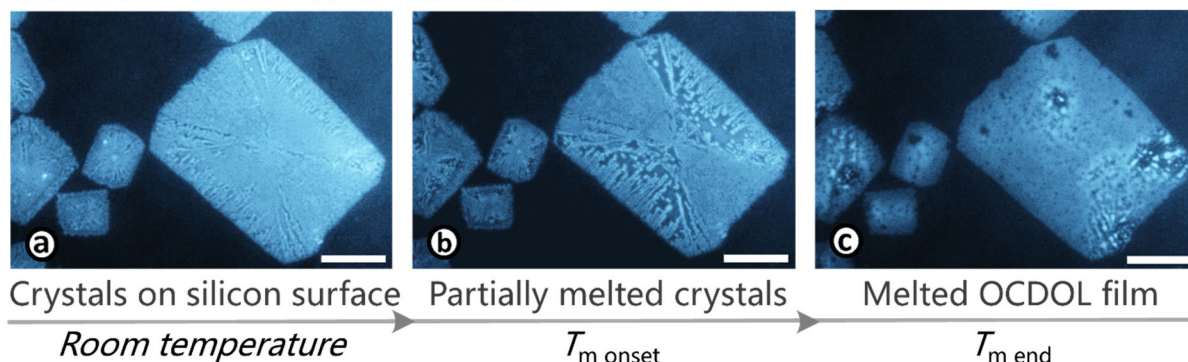


Figure S5: Optical microscope images at air-solid interface of (a) Langmuir Schaefer transferred OCL diol crystals (crystallized at MMA 8.5 \AA^2 ; crystallization temperature (T_c) $21 \text{ }^\circ\text{C}$; transferred on solid silicon) (b) partially melted OCL film obtained at $T_{m, \text{onset}} 57 \text{ }^\circ\text{C}$ and (c) the melted film image obtained after $T_{m, \text{end}} 59 \text{ }^\circ\text{C}$ (scale bar = $20 \text{ }\mu\text{m}$). Recrystallization of the melted OCL crystals at air-solid interface is not identifiable.

Mean crystal thickness calculation from histograms

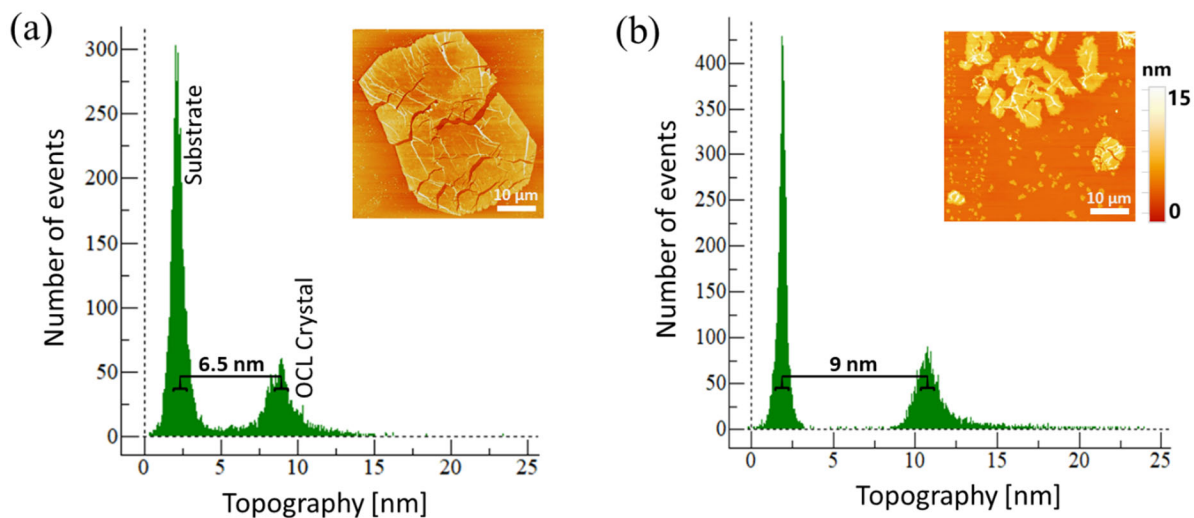


Figure S6: Histograms of the Atomic Force Microscopy (AFM) images (intermittent contact mode; $21 \pm 0.5 \text{ }^\circ\text{C}$) of (a) Langmuir–Schaefer (LS) transferred OCL diol crystals (crystallized at MMA 15 \AA^2 ; $T_c 21 \text{ }^\circ\text{C}$; transferred on solid silicon) (b) LS transferred OCL diol recrystallized structures (recrystallized at MMA 8.5 \AA^2 ; recrystallization temperature, $T_{\text{rec}} 39 \pm 1 \text{ }^\circ\text{C}$; transferred on solid silicon). OCL crystal thickness values calculated from subtracting peaks of thickness curves by OCL crystal and substrate. The statistical error of the crystal thickness is calculated by mean deviation of $\frac{1}{2}$ of thickness curves slope values obtained from at least three AFM images.



Appendix II: Degradation kinetics of oligo(ϵ -caprolactone) ultrathin films: Influence of crystallinity

Shivam Saretia^{1,2} · Rainhard Machatschek^{1,2} · Andreas Lendlein^{1,2} 

Received: 26 March 2021 / Accepted: 8 May 2021

© Helmholtz-Zentrum Hereon 2021

Abstract

The potential of using crystallinity as morphological parameter to control polyester degradation in acidic environments is explored in ultrathin films by Langmuir technique. Films of hydroxy or methacrylate end-capped oligo(ϵ -caprolactone) (OCL) are prepared at the air–water interface as a function of mean molecular area (MMA). The obtained amorphous, partially crystalline or highly crystalline ultrathin films of OCL are hydrolytically degraded at pH ~ 1.2 on water surface or on silicon surface as-transferred films. A high crystallinity reduces the hydrolytic degradation rate of the films on both water and solid surfaces. Different acceleration rates of hydrolytic degradation of semi-crystalline films are achieved either by crystals complete melting, partially melting, or by heating them below their melting temperatures. Semi-crystalline OCL films transferred via water onto a solid surface retain their crystalline morphology, degrade in a controlled manner, and are of interest as thermoswitchable coatings for cell substrates and medical devices.

Introduction

One of the primary benefits of choosing poly(ϵ -caprolactone) (PCL) as material for drug release systems and medical implants is its (bio)degradability. Besides the hydrolysis rate of the ester bonds, the degradation behavior of PCL is also influenced by its crystallinity, since the tight assembly of polymer chains restricts the access of water/ions to cleavable chemical bonds [1]. Another feature making PCL a promising candidate material for medical devices is that its crystals can melt around the body temperature, thereby enabling shape-shifting of implants [2]. Since the overall degradation profile of PCL devices depends on their crystalline morphology, implementing or executing a shape-shifting capability affects their degradation behavior [3].

It is therefore highly relevant to characterize how crystallinity and activation of thermal transitions affect the degradation behavior of PCL, yet this is difficult in bulk systems.

Degradation studies of bulk PCL in pellets, scaffolds, fibers, or thick films can take weeks to months. At pH 1, bulk PCL undergoes an induction period (~300 h) prior to exhibiting steady degradation [4]. To shorten the degradation time, frequently studies employ extreme pH values or high temperatures [5]. Care has to be taken when extrapolating their results to physiological conditions [6]. For extreme pH values, the bond scission rate is accelerated, while the water diffusion is not, which favors surface erosion [5]. Also, catalytic effects might be so strong that crystalline and amorphous bonds are broken equally, while elevated temperatures result in the melting of crystals. Moreover, it is extremely challenging to determine the degradation rates of crystalline domains, since degradation can induce chemi-crystallization, resulting in an interplay between degradation and formation of crystallites [7].

Therefore, here we use ultrathin films of semi-crystalline PCL as model systems for systematic and fast evaluation of the influence of crystals on the degradation profile of PCL.

By means of the Langmuir technique, we are able to generate ultrathin OCL films at the air–liquid interface with precisely adjusted semi-crystalline morphology, including crystal size, number density, thickness, and melting temperature. The polymer films with adjustable semi-crystalline

Supplementary Information The online version contains supplementary material available at <https://doi.org/10.1557/s43580-021-00067-4>.

✉ Andreas Lendlein
lendlein@uni-potsdam.de

¹ Institute of Active Polymers and Berlin-Brandenburg Center for Regenerative Therapies, Helmholtz-Zentrum Hereon, 14513 Teltow, Germany

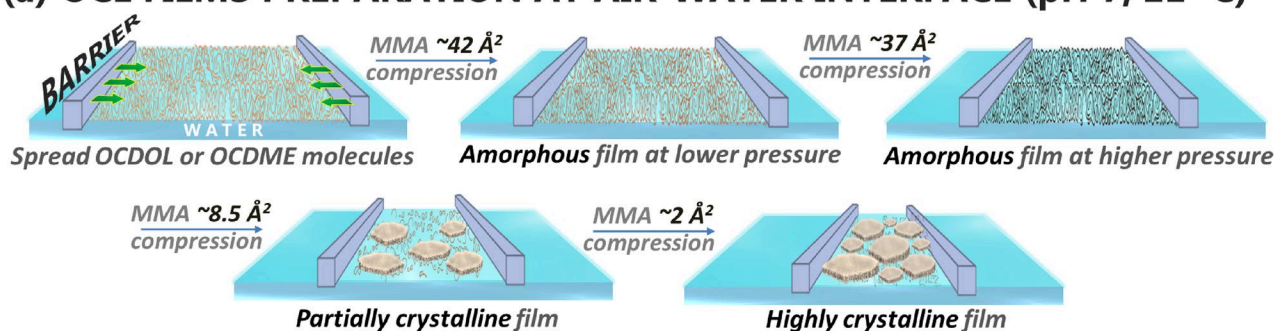
² Institute of Chemistry, University of Potsdam, 14476 Potsdam, Germany

morphology are transferable to solid substrates for further characterization [8]. It is also possible to subject these films to thermal treatments that reflect the activation of a shape-shifting effect while measuring the influence on degradation in real time. We therefore hypothesize that the degradation rate of chain segments in amorphous and crystalline domains can be determined systematically in ultrathin films prepared using different OCL telechelics.

In this study, semi-crystalline or amorphous films of hydroxy (OCL diol; OCDOL) and methacrylate (OCL dimethacrylate; OCDME) end-capped linear oligomers are prepared at the air–water interface at pH 7 at 21 °C (Fig. 1a). The prepared films are hydrolytically degraded by shifting the pH to ~1.2. Amorphous films are degraded at different surface pressures to prove an influence of OCL chain-packing on the hydrolytic degradation (Fig. 1b:1).

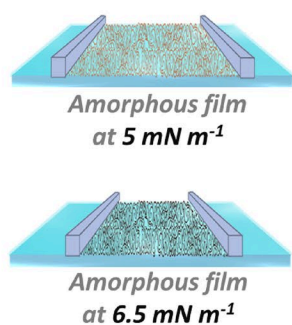
Partially crystalline OCL films are hydrolytically degraded at different constant degradation temperatures (T_{deg}) close to the melting and recrystallization range (Fig. 1b:2). These are compared to highly crystalline films, where the influence of OCL end groups (hydroxy or methacrylate) or temperature (21 or 37 °C) on degradation is determined (Fig. 1b:3). Both highly crystalline and molten films are transferred to silicon surfaces to further investigate their change in morphology during degradation. (Fig. 1b:3).

(a) OCL FILMS PREPARATION AT AIR-WATER INTERFACE (pH 7; 21 °C)

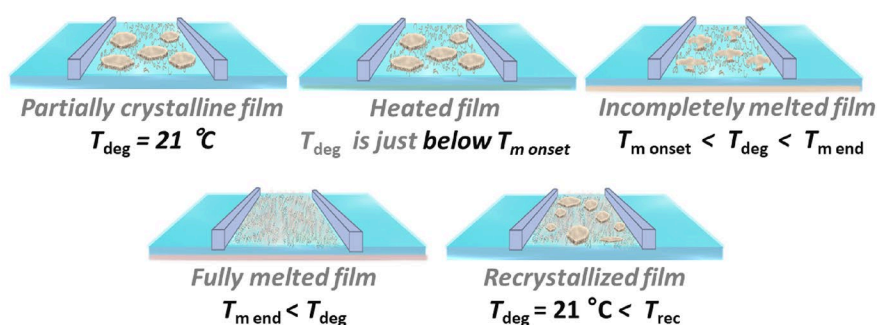


(b) HYDROLYTIC DEGRADATION OF OCL FILMS AT pH 1.2

① AMORPHOUS FILMS



② PARTIALLY CRYSTALLINE FILMS



③ HIGHLY CRYSTALLINE FILMS

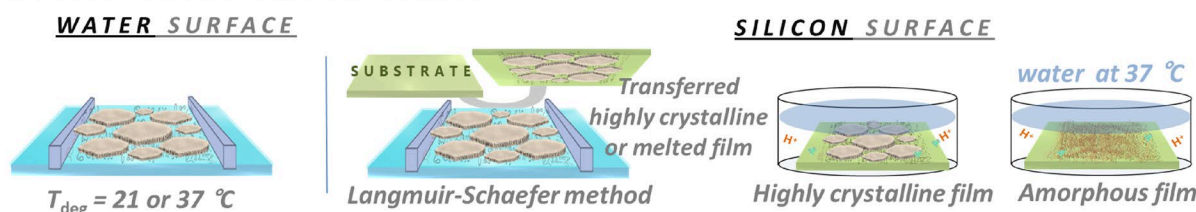


Fig. 1 Schematic representation of the experimental protocol for **a** preparing and **b** hydrolytically degrading (b:1) amorphous, (b:2) partially crystalline, and (b:3) highly crystalline OCL ultrathin films

Experimental

Materials

Oligo(ϵ -caprolactone) diol (OCDOL, trade name CAPA 2803, Solvay Caprolactones, Warrington, U.K.) and oligo(ϵ -caprolactone) dimethacrylate (OCDME, Sigma-Aldrich, Germany) were used without any further purification. Bulk material characteristics of OCDOL and OCDME are summarized in Table S1 of supplementary information.

Preparation of OCL ultrathin films at air–water interface by Langmuir technique

Langmuir technique setup and details on the cleaning of the Teflon trough used for investigation of OCL films at air–water interface were described previously [8]. Briefly, to prepare OCL ultrathin films differing in their crystallinity, chloroform solution ($0.2\text{--}0.3\text{ mg mL}^{-1}$) of OCDOL or OCDME was spread dropwise on the surface of water at $21 \pm 0.5\text{ }^\circ\text{C}$ in the Langmuir trough using a micro syringe (Hamilton Co., Reno, NV, USA). After a waiting time of 30 min for chloroform evaporation, the film was symmetrically compressed to specific MMA (see supplementary information; Table S2) at a barrier speed of 10 mm min^{-1} . MMA is the mean surface area occupied per ϵ -caprolactone repeat unit at the air–water interface and is calculated from the number of spread repeat units and the total area of the film. Details of hydrolytic degradation of OCL films at the air–water interface or of Langmuir-Schaefer (LS) transferred films at silicon surface are described in supplementary information; Table S3.

Statistics experimental errors and error considerations with respect to instrumentation

OCL films preparation and hydrolytic degradation at the air–water interface or of LS transferred films at silicon

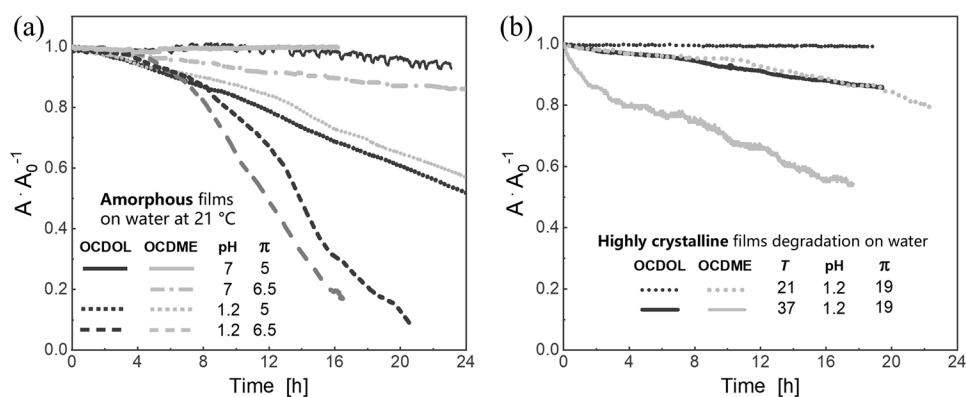
surface were performed at least three times. The systematic error range of the surface pressure sensor is $\pm 0.7\text{ mN m}^{-1}$ and $\pm 0.2\text{ }^\circ\text{C}$ for the temperature sensor. At the air–water interface, the experimental error during spreading of polymer solution and environmental impurities like dust/lint particles can lead to irregularities in OCL film MMA measurements by $\pm 1\text{ \AA}^2$.

Results and discussion

Ultrathin films of OCDOL or OCDME were prepared at the air–water interface by compressing molecules to different MMAs (~ 42 or 37 \AA^2 = amorphous films; 8.5 \AA^2 = partially crystalline; $\sim 2\text{ \AA}^2$ = highly crystalline) using the Langmuir trough barriers. The related compression isotherms (MMA versus surface pressure) and morphology of OCL ultrathin films on water at pH 7 under room temperature are shown in supplementary information Fig. S1. A detailed explanation on differences in the compression isotherms, crystallization, and melting behavior of OCDOL and OCDME films at the air–water interface can be found elsewhere [8–10].

Figure 2a shows the hydrolytic degradation of amorphous OCL films at two different surface pressures, where 6.5 mN m^{-1} is closer to the crystallization transition than 5 mN m^{-1} [9]. During a 24-h period at pH 7, amorphous OCL films at 6.5 mN m^{-1} (Fig. 2a) show an area reduction of about 5%. This confirms that the film is stable enough to carry out long-term degradation studies at both surface pressures. The degradation curve of amorphous OCLs at 6.5 mN m^{-1} shows the typical sigmoid shape of solubility-controlled polymer degradation (Fig. 2a). Since the molecular weight is initially far above the solubility threshold, chain cuts have a low probability of producing short, water-soluble fragments. Once the molecular weight is sufficiently low, chain cuts have a high probability of creating water-soluble fragments. The slightly faster dissolution of OCDME compared to OCDOL is expected due to its lower initial molecular mass. At a lower surface pressure of 5 mN m^{-1} , the OCL films

Fig. 2 Hydrolytic degradation of **a** amorphous OCL films and **b** highly crystalline OCL films on air–water interface at different conditions. Constant surface pressure (mN m^{-1}) of degradation is represented by π



are even more stable at pH 7 (Fig. 2a). When changing the pH to 1.2, an almost linear mass loss is observed, resulting in slower erosion than at higher surface pressure (Fig. 2a). Such a pressure dependence of the degradation curve could be explained by the surface-pressure-dependent solubility of fragments. In general, the higher the surface pressure, the greater the tendency for molecules to desorb from the interface. That means that at lower surface pressure, the chance that small fragments remain at the surface is higher. Then, the solubility transition becomes less sharp and the effect of initial molecular weight becomes even smaller (Fig. 2a).

The hydrolytic degradation of partially crystalline films (crystallized at MMA 8.5 Å²; 21 °C) on water at pH 1.2 at different temperatures is shown in supplementary information; Fig. S2. Partially crystalline films display competition of melting and degradation, together with the abundance of much faster degrading amorphous segments, and makes them a far from ideal system to study the influence of crystallinity on OCL degradation.

To get a clear understanding of the degradation rate of OCL crystals, highly crystalline OCDOL and OCDME films were degraded at 21 °C (room temperature) or 37 °C (body temperature) at the air–water interface (Fig. 2b). At 21 °C, pH 1.2 highly crystalline films (Fig. 2b) are far more stable against hydrolytic degradation than partially crystalline films (supplementary information; Fig. S2) or amorphous films (Fig. 2a). The deceleration is on the order of three times for OCDME, and even greater for OCDOL, where no dissolution was observed. Heating the highly crystalline films to body temperature increased the degradation rate (Fig. 2b). For OCDME, the effect was again well within the range expected for thermal activation, i.e., it does not seem that there are additional accelerating effects like partial crystal melting (the highly crystalline films have a much higher T_m (47 to 49 °C) than the partially crystalline ones (27 to 43 °C)). For OCDOL, the effect cannot be quantified since no degradation was observed of its highly crystalline films at room temperature at the air–water interface (Fig. 2b).

Highly crystalline OCDME films at 21 or 37 °C degrade faster than highly crystalline OCDOL films at the air–water interface (Fig. 2b). This effect is attributed to differences in chain-packing and larger free volume in OCDME crystals, which is evidenced by the prevalence of growth sectors with a lower melting temperature [8]. Nevertheless, for both OCDOL and OCDME, the highly crystalline films degrade slowly and almost linearly at 37 °C. Such a behavior is highly demanded for applications like erosion-controlled drug release, but very different from the mechanism observed for erosion of highly crystalline OCL layers under enzymatic catalysis [10], where the sigmoid-shaped mass loss indicated a solubility-controlled degradation.

To gain further insights into the difference between degradation of amorphous and crystalline OCL under acidic conditions, highly crystalline OCL films and amorphous films (melted highly crystalline films at 49 °C) were transferred to silicon substrates by the LS method (Fig. 3). Where OCL crystals are transferable with minor fractures, the amorphous films show dewetting (Fig. 3). All LS transferred films were hydrolytically degraded by incubation under water at pH 1.2 at 37 °C (Fig. 3).

Degradation of transferred highly crystalline and amorphous (melted) films of OCDOL and OCDME transferred on silicon at 37 °C; pH 1.2 resulted in visible differences in the crystal morphologies after 72 h (Fig. 3). It is very clear that under these conditions, the crystals are not shrinking laterally in a homogeneous way. If they were, an exponentially decreasing degradation rate, which is proportional to the remaining area, would be expected. Rather, cracks and channels are generated within the crystals. The existence of regions with different perfection of chain-packing was also concluded from enzymatic degradation experiments [11]. Therefore, the linear degradation of the single crystals is attributed to the propagation of the degradations through these regions of different chain-packing. Compared to the single crystals, the films, which were transferred in a molten state were nearly completely degraded after 72 h (Fig. 3).

Conclusion

Amorphous and semi-crystalline films of dihydroxy- or dimethacrylate-terminated linear OCL were prepared by compression of molecules to different MMAs on water at 21 °C and pH 7. The prepared films were hydrolytically degraded at pH 1.2 at different physiologically applicable temperatures. At room temperature, the mass loss of highly crystalline OCL diol films was negligible for 24 h, proving that crystals are hydrolytically far more stable than amorphous chains. In general, the highly crystalline OCL layers displayed linear mass loss, making them attractive candidates, for e.g., drug-releasing coatings. The strongly retarded degradation of OCL crystals was also observed after transfer to solid substrates. The perfection in chain-packing seems to play an important part in the degradation of OCL crystals, as evidenced by pattern formation and lower hydrolytic stability of crystals with lower melting temperature. An acceleration of degradation was observed upon melting of semi-crystalline layers, but the effect was fully reversible when the layers were cooled back to the initial temperature. The present work demonstrates the option to control the hydrolytic degradation of OCL physically via crystallization and chemically via chain termination. Future investigations could encompass adjusting the melting temperature of

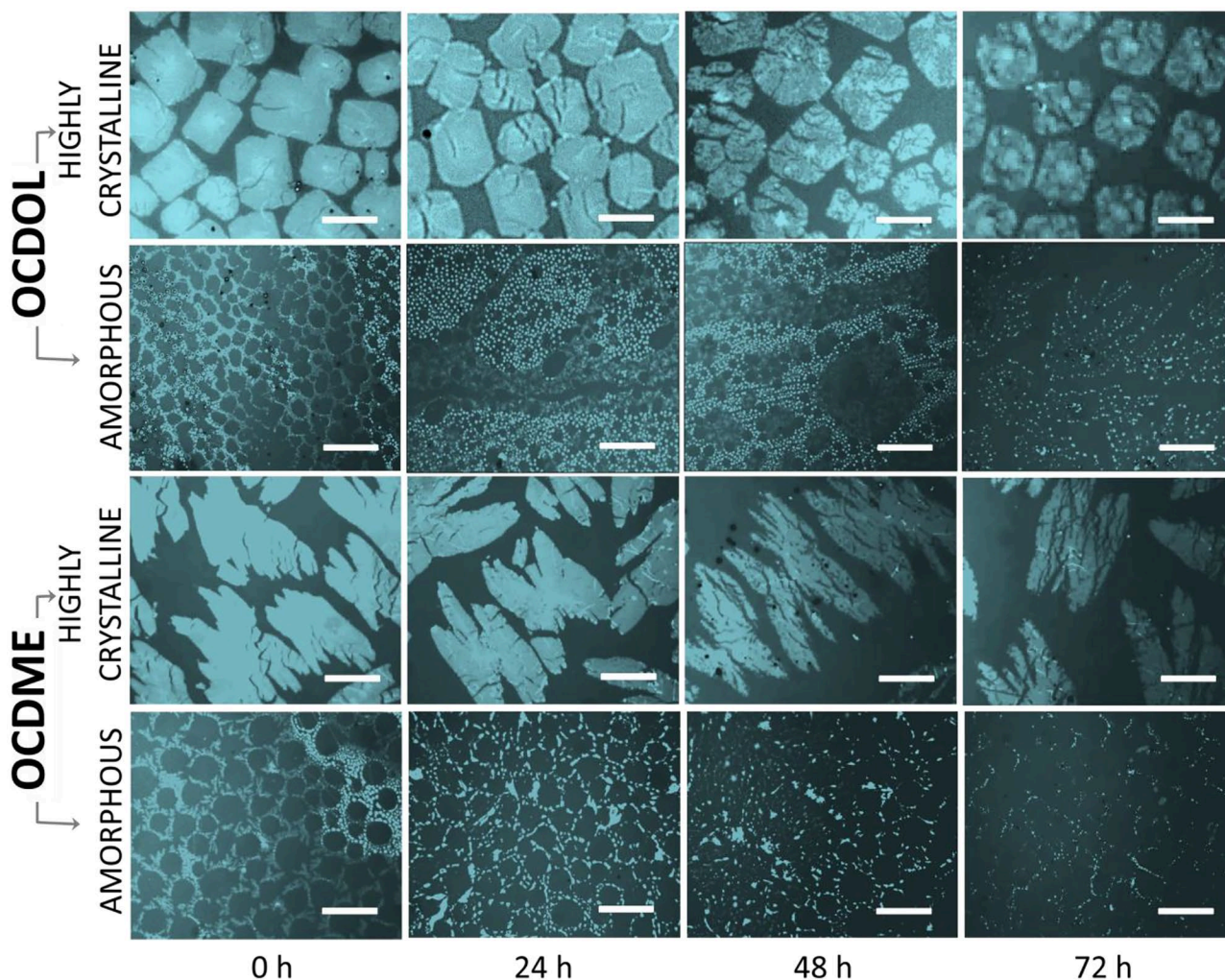


Fig. 3 Optical microscopy images of LS transferred highly crystalline and melted (amorphous) OCL films incubated in water at 37 °C and pH 1.2. (scale bar 20 μ m)

highly crystalline layers to produce functional coatings that degrade in response to a defined thermal stimulus.

Acknowledgments The authors acknowledge Dr. Natalia Tarazona and Ms. Manuela Keller for their assistance in Langmuir setup. This work is financially supported by the Helmholtz Association of German Research Centers through program-oriented funding and through Helmholtz Graduate School for Macromolecular Bioscience (MacroBio, VH-GS-503).

Funding Open Access funding enabled and organized by Projekt DEAL.

Data availability Data will be made available on reasonable request.

Declarations

Conflict of interest The authors declare no conflict of interest.

Open Access This article is licensed under a Creative Commons Attribution 4.0 International License, which permits use, sharing, adaptation, distribution and reproduction in any medium or format, as long as you give appropriate credit to the original author(s) and the source, provide a link to the Creative Commons licence, and indicate if changes were made. The images or other third party material in this article are included in the article's Creative Commons licence, unless indicated otherwise in a credit line to the material. If material is not included in the article's Creative Commons licence and your intended use is not permitted by statutory regulation or exceeds the permitted use, you will need to obtain permission directly from the copyright holder. To view a copy of this licence, visit <http://creativecommons.org/licenses/by/4.0/>.

References

1. M. Bartnikowski, T.R. Dargaville, S. Ivanovski, D.W. Huttmacher, *Prog. Polym. Sci.* **96**, 1 (2019)
2. A. Lendlein, O.E.C. Gould, *Nat. Rev. Mater.* **4**(2), 116 (2019)
3. R. Machatschek, S. Saretia, A. Lendlein, *Adv. Mater. Interfaces* **8**(6), 2001926 (2021)

4. J.H. Jung, M. Ree, H. Kim, *Catal. Today* **115**(1), 283 (2006)
5. L.N. Woodard, M.A. Grunlan, *ACS Macro Lett.* **7**(8), 976 (2018)
6. H. Sun, L. Mei, C. Song, X. Cui, P. Wang, *Biomaterials* **27**(9), 1735 (2006)
7. D.C. França, D.D. Morais, E.B. Bezerra, E.M. Araújo, R.M.R. Wellen, *Mater. Res.* **21**, 1–8 (2018)
8. S. Saretia, R. Machatschek, T. Bhuvanesh, A. Lendlein, *Adv. Mater. Interfaces* **200**, 2021 (1940)
9. S. Saretia, R. Machatschek, B. Schulz, A. Lendlein, *Biomed. Mater.* **14**(3), 034103 (2019)
10. S. Saretia, R. Machatschek, A. Lendlein, *MRS Adv.* (2021). <https://doi.org/10.1557/s43580-021-00020-5>
11. T. Iwata, Y. Doi, *Polym. Int.* **51**(10), 852 (2002)

SUPPLEMENTARY INFORMATION

Degradation kinetics of oligo(ϵ -caprolactone) ultrathin films: influence of crystallinity

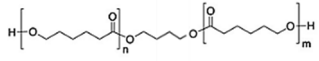
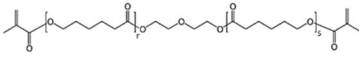
Shivam Saretia^{1,2}, Rainhard Machatschek^{1,2}, Andreas Lendlein^{1,2*}

¹ Institute of Active Polymers and Berlin-Brandenburg Center for Regenerative Therapies,
Helmholtz-Zentrum Hereon, 14513 Teltow, Germany

² Institute of Chemistry, University of Potsdam, 14476 Potsdam, Germany

* corresponding author, e-mail: lendlein@uni-potsdam.de

Table S1: Bulk characteristics of OCL samples determined by GPC, ¹H NMR and DSC

Sample	M_n (GPC) ^a [g mol ⁻¹]	M_n (¹ H NMR) ^a [g mol ⁻¹]	End group functionalization (¹ H NMR) ^b [%]	PDI (GPC)	T_c (DSC) ^c [°C]	T_m (DSC) ^c [°C]
OCDOL 	8300	7900	95±3	1.2	29±4.5	56±4
OCDME 	5900	4300	85±2	1.2	18±4.5	39±4.5

a The shift of molecular weights to higher values in GPC than ¹H NMR can be related to fractionation of molecules by precipitation.

b End group functionalization determined by ¹H NMR analysis was within the limits of experimental error of signal integration.

c The temperature range of T_c and T_m was estimated by extrapolation of slopes of exotherms and endotherms from DSC measurements.

Detailed descriptions of the bulk characterization methods can be found in [1]

Table S2: OCL ultrathin films applied for hydrolytic degradation at the air-water interface

OCL sample	Ultrathin film properties			
	Type	MMA ^a [Å ²]	Surface pressure ^b [mN m ⁻¹]	Constant surface pressure of degradation [mN m ⁻¹]
OCDOL	Amorphous	42	5	5
	Amorphous	37	6.5	6.5
	Partially crystalline	8.5	11	7.5 ^c
	Highly crystalline	2	20	19 ^c
OCDME	Amorphous	42	5	5
	Amorphous	37	6.5	6.5
	Partially crystalline	8.5	14	12.5 ^c
	Highly crystalline	2	20	19 ^c

a Statistical error of mean molecular area is within the range of ± 1 Å². For highly crystalline films, the statistical error for MMA is ± 0.5 Å².

b Surface pressure acquired during OCL molecules compression to different MMA at the air-water interface (Figure S1). Statistical error of surface pressure is ± 0.7 mN m⁻¹

c Stabilised surface pressure of degradation for semi-crystalline films obtained after relaxation for ~3 h at their crystallization MMA at room temperature. Statistical error of surface pressure is ± 0.7 mN m⁻¹

Table S3: Hydrolytic degradation OCL ultrathin films at different interfaces

Hydrolytic degradation of OCL films	Method
On water surface	Hydrolytic degradation of OCL ultrathin films at the air-water interface was performed at constant surface pressures and temperatures. A Milli-Q Gradient A-10 water purification system (Millipore, 18.2 MU cm, toc < 4 ppb) provided water for the aqueous subphase in Langmuir trough and was used for degradation experiments. Concentrated hydrochloric acid (9 mL of 8.23 M HCl; Merck KGaA, Darmstadt, Germany) was diluted with water to a volume of 12 mL and inserted into the aqueous subphase (240 mL) using glass pipettes to make final subphase concentration of 0.3 M HCl. The obtained pH 1.2 ± 0.2 was monitored by the glass electrode of a pH meter (Mettler Toledo, Germany) outside the barriers of the trough. Before the insertion of HCl into the subphase, all semi-crystalline films were allowed to relax for at least ~3 h at their crystallization MMA at room temperature for the stabilization of the surface pressure. $A_t \cdot A_0^{-1}$, as function of time, was recorded where A_0 was the initial surface area occupied by the OCL film at $t = 0$ (time point of HCl insertion into the subphase) and A_t was the film surface area after a certain degradation time period t .
On silicon surface	The highly crystalline and the melted (amorphous) OCL films prepared at the air-water interface were transferred to silicon substrates (Plano GmbH, Germany) by the LS (Langmuir-Schaefer) method. LS transferred OCL films were immersed in aqueous HCL solution at pH 1.2 ± 0.2 and 37 ± 0.5 °C which was under continuous stirring. The change in morphology of the OCL films was observed using an optical microscope in reflection mode (Zeiss Axio Imager A1m, Carl Zeiss, Jena, Germany) equipped with crossed polarizers and 50x magnification objective (Objective LD Epiplan 50x/0,50).

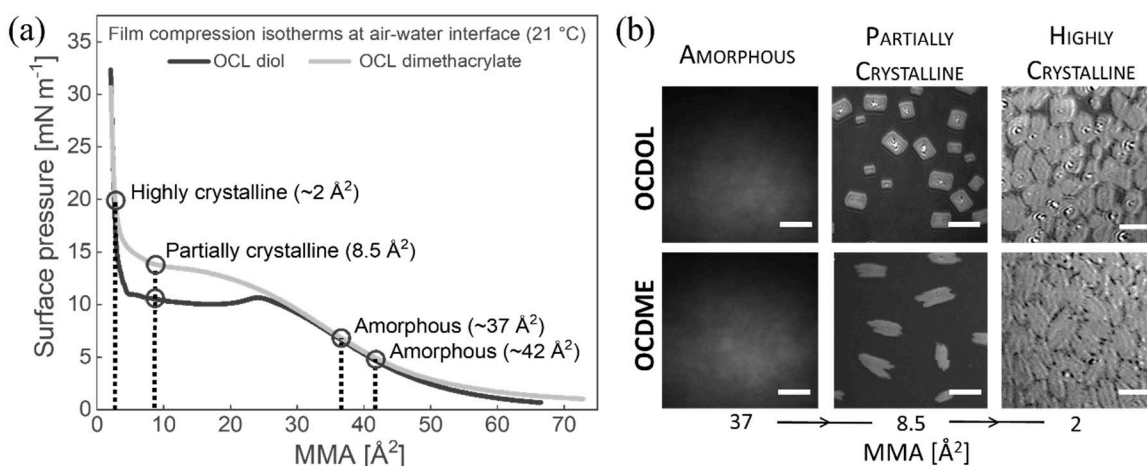


Figure S1: OCDOL and OCDME film (a) compression isotherms at the air-water interface at 21 °C; pH 7. Acquired (b) BAM images during compression of OCL films to different MMA at the air-water interface on 21 °C; pH 7 (scale bar: 50 μm). OCL films at MMA $\sim 37 \text{ \AA}^2$ are in a highly compressed, amorphous state and have highest theoretical value of static elasticity modulus. Further compression of the OCL film to lower MMAs leads to 2D-3D chain transitions and with formation of microscopically observable single crystals at a critical surface pressure (pressure between MMA 25-20 \AA^2). When OCL films are crystallized at different MMA values from 22 to 2 \AA^2 , the crystallinity in the film decreases with increasing MMA. That means the OCL films at MMA 2 \AA^2 have higher crystallinity than the films at MMA 8.5 \AA^2 , which is apparent in acquired (b) BAM images. In highly crystalline films, only a minimal amorphous area can be found between the tightly packed crystals. Bulkier methacrylate end groups retard crystallization at room temperature, where OCDME crystals have wavy edges while OCDOL crystals have smoother edges.

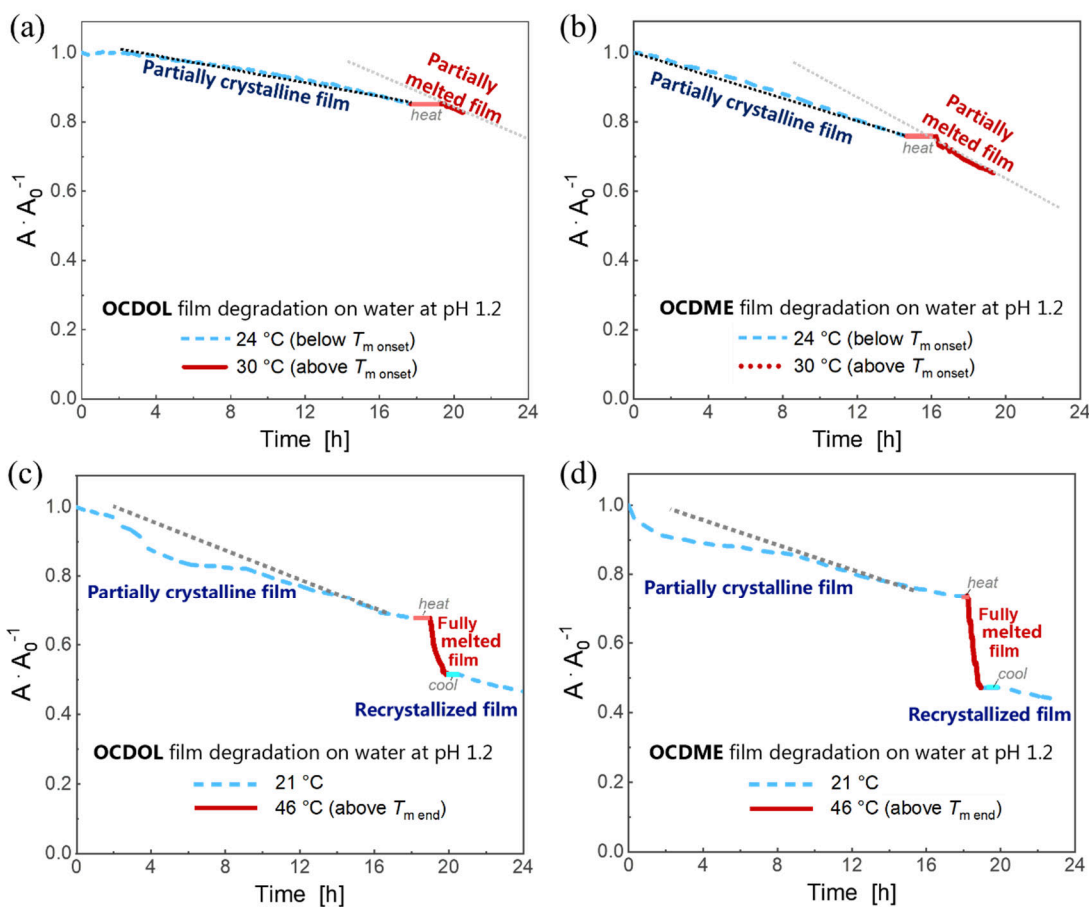


Figure S2: Hydrolytic degradation of partially crystalline OCL films including (a-b) partial film melting and (c-d) complete film melting and recrystallization at the air-water interface. Red section at ~ 19 h shows degradation during heating of partially crystalline OCL films. Extrapolated dotted lines represent the steady state of mass-loss at constant degradation temperatures. The mass-loss of the partially crystalline films at 21 °C (c-d) is overall very similar to the mass-loss of the amorphous films (roughly 30% in 16 h; Figure 2a). This suggests that the degradation happens predominantly in the amorphous parts around the crystals (dark region in BAM images; Figure S1b). Then, the lower mass-loss at 24 °C (a-b) could be explained by a more efficient melting of crystals to compensate the disappearance of the amorphous layer by degradation. Subsequently, the area reduction becomes lower as well (a-b). The films were heated above the onset and the end of the melting transition in order to understand how heating affects degradation, e. g. due to implantation or due to activation of a related function. Partial melting (above $T_{m\text{ onset}} = \sim 30$ °C; a-b) results in a substantial increase of the degradation rate. However, that increase is at least partly an effect of temperature. When completely melting the crystals (above $T_{m\text{ end}} = \sim 43$ °C; c-d), a dramatic increase in the degradation rate is observed. Interestingly, the degradation rate goes back to its initial value when the film is recrystallized by cooling (c-d). This suggests that a short thermal stimulus does not affect long-term degradation behavior of OCL based devices.

1. S. Saretia, R. Machatschek, T. Bhuvanesh and A. Lendlein, *Adv. Mater. Interfaces* **8**(7) 2001940 (2021).



Appendix III:

Highly crystalline PCL ultrathin films as thermally switchable biomaterial coatings

Shivam Saretia^{1,2} · Rainhard Machatschek^{1,2} · Andreas Lendlein^{1,2}

Received: 15 December 2020 / Accepted: 31 January 2021 / Published online: 23 March 2021

© The Author(s), under exclusive licence to The Materials Research Society 2021

Abstract

Semi-crystalline oligomers are explored as functionalized thermoswitchable coatings for modification of biomaterials surface. Highly crystalline oligo(ϵ -caprolactone) (OCL) films are prepared at the air–water interface by the Langmuir technique, which consist of tightly packed single crystals. Their morphology and melting temperature can be tuned by the chemical structure of the OCL end-groups (hydroxy or methacrylate) and by the crystallization temperature (12 or 21 °C) as physical parameter. This demand of high crystallite density and adjustable morphology of coatings is not met by conventional methodologies for preparing thin films, e.g., spin coating, spray coating, or solvent evaporation. The high crystallinity reduces the enzymatic degradation rate of the films on both water and solid surfaces. The high density of methacrylate end-groups at the crystal surfaces enables post-functionalization, which was demonstrated using fluorescein dimethacrylate as chemically linked label. The thermoswitching behavior (melting and recrystallization) of fluorescein functionalized, highly crystalline OCL films shows temperature-dependent distribution of the chemically linked fluorescein moieties, which are accumulated on the surfaces of crystals, and homogeneously dispersed when the crystals are molten. Thermally switchable highly crystalline films are relevant for cell substrates modulating adhesion at the biointerface or for coatings as barrier layer influencing the degradation rate.

Introduction

Degradable, semi-crystalline polymers such as poly(ϵ -caprolactone) (PCL) telechelics are of high technological relevance for switchable biomaterial surfaces to influence cell adhesion at the biointerface and for implant coating as phase-changing lubricant [1]. PCL is established in clinical applications and its enzymatic degradability is well-documented [2]. In particular, PCL crystals can be used as thermoswitchable units and exhibit, e.g., a change in stiffness and degradability upon melting [3]. The melting temperature of PCL crystals can be adjusted to be very close

to physiological conditions, producing a polymer layer that changes a broad variety of its functional properties upon application of a small thermal stimulus [1, 4]. Maximizing the effect of the thermal switching requires a high density of crystals having identical orientation. Conventional methods for preparing thin films such as spin coating, spray coating, or solvent evaporation are usually not suited to produce such morphologies [5, 6]. Yet, they require processing conditions involving, e.g., elevated temperatures, centrifugal forces, or organic solvents, which are not well suited for post-functionalization of polymeric biomaterials.

The air–water interface provides an elegant solution for the controlled crystallization of PCL ultrathin films under mild conditions. Using the Langmuir technique, the semi-crystalline morphology, including crystal size, number density, thickness, and melting temperature can be precisely adjusted by varying physical parameters such as the aqueous subphase temperature (crystallization temperature), the distance between the barriers, changing the film Mean Molecular Area (MMA), the compression speed or by chemical features such as the OCL telechelic functional end-groups or molecular weight [7, 8]. The nanostructured polymer films prepared at the air–water interface are transferable on

Supplementary Information The online version of this article contains supplementary material available at <https://doi.org/10.1557/s43580-021-00020-5>.

✉ Andreas Lendlein
andreas.lendlein@hzg.de

¹ Institute of Active Polymers and Berlin-Brandenburg Center for Regenerative Therapies, Helmholtz-Zentrum Geesthacht, Kantstr. 55, 14513 Teltow, Germany

² Institute of Chemistry, University of Potsdam, Karl-Liebknecht-Straße 24–25, 14476 Potsdam, Germany

different kinds of substrates—hydrophilic or hydrophobic with smooth or rough surfaces [9].

Degradability is a highly relevant function for polymeric biomaterials that is particularly influenced by crystallinity [3]. Here, the Langmuir technique offers the opportunity not only to prepare almost entirely crystalline materials (Fig. 1a), but also to study their degradation behavior and to exactly identify the influence of crystallinity on degradability. It is thereby possible to quantify the extent of adjustment that can be made to the lifetime of a highly crystalline material by thermal switching. In this work, this investigation is carried out using enzymatic catalysis both at the air–water interface and on solid surfaces (Fig. 1b). The exclusion of defects from the polymeric lattice leads to a segregation of chain-ends to the crystal surface [10]. Therefore, single crystals of oligomeric macromolecules are densely covered with chain-ends, which can be converted in a chemical functionalization [11]. Upon melting, the functional end-groups accumulated at the crystalline surface get redistributed in the amorphous phase, resulting in a change of the chemical composition of the material surface. While any chemical functionalization is possible, here a highly crystalline OCL

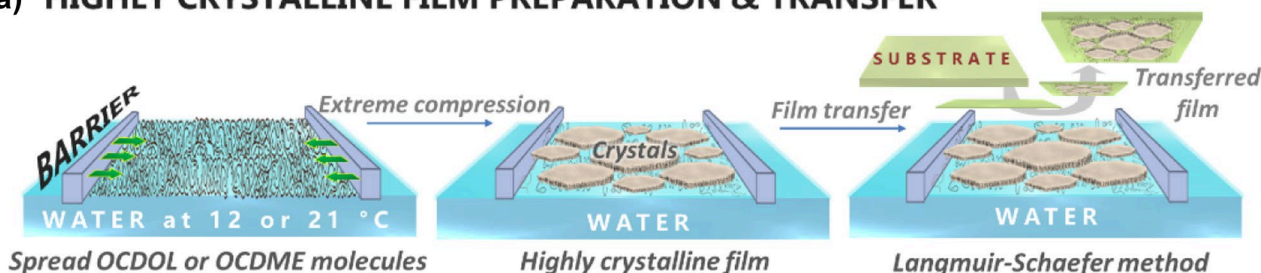
dimethacrylate (OCDME) transferred film was equipped with chemically linked fluorescent moieties (Fig. 1c). The fluorescence emission by fluorescein will be used to distinguish preferable film regions for dye attachment. This dye will also be used to follow the change in the phase morphology during thermally controlled switching.

Experimental

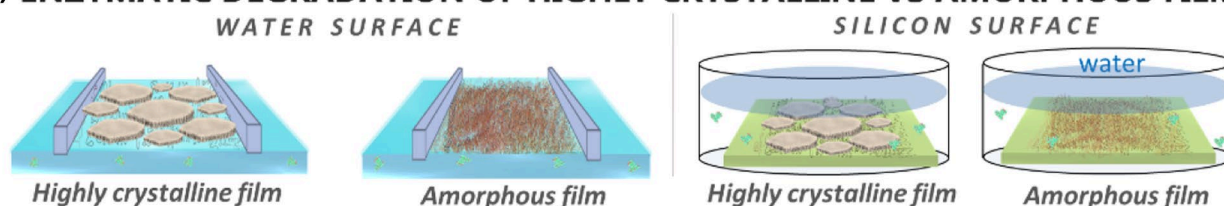
Materials

Oligo(ϵ -caprolactone) diol (OCDOL, trade name CAPA 2803, Solvay Caprolactones, Warrington, U.K.) and oligo(ϵ -caprolactone) dimethacrylate (OCDME, Sigma Aldrich, Darmstadt, Germany) were used without any further purification. CDCl_3 (99.8%, VWR) for ^1H NMR and chloroform (HPLC grade, Roth) for GPC were used as the solvents. Bulk material characteristics of OCDOL and OCDME are summarized in Table 1. Details on the bulk characterization methods of OCL samples are given in the supplementary information (Figures S1–S3; Table S1).

(a) HIGHLY CRYSTALLINE FILM PREPARATION & TRANSFER



(b) ENZYMATIC DEGRADATION OF HIGHLY CRYSTALLINE VS AMORPHOUS FILMS



(c) FUNCTIONALIZATION OF HIGHLY CRYSTALLINE OCDME FILM & MELTING

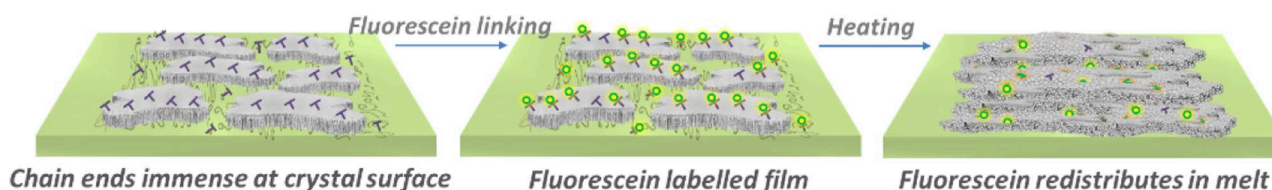
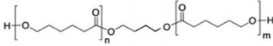
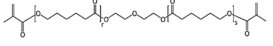


Fig. 1 Schematic representation of the experimental protocol for **a** preparing, **b** transferring and **c** investigating highly crystalline OCL ultrathin films

Table 1 Bulk characteristics of OCL samples determined by GPC, ^1H NMR, and DSC

Sample	M_n (GPC) ^a [g mol ⁻¹]	M_n (^1H NMR) ^a [g mol ⁻¹]	End-group functionalization (^1H NMR) ^b [%]	PDI (GPC)	T_c (DSC) ^c [°C]	T_m (DSC) ^c [°C]
OCDOL 	8300	7900	95 ± 3	1.2	29 ± 4.5	56 ± 4
OCDME 	5900	4300	85 ± 2	1.2	18 ± 4.5	39 ± 4.5

^aThe shift of molecular weights to higher values in GPC than ^1H NMR can be related to fractionation of molecules by precipitation

^bEnd-group functionalization determined by ^1H NMR analysis was within the limits of experimental error of signal integration. The M_n determined previously via quantification of hydroxy group concentration (OH-value) by potentiometric titration is 8000 g mol⁻¹. [12]

^cThe temperature range of T_c and T_m was estimated by extrapolation of slopes of exotherms and endotherms from DSC measurements

A Milli-Q Gradient A-10 water purification system (Millipore, Darmstadt, Germany, 18.2 MU cm, toc < 4 ppb) provided water for the aqueous subphase in Langmuir trough and for dissolution of the lipase enzyme (*Pseudomonas cepacia*; Sigma, Darmstadt, Germany; 0.007 mg·mL⁻¹) used for degradation experiments. Ethanol (HPLC grade; Bernd Kraft, Duisburg, Germany) and chloroform (HPLC grade, Roth, Karlsruhe, Germany) were used for cleaning of Teflon trough surface, or preparing OCL chloroform solution.

Preparation of OCL film at air–water interface by Langmuir technique

Details on the Langmuir technique setup and the Teflon trough purification for investigation of films at air–water interface are described in supplementary information (see supplementary information; Table S2). Visualization of OCL film crystallization at the air–water interface was performed by Brewster Angle Microscopy (BAM; ellipsometer nanofilm_ep3, Accurion, Göttingen, Germany) equipped with a high performance CCD camera, a 10× magnification lens with a maximum lateral resolution of 2 μm and a 658 nm class IIIB laser source. To prepare highly crystalline OCL films at the air–water interface, chloroform solution (0.2–0.3 mg·mL⁻¹) of OCDOL or OCDME was spread dropwise on the surface of water in the Langmuir trough using a micro syringe (Hamilton Co., Reno, NV, USA) such that the OCL film Mean Molecular Area (MMA) was above 7 Å². After a waiting time of 30 min for chloroform evaporation, the OCL film was symmetrically compressed to an MMA of ~2 Å² at a barrier speed of 10 mm·min⁻¹.

Enzymatic degradation of OCL films on water surface

Enzymatic degradation of highly crystalline OCL films was compared with amorphous (melted) OCL films on water surface. The amorphous film at the air–water interface was

prepared by melting the highly crystalline OCL film (crystallized at MMA ~2 Å²) at temperatures ≥ 49 °C. Thereafter, the aqueous subphase was cooled to 46 °C, where recrystallization still does not occur and the film was in the amorphous state. Before degrading the highly crystalline OCL film, the subphase was also heated to 46 °C, where the OCL crystals do not melt. Hence, both highly crystalline and amorphous OCL films at MMA ~2 Å² were degraded at a constant temperature of 46 °C at the air–water interface. Enzymatic degradation was carried out at constant surface pressure, where lipase solution was inserted into the subphase and A_t/A_0^{-1} , as function of time, was recorded where A_0 was the initial surface area occupied by the OCL film at $t=0$ and A_t was the film surface area after a certain degradation time period t .

Enzymatic degradation of OCDOL films on silicon surface

For enzymatic degradation of OCL films on solid surfaces, highly crystalline OCDOL films (crystallized at MMA ~2 Å²) and amorphous (melted) OCDOL films were transferred to silicon substrates (Plano GmbH, Wetzlar, Germany) by the Langmuir–Schaefer method. They were immersed in enzyme solution at 37 ± 0.5 °C which was continuously stirred to avoid enzyme accumulation at the air–water interface. The change in film morphology was observed by optical microscopy and AFM (see supplementary information; Table S3).

OCDME films fluorescein labeling, melting, and recrystallization

The transferred, highly crystalline OCDME films were reacted with fluorescein dimethacrylate (Sigma, Darmstadt, Germany; 0.5 mg·mL⁻¹; buffer at pH 10; lactone form of fluorescein at acidic or neutral pH has very low fluorescence while quinoid form at pH 10 is fluorescent active).

For this purpose, the OCDME films were incubated with fluorescein dimethacrylate solution for 4 h under presence of UV light (2.4 mW cm^{-2} ; Analytik Jena AG, Germany) and washed thrice with pH 10 buffer. Optical and fluorescent (Carl Zeiss- Filter Set 46) images were acquired during melting and cooling of fluorescence-labeled OCDME crystals in presence of water (Objective Zeiss, W N-Achroplan 63x/0,9).

Statistical experimental errors

OCL films preparation, melting, and degradation experiments were performed at least three times. At the air–water interface, the systematic error range of the surface pressure sensor is $\pm 0.3 \text{ mN}\cdot\text{m}^{-1}$ and $\pm 0.2 \text{ }^\circ\text{C}$ for the temperature sensor. At the air–water interface, the experimental error during spreading of polymer solution and environmental impurities like dust particles can lead to irregularities in OCL film MMA measurements by $\pm 1 \text{ } \text{Å}^2$. The instrumentation error of rate of heating or cooling at the air–water or air–solid interface is less than $\pm 0.5 \text{ }^\circ\text{C min}^{-1}$. The systematic error of the melting temperature at the air–water interface is given as a temperature range between the points where the first signs of melting and complete melting in the BAM were observed.

Results and discussion

The spread OCL molecules at the air–water interface were compressed to low MMA by the Langmuir trough barriers. The related compression isotherms (MMA versus surface pressure) are shown in Fig. 2a for two different temperatures of the aqueous subphase. The compression isotherm of both OCDOL and OCDME films is at slightly lower surface pressure values at the lower aqueous subphase temperature of $12 \text{ }^\circ\text{C}$, suggesting an influence of temperature

on crystallization process at the air–water interface. The crystallization during compression (Fig. 2a) of the OCL films at the air–water interface is visualized by Brewster angle microscopy (Fig. 2b), which shows that the OCL crystals get located closer to each other with increasing compression (Fig. 2b:1–3) and therefore the overall crystallinity increases. At the same time, the amorphous phase represented by the dark region, which surrounds the crystals (Fig. 2b:1), gradually disappears during film compression (Fig. 2b:3). Either new crystals are formed or the existing crystals grow in their lateral size when folded chains further add to their growth front.

At a threshold MMA range ($MMA_{\text{high crys}}$) between 3.0 and $2.0 \text{ } \text{Å}^2$, which is accompanied with a sudden shoot up of surface pressure (Fig. 2a), the Brewster angle microscopic image (Fig. 3a–d) shows the appearance of highly crystalline OCDOL or OCDME films at the air–water interface at different aqueous subphase temperatures (12 or $21 \text{ }^\circ\text{C}$). At $MMA_{\text{high crys}}$, the OCL crystals (bright regions; Fig. 3a–d) are tightly packed and rather fixed, i.e., no longer change their lateral position on the water surface, whereas the amorphous regions (dark regions; Fig. 3a–d) are minimal implying that the film is highly crystalline. In terms of morphology, the OCDOL crystal size on water at $12 \text{ }^\circ\text{C}$ is smaller than OCDOL crystals at $21 \text{ }^\circ\text{C}$ (Fig. 3a–b; Table 2). The OCL crystal shape is influenced by the OCL functional end-group as well. The hydroxy-terminated OCL (OCDOL) forms crystals with smoother edges while OCL dimethacrylate (OCDME) forms crystals with wavy edges. Therefore, highly crystalline films comprised of OCL crystals with different shapes and size are prepared by exploiting OCL functional end-groups (hydroxy or methacrylate) and aqueous subphase temperature (Fig. 3a–d; Table 2) at $MMA_{\text{high crys}}$.

For investigating thermoswitching function, i.e., melting and recrystallization of highly crystalline OCL films at the air–water interface, the OCL samples were compressed

Fig. 2 OCDOL and OCDME film compression isotherms **a** at the air–water interface at different aqueous subphase temperatures (12 or $21 \text{ }^\circ\text{C}$). Acquired BAM images **b** during compression of OCDOL film on aqueous subphase at $21 \text{ }^\circ\text{C}$ at the air–water interface (scale bar: $100 \text{ } \mu\text{m}$)

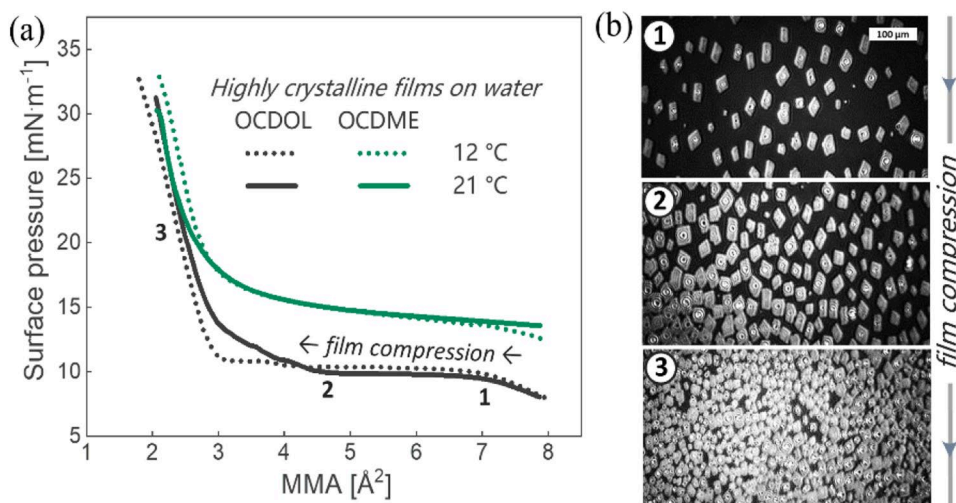


Fig. 3 Acquired BAM images (scale bar: 100 μm) of highly crystalline OCDOL (a, b) and OCDME films (c, d) (MMA $\sim 2 \text{ \AA}^2$) at the air–water interface at different aqueous subphase temperatures [12 $^\circ\text{C}$ (a, c) or 21 $^\circ\text{C}$ (b, d)]

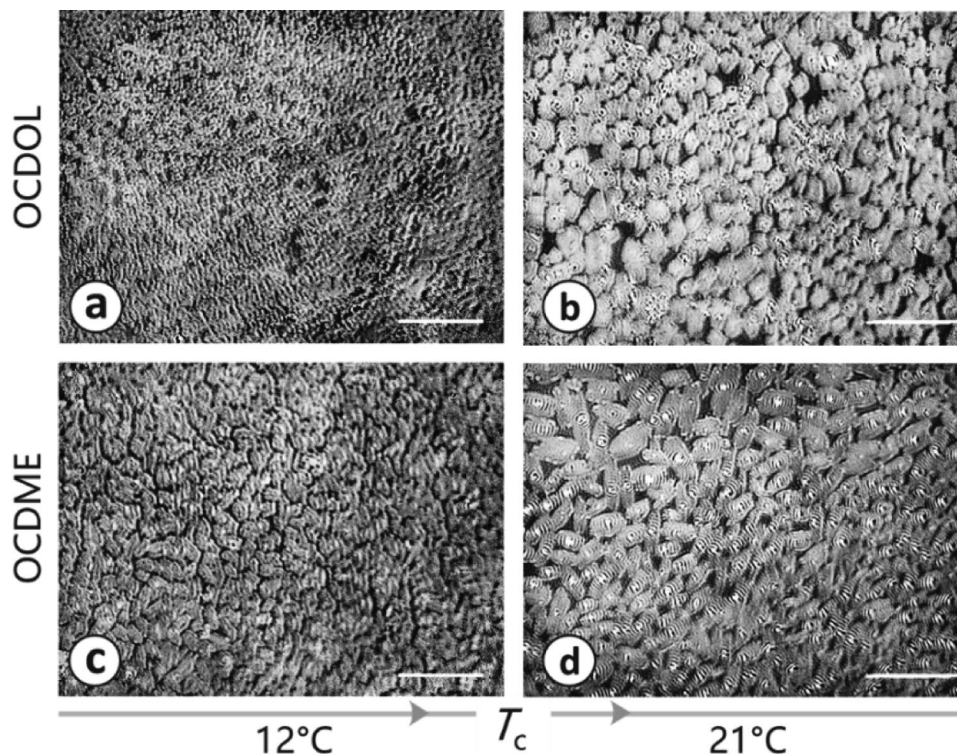


Table 2 Morphological and thermal characteristics of highly crystalline OCL films (MMA 2 \AA^2) at the air–water interface

OCL sample	T_c^a [$^\circ\text{C}$]	Crystals morphology	$T_{m \text{ onset}}^a$ [$^\circ\text{C}$]	$T_{m \text{ end}}^a$ [$^\circ\text{C}$]	T_{rec}^a [$^\circ\text{C}$]
OCDOL	12	Smooth edges; $\sim 10 \mu\text{m}$ (Fig. 3a)	33	48	44
	21	Smooth edges; $\sim 30\text{--}60 \mu\text{m}$ (Fig. 3b)	48	50	44
OCDME	12	Wavy edges; $\sim 20\text{--}50 \mu\text{m}$ (Fig. 3c)	34	43	39
	21	Wavy edges; $\sim 30\text{--}60 \mu\text{m}$ (Fig. 3d)	47	49	43

The statistical error of T_c , $T_{m \text{ onset}}$ and $T_{m \text{ end}}$ is $\pm 0.5 \text{ }^\circ\text{C}$ and of T_{rec} is $\pm 1.5 \text{ }^\circ\text{C}$

to MMA of 2 \AA^2 , and after a waiting time of 10 min, the underlying aqueous subphase was heated. By observing the film under BAM, the onset of melting ($T_{m \text{ onset}}$; crystals begin to melt), endpoint of melting ($T_{m \text{ end}}$; clear BAM image without any crystals), and recrystallization temperature (T_{rec} ; appearance of crystalline structures during cooling) were identified (Table 2).

The highly crystalline OCL films melt under physiologically applicable temperatures and the molten films recrystallize below $45 \text{ }^\circ\text{C}$ during cooling of the aqueous subphase (Table 2). Interestingly, the $T_{m \text{ onset}}$ of both OCDOL and OCDME samples is of lower value when the highly crystalline films are prepared at a water temperature of $12 \text{ }^\circ\text{C}$. Therefore, the melting temperature range of highly crystalline films at the air–water interface can be adjusted by varying the crystallization temperature (T_c). Comparing the different molecules, the slightly higher melting temperature range of OCDOL films than OCDME films is attributed to its higher molecular weight.

The enzymatic degradation of bulk polymers proceeds in a surface erosion process, since the enzymes are usually not able to penetrate into the bulk polymer. Therefore, a highly crystalline layer at the surface could serve as a thermally switchable barrier for enzymatic degradation. Here, this effect was investigated for OCDOL and OCDME films at MMA 2 \AA^2 , either in highly crystalline or amorphous (melt) state at the air–water interface in the presence of *Pseudomonas cepacia* lipase both at an identical temperature of $46 \text{ }^\circ\text{C}$ (Fig. 4). The highly crystalline OCDOL films are degradable by lipase but with a ca. $3 \times$ slower rate compared to amorphous OCDOL films. The highly crystalline OCDME film degradation is only slightly slower than the OCDME amorphous film degradation. The difference might be explained by the functional end-groups interaction with the enzyme and by the degradation temperature of $46 \text{ }^\circ\text{C}$ being much closer to the OCDME melting temperature range ($48 \pm 1 \text{ }^\circ\text{C}$). Also, the OCDME crystals could have a larger degree of internal disordering than the OCDOL

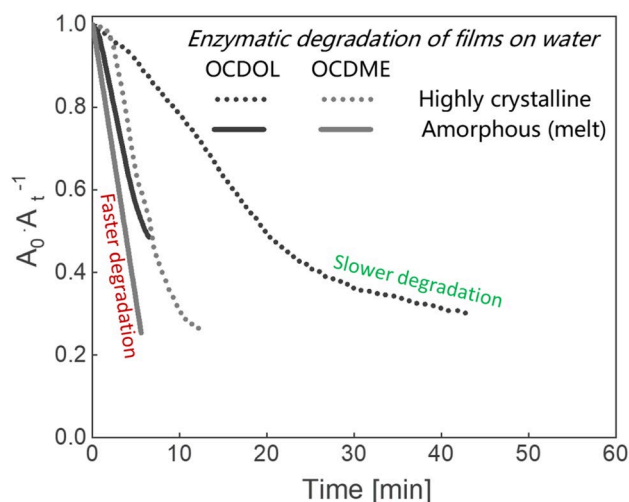


Fig. 4 Enzymatic degradation of highly crystalline OCL films (dotted line) compared to amorphous OCL films (straight line) on the water surface at 46 °C

crystals due to the different chain packing. Altogether, the effect was not very pronounced. Contrary to the hypothesis, crystalline barrier layers are not able to efficiently decelerate the enzymatic degradation of OCL, since the enzymes are catalyzing the degradation of OCL single crystals with great efficiency. Possibly, thicker crystals or multiple layers are required to produce an effective coating stable against enzymatic degradation.

This observation was further substantiated for OCL films on silicon surfaces, when OCDOL films were transferred

in their highly crystalline (Fig. 5a:1) or amorphous state (Fig. 5a:2) by the Langmuir–Schaefer method. While the high density of OCDOL crystals (Fig. 5a:1) was maintained upon transfer, the amorphous OCDOL film (Fig. 5a:2) on silicon showed many holes as a consequence of dewetting.

The enzymatic degradation of these transferred OCDOL films (Fig. 5b) proceeded faster than on the water surface (Fig. 4) due to non-identical conditions. The constant stirring and the temperature of 37 °C (highest activity of enzyme) led to complete dissolution after few minutes (Fig. 5b). While the relative effect was somewhat similar (ca. 2× slower degradation of highly crystalline vs. amorphous films), the difference in absolute numbers was very small (Fig. 5b).

Bulky end-groups are expelled to the crystal surface during chain packing for crystals formation [11]. The density is inversely proportional to molecular weight and hence very pronounced for oligomers. Therefore, a distinct feature of highly crystalline OCL films is the high density of free unreacted end-groups presented at their surface. Here, this was demonstrated by chemically linking methacrylate end-groups apparent in the OCDME film, which are primarily present at the surface of the crystals, to fluorescein dimethacrylate. The redistribution of the functionalized end-groups during film melting and recrystallization was observed by fluorescence microscopy (Fig. 6). For fluorescein labeling, highly crystalline OCDME film was incubated in fluorescein dimethacrylate solution in the presence of UV light for 4 h. After the photo-reaction, the crystals in the OCDME film (Fig. 6e) showed a high degree of fluorescence suggesting successful linking

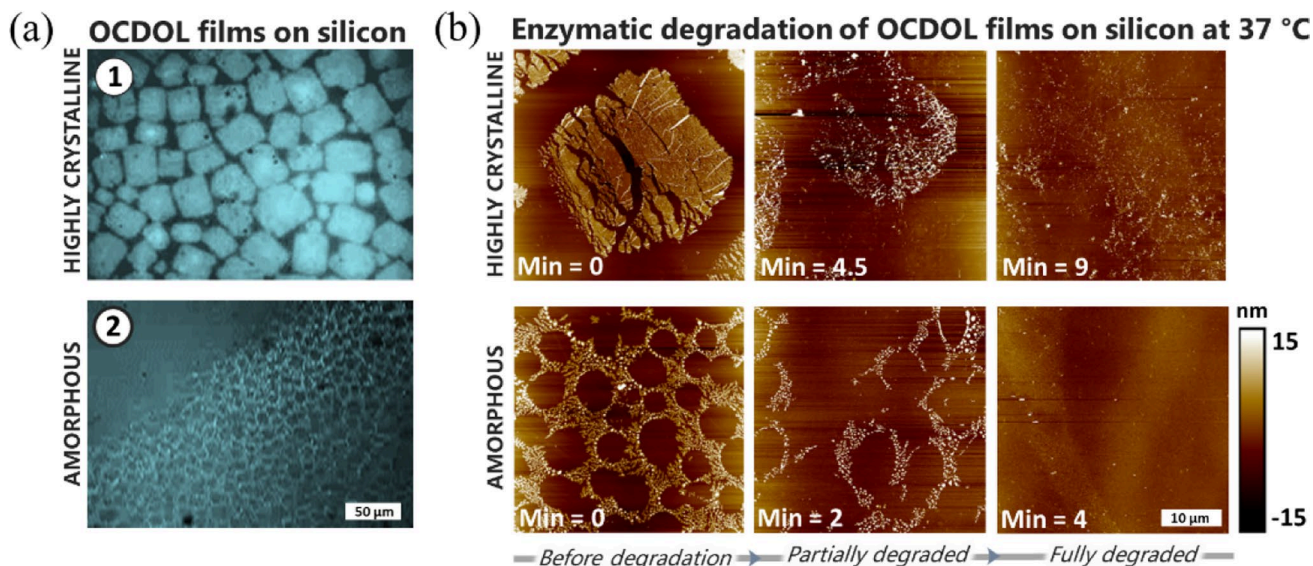


Fig. 5 Optical microscopy images **a** of transferred highly crystalline OCDOL films (a:1) and amorphous OCDOL films (a:2) on silicon by Langmuir–Schaefer method. High amount of crystals from a highly crystalline film are transferable on silicon with minor fractures (a:1),

while transferred amorphous film undergoes dewetting process with holes formation (a:2). AFM images acquired at different intervals of enzymatic degradation **b** show that the highly crystalline OCDOL films degrade ca. 2× slower than the amorphous OCDOL film

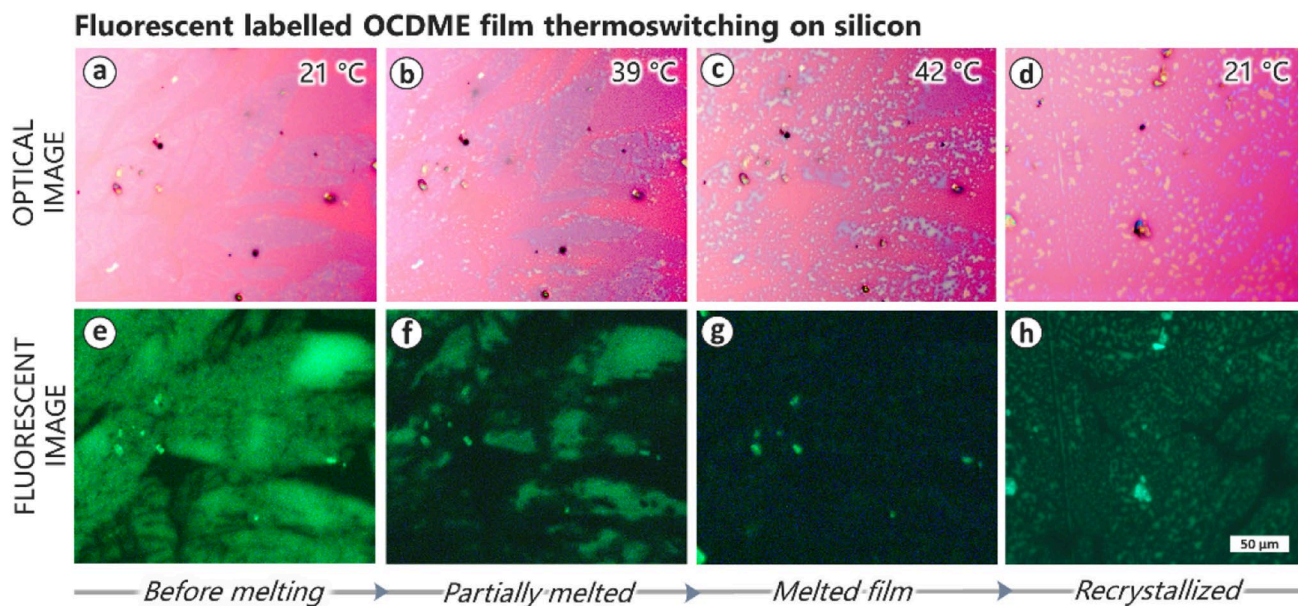


Fig. 6 Optical **a–d** and fluorescent **e–h** microscopy during thermoswitching of highly crystalline OCME films with chemically linked fluorescein label. **a, e**: Fluorescein dimethacrylate links to high density of methacrylate end-groups at the OCDME crystals surface evident by their greater degree of fluorescence compared to the surrounding dark amorphous phase. **b, c; f, g**: Melting of highly crystalline OCME films with chemically linked fluorescein is accompanied

with drastic, uneven lowering of fluorescence intensity in the crystals suggesting redistribution of fluorescein linked OCL end-groups with a possible phase separation. **d, h**: Recrystallized film shows higher fluorescence than the melted film meaning that the fluorescein linked, bulky chain-ends are expelled on the recrystallized structures. The statistical error of temperatures is within limit of ± 1.5 °C

of fluorescein to the chain-ends. During the melting of the film in water, (Fig. 6a–c, e–g) the fluorescence intensity of the film is drastically reduced. After cooling, the recrystallized film (Fig. 6h) has a greater fluorescence intensity than the molten film (Fig. 6g). Since the thin polymer layer should be completely transparent for light, a redistribution of fluorescence was expected, but the almost complete quenching of fluorescence intensity in the molten film was unexpected. Some of the polymer chains were certainly dissolved into the heated water, yet the partial recovery of the fluorescence upon recrystallization demonstrates that there must be an additional reason for the quenching in the molten state. For instance, the wettability of the underlying substrate changes with temperature and therefore can influence polymer chains adhesion and the fluorescence emission [13], while the fluorescein dye is also susceptible to photobleach by environmental oxygen and water [14, 15]. Nevertheless, the example of fluorescence shows very clearly how the availability and assembly of functional molecules at the surfaces of these highly crystalline films can be switched with temperature.

Conclusion

Highly crystalline films of dihydroxy or dimethacrylate-terminated linear OCL molecules were prepared at the air–water interface by compressing the molecules to a very low mean molecular area of ~ 2 Å². Brewster angle microscopy at the air–water interface showed that crystals morphology and thermoswitching behavior (melting and recrystallization) of the highly crystalline OCL films is adjustable by varying the OCL functional end-groups and crystallization temperature. The highly crystalline OCL films were transferred to silicon substrates by the Langmuir–Schaefer method, where transferred OCL crystals are transferable with minor fractures while amorphous films showed dewetting. Highly crystalline OCDOL films are around three times more stable against enzymatic degradation than amorphous OCL films on both water and silicon surfaces; however, they are not very stable in absolute numbers. Fluorescence microscopy of highly

crystalline films of ODCME functionalized with fluorescein dimethacrylate showed a pronounced change in fluorescence intensity during thermoswitching of the film. This study demonstrates a systematic method for developing highly crystalline OCL films with adjustable morphology, thermoswitching, and degradation behavior. The approach used to prepare the crystals is scalable and can be applied at different biointerfaces. Future investigations could encompass the degradation of these highly crystalline coatings in the absence of enzymes at different pH-values, and the exploration of the films as thermosensitive lubricant for surgical implants to reduce friction in contact with tissue.

Acknowledgments The authors acknowledge the support in characterization by Ms. Manuela Keller for AFM, Dr. Skadi Lau for optical microscopy, Dr. Maria Balk for GPC, Ms. Susanne Schwanz for DSC, and Mr. Olaf Lettau for infrared spectroscopy. This work is financially supported by the Helmholtz Association through program-oriented funding and through Helmholtz Graduate School for Macromolecular Bioscience (MacroBio, VH-GS-503).

Funding Open Access funding enabled and organized by Projekt DEAL.

Data availability Data will be made available on reasonable request.

Compliance with ethical standards

Conflict of interest The Authors declare that they have no conflicts of interest.

Open Access This article is licensed under a Creative Commons Attribution 4.0 International License, which permits use, sharing, adaptation, distribution and reproduction in any medium or format, as long as you give appropriate credit to the original author(s) and the source, provide a link to the Creative Commons licence, and indicate if changes were made. The images or other third party material in this article are included in the article's Creative Commons licence, unless indicated otherwise in a credit line to the material. If material is not included in the article's Creative Commons licence and your intended use is not permitted by statutory regulation or exceeds the permitted use, you will need to obtain permission directly from the copyright holder. To view a copy of this licence, visit <http://creativecommons.org/licenses/by/4.0/>.

References

1. A. Lendlein, O.E.C. Gould, Reprogrammable recovery and actuation behaviour of shape-memory polymers. *Nat. Rev. Mater.* **4**, 116 (2019)
2. H. Sun, L. Mei, C. Song, X. Cui, P. Wang, The in vivo degradation, absorption and excretion of PCL-based implant. *Biomaterials* **27**, 1735 (2006)
3. M. Bartnikowski, T.R. Dargaville, S. Ivanovski, D.W. Huttmacher, Degradation mechanisms of polycaprolactone in the context of chemistry, geometry and environment. *Prog. Polym. Sci.* **96**, 1 (2019)
4. W. Ryu, L. Xiang, T. Jeon, M. Ree, Melt density, equilibrium melting temperature, and crystallization characteristics of highly pure cyclic poly(ϵ -Caprolactone)s. *Polymer* **207**, 122899 (2020)
5. B. Lotz, T. Miyoshi, S.Z.D. Cheng, 50th Anniversary perspective: polymer crystals and crystallization: personal journeys in a challenging research field. *Macromolecules* **50**, 5995 (2017)
6. Y.-X. Liu, E.-Q. Chen, Polymer crystallization of ultrathin films on solid substrates. *Coord. Chem. Rev.* **254**, 1011 (2010)
7. B. Li, A. Esker, Molar mass dependent growth of poly(ϵ -caprolactone) crystals in langmuir films. *Langmuir* **23**, 2546 (2007)
8. S. Saretia, R. Machatschek, B. Schulz, A. Lendlein, Reversible 2D networks of oligo(ϵ -caprolactone) at the air-water interface. *Biomed. Mater.* **14**, 34103 (2019)
9. K. Ariga, Y. Yamauchi, T. Mori, J.P. Hill, 25th anniversary article: what can be done with the langmuir-blodgett method? recent developments and its critical role in materials science. *Adv. Mater.* **25**, 6477 (2013)
10. S. Yuan, K. Schmidt-Rohr, Immobilized ^{13}C -labeled polyether chain ends confined to the crystallite surface detected by advanced NMR. *Sci. Adv.* **6**, 59 (2020)
11. S. Agbolaghi, S. Abbaspoor and F. Abbasi: A comprehensive review on polymer single crystals-From fundamental concepts to applications. *Progress Polym. Sci.* (2017).
12. A.-C. Schöne, K. Kratz, B. Schulz and A. Lendlein: Polymer architecture versus chemical structure as adjusting tools for the enzymatic degradation of oligo(ϵ -caprolactone) based films at the air-water interface. *Polym. Degradat. Stab.* **131** (2016).
13. R. Gupta, R. Thomas, G.U. Kulkarni, Tunable solid state fluorescence behavior of a methoxy substituted oligo(phenyleneethynylene): influence of cooling rate and surface crystallization. *J. Mater. Chem.* **22**, 19139 (2012)
14. J.R. Saylor, Photobleaching of disodium fluorescein in water. *Exp. Fluids* **18**, 445 (1995)
15. L. Song, E.J. Hennink, I.T. Young, H.J. Tanke, Photobleaching kinetics of fluorescein in quantitative fluorescence microscopy. *Biophys. J.* **68**, 2588 (1995)

SUPPLEMENTARY INFORMATION

Highly crystalline PCL ultrathin films as thermally switchable biomaterial coatings

Shivam Saretia^{1,2}, Rainhard Machatschek^{1,2}, Andreas Lendlein^{1,2*}

¹Institute of Active Polymers and Berlin-Brandenburg Center for Regenerative Therapies, Helmholtz-Zentrum Geesthacht, Kantstr. 55, 14513 Teltow, Germany

²Institute of Chemistry, University of Potsdam, Karl-Liebknecht-Straße 24-25, 14476 Potsdam, Germany

*Correspondence to: Andreas Lendlein

E-mail: andreas.lendlein@hzg.de

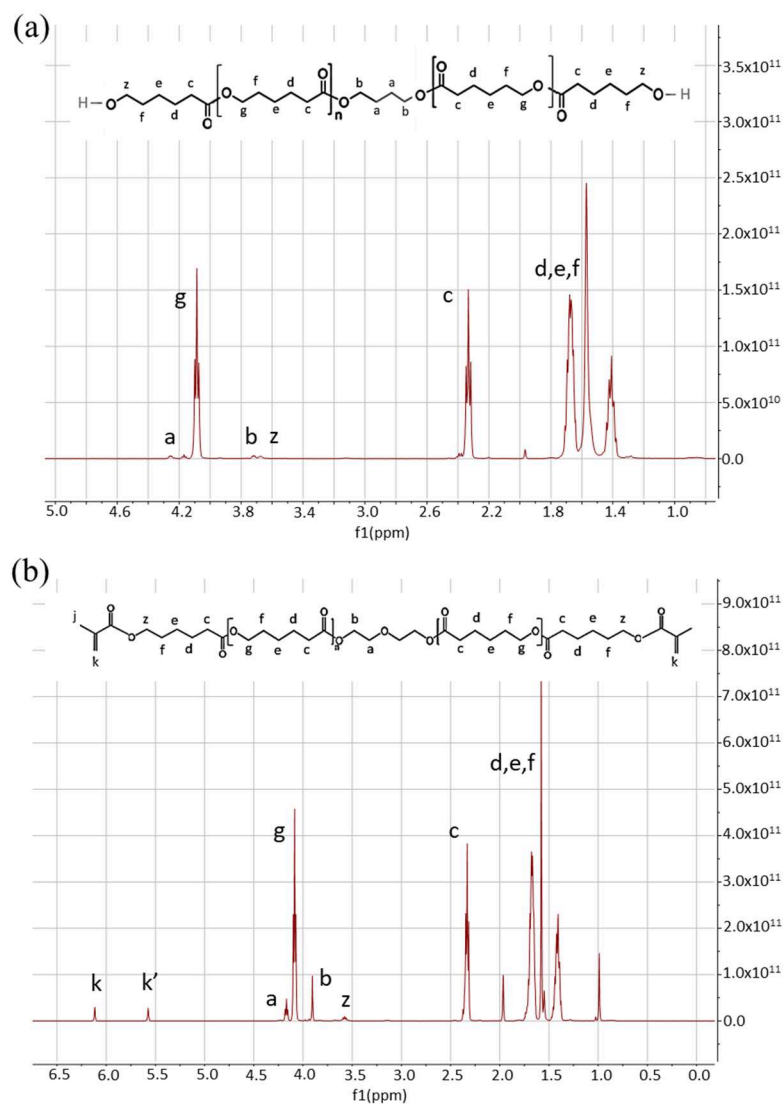


Figure S1: ¹H NMR spectra of OCL diol (a) and OCL dimethacrylate (b) in deuterated chloroform at room temperature.

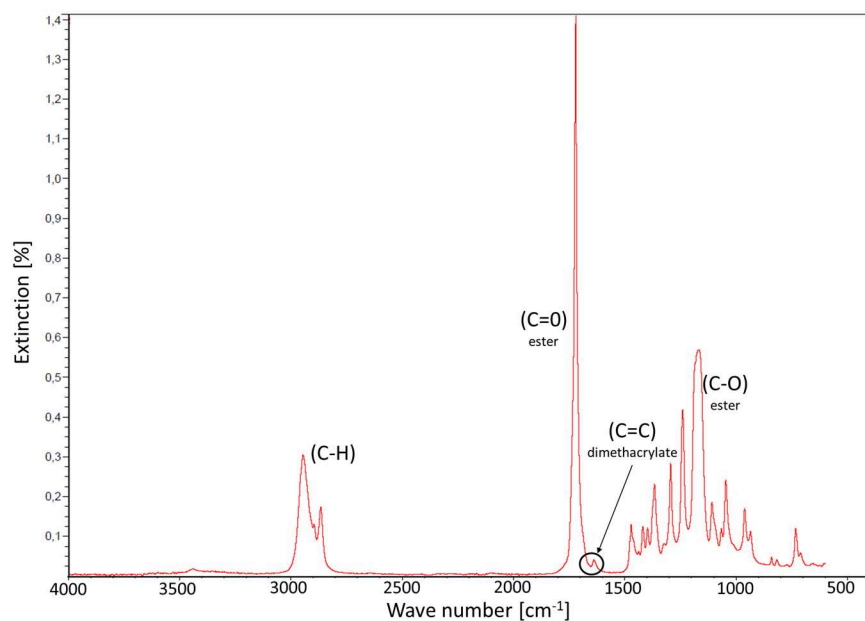


Figure S2: Infrared spectra of OCL dimethacrylate of solid sample under vacuum at room temperature.

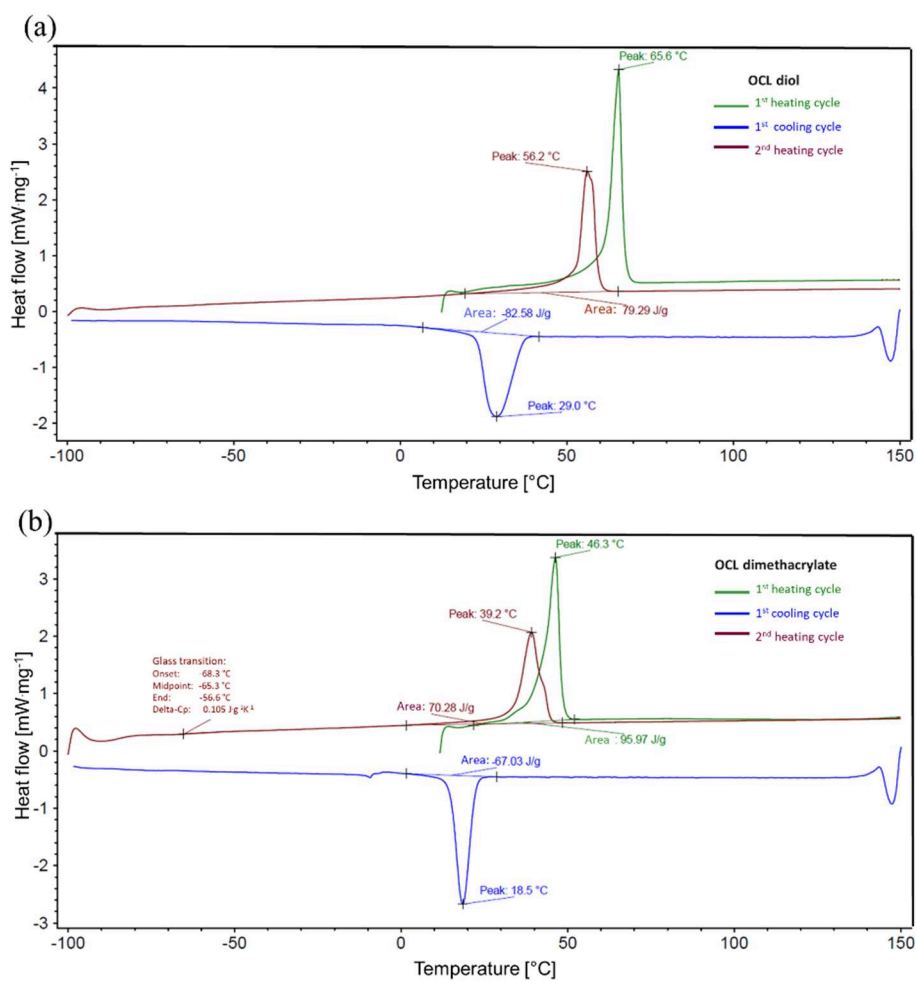


Figure S3: Differential Scanning Calorimetry (DSC) thermograms of OCL diol (a) and OCL dimethacrylate (b).

Table S1: Methods for investigating bulk OCL samples M_n , degree of end group functionalization, chemical structure and thermal properties.

Method	Description
GPC	The set up for determining M_n by Gel Permeation Chromatography (GPC) consisted of a mixed D column (600 mm \times 7.5 mm, Polymer Laboratories Ltd.), a T60A dual detector and a refractive index detector (Shodex RI-101, Showa Denko, Japan). Chloroform (HPLC grade, Roth) was used as eluent at a flow rate of 1.0 mL \cdot min $^{-1}$, and polystyrene as the standard for universal calibration.
^1H NMR (Figure S1)	Structure elucidation and molecular weight analysis of OCL samples was performed by ^1H NMR using a Bruker Avance 300 spectrometer (300 MHz), in CDCl_3 (99.8%, VWR) at 25 ± 0.5 °C. By ^1H NMR, the molecular weight, M_n was determined by calculating the number of repeating monomer units, $n = (\text{sum of CH}_2 \text{ proton integrals}) / (\text{sum of CH}_2 \text{ protons}) / (\text{integral per proton value})$. Value of n for OCL diol is 70 ± 2 and for OCL dimethacrylate is 35 ± 2 . For calculating the M_n , following formula is used, $M_n = (\text{MW end groups}) + (\text{MW core group}) + (\text{MW repeating caprolactone unit}) \cdot (n)$. M_n of OCL diol = $(31+31) + (104) + (114) \cdot (69) \text{ g}\cdot\text{mol}^{-1} = 7900$ to $8200 \text{ g}\cdot\text{mol}^{-1}$. M_n of OCL dimethacrylate = $(69 + 69) + (104) + (114) \cdot (34) \text{ g}\cdot\text{mol}^{-1} = 4200$ to $4300 \text{ g}\cdot\text{mol}^{-1}$. Degree of end group functionalization, from OCL diol ^1H NMR spectra (a) was calculated by the formula, $D_{\text{OCDOL}} = (I < z > / I < a \text{ or } b >) \cdot 100 \%$, coming out to be $\geq 95 \%$. Degree of end group functionalization from OCL dimethacrylate ^1H NMR spectra (b) was calculated as $D_{\text{OC DME}} = (I < k > / I < b >) \cdot 100 \%$, yielding $\sim 85 \%$.
IR analysis (Figure S2)	Infrared analysis (Nicolet spectrometer) was carried out for a solid sample of OCL dimethacrylate. IR revealed typical stretches for OCL and methacrylate. At $\sim 1620 \text{ cm}^{-1}$, a small peak due to C=C bonds is visible. The encircled stretches at 810 cm^{-1} (=CH) and 1408 cm^{-1} (=CH $_2$) are also contributions from methacrylate-groups.
DSC (Figure S3)	Thermal properties of OCL bulk samples were evaluated on a DSC 204F1 (Perkin Elmer). Under nitrogen purge, the sample was heated from 4 °C to 150 °C (green), followed by the first cooling cycle (blue) to -100 °C and a final second heating cycle (red) till 150 °C. The rate of heating or cooling was 10 K \cdot min $^{-1}$. Thermal properties are determined from the first cooling and second heating cycle run. For thermal analysis of the bulk material, the DSC has an instrumentation error of ± 0.5 °C.

Table S2: Langmuir technique setup for investigating OCL films at the air-water interface.

Langmuir technique	Description
Apparatus	The Langmuir trough (KSV NIMA, Finland) and Brewster angle microscope (BAM) were placed on an active vibration isolation system (Halcyonics variobasic 40, Accurion, Germany) within a laser safety cabinet. The temperature of the aqueous subphase was controlled with a circulating water bath at the exterior of Langmuir trough. The surface pressure (π) at the air-water interface was measured by the Wilhelmy technique (hanging platinum plate) with a calibrated sensor placed at the centre between the barriers in the Langmuir trough. To maintain the water level during the experiment, the evaporated water in the Langmuir trough was compensated by the digitally controlled water pump (Ismatec, Germany).
Software	The Langmuir trough software (KSV NIMA) uses the input variables of spread amount of OCL solution at air-water interface, trough surface area, and molecular weight of repeat unit (ϵ -caprolactone; $114 \text{ g}\cdot\text{mol}^{-1}$) to calculate the OCL film mean molecular area (MMA). The output curves show relationships between MMA, surface pressure, temperature, compression speed and time.
Cleaning	For cleaning of the Langmuir trough, its surface was wiped thoroughly with ethanol (HPLC grade; Bernd Kraft, Duisburg, Germany) soaked tissue wipes (Kimtech Science, Germany) followed by chloroform (HPLC grade, Roth, Germany) soaked tissue wipes. Deionized water was filled in the Langmuir trough and removed, at least three times.
Final subphase	The final aqueous subphase in the Langmuir trough was deionized water at 12 or 21 °C. By monitoring the surface pressure, the final purity of the Langmuir trough and the subphase was controlled. In the final aqueous subphase, the total change of the surface pressure at air-water interface while closing the Langmuir trough compression barriers was below $0.2 \text{ mN}\cdot\text{m}^{-1}$.

Table S3: Methods for investigating enzymatic degradation of transferred OCL films on silicon surface.

Method	Description
Optical microscopy	The change in morphology of the films was observed using a polarized optical microscope (Zeiss Axio Imager A1m, Carl Zeiss, Jena, Germany) equipped with crossed polarizers and a 40x magnification objective (Objective Zeiss A-Plan Plan 40x/0,65 Pol).
AFM	The topography of the OCL films degraded at different intervals was recorded in air using AFM (MultiMode 8, Bruker, Karlsruhe, Germany) operating in the intermittent contact mode in air at 21 ± 0.5 °C and RTESPW-150 tips (150 kHz frequency; $5 \text{ N}\cdot\text{m}^{-1}$ spring constant). All AFM images were line-flattened with a first order polynomial using the software NanoScope Analysis 2.0.

Biomedical Materials

Appendix IV:



PAPER

Reversible 2D networks of oligo(ϵ -caprolactone) at the air–water interface

OPEN ACCESS

RECEIVED

27 September 2018

REVISED

30 January 2019

ACCEPTED FOR PUBLICATION

5 March 2019

PUBLISHED

3 April 2019

Original content from this work may be used under the terms of the [Creative Commons Attribution 3.0 licence](https://creativecommons.org/licenses/by/4.0/).

Any further distribution of this work must maintain attribution to the author(s) and the title of the work, journal citation and DOI.

Shivam Saretia^{1,2}, Rainhard Machatschek¹, Burkhard Schulz^{1,2} and Andreas Lendlein^{1,2,3}¹ Institute of Biomaterial Science and Berlin-Brandenburg Center for Regenerative Therapies, Helmholtz-Zentrum Geesthacht, Kantstraße 55, D-14513 Teltow, Germany² Institute of Chemistry, University of Potsdam, Karl-Liebknecht-Straße 24-25, D-14476 Potsdam, Germany³ Author to whom any correspondence should be addressed.E-mail: andreas.lendlein@hzg.de**Keywords:** poly(ϵ -caprolactone), langmuir monolayer, two dimensional network, crystallization, cross-linking**Abstract**

Hydroxyl terminated oligo(ϵ -caprolactone) (OCL) monolayers were reversibly cross-linked forming two dimensional networks (2D) at the air–water interface. The equilibrium reaction with glyoxal as the cross-linker is pH-sensitive. Pronounced contraction in the area of the prepared 2D OCL films in dependence of surface pressure and time revealed the process of the reaction. Cross-linking inhibited crystallization and retarded enzymatic degradation of the OCL film. Altering the subphase pH led to a cleavage of the covalent acetal cross-links. The reversibility of the covalent acetal cross-links was proved by observing an identical isotherm as non-cross-linked sample. Besides as model systems, these customizable reversible OCL 2D networks are intended for use as pH responsive drug delivery systems or functionalized cell culture substrates.

1. Introduction

Poly(ϵ -caprolactone) (PCL) plays a paramount role as degradable implant material or as matrix for controlled drug delivery systems. It can be processed to nanoparticles, micelles, microspheres, electro spun mats, scaffolds or films [1–4]. End-group functionalized poly- or oligo(ϵ -caprolactone)s as telechelics are starting materials for building complex architectures. In such polymer systems, thermal properties and degradation profiles are adjustable by controlling the number of arms and chain lengths of the telechelics. With capability of further polymerization, one dimensional telechelics give new opportunities for creating three dimensional dendrimers, bulk polymer networks and 2D nanostructures [5, 6]. Reversibly cross-linked polymer networks of PCL can be stimuli responsive. Temperature sensitive net-points can induce a shape memory response [7, 8] while reversible chemical bonds promote self-healing characteristics [9, 10]. Permanently cross-linked PCL networks are applied for tissue regeneration [11, 12] and in printing technologies [13, 14]. An important parameter in PCL networks modulated by cross-linking is ester bond cleavage by degradation [15–19]. The rate-

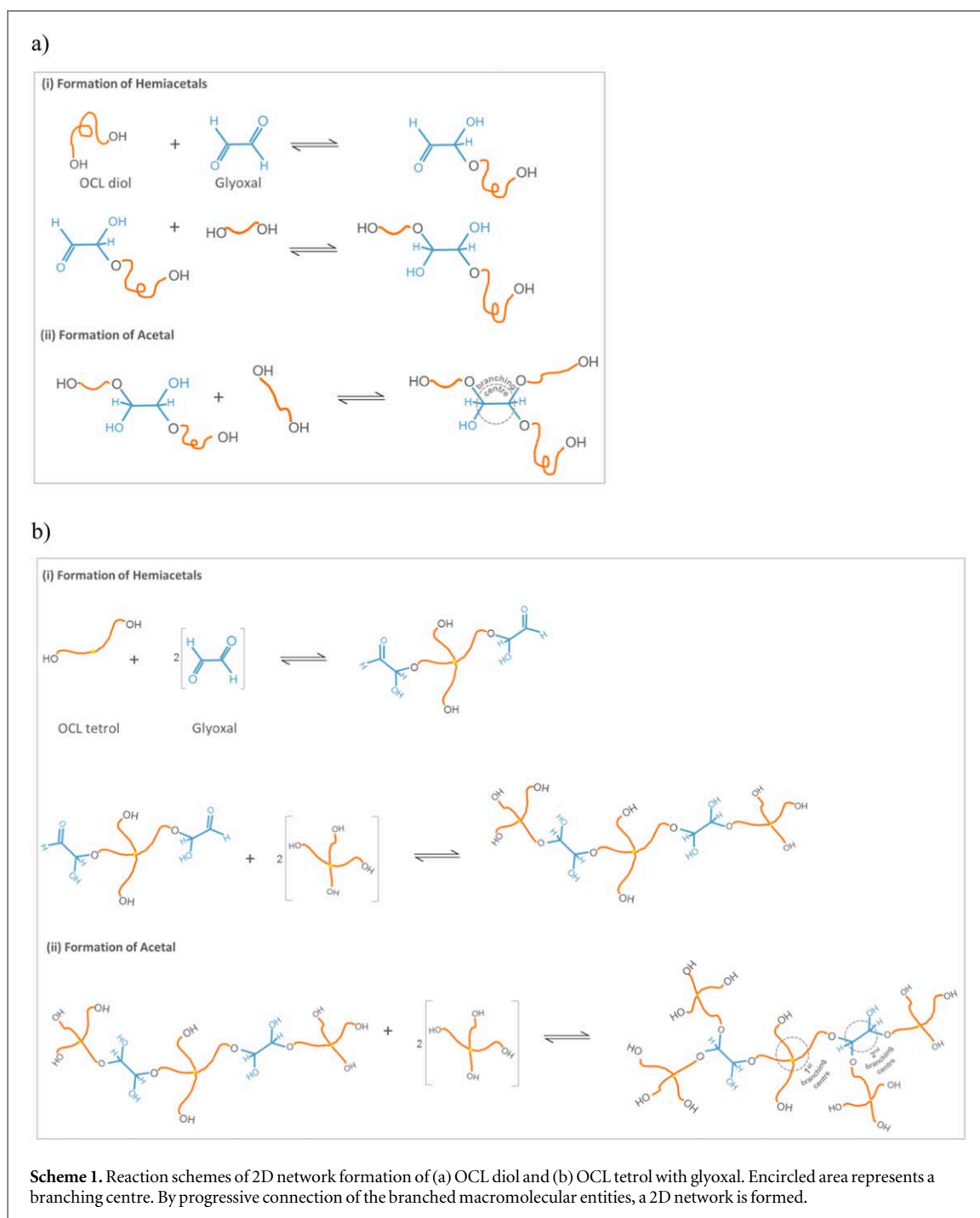
determining step in PCL degradation by enzymatic hydrolysis generally slows down in the presence of netpoints formed by crystalline domains [20–22]. PCL based elastomers enzymatically hydrolyse completely over a wide range of temperatures at pH 7 when lacking crystalline domains. PCL elastomers combining controlled biodegradation and reasonable mechanical strength can be prepared by cross-linking a star-shaped hydroxyl-terminated poly(γ -methyl- ϵ -caprolactone) with bis(β -lactone) [15]. Implants prepared by cross-linking PCL during ring-opening polymerization of caprolactone with bis(trimethylene carbonate) exhibit reduced crystallinity and form-stability, but show suppressed enzymatic degradation [16]. Degradation kinetics are also influenced for benzoperoxide cross-linked PCL membranes in phosphate buffered saline [17]. Interestingly, PCL films prepared by photocross-linking with benzophenone or benzil exhibit faster hydrolysis due to enhancement in overall polarity of the film [18, 19]. These examples show that the physico-chemical properties, mechanical stability and degradation profiles of 3D networks can be tailored in a controlled fashion by cross-linking. On the other hand, 2D polymer systems with interconnected telechelics in lateral plane can also lead to

generation of new material features as seen for 2D materials such as graphene and its derivatives, which modulate responses with cells, tissues or other bio-interfaces [23, 24]. Although graphene materials have immense potential in healthcare such as for drug delivery, bio imaging, capturing pathogens and tissue engineering, several contradictory results are reported in literature due to graphene shape, size, concentration, carbon source, and cytotoxicity [25, 26]. Therefore, it is still a challenge to develop alternatives to conventional 2D materials for biological applications. We hypothesize that functionalized 2D polymer networks based on OCL telechelics with different chemical functionalities can be used as building blocks for creating bioresponsive polymer 2D networks. Besides network stability, the degradability should be altered by an external stimulus such as by pH and has to be systematically investigated. Chemical functions sensitive to pH are of specific interest, since gradients of pH exist at different physiological levels and in nature. Sites of tumour and inflammatory tissues have a slightly acidic pH when compared to their surrounding healthy tissues. Moreover, the environment of endosomes and lysosomes that carry substances inside cells is acidic. Hence, systems with pH sensitive chemical cross-links have attracted a key focus in developing drug delivery systems and in tissue regeneration [16, 27–29]. There are several possibilities to have OCL cross-links sensitive to pH, such as by using ortho ester [30], cis-aconityl bond [31], Schiff base formed between hydrazine and ketone groups [32] and acetal cross-links [33].

The Langmuir technique is ideally suited for preparing 2D materials of non-water or partially water soluble precursors. It allows for positioning of reactive end groups of monomers at the air–water interface for linking by different reaction mechanisms such as by irradiation [34], enzyme [35], catalyst [36], metal ions [37, 38] and ‘click’ reactions [39]. Additionally, faster analysis of biodegradation processes are possible by this technique at molecular level [40]. While various ideally symmetric, small molecules are linked using Langmuir technique to form 2D materials [34, 37, 39, 41–44], only few studies described 2D cross-linking of oligomers or polymers using the Langmuir technique in recent years [5, 38, 45–49]. For example, a semi-interpenetrating oligomeric network is achievable by embedding cross-linked methacryloxypropyl-terminated polydimethylsiloxane in a cellulose acetate butyrate matrix [5]. In our concept for preparing biodegradable 2D polymer networks, we use OCL telechelics end-capped with hydroxyl groups, because of their stability and well-studied behaviour at the air–water interface [50]. Acetal cross-links in hydroxyl terminated OCL monolayers are favoured since they are well described, can be used with different types of hydroxyl groups [51] and form under the conditions of the Langmuir technique experimental setup (aqueous subphase at room temperature). Acetal bonds

form reversibly and provide the required pH sensitivity for a stimulus responsive material. This is a key advantage over traditional 2D materials forming irreversibly. The lateral size of 2D sheets is limited due to the nearly inevitable formation of grain boundaries when several sheets grow simultaneously next to each other. With reversible reactions, the grain boundaries can be cured and large lateral sizes can be achieved. The chemical equilibrium determines the number of unreacted chain ends that are available for further functionalization. As a proof of principle, the dialdehyde glyoxal is used, which imparts hemiacetal and acetal links in the hydroxyl terminated OCL polymer system and can react with four hydroxyl terminated chain ends of OCL. An idealised acetalization reaction scheme is shown in scheme 1.

The carbonyl group of glyoxal protonates under water, which is attacked by the nucleophilic hydroxyl group of an OCL molecule [52, 53]. After subsequent deprotonation of the intermediate species, hemiacetal bonds are formed. Hemiacetal is an unstable intermediate and can react with hydroxyl groups of an OCL chain present in the vicinity to form an acetal [51]. The acetal bonds are stable in alkaline pH while under acidic pH, cleavage of some acetals occurs to release free end groups. The density of OCL hydroxyl groups at the air–water interface can be influenced by modulating OCL molecule packing density. Here, we examine two approaches to form a covalent 2D network. With linear, hydroxyl terminated OCL diol, a network is formed because each glyoxal molecule can connect up to four linear molecules and act as a branching centre (scheme 1(a)). Here, a branching centre is a point in the network where more than two OCL chains are covalently connected. When eventually more chain-ends are connected in the branching centres, the branched macromolecular entities link and ultimately form a 2D network. When using star shaped OCL tetrols, a certain number of branching centres are already provided by the tetrols (scheme 1(b)). Hence, we expect a faster network formation for tetrols, compared to diols. The maximum cross-link density for both linear molecules and tetrols is determined by molecular weight or arm length, respectively. Here, we use tetrols with an arm length (3200 g mol^{-1}) that is similar to the molecular weight of the diol (2800 g mol^{-1}), and therefore, in the diol monolayer, the hydroxyl end-groups concentration per unit area is double compared to the tetrol monolayer. It is known that PCL chain segments near covalent network points have limited mobility due to steric hindrance and hence their crystallization is hindered. We will use this effect to qualitatively evaluate the progress of the cross-linking reaction by studying the surface pressure induced crystallization of the layer. Furthermore, cross-links delay the biodegradation of OCL by reducing the number of free chain ends where small fragments can be generated relatively fast, so the



enzymatic degradation of OCL is studied to obtain further information on the degree of cross-linking.

To free OCL molecules from a cross-linked OCL 2D network, the formation of branching centres is reversed. This is achieved by breaking the acetal bonds. We expect that acetal bonds in the network can be cleaved to release free chain ends by reducing the pH. The reversion of the network formation after lowering of the pH is studied by π -A isotherms and pressure induced crystallization. The prepared pH triggered OCL 2D network aims in broadening applications of 2D crystallisable polymers, such as for forming pH triggered enteric drug delivery systems.

2. Experimental

2.1. Materials

Oligo(ϵ -caprolactone) diol (OCL diol, trade name CAPA 2304, Solvay Caprolactones, Warrington, UK) was used without any further purification. Star-shaped polymer based on ϵ -caprolactone with four-arms (4 arm OCL) was synthesized using the catalyst dibutyltin oxide and the initiator pentaerythritol [54]. Glyoxal (40% w/v, Sigma Aldrich, Germany) used as the cross-linker was dissolved in up to 5 ml water in required concentration before injecting into the sub-phase. The aqueous subphase and water for dissolution of glyoxal was obtained by a Milli-Q Gradient

A-10 water purification system (Millipore, 18.2 MU cm, toc < 4 ppb). For cleaning of trough, ethanol (HPLC grade; Bernd Kraft, Duisburg, Germany) and chloroform (HPLC grade, Roth) were used. For the used OCL diol and 4 arm OCL, the characterisation data were reported previously [55]. The average number molecular weight (M_n), determined by gel permeation chromatography (GPC) was 2800 g mol^{-1} and $13\,000 \text{ g mol}^{-1}$, respectively. The determined M_n (GPC) per end group for OCL diol and 4 arm OCL was 1400 g mol^{-1} and 3200 g mol^{-1} , respectively.

2.2. Langmuir monolayer technique

The surface pressure-area (π -A) isotherms were recorded with a Langmuir trough (KSV NIMA, Finland) placed on an active vibration isolation system (Halcyonics variobasic 40, Accurion, Germany) within a laser safety cabinet. The surface pressure (π) was measured by the Wilhelmy technique with a calibrated sensor located in the centre between the barriers. Water level compensation system was used to compensate the loss of water due to evaporation during the course of experiment to avoid false changes in the recorded surface pressure. The trough was cleaned thoroughly with ethanol followed by chloroform. Afterwards, the deionized water was filled and removed at least three times. By monitoring the surface pressure, the purity of the trough and the subphase was controlled. In the final aqueous subphase, while closing the barriers, the total change of the surface pressure was below 0.2 mN m^{-1} . For all OCL samples, the chloroform stock solutions had a concentration in the range of 0.2 – 0.4 mg ml^{-1} . The solution was applied drop-wise onto the air-water interface using a microsyringe (Hamilton Co., Reno, NV, USA). The chloroform was allowed to evaporate for ten minutes before the start of compression. The rate of compression and expansion of monolayer was 10 mm min^{-1} . The surface pressure was recorded as a function of the mean molecular area per repeating unit (MMA).

The elasticity modulus was determined using the formula, $\kappa = A^{-1} (\delta\pi \cdot \delta A^{-1})$ where A is the area per molecule and π is the surface pressure. At the maximum of elasticity modulus, the corresponding surface pressure and mean molecular area is π_i and MMA_i , respectively.

2.3. Cross-linking of OCL monolayer

For cross-linking by dialdehyde, OCL molecules were compressed and withheld at a constant surface pressure. Thereafter, glyoxal (Sigma Aldrich, Germany; vapour pressure of glyoxal 40% at 20°C : 24 mbar) was injected into subphase (glyoxal/caprolactone molar ratio in the subphase = 20 000) and the monolayer was withheld at a specific constant surface pressure. Glyoxal is highly water soluble and its hydrate forms, which are considered non-volatile, contain reactive

carbonyl groups [56]. After the fixed period of reaction time, the barriers were opened completely to initial position of the Langmuir trough and π -A isotherms of the cross-linked layers were recorded.

2.4. Degradation by lipase

For enzymatic degradation of OCL 2D networks, lipase (Sigma, Germany) from *Pseudomonas cepacia* (0.007 mg ml^{-1}) was injected into the subphase. For degradation of the control sample, glyoxal was also added just before the injection of the enzyme into the subphase. $A_t A_0^{-1}$, as function of time was recorded where A_0 is the initial surface area occupied by Langmuir film at $t = 0$ and A_t is the acquired surface area after a certain time interval, t . The degradation experiment of Langmuir film was performed at 7 mN m^{-1} ; $22 \pm 0.5^\circ\text{C}$.

2.5. Brewster angle microscopy (BAM) studies

BAM images were recorded with ellipsometer nano-film_ep3 (Accurion, Gottingen, Germany) equipped with a high performance CCD camera, a $10\times$ magnification lens with a maximum lateral resolution of $2 \mu\text{m}$, and a 658 nm class IIIB laser source.

2.6. Interfacial infrared spectroscopy

Polarization Modulation Infrared Reflection Adsorption Spectroscopy (PM-IRRAS; KSV NIMA) was used together with a Langmuir trough (KSV NIMA) with water level compensation to study the change in chemical composition of film under spectral range of 800 – 4000 cm^{-1} .

3. Results and discussion

3.1. Langmuir film isotherms

The π -A isotherm of a non-cross-linked OCL diol monolayer was recorded first to evaluate the suitable conditions for the acetalization reaction. It shows the typical Langmuir monolayer behaviour reported for PCL [57], and is marked by a sudden reduction of surface pressure (collapse pressure $\sim 11.2 \text{ mN m}^{-1}$; figure 1). Based on the values of static elastic modulus of control (non-cross-linked) sample of OCL diol monolayer, acetalization reaction was performed at three different surface pressure values 2, 5 and 7 mN m^{-1} , corresponding to the increasing concentration of OCL end groups per area. To avoid hydrolysis of ester bonds, mild reaction conditions (pH 5.7; room temperature) were realized. After the reaction, the barriers were opened to initial position of the trough and π -A isotherms were recorded to compare reacted OCL 2D film with the control sample.

Apparently, compared to the control sample, lowering of mean molecular area, an increased π_i (table 1) and an elevated collapse pressure was observable for all cases of OCL diol monolayer reaction. Rather, a clear

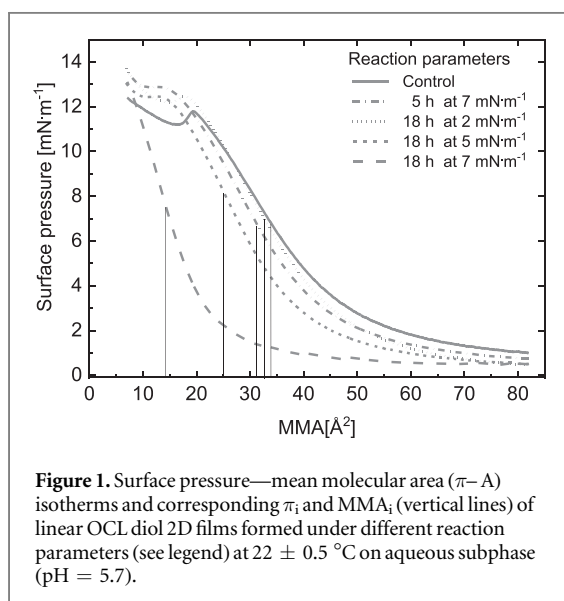


Table 1. Surface pressure and mean molecular area values at the highest point of static elasticity modulus.

OCL monolayer reaction parameters	π_i (mN m ⁻¹)	MMA _i (Å ²)
Bi functional, OCL diol		
Control	6.9 ± 0.3	33 ± 1.0
5 h; 7 mN m ⁻¹	7.1 ± 0.4	31 ± 1.5
18 h; 2 mN m ⁻¹	7.4 ± 0.7	32 ± 2.0
18 h; 5 mN m ⁻¹	8.2 ± 0.3	25 ± 1.0
18 h; 7 mN m ⁻¹	8.1 ± 0.6	14 ± 1.0
Tetra functional, 4 arm OCL		
Control	6.0 ± 0.3	32 ± 1.0
7.5 h; 7 mN m ⁻¹	7.5 ± 0.5	18 ± 1.0

effect on relative reduction of MMA_i was observed for all OCL 2D films prepared depending on end-groups concentration (figure 1). Such a contraction of a monolayer at the air–water interface by cross-linking was also reported for cross-linked PDMS 2D networks [5]. For OCL 2D films, a twofold decrease in MMA_i

compared to the control sample was observed only after OCL diol monolayer was reacted at a high packing density of 7 mN m⁻¹ for 18 h. The acetalization reaction at air–water interface is slow and depends on the OCL molecule end-group concentration. Thus, it is expected that increasing the end-group concentration promotes cross-linking via acetal formation [58]. After reaching the collapse surface pressure, OCL 2D networks formed during 18 h reaction at 5 mN m⁻¹ and 5 h reaction at 7 mN m⁻¹ showed no sudden decrease, rather a plateau region. Additionally, a collapse pressure in π -A isotherm was not observable until the end of compression for the OCL 2D film formed at the high packing density at 7 mN m⁻¹ for 18 h reaction time. The shifting of collapse pressure of all OCL 2D films to a higher value compared to the control sample proves an increase in stability of the film due to acetalization reaction. To prove the acetalization reaction, Polarization Modulation-Infrared Reflection Absorption Spectroscopy (PM-IRRAS) spectra under different reaction times were recorded. The spectrum (figure 2(a)) before injection of glyoxal had no discernible peaks and was used as the reference spectrum, i.e. all spectra were normalized with respect to the spectrum at $t = 0$. The PM-IRRAS signal of the OCL 2D network for visualizing acetal links was weak owing to molecular level ultrathin film. Nevertheless, the acetal doublet peaks (1060 and 1100 cm⁻¹) were clearly distinguishable. The peaks at 1100 and 1060 cm⁻¹ were absent in the non-cross-linked OCL diol monolayer (figure 2(a)) and became visible in all spectra recorded after 21 h glyoxal reaction (figure 2(b)) with the monolayer. The bands are characteristic for acetals and attributed to symmetric COCOC (1100 cm⁻¹) and antisymmetric COCOC (1060 cm⁻¹) stretching.

Further evidence of occurrence of cross-linking was demonstrated by 4 arm OCL. Compared to 2D film of OCL diol, a ~2 fold decrease in MMA_i was reached in 2D film of 4 arm OCL in a relative less

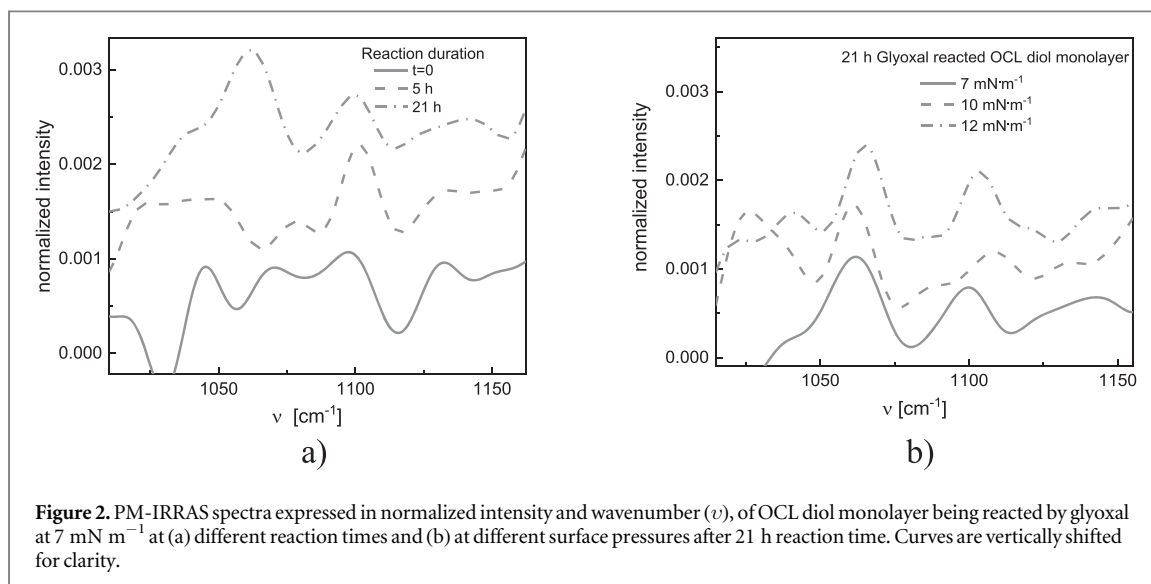
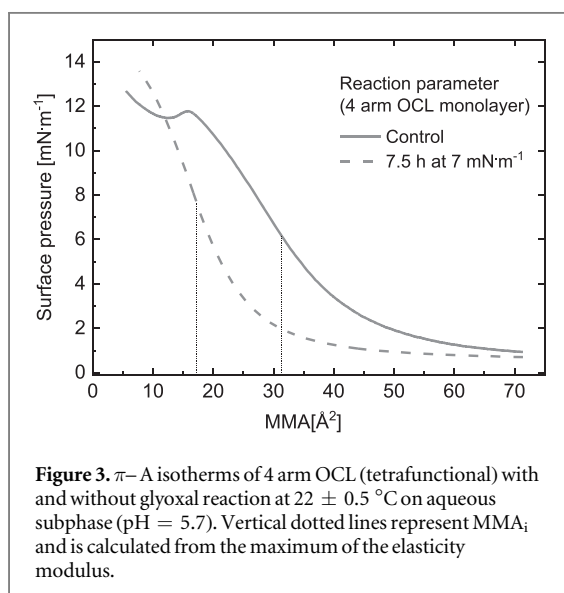


Figure 2. PM-IRRAS spectra expressed in normalized intensity and wavenumber (ν), of OCL diol monolayer being reacted by glyoxal at 7 mN m⁻¹ at (a) different reaction times and (b) at different surface pressures after 21 h reaction time. Curves are vertically shifted for clarity.



duration of acetalization reaction (figure 3). This effect can be correlated to the structure and chemical composition of the molecules. In comparison to linear bifunctional OCL diol molecule, in tetrafunctional OCL, 4 arms of the OCL are connected to a central molecule which can be assumed as a branching centre. Hence, when the duration of the acetalization reaction for 4 arm OCL is decreased to 7.5 h (~60% time less compared to 18 h), a similar progression of isotherm as 18 h reacted bifunctional OCL diol monolayer at 7 mN m^{-1} is observed.

3.2. Crystallization behaviour of OCL 2D network

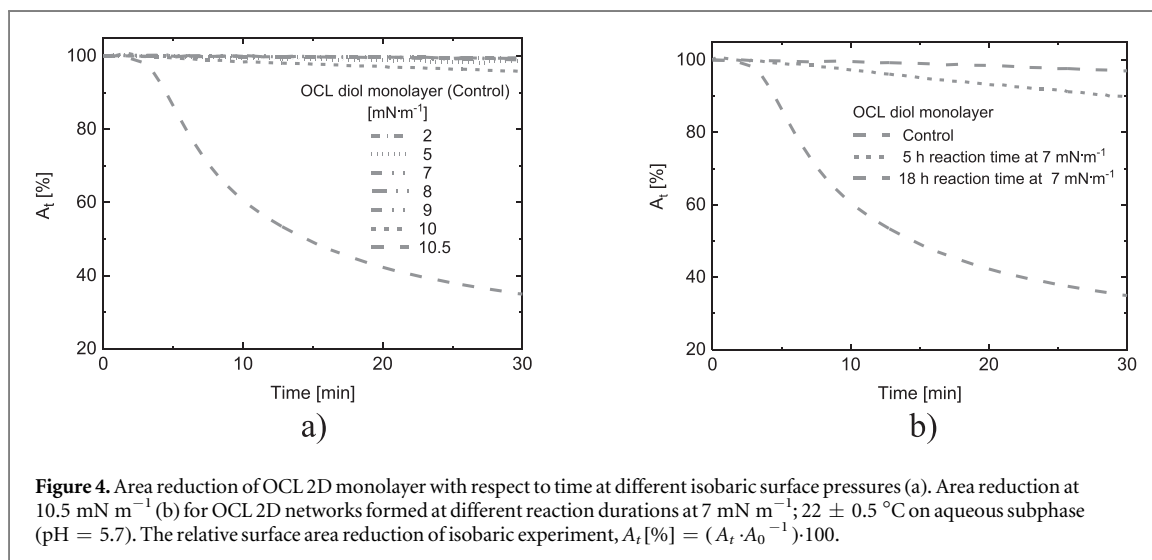
The crystallization behaviour of OCL in restricted geometries is well studied and is affected by molar mass, film thickness, temperature, the field for chain diffusion and many other factors [50, 57, 59]. At the constant surface pressure of 10.5 mN m^{-1} , which is between π_i (6.9 mN m^{-1}) and the collapse pressure (11.2 mN m^{-1}), the non-cross-linked OCL monolayer (control) shows an area reduction (figure 4(a)) due to

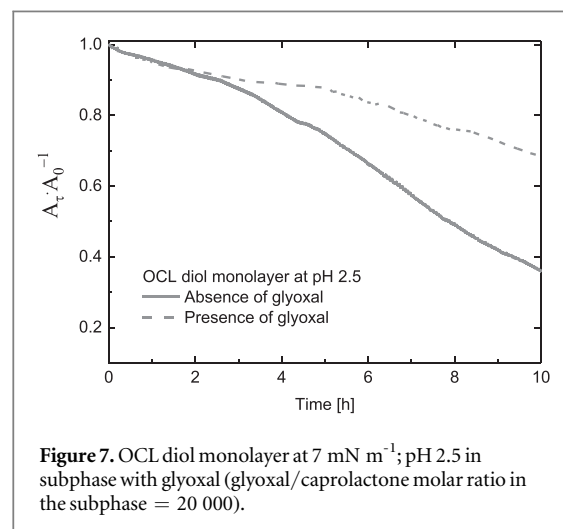
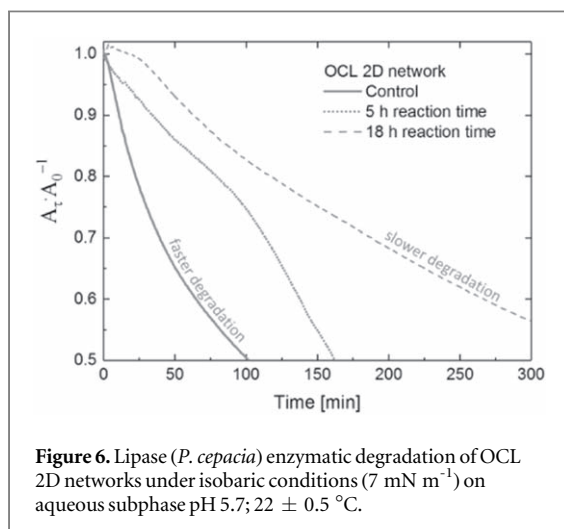
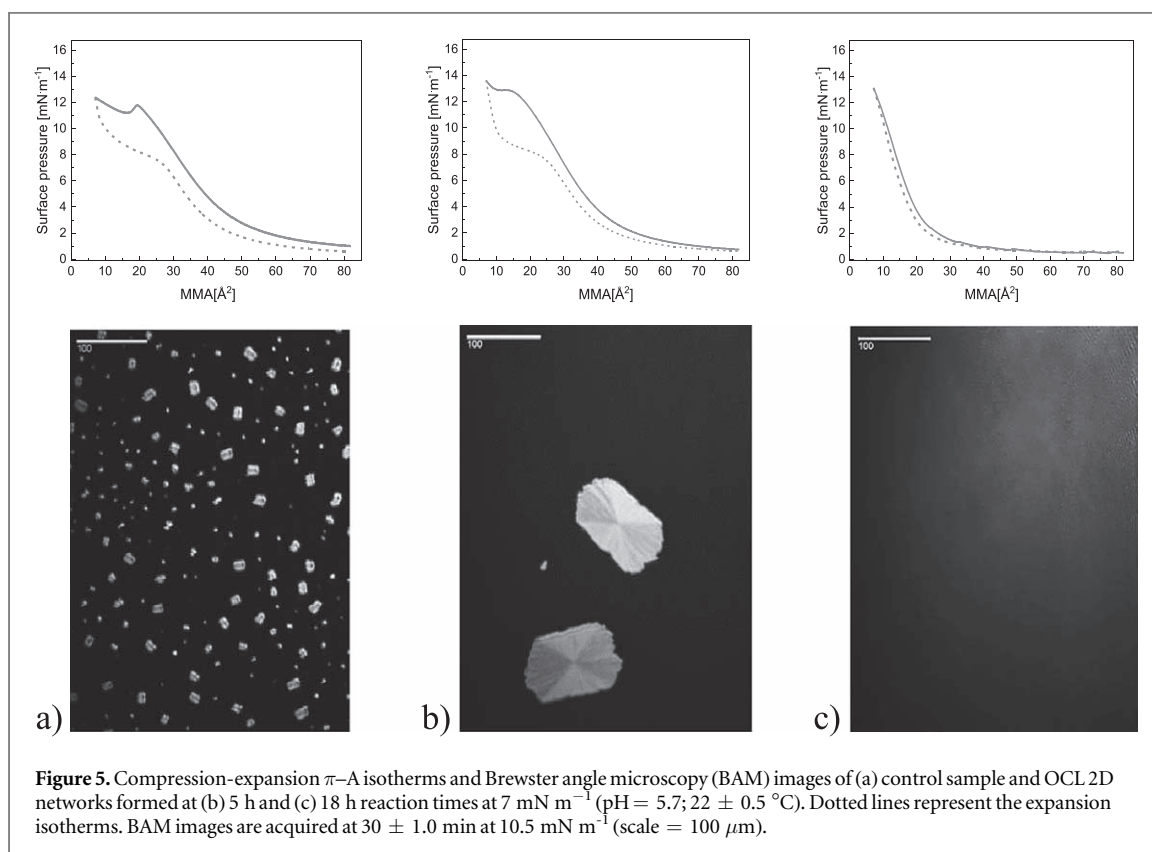
formation of typical small sized 3D domains under BAM (figure 5(a)). These 3D domains of OCL seen as bright regions in the BAM image are the spherulites, which are surrounded by the amorphous layer (dark region). To study the crystallization behaviour of OCL 2D networks, we cross-linked OCL monolayers at 7 mN m^{-1} (in absence of spherulites) for different reaction times and then compressed the layers to the elevated surface pressure of 10.5 mN m^{-1} .

Introduction of branching structure in PCL bulk systems lowers crystallization ability and T_m (melting temperature) while it increases the mechanical stability [60–62]. Since random cross-linking of OCL molecules in Langmuir monolayer presumably leads to branching of OCL chains to form a 2D network, we expect that a retardation of the crystallization process can provide an indirect proof of cross-linking of OCL monolayer.

For OCL 2D networks formed at 5 h reaction time at 7 mN m^{-1} , the normalized area reduction at 10.5 mN m^{-1} was decreased compared to the control sample (figure 4(b)), with accompaniment of large sized spherulites observed in BAM (figure 5(b)). Such an increase in lateral dimensions can be asserted to an increased molar mass of the molecules after cross-linking and therefore such large spherulites, typically formed for intermediate molar mass (~8 kDa) of OCL molecules were observed [57].

On the contrary, the relative area reduction at 10.5 mN m^{-1} was minimal for the OCL 2D network formed at 18 h reaction time at 7 mN m^{-1} (figure 4(b)), with no visible crystals in BAM images (figure 5(c)). This strongly projects that cross-linking impedes the surface pressure induced lateral crystallization of OCL monolayer. By connection of OCL chains by acetal cross-links, molar mass in the monolayer increases while due to formation of cross-linking netpoints, the OCL chain mobility is decreased leading to a retarded crystallization. However, lateral surface pressure induced crystallization in ultrathin films is a dynamic process and cannot be directly interpreted





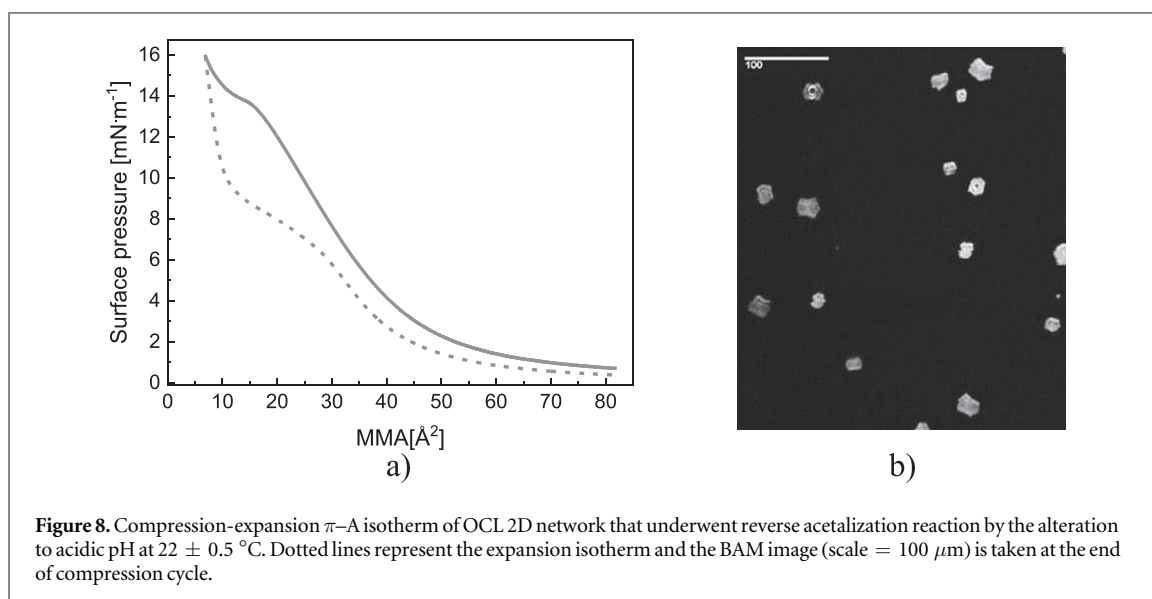
and therefore can be seen only as an indirect proof of cross-linking.

A further insight into the crystallization behaviour is available by recording the expansion π -A isotherms (figure 5). Expansion isotherms formed by opening the Langmuir trough barriers after the end of compression at a constant rate indicate the melting behaviour of surface pressure induced spherulites. The spherulites of the control sample dissolve during the expansion of the monolayer, where the polymer chains of the spherulites continuously unfold to render initial '2D' monolayer state. This marks a faster initial decrease in surface pressure in the expansion isotherm followed by a plateau around 8.5 mN m^{-1}

(figure 5(a)). Such a similar progression of the expansion isotherm was also seen by OCL 2D networks formed after 5 h cross-linking at 7 mN m^{-1} (figure 5(b)). However, for OCL 2D network formed after 18 h cross-linking at 7 mN m^{-1} , a plateau in the expansion isotherm was not observable, while the curve follows a similar trend as its compression cycle (figure 5(c)).

3.3. Degradation of OCL 2D networks

Figure 6 shows enzymatic degradation isotherms of OCL 2D networks formed under different cross-linking reaction durations at the surface pressure of 7 mN m^{-1} , in the absence of any 3D domains in the



layer. The catalytic triad of the enzyme lipase cleaves OCL chains into water-soluble fragments, causing monolayer area reduction. For control sample, after injection of lipase into the subphase (time = 0), a fast degradation was detected. It was previously shown that OCLs below molar masses of $10\,000 \text{ g mol}^{-1}$ present identical degradation isotherms [55]. On the contrary, the degradation isotherm for OCL 2D networks shifts substantially compared to the control sample. The slowest degradation rate was observed for OCL 2D networks formed after 18 h reaction time at 7 mN m^{-1} . Such a dense 2D network with modified and interconnected end groups of OCL molecules possibly hinders interaction of enzyme with OCL segments or has slow formation of water-soluble OCL fragments.

3.4. Reversibility of the cross-links

Figure 7 shows the behaviour of OCL diol monolayer at acidic pH of 2.5 with and without the presence of glyoxal in the subphase. A slower area reduction of OCL diol monolayer at pH 2.5 in presence of glyoxal suggests an interplay of acidic hydrolysis of ester bonds and the cross-linking reaction phenomenon. To prove that the acetal cross-links in the OCL 2D network are reversible, the reverse cross-linking reaction was promoted for retrieval of free OCL molecules by altering the pH and π -A isotherm (figure 8(a)) was recorded.

OCL 2D network was formed at 7 mN m^{-1} after 18 h of glyoxal reaction of OCL diol monolayer in aqueous subphase of pH 5.7. To carry out the reverse acetalization reaction, the pH was shifted to 2.5 for the next 9 h. The barriers were opened to initial Langmuir trough position and compression-expansion isotherms were recorded (figure 8(a)). The π -A curve of OCL 2D network after alteration to acidic pH (figure 8(a)) deviates from the π -A curve of OCL 2D network formed at pH 5.7 (figure 5(c)). Indeed, it follows an identical slope with the control sample

(figure 5(a)), with observance of collapse pressure at $\sim 13.5 \text{ mN m}^{-1}$.

Change in crystallization behaviour further validates the reversibility of cross-links in the network. In contrast to the BAM image of OCL 2D network which shows no 3D domains at 10.5 mN m^{-1} (figure 5(c)), the BAM image for OCL 2D network that underwent reverse acetalization reaction (figure 8(b)) shows occurrence of relatively larger spherulites comparable to the ones observed in non-cross-linked OCL layer at 10.5 mN m^{-1} (figure 5(a)). This implies that alteration to acidic pH caused a decrease in the covalent acetal link density of the cross-linked OCL 2D network, allowing OCL chains to fold and participate again in the lateral crystallization process.

The similar compression-expansion π -A isotherm behaviour as the control sample and occurrence of spherulites implies an increase in the conformational freedom in OCL chain segments and enhanced crystallization degree in the film by the decrease of acetal cross-link density. Therefore, acetal links orchestrated the forming of a reversible OCL 2D network that is reversible by means of pH.

4. Conclusion

The 2D cross-linking of hydroxyl end-capped OCL monolayer by glyoxal at the air-water interface was demonstrated by changes in π -A isotherms, film crystallization behaviour and film degradation rate. Additionally, interfacial infrared spectroscopy demonstrated the acetal bond formation in the OCL 2D film. After cross-linking, π -A isotherm displayed a higher reduction in the mean molecular area for OCL 2D networks formed under high OCL molecular packing density and longer reaction time. Moreover, π -A isotherms demonstrated that reduction in mean molecular area is achieved faster for the 2D network based on tetrafunctional OCL tetrol compared with

bifunctional OCL diol. Reversibility of acetal cross-links in the OCL 2D network is demonstrated by altering the subphase pH to promote the reverse reaction. Such a film exhibited comparative crystallization and π -A isotherm of non-cross-linked OCL monolayer.

Such 2D networks of polymers can give fundamental insights on physical chemistry and rational design of bulk polymer networks. Further work on covalent functionalization of unreacted end-groups will explore how such a stimuli responsive 2D polymer network can be used for delivery of bioactive substances, as coating for medical devices and as functionalized substrates for studying cell behaviour.

Acknowledgments

This work was financially supported by the Helmholtz Graduate School for Macromolecular Bioscience and the Helmholtz Association through programme-oriented funding.

ORCID iDs

Andreas Lendlein  <https://orcid.org/0000-0003-4126-4670>

References

- [1] Malikmammadov E, Tanir T E, Kiziltay A, Hasirci V and Hasirci N 2017 PCL and PCL-based materials in biomedical applications *J. Biomater. Sci. Polym. Ed.* **29** 863–93
- [2] de Melo F, Nicolau P, Piovano L, Lin S-L, Baptista-Fernandes T, King M I, Camporese A, Hong K, Khattar M M and Christen M-O 2017 Recommendations for volume augmentation and rejuvenation of the face and hands with the new generation polycaprolactone-based collagen stimulator (Ellans[®]) *Clin. Cosmetic Investigational Dermatology* **10** 431–40
- [3] Bezwada R S, Jamiolkowski D D, Lee I Y, Agarwal V, Persivale J, Trenka-Benthin S, Ernetta M, Suryadevara J, Yang A and Liu S 1995 Monocryl suture, a new ultra-pliable absorbable monofilament suture *Biomaterials* **16** 1141–8
- [4] Lotfi M, Ghasemi N, Rahimi S, Vosoughhosseini S, Saghir M A and Shahidi A 2013 Resilon: a comprehensive literature review *J. Dental Res. Dental Clinics Dental Prospect.* **7** 119–30
- [5] El Haitami A, Backus E H G and Cantin S 2014 Synthesis at the air–water interface of a two-dimensional semi-interpenetrating network based on poly(dimethylsiloxane) and cellulose acetate butyrate *Langmuir* **30** 11919–27
- [6] Sisson A L, Ekin D and Lendlein A 2013 The contemporary role of ϵ -caprolactone chemistry to create advanced polymer architectures *Polymer* **54** 4333–50
- [7] Lendlein A, Schmidt A M, Schroeter M and Langer R 2005 Shape-memory polymer networks from oligo(ϵ -caprolactone) dimethacrylates *J. Polym. Sci. A* **43** 1369–81
- [8] Zhu G, Liang G, Xu Q and Yu Q 2003 Shape-memory effects of radiation crosslinked poly(ϵ -caprolactone) *J. Appl. Polym. Sci.* **90** 1589–95
- [9] Mallek H, Jegat C, Mignard N, Abid M, Abid S and Taha M 2013 Reversibly crosslinked self-healing PCL-based networks *J. Appl. Polym. Sci.* **129** 954–64
- [10] Kuhl N, Bode S, Hager M D and Schubert U S 2016 Self-healing polymers based on reversible covalent bonds *Adv. Polym. Sci.* **273** 1–58
- [11] Wang S, Yaszemski M J, Gruetzmacher J A and Lu L 2008 Photo-crosslinked poly(ϵ -caprolactone fumarate) networks: roles of crystallinity and crosslinking density in determining mechanical properties *Polymer* **49** 5692–9
- [12] Wang S, Yaszemski M J, Knight A M, Gruetzmacher J A, Windebank A J and Lu L 2009 Photo-crosslinked Poly(ϵ -caprolactone fumarate) networks for peripheral nerve regeneration: physical properties and preliminary biological evaluations *Acta Biomaterialia* **5** 1531–42
- [13] Elomaa L, Teixeira S, Hakala R, Korhonen H, Grijpma D W and Seppälä J V 2011 Preparation of poly(ϵ -caprolactone)-based tissue engineering scaffolds by stereolithography *Acta Biomaterialia* **7** 3850–6
- [14] He Y, Tuck C J, Prina E, Kilsby S, Christie S D R, Edmondson S, Hague R J M, Rose F R A J and Wildman R D 2017 A new photocrosslinkable polycaprolactone-based ink for three-dimensional inkjet printing *J. Biomed. Mater. Res. B* **105** 1645–57
- [15] De Hoe G X, Zumstein M T, Tieghe B J, Brutman J P, McNeill K, Sander M, Coates G W and Hillmyer M A 2018 Sustainable polyester elastomers from lactones: synthesis, properties, and enzymatic hydrolyzability *J. Am. Chem. Soc.* **140** 963–73
- [16] Yang L, Li J, Jin Y, Li M and Gu Z 2015 *In vitro* enzymatic degradation of the cross-linked poly(ϵ -caprolactone) implants *Polym. Degrad. Stab.* **112** 10–9
- [17] Yin G, Zhang L, Zhou Z and Li Q 2016 Preparation and characterization of cross-linked PCL porous membranes *J. Polym. Res.* **23** 229
- [18] Kósa C, Sedlacik M, Fiedlerová A, Chmela S, Borská K and Mosnacek J 2015 Photochemically cross-linked poly(ϵ -caprolactone) with accelerated hydrolytic degradation *Eur. Polym. J.* **68** 601–8
- [19] Mosnacek J, Borská K, Danko M and Janigová I 2013 Photochemically promoted degradation of poly(ϵ -caprolactone) film *Mater. Chem. Phys.* **140** 191–9
- [20] Zumstein M T, Kohler H-P E, McNeill K and Sander M 2016 Enzymatic hydrolysis of polyester thin films: real-time analysis of film mass changes and dissipation dynamics *Environ. Sci. Technol.* **50** 197–206
- [21] Zumstein M T, Kohler H-P E, McNeill K and Sander M 2017 High-throughput analysis of enzymatic hydrolysis of biodegradable polyesters by monitoring cohydrolysis of a polyester-embedded fluorogenic probe *Environ. Sci. Technol.* **51** 4358–67
- [22] Zumstein M T, Rechsteiner D, Roduner N, Perz V, Ribitsch D, Guebitz G M, Kohler H-P E, McNeill K and Sander M 2017 Enzymatic hydrolysis of polyester thin films at the nanoscale: effects of polyester structure and enzyme active-site accessibility *Environ. Sci. Technol.* **51** 7476–85
- [23] Wang R, Sing M K, Avery R K, Souza B S, Kim M and Olsen B D 2016 Classical challenges in the physical chemistry of polymer networks and the design of new materials *Acc. Chem. Res.* **49** 2786–95
- [24] Dong R, Zhang T and Feng X 2018 Interface-assisted synthesis of 2D materials: trend and challenges *Chem. Rev.* **118** 6189–235
- [25] Tu Z, Guday G, Adeli M and Haag R 2018 Multivalent Interactions between 2D nanomaterials and biointerfaces *Adv. Mater.* **30** 1706709
- [26] Kurapati R, Kostarelos K, Prato M and Bianco A 2016 Biomedical uses for 2D materials beyond graphene: current advances and challenges ahead *Adv. Mater.* **28** 6052–74
- [27] Nowag S and Haag R 2013 pH-Responsive micro- and nanocarrier systems *Angew. Chem. Int. Ed.* **53** 49–51
- [28] Li F, Chen C, Yang X, He X, Zhao Z, Li J, Yu Y, Yang X and Wang J 2018 Acetal-linked hyperbranched polyphosphoester nanocarriers loaded with chlorin e6 for pH-activatable photodynamic therapy *ACS Appl. Mater. Interfaces* **10** 21198–205

- [29] Washington K E, Kularatne R N, Karmegam V, Biewer M C and Stefan M C 2018 Stimuli-responsive poly(ϵ -caprolactone)s for drug delivery applications *Stimuli Responsive Polymeric Nanocarriers for Drug Delivery Applications* ed A S H Makhlof and N Y Abu-Thabit vol. 1 (Duxford, United Kingdom: Woodhead Publishing) ch 18 pp 501–29
- [30] Qiu L, Zhu M, Gong K, Peng H, Ge L, Zhao L and Chen J 2017 pH-triggered degradable polymeric micelles for targeted anti-tumor drug delivery *Mater. Sci. Eng. C* **78** 912–22
- [31] Hu F Q, Liu L N, Du Y Z and Yuan H 2009 Synthesis and antitumor activity of doxorubicin conjugated stearic acid-g-chitosan oligosaccharide polymeric micelles *Biomaterials* **30** 6955–63
- [32] Younsoo B, Shiget F, Atsushi H and Kazunori K 2003 Design of environment-sensitive supramolecular assemblies for intracellular drug delivery: polymeric micelles that are responsive to intracellular pH change *Angew. Chem. Int. Ed.* **42** 4640–3
- [33] Gillies E R, Goodwin A P and Fréchet J M J 2004 Acetals as pH-sensitive linkages for drug delivery *Bioconjugate Chem.* **15** 1254–63
- [34] Payamyar P et al 2014 Synthesis of a covalent monolayer sheet by photochemical anthracene dimerization at the air/water interface and its mechanical characterization by AFM indentation *Adv. Mater.* **26** 2052–8
- [35] Bruno F F, Akkara J A, Kaplan D L, Sekher P, Marx K A and Tripathy S K 1995 Enzyme-mediated two-dimensional polymerization of aromatic derivatives on a langmuir trough *Ind. Eng. Chem. Res.* **34** 4009–15
- [36] Kosif I, Kratz K, You S S, Bera M K, Kim K, Leahy B, Emrick T, Lee K Y C and Lin B 2017 Robust gold nanoparticle sheets by ligand cross-linking at the air–water interface *ACS Nano* **11** 1292–300
- [37] Dai W et al 2017 Three-legged 2, 2'-bipyridine monomer at the air/water interface: monolayer structure and reactions with Ni(II) ions from the subphase *Langmuir* **33** 1646–54
- [38] Upcher A, Lifshitz Y, Zeiri L, Golan Y and Berman A 2012 Effect of metal Cations on Polydiacetylene langmuir films *Langmuir* **28** 4248–58
- [39] Kayal H, Ahmida M M, Dufour S, Taing H and Eichhorn S H 2013 Cross-linking of discotic tetraazaporphyrin dyes in 2 and 3 dimensions by 'click' chemistry *J. Mater. Chem. C* **1** 7064–72
- [40] Schöne A C, Roch T, Schulz B and Lendlein A 2017 Evaluating polymeric biomaterial-environment interfaces by Langmuir monolayer techniques *J. R. Soc. Interface* **14** 20161028
- [41] Bauer T, Zheng Z, Renn A, Enning R, Stemmer A, Sakamoto J and Schlüter A D 2011 Synthesis of free-standing, monolayered organometallic sheets at the air/water interface *Angew. Chem. Int. Ed.* **50** 7879–84
- [42] Dong R, Pfeiffermann M, Liang H, Zheng Z, Zhu X, Zhang J and Feng X 2015 Large-area, free-standing, two-dimensional supramolecular polymer single-layer sheets for highly efficient electrocatalytic hydrogen evolution *Angew. Chem. Int. Ed.* **54** 12058–63
- [43] Murray D J, Patterson D D, Payamyar P, Bhola R, Song W, Lackinger M, Schlüter A D and King B T 2015 Large area synthesis of a nanoporous two-dimensional polymer at the air/water interface *J. Am. Chem. Soc.* **137** 3450–3
- [44] Zheng Z, Ruiz-Vargas C S, Bauer T, Rossi A, Payamyar P, Schutz A, Stemmer A, Sakamoto J and Schlüter A D 2013 Square-micrometer-sized, free-standing organometallic sheets and their square-centimeter-sized multilayers on solid substrates *Macromol. Rapid Commun.* **34** 1670–80
- [45] Scheibe P, Schoenhentz J, Platen T, Hoffmann-Röder A and Zentel R 2010 Langmuir–blodgett films of fluorinated glycolipids and polymerizable lipids and their phase separating behavior *Langmuir* **26** 18246–55
- [46] Matmour R, Joncheray T J, Gnanou Y and Duran R S 2007 Two-dimensional polymeric nanomaterials through cross-linking of Polybutadiene-*b*-poly(ethylene oxide) monolayers at the air/water interface *Langmuir* **23** 649–58
- [47] Matmour R, Joncheray T J, Gnanou Y and Duran R S 2007 Cross-linking of polybutadiene at the air/water interface: toward an easy access to two-dimensional polymeric materials *J. Colloid Interface Sci.* **311** 315–21
- [48] Carino S R, Duran R S, Baney R H, Gower L A, He L and Sheth P K 2001 Chemical cross-linking, surface compressional modulus, and viscosity of n-octadecyltrimethoxy silane monolayers *J. Am. Chem. Soc.* **123** 2103–4
- [49] Kloeppner L J, Batten J H and Duran R S 2000 Surface behavior and polymerization of 2- and 3-(1-octadecynyl)aniline at the air–aqueous interface *Macromolecules* **33** 8006–11
- [50] Li B, Wu Y, Liu M and Esker A R 2006 Brewster angle microscopy study of poly(ϵ -caprolactone) crystal growth in langmuir films at the air/water interface *Langmuir* **22** 4902–5
- [51] Brachvogel R-C and von Delius M 2016 The dynamic covalent chemistry of esters, acetals and orthoesters *Eur. J. Org. Chem.* **2016** 3662–70
- [52] Whipple E B 1970 Structure of glyoxal in water *J. Am. Chem. Soc.* **92** 7183–6
- [53] Gomez M E, Lin Y, Guo S and Zhang R 2015 Heterogeneous chemistry of glyoxal on acidic solutions. An Oligomerization pathway for secondary organic aerosol formation *J. Phys. Chem. A* **119** 4457–63
- [54] Zotzmann J, Behl M, Hofmann D and Lendlein A 2010 Reversible triple-shape effect of polymer networks containing poly(pentadecalactone)- and poly(epsilon-caprolactone)-segments *Adv. Mater.* **22** 3424–9
- [55] Schöne A-C, Kratz K, Schulz B and Lendlein A 2016 Polymer architecture versus chemical structure as adjusting tools for the enzymatic degradation of oligo(ϵ -caprolactone) based films at the air–water interface *Polym. Degrad. Stab.* **131** 114–21
- [56] Loeffler K W, Koehler C A, Paul N M and De Haan D O 2006 Oligomer formation in evaporating aqueous glyoxal and methyl glyoxal solutions *Environ. Sci. Technol.* **40** 6318–23
- [57] Li B and Esker A R 2007 Molar mass dependent growth of poly(ϵ -caprolactone) crystals in langmuir films *Langmuir* **23** 2546–54
- [58] Sorrell T 2006 *Organic Chemistry* (Sausalito, California: University Science Books)
- [59] Liu Y-X and Chen E-Q 2010 Polymer crystallization of ultrathin films on solid substrates *Coord. Chem. Rev.* **254** 1011–37
- [60] Lee K W, Chung J W and Kwak S-Y 2018 Highly branched polycaprolactone/glycidol copolymeric green plasticizer by one-pot solvent-free polymerization *ACS Sustain. Chem. Eng.* **6** 9006–17
- [61] Nguyen N T, Thurecht K J, Howdle S M and Irvine D J 2014 Facile one-spot synthesis of highly branched polycaprolactone *Polym. Chem.* **5** 2997–3008
- [62] Straßburg A, Lützen H and Hartwig A 2015 Crystallinity as new toughening concept for epoxy resins: influence of branching of integrated polyester *J. Adhes. Soc. Japan* **51** 286–92

Appendix V: List of Publications and Contributions to Conferences

Publications

1. Shivam Saretia, Rainhard Machatschek, Thanga Bhuvanesh and Andreas Lendlein, **Effect of water on crystallization and melting of telechelic oligo(ϵ -caprolactone)s in ultrathin films**, *Advanced Materials Interfaces*, 8, 2001940, 2021, DOI: 10.1002/admi.202001940
2. Shivam Saretia, Rainhard Machatschek, and Andreas Lendlein, **Degradation kinetics of oligo(ϵ -caprolactone) ultrathin films: influence of crystallinity**, *MRS Advances*, 2021, DOI: 10.1557/s43580-021-00067-4
3. Shivam Saretia, Rainhard Machatschek, and Andreas Lendlein, **Highly crystalline PCL ultrathin films as thermally switchable biomaterial coatings**, *MRS Advances*, 6, 283–290, 2021, DOI: 10.1557/s43580-021-00020-5
4. Shivam Saretia, Rainhard Machatschek, Burkhard Schulz and Andreas Lendlein, **Reversible 2D networks of oligo(ϵ -caprolactone) at the air-water interface**, *Biomedical Materials*, 14(3), 034103, 2019, DOI: 10.1088/1748-605X/ab0cef
5. Rainhard Machatschek, Shivam Saretia and Andreas Lendlein, **Assessing the influence of temperature-memory creation on the degradation of copolyesterurethanes in ultrathin films**, *Advanced Materials Interfaces*, 8, 2001926, 2021, DOI: 10.1002/admi.202001926
6. Rainhard Machatschek, Shivam Saretia and Andreas Lendlein, **The interplay between network morphology and degradation kinetics of polymers: Theoretical and experimental analysis by means of a 2D model system**, *MRS Advances*, 5, 679–691, 2020, DOI: 10.1557/adv.2019.457
7. Thanga Bhuvanesh, Shivam Saretia, Toralf Roch, Anne-Christin Schöne, Falko O. Rottke, Karl Kratz, Weiwei Wang, Nan Ma, Burkhard Schulz and Andreas Lendlein, **Langmuir–Schäfer films of fibronectin as designed biointerfaces for culturing stem cells**, *Polymers for Advanced Technologies*, 28(10), 1305–1311, 2017, DOI: 10.1002/pat.3910

Journal front cover

1. Shivam Saretia, Rainhard Machatschek, Thanga Bhuvanesh and Andreas Lendlein, **Semi-crystalline oligomers: Effect of water on crystallization and melting of telechelic oligo(ϵ -caprolactone)s in ultrathin films**, *Advanced Materials Interfaces*, 8, 2001940, 2021, DOI: 10.1002/admi.202170035

Contributions to Conferences

1. Shivam Saretia, Rainhard Machatschek, and Andreas Lendlein, **Degradation kinetics of oligo(ϵ -caprolactone) ultrathin films: influence of crystallinity**, Materials Research Society Spring Meeting, Symposium - SM10: Progress in Green Chemistry Approaches for Sustainable Polymer Materials, April 17 – 23, 2021, Boston, USA, (*Abstract & oral presentation*)
2. Shivam Saretia, Rainhard Machatschek, and Andreas Lendlein, **Highly crystalline PCL ultrathin films as thermally switchable biomaterial coatings**, Materials Research Society Fall Meeting, Symposium - F.SM03: Materials and Mechanics Challenges in Haptics for Human–Machine Interfaces, November 27 – December 4, 2020, Boston, USA, (*Abstract & poster presentation*)
3. Shivam Saretia, Rainhard Machatschek, Burkhard Schulz and Andreas Lendlein, **Modulating enzymatic degradation of poly(ϵ -caprolactone) monolayer at air-water interface by two dimensional crosslinking**, PolyDays, September 11 – 13, 2019, Berlin, Germany (*Abstract & poster presentation*)
4. Shivam Saretia, Rainhard Machatschek, Burkhard Schulz and Andreas Lendlein, **Reversible 2D networks of oligo(ϵ -caprolactone) at the air-water interface**, *Advanced Functional Polymers in Medicine*, May 16 – 18, 2018, Montpellier, France (*Abstract & poster presentation*)

Appendix VI: Curriculum Vitae

For reasons of data protection, this section is excluded in the electronic version